2016

PORE PRESSURE MEASUREMENT INSTRUMENTATION RESPONSE TO BLASTING

Kylie M. Larson-Robl
University of Kentucky, larsonrobl@gmail.com
Digital Object Identifier: http://dx.doi.org/10.13023/ETD.2016.271

STUDENT AGREEMENT:

I represent that my thesis or dissertation and abstract are my original work. Proper attribution has been given to all outside sources. I understand that I am solely responsible for obtaining any needed copyright permissions. I have obtained needed written permission statement(s) from the owner(s) of each third-party copyrighted matter to be included in my work, allowing electronic distribution (if such use is not permitted by the fair use doctrine) which will be submitted to UKnowledge as Additional File.

I hereby grant to The University of Kentucky and its agents the irrevocable, non-exclusive, and royalty-free license to archive and make accessible my work in whole or in part in all forms of media, now or hereafter known. I agree that the document mentioned above may be made available immediately for worldwide access unless an embargo applies.

I retain all other ownership rights to the copyright of my work. I also retain the right to use in future works (such as articles or books) all or part of my work. I understand that I am free to register the copyright to my work.

REVIEW, APPROVAL AND ACCEPTANCE

The document mentioned above has been reviewed and accepted by the student's advisor, on behalf of the advisory committee, and by the Director of Graduate Studies (DGS), on behalf of the program; we verify that this is the final, approved version of the student's thesis including all changes required by the advisory committee. The undersigned agree to abide by the statements above.

Kylie M. Larson-Robl, Student

Dr. Jhon Silva-Castro, Major Professor

Dr. Braden Lusk, Director of Graduate Studies

PORE PRESSURE MEASUREMENT INSTRUMENTATION RESPONSE TO BLASTING

THESIS

A thesis submitted in partial fulfillment of the requirements for the degree of Master of Science in Mining Engineering in the College of Engineering at the University of Kentucky

By:

Kylie M. Larson-Robl

Lexington, Kentucky

Direction: Dr. Jhon Silva-Castro, Assistant Professor of Mining Engineering

Lexington, Kentucky

2016

ABSTRACT OF THESIS

PORE PRESSURE MEASUREMENT INSTRUMENTATION RESPONSE TO BLASTING

Coal mine impoundment failures have been well documented to occur due to an increase in excess pore pressure from sustained monotonic loads. Very few failures have ever occurred from dynamic loading events, such as earthquakes, and research has been done regarding the stability of these impoundment structures under such natural seismic loading events. To date no failures or damage have been reported from dynamic loading events caused by near-by production blasting, however little research has been done considering these conditions. Taking into account that current environmental restrictions oblige to increase the capacity of coal impoundments, thus increasing the hazard of such structures, it is necessary to evaluate the effects of near-by blasting on the stability of the impoundment structures. To study the behavior of excess pore pressure under blasting conditions, scaled simulations of blasting events were set inside a controlled sand tank. Simulated blasts were duplicated in both saturated and unsaturated conditions. Explosive charges were detonated within the sand tank at various distances to simulate different scaled distances. Information was collected from geophones for dry and saturated scenarios and additionally from pressure sensors under saturated conditions to assess the behavior of the material under blasting conditions.

KEYWORDS: Pore Pressure, Blasting, Coal Impoundments, Tourmaline Sensors, Shock Loading, Soil Dynamics

Kylie M. Larson-Robl

06/18/2016

PORE PRESSURE MEASUREMENT INSTRUMENTATION RESPONSE TO BLASTING

By:

Kylie M. Larson-Robl

Dr. Jhon Silva-Castro

Director of Thesis

Assistant Professor

Dr. Braden Lusk

Director of Graduate Studies

Professor

06/18/2016

Acknowledgements

Support for this work was funded by The Office of Surface Mining (OSM).

The author would like to thank:

Dr. Jhon Silva-Castro, thesis advisor and assistant professor of mining engineering at the University of Kentucky;

Dr. Braden Lusk and Dr. Kyle Perry for serving on this thesis committee;

Dr. Joshua Calnan, Dr. Braden Lusk, and Tristan Worsey as our certified blasters for support in test setup, troubleshooting, and charge detonation;

Nelson Brothers for providing the explosives;

My husband-to-be, Phillip Begley.

Contents

List of Tables

List of Figures

CHAPTER 1: INTRODUCTION

Coal refuse impoundments are a typical mine waste disposal system for coal mines in the Eastern United States. As of 2013, NIOSH lists 1,204 surface coal mine operations in the United States (Figure 1). Although impoundment dams (or tailings dams) are not exclusive to coal operations, as of 2016, MSHA lists approximately 2,000 impoundments/dams in its dam inventory with over 400 of those being classified as “high hazard potential” (Department of Labor, MSHA Dam Safety). Due to the topographic nature of the Appalachian region much of these coal refuse impoundments are cross valley structures, Figure 2. These cross valley impoundment structures may be built using an upstream staging method (Figure 3), centerline staging method (Figure 4), or a downstream staging method (Figure 5) (Engineering and Design Manual. Coal Refuse Disposal Facilities, 2009).

Historically there have been numerous failures of these impoundments since the most devastating failure in Buffalo Creek, West Virginia in 1972. This failure was the result of the combination of heavy rainfall and inadequate construction. The Buffalo Creek failure sent approximately 132 million gallons of slurry into the mining community below which resulted in 125 people killed, 1,100 injured, more than 4,000 homeless, and an estimated $50 million in property damages (Davies et. al., 1972). At the time of the Buffalo Creek disaster there were no federal regulations on coal impoundments. Since then, there have been regulations regarding structure size, slurry capacity, and monitoring systems put in place. Much of the monitoring system requirements include a pore pressure monitoring

system. The majority of failures have been circumstance of heavy precipitation causing an excess in pore pressure to reduce effective stress for a period of time long enough to allow gravity to act upon that slope (National Research Council, 2002).

A similar production of excess pore pressure can occur due to vibration from seismic events; e.g. liquefaction during an earthquake (Engineering and Design Manual. Coal Refuse Disposal Facilities, 2009). Damage to earth fill dams from earthquakes, although rare, has been documented. A near failure of the Lower Van Norman Dam during the 1971 San Fernando earthquake prompted modern dynamic analysis methods and design recommendations (FEMA, 2005). These recommendations take in to consideration the largest expected seismicity to the area as a result of earthquakes and require a safety factor greater than or equalling to 1.2. Although these recommendations do not consider the vibrations caused by mine blasting, worldwide experience with these structures indicate a high success rate even under significant seismic events. In the absence of reference to, and the insufficient research done, the dynamic conditions produced by mine blasting and the potential effect on slope stability of impoundments should be examined (Larson-Robl, K. et al., 2015).

Prior to attempting to measure and model excess pore pressures within a full scale impoundment structure, it was important to model and understand the pore pressure response and its relationship to traditional blasting parameters in a scaled, controlled environment. The results from these scaled experiments are presented in this thesis.

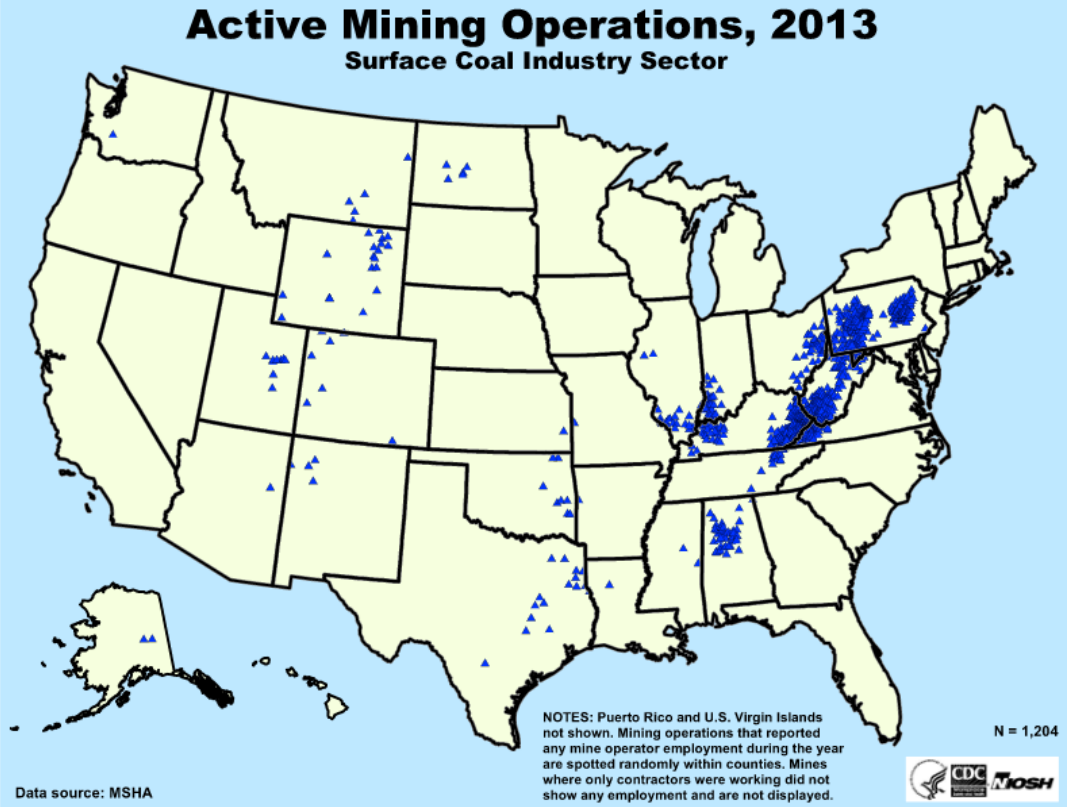

Figure 1: Most current map of all 1,204 surface coal operations from the National Institute for Occupational Safety and Health (NIOSH)

Figure 2: Upstream cross valley impoundment in Raleigh County, West Virginia where Marsh Fork Elementary operated at the base until 2013; photo credited to Carl Galie

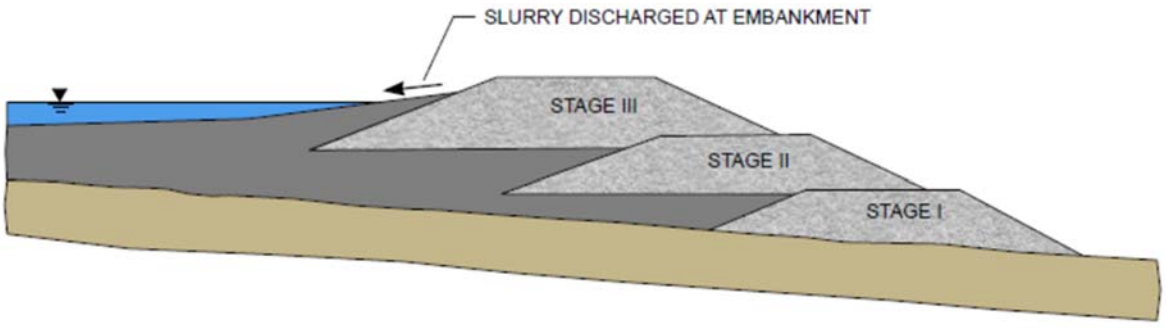

Figure 3: Upstream staging method (Engineering and Design Manual. Coal Refuse Disposal Facilities, 2009)

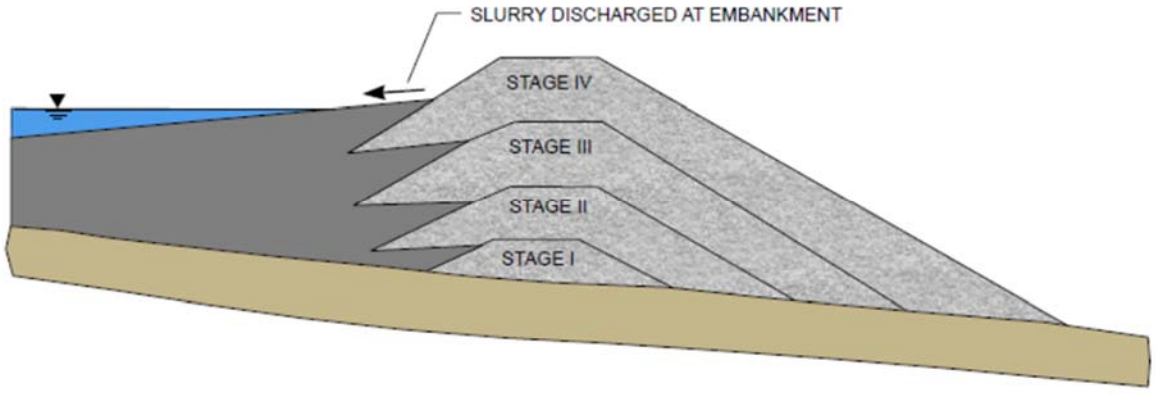

Figure 4: Centerline staging method (Engineering and Design Manual. Coal Refuse Disposal Facilities, 2009)

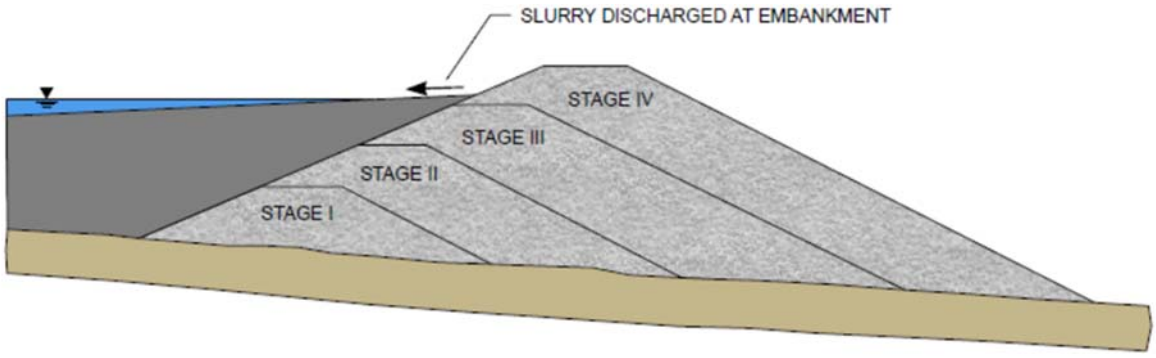

Figure 5: Downstream staging method (Engineering and Design Manual. Coal Refuse Disposal Facilities, 2009)

CHAPTER 2: BACKGROUND INFORMATION

2.1 Terminology

Impoundment dams are constructed using the unconsolidated course mine refuse, and the fine refuse slurry is pumped behind this containment. An unconsolidated medium, whether that be a sand, gravel, or soil, is comprised of the matrix of particles as well as the pore space between them. These pores can be filled with air, water, or any other present gas or liquid. In the interest of this study, it will be considered when all of the pore spaces are filled with water for a condition of 100% saturation. The greatest risk of failure within impoundment structures occurs in the unconsolidated, saturated, fine slurry material under the successive overlying stages especially in the upstream staging method (National Research Council, 2002). The force of the grain-to-grain contacts of the particle matrix is termed the effective stress, Figure 6 (black arrows). Effective stress is mainly a function of density and depth, but may be influenced by geometric or geologic features. The force of the gas or liquid in the pore space, in this case water, acting upon the particles is termed the pore pressure, Figure 6 (blue arrows).

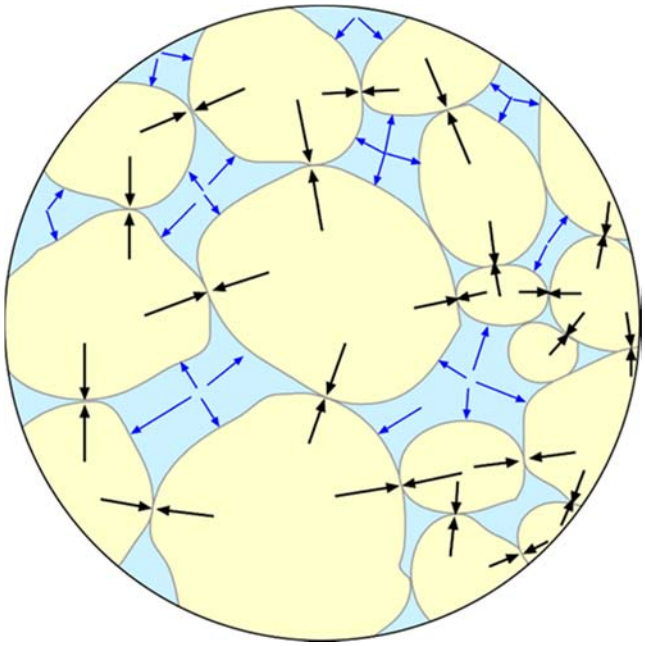

Figure 6: Depiction of effective stress (black arrows) and pore pressures (blue arrows).

The combination of the effective stress, σ'_0, and the pore pressure, u, is the total stress, σ_{total}:

$$\sigma_{total} = \sigma'_0 + u \quad (1)$$

The most basic calculation of effective stress is subtracting the static pore pressure from the total stress, both as a function of the unit weight and depth:

$$\sigma'_0 = \sigma_{total} - u = z\gamma_{soil} - z\gamma_{water} \quad (2)$$

Where z, is depth and γ_{soil} and γ_{water} are the unit weight of the soil/unconsolidated material and the unit weight of water, respectively. This being the calculation for a one layer system; each additional layer above the

desired depth would have to be added with its respective depth multiplied by its respective unit weight. For example from Figure 7:

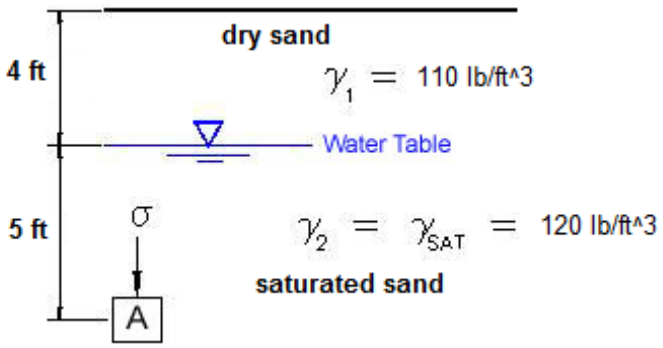

Figure 7: example for calculation of effective stress at location A

$$\sigma_{total} = z\gamma_{soil} = (4\,ft)\left(110\frac{lb}{ft^3}\right) + (5\,ft)\left(120\frac{lb}{ft^3}\right) = 1040\frac{lb}{ft^2} \quad (3)$$

$$u = z\gamma_{water} = (5\,ft)\left(62.4\frac{lb}{ft^3}\right) = 312\frac{lb}{ft^2} \quad (4)$$

$$\sigma'_0 = \sigma_{total} - u = 1040\frac{lb}{ft^2} - 312\frac{lb}{ft^2} = 728\frac{lb}{ft^2} \quad (5)$$

There are generally two different types of loading scenarios that are discussed here; monotonic loading and dynamic loading. Monotonic loading is that of an increasing load at low rates, such as those used in triaxial or uniaxial compression strength tests. For the purpose of this study, dynamic loading is broken into two different types; dynamic cyclic loading and dynamic shock wave loading. Dynamic cyclic loading refers to a loading that is periodic or oscillatory, i.e. earthquakes. Dynamic shock wave loading refers to the loading typical of an explosive detonation at close range. At further distances the loading from an explosive detonation resembles that of a dynamic cyclic loading event.

When a saturated unconsolidated material is subject to conditions of undrained loading (occurring when the pore water is unable to drain from the soil) the shear stress may rise to a point of failure; a stress loading past this point causes an increase in the pore pressure, since this pore pressure is in addition to the initial hydrostatic pore pressure it is termed excess pore pressure (Woldeselassie, 2012). Skempton (1954), based on axisymmetric triaxial tests on hydrostatically consolidated specimens, proposed a relationship to quantify the amount of excess pore pressure generated in a triaxial compression test (using a monotonic load) in terms of major and minor principal stress increments as:

$$\Delta u = B(\Delta\sigma_3 + A(\Delta\sigma_1 - \Delta\sigma_3)) \quad (6)$$

Where A and B are pore pressure coefficients known as Skempton's pore pressure parameters; B being dependent on the degree of saturation and A accounting for the shear induced pore pressure.

$$B = \frac{1}{1+n\left(\frac{C_F}{C_{Sk}}\right)} \quad (7)$$

Where, n is the porosity, C_F is the compressibility of the pore fluid, and C_{Sk} is the compressibility of the soil skeleton. In the case of a fully saturated medium where the pore liquid is water C_F is negligible compared to C_{Sk}, and thusly $B \cong 1$ (Skempton, 1954). A has typically been determined experimentally and is taken at failure. A has been demonstrated by Skempton to be equal to $\frac{1}{3}$ for isotropic elastic materials, but range in value for naturally occurring soils. An attempt by

Terzaghi et al. (1996) to predict excess pore pressure in three dimensional loading has produced the following equation:

$$\Delta u = B(\Delta\sigma_3 + A_1(\Delta\sigma_1 - \Delta\sigma_3) + A_2(\Delta\sigma_2 - \Delta\sigma_3)) \quad (8)$$

Not enough experimental research has been done to accurately define A_1 and A_2. Equations 6 and 8 were developed for monotonic loading, and there are few non-theoretical proposals for the assessment of excess pore pressure under dynamic shock type loads such as blasting.

When soil or unconsolidated material is loaded dynamically or monotonically under undrained conditions, there is a generation of excess pore pressure referred to as residual pore pressure. This residual pore pressure increase occurs when the saturation fluid deforms elastically while the soil matrix deforms plastically (Charlie et al., 2001). When both the fluid and soil matrix respond to a strain elastically the pore pressure does not maintain an increased residual pore pressure. At the point of failure of the shear stress, where excess pore pressure is generated, the effective stress between particles goes to zero (Figure 6 particles are no longer in contact), thus all stress is transferred to the pore pressure liquid. This phenomena is termed liquefaction.

Traditionally, liquefaction has been studied as a result of dynamic cyclic loading; i.e. earthquakes, but the initiation of liquefaction due to a dynamic shock wave load (like blasting) is less understood. It is important to note that liquefaction may be induced when either loose unconsolidated material are rearranged and packed more densely due to shearing, or when dense unconsolidated material

dilates due to shearing (Woldeselassie, 2012). It is understood that under cyclic loading the cause of liquefaction of loose unconsolidated material is the densification of the matrix and dilation often plays little role (Woldeselassie, 2012). Although, it has been shown that severe vibration can induce dilation. Much of the existing literature examines blast-induced pore pressures in the scope of cyclic loading, as the loading event from a blast resembles a cyclic loading event at large scaled distances.

2.2 Pore Pressures and Stress Measurements from Loading Events

In development of this research, it is necessary to make the distinction between different loading conditions of a blast. In this study and those studies examined, spherical or cylindrical (non-directional or planar) explosives produce spherical or cylindrical stress waves. At close scaled distances the ground response, measured by peak particle velocity (PPV), is that of a dynamic shock wave loading event that produces a transient peak and attenuates back to static state very quickly. At further scaled distances the ground response, PPV, resembles that of a dynamic cyclic loading event that has an oscillatory waveform that is sustained over a longer period of time.

The peak particle velocity (PPV) and peak radial compressive stress occur simultaneously with the wave front (Charlie et al., 2013). Whereas peak shear strain occurs shortly after the pass of the stress wave peak (Charlie et al., 2013). Because the transient pore pressure peak is due to the initial compressional wave

produced from the blast, this peak is almost instantaneous and quickly goes back to zero within milliseconds, Figure 8.

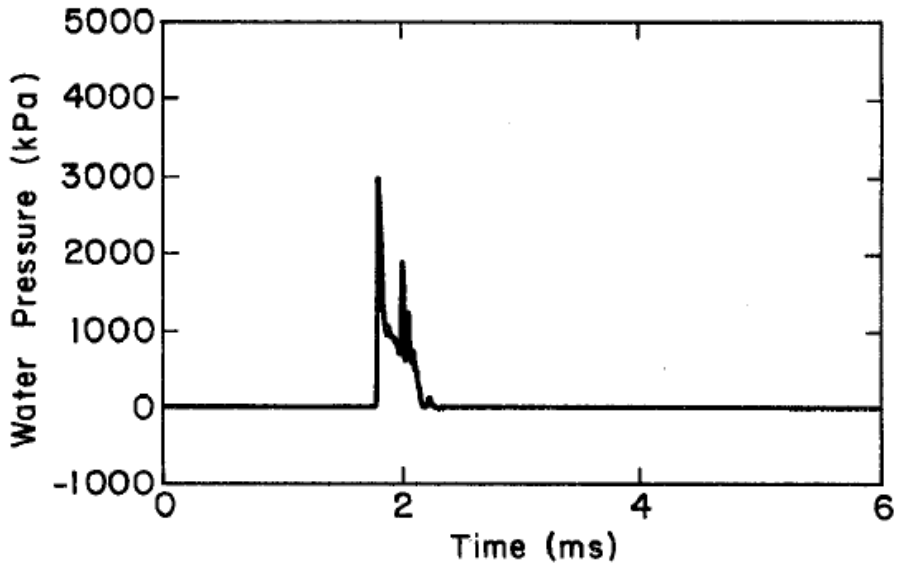

Figure 8: Tourmaline waveform results from a test depicting only the transient pore pressure from a test with 0.43 kg of explosives at a distance of 2.7 m (Charlie et al., 2001).

The residual pore pressure on the other hand, has a more gradual increase after the pass of the initial stress wave and dissipates slowly (Charlie et al., 2001). The dissipation occurs as the excess pore pressure subsides and the soil consolidates; a function of the permeability of the material and the geology or geometry of the location. This gradual rise and fall of residual pore pressure may remain over a period of time ranging from seconds to minutes. Figure 9 shows a waveform result depicting residual pore pressures.

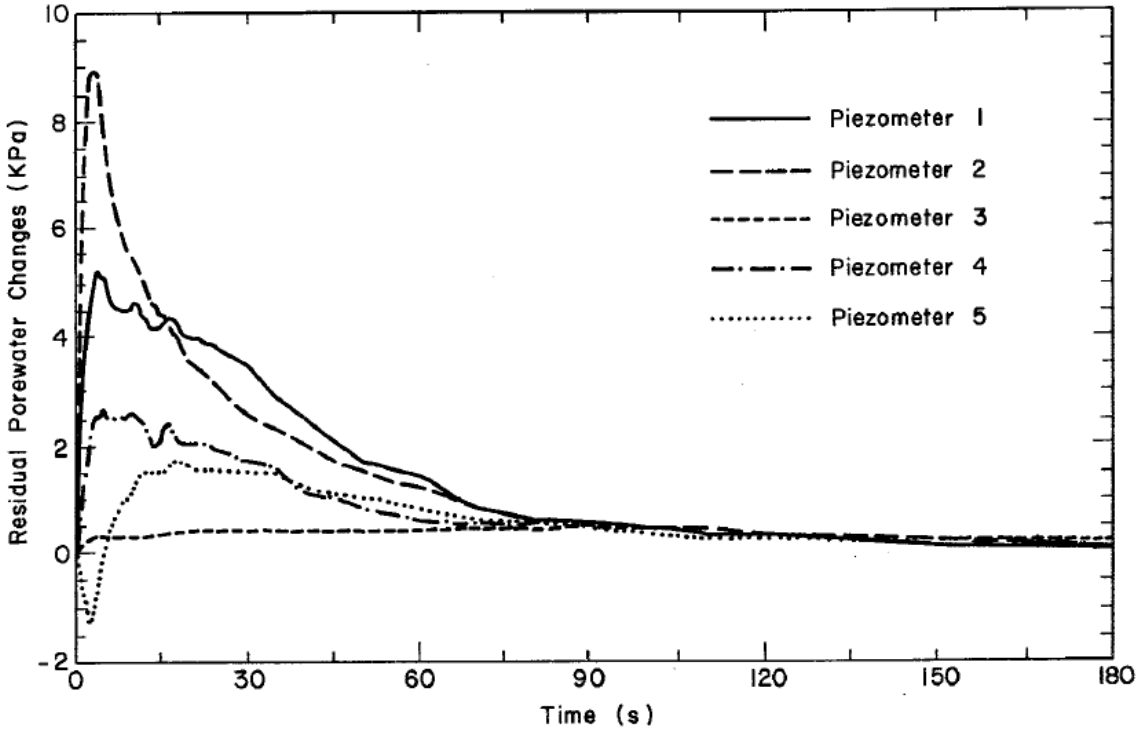

Figure 9: Tourmaline waveform results from a test depicting residual excess pore pressures from a blast of 0.43 kg of explosives at scaled distances of 6.9, 9.55, 12.2, 7.69, 9.55 m/kg$^{1/3}$ for piezometers 1, 2, 3, 4, and 5 respectively (Charlie et al., 2013).

Liquefaction exists when the pore pressure is equal to or exceeds the initial grain-to-grain effective stress of the soil matrix. This phenomena under cyclic loading is often looked at in the terms of pore pressure ratio, PPR; that is the ratio of the change in residual excess pore pressure, Δu_{res}, to the initial effective stress, σ'_0 (Charlie et al., 2001).

$$PPR = \frac{\Delta u_{res}}{\sigma'_0} \qquad (9)$$

Such that, when the PPR exceeds or equals one, liquefaction occurs. It is known that as relative density and effective stress increase the required PPV and peak strain required to induce liquefaction increases.

The interests of this study are the excess pore pressure measurements in a saturated medium and their relation to the other typical values measured in blasting. Due to the nature of dynamic shock wave loading events, the other typical values of interest are peak ground motion (also referred to as peak particle velocity (PPV)), strain, and pressure. In the event of a charge detonation, a compressive stress wave is produced that can cause peak accelerations several orders of magnitude greater than an earthquake. Since these values are largely dependent on the amount of explosives used, they are commonly related to a scaled distance. Scaled distance is typically either in the form of square-root or cube-root scaling. This scaled distance, SD, is typically the distance measured from the charge location, d, divided by the square-root or cube-root of the mass of explosives, $M^{\frac{1}{2}}$ or $M^{\frac{1}{3}}$,

$$SD = \frac{d}{M^{\frac{1}{2}}} \quad (10)$$

$$SD = \frac{d}{M^{\frac{1}{3}}} \quad (11)$$

The square-root scaling is typically used for row charges, line charges, and near-surface charges resulting in surface waves, whereas cube-root scaling is typically used for point-charges that are deeply buried (Charlie et al., 2001). For this study the cube-root scaling method will be utilized, as single detonations are used. It is

important to note that multiple detonations typically cause increased residual pore pressures at greater scaled distances and at smaller PPVs and peak strains than single detonations (Charlie et al., 2013).

Peak particle velocity, PPV, is the most common value assessed during blasting due to its ease of measurement and thoroughly studied implications. It can be measured by mounting or burying a geophone connected to a seismograph at the desired location. It is also important to note the relationship between the PPV and the peak compressive strain, ε_{peak}, in percent and the peak transient compressive stress, σ_{peak}, in kPa (Charlie et al., 2001).

$$\varepsilon_{peak} = \frac{PPV}{V_c}\,(100\%) \qquad (12)$$

$$\sigma_{peak} = (\rho_t V_c) PPV \qquad (13)$$

Where, V_c, is the compressive wave velocity, ρ_t, is the total mass density. Although, the equations for peak radial compressive strain (ε_{peak}) and peak radial compressive stress (σ_{peak}) were developed for planar stress waves they are valid on the stress wave for expanding spherical stress waves (Charlie et al., 2013). It can be approximated that peak shear strain, γ_{peak}, is equal to the peak compressive strain at the front of the stress wave (Charlie et al., 2013):

$$\gamma_{peak} \cong \varepsilon_{peak} = \left(\frac{PPV}{V_c}\right)(100\%) \qquad (14)$$

Peak tensional strain, ε_{peakd}, occurs at peak displacement for expanding spherical stress waves, which often occurs after the stress wave front has passed (Charlie et al., 2013):

$$\varepsilon_{peakd} = \frac{d_{peak}}{R}(100\%) \quad (15)$$

Where d_{peak} is the peak displacement in meters and R is the radial distance from the detonation in meters. Similarly, the peak tensional strain, γ_{peakd}, occurring after the stress wave front, can be approximated with the peak tensional strain, ε_{peakd}, at peak displacement, d_{peak} (Charlie et al., 2013):

$$\gamma_{peakd} \cong \varepsilon_{peakd} = \frac{d_{peak}}{R}\ (100\%) \quad (16)$$

With the assumption that peak radial compression strain and peak displacement occurs at the same time, Hryciw (1986) and Pathirage (2000) the peak shear strain, γ_{peak}, from a spherical expanding stress wave is:

$$\gamma_{peak} = 0.5\ \left(\frac{PPV}{V_c} + \frac{d_{peak}}{R}\right)(100\%) \quad (17)$$

Where PPV is the peak particle velocity in m/s, V_c is the compressional wave velocity in m/s.

Due to the importance of these values in blasting stability of other mine features there have been empirical studies to attempt to predict these values in saturated, unconsolidated material. Crawford et al. (1974) and Drake and Little (1983) produced the following equations based on over 100 explosions tests in soil utilizing spherical shaped explosives:

$$PPV = 48.8\,(2.52)^{-n}\,(SD)^{-n} \quad (18)$$

$$\sigma_{peak} = 48.8\,(2.52)^{-n}\,(\rho_t V_c)(SD)^{-n} \quad (19)$$

$$d_{peak} = 60.4\,(2.52)^{-n+1}\left(\frac{M^{\frac{1}{3}}}{V_c}\right)(SD)^{-n+1} \quad (20)$$

Where PPV is the peak radial particle velocity in m/s, n is the attenuation coefficient, SD is the cube-root scaled distance in m/kg$^{1/3}$ of trinitrotoluene (TNT) equivalent explosives mass, σ_{peak} is the peak compressive stress in Pa, ρ_t is the total soil density in kg/m^3, V_c is the compressive wave velocity in m/s, d_{peak} is the peak ground displacement in meters, and M is the mass of explosives used in kg. The value of $\rho_t V_c$ is the acoustic impedance of the soil in kg/m^{2}s. The tests comprising these equations ranged from soils of loose dry sand to soils of saturated clay. The proposed attenuation coefficient for saturated soil with a seismic velocity greater than 1,500 m/s is 1.5 (Drake and Little, 1983), and an attenuation coefficient of 1.13 is suggested by Cole (1948) for water alone. Utilizing the suggested attenuation coefficient of 1.5 these equations reduce to:

$$PPV = 12.2\,(SD)^{-1.5} \quad (21)$$

$$\sigma_{peak} = 12.2\,(\rho_t V_c)(SD)^{-1.5} \quad (22)$$

$$d_{peak} = 38.0\left(\frac{M^{\frac{1}{3}}}{V_c}\right)(SD)^{-0.5} \quad (23)$$

Historically, impoundment and earth fill dam damage has occurred under cyclic loading events that tend to cause lasting residual pore pressure increases leading to liquefaction. At this time very limited instrumentation exists to function in and accurately measure the complex environment and stress field of pore pressures subject to shock waves from blasting.

2.3 Pressure Sensors

There are a few different instruments that are capable of measuring pore pressure. The instruments commonly used for dynamic blasting pressures are piezoresistive strain gauges that use a diaphragm to convert changes in pressure to an electrical signal, but these have been typically developed for air pressures. Previous studies have favored the Endevco piezoresistive pressure transducer model 8511A, Figure 10, to measure dynamic transient pore pressure due to its high sampling rate and pressure capability up to 140,000 kPa (Charlie et al., 2001, Charlie et al., 2013, Veyera et al., 2002). These Endevco pressure transducers are originally designed for air blasts and require retrofitting with a steel porous plate over the diaphragm for use in unconsolidated material.

Figure 10: Endevco piezoresistive pressure transducer model 8511A with retrofitted steel porous plate.

The most common pore pressure instruments are standard piezometers, Figure 11. Standard piezometers come in many varieties, and function by measuring the changes in the water column above the sensor. Standard piezometers have typically been used to measure residual excess pore pressures, but since they have a much lower sampling rate, they cannot measure transient pore pressures from a dynamic shock wave loading event occurring within milliseconds. In this study, it was attempted to use a RST Instruments piezometer, but with a sampling rate of 33 samples/minute (approximately every three seconds), attempts were unsuccessful. Typical instruments used to measure vibration in blasting have sampling rates on the order of 1,000 to 2,000 samples per second.

Figure 11: standard piezometers

Tourmaline piezoelectric pressure sensors, Figure 12, work similarly to the pressure transducers by converting the pressure changes to an electrical signal, where the clear, flexible, cylindrical casing surrounding the filament acts as a diaphragm. Tourmaline pressure sensors were designed specifically to respond to underwater blasts. These sensors come in multiple sensitivities up to 10,000 psi (68950 kPa) capabilities, and are designed specifically for underwater blasts. For this study we acquired two tourmaline sensors with 1,000 psi thresholds and another tourmaline sensor with a 50 psi threshold. Tourmaline pressure sensors are expensive, sensitive and sophisticated instruments, and publications on their applications are limited.

Figure 12: PCB Tourmaline pressure sensors

CHAPTER 3: REVIEW OF LITERATURE

3.1 Existing Empirical Thresholds for Liquefaction and Residual Pore Pressures

3.1.1 Peak Particle Velocity

Where peak particle velocity, PPV, is the most common measurement during blasting events, it is not surprising much of the current research and recommendations for excess pore pressure are relating to PPV. According to Puchkov (1962), horizontal deposits of saturated soil did not experience liquefaction at PPVs less than 0.11 m/s (4.3 in/s) (Charlie et al., 2013). A study done by Charlie et al. in 1992 reported liquefaction occurring at PPVs exceeding 0.9 m/s (35 in/s) in dense alluvial sand, and a study by Al-Qassimi et al. (2005) reported liquefaction occurring at PPVs exceeding 0.6 m/s (24 in/s) for loose tailings. Where, the designation of granular soils based on relative density, D_r, are as follows: 0-20% D_r is very loose, 20-40% D_r is loose, 40-70% D_r is medium dense, 70-85% D_r is dense, and 85-100% is very dense (Kalinski, 2011). A study by Charlie et al. (2013) in angular, poorly graded sand resulted in liquefaction at PPVs of 0.49, 0.52, and 0.71 m/s (19, 20, and 28 in/s) for loose, dense, and very dense sand, respectively. According to Long et al. (1981), residual pore pressures occurred in loose saturated sand when PPV exceeded 0.05 m/s (2.0 in/s) (Charlie et al., 2013). Obermeyer (1980) reported no significant pore pressure increase (PPR < 0.1) at PPV up to 0.02 m/s (0.79 in/s) (Charlie et al., 2013). Charlie et al. (2013) reported no significant residual pore pressure at PPVs less than 0.07 m/s (2.8 in/s) for loose, dense, and very dense sands. Obermeyer (1980), Long et al.

(1981), and Charlie (1985) reported that no significant increase in residual pore pressure occurred in loose sands with peak particle velocities less than 0.01 to 0.05 m/s (0.39 to 2.0 in/s). Charlie et al. (2001) did not see significant increases in residual pore pressure between PPV of 0.015 m/s (0.59 in/s) at effective stress of 3.9 kPa (0.57 psi) and PPV of 0.035 m/s (1.4 in/s) at 29.3 kPa (4.2 psi) effective stress. Charlie et al. (2001) recommends that for hydraulic fill dams or dams constructed of loose sands or silts PPV should not exceed 0.025 m/s (0.98 in/s), and for dams of medium dense sand or silts PPV should not exceed 0.05 m/s (2.0 in/s). Charlie et al. (2013) suggests that PPV for earthfill dams and tailing dams be kept under 0.025, 0.05, and 0.10 m/s (0.98, 2.0, and 3.9 in/s) for those unconsolidated materials that are sensitive, moderately sensitive, and not sensitive to vibration, respectively. These thresholds are summarized in Table 1.

Table 1: Reported Liquefaction and Residual Pore Pressure Thresholds for peak particle velocity (Charlie et al., 2013)

PPV (m/s)	Density	Reference
Liquefaction (field explosive tests)		
>0.49	loose	Charlie et al. (2013)
>0.71	very dense	Charlie et al. (2013)
>0.52	dense	Charlie et al. (2013)
>0.49	loose	Charlie et al. (2013)
>0.6	loose	Al-Qassimi et al. (2005)[a]
>0.8±	loose	Pathirage (2000)[a]
>0.16	dense	Charlie et al. (1992)
>0.08	very loose	Puchkov (1962)
>0.11	very loose	Lyakhov (1961)
Liquefaction (one-dimensional laboratory shock tests)		
>0.1	loose	Hubert (1986)
>0.4	loose	Veyera (1985)
Significant residual pore pressure: PPR >0.1 (field explosive tests)		
>0.07	loose-dense	Charlie et al. (2013)
>0.07	loose-dense	Charlie et al. (2013)
>0.01	loose	Al-Qassimi et al. (2005)[a]
>0.03	dense	Charlie et al. (1992)
>0.05	loose	Long et al. (1981)
>0.02	hydraulic fill tailings	Obermeyer (1980)
Significant residual pore pressure: PPR >0.1 (one-dimensional laboratory shock tests)		
>0.08		Veyera (1985) and Hubert (1986

Note: All values are for single detonations unless where noted.
[a]Multiple millisecond-delayed detonations

3.1.2 Peak Compressive Strain

A peak compressive strain, ε_{peak}, of less than 0.001-0.01% is generally accepted as being in the elastic range of the soil matrix and small enough to ensure there is no generation of residual pore pressure (Dobry, et al., 1982; Charlie 1985). Using the previous equations and an estimated 1500 m/s compressive wave velocity, V_c, for loose soil saturated with deaired water, this PPV is between about 0.015 m/s

(0.6 in/s) and 0.15 m/s (6.0 in/s) (Charlie et al., 2001). Charlie et al. (1992) and Pathirage (2000) reported liquefaction occurring at strains greater than 0.06%. Al-Qassimi et al. (2005) reported liquefaction occurring at strains greater than 0.04%. Charlie et al. (2013) reported liquefaction at strains of 0.03, 0.03, and 0.04% for loose, dense, and very dense sands, respectively. Veyera (1985), Hubert (1986), Bolton (1989), and Charlie et al. (2013) reported no significant residual pore pressure at peak strains less than approximately 0.005%. Pathirage (2000) and Gohl et al. (2001) reported no significant residual pore pressure at peak strains less than 0.01% and 0.02%, respectively. Charlie et al. (1992) reported that at peak strains less than 0.002% no significant residual pore pressure occurred and Al-Qassimi et al. (2005) reported no significant residual pore pressure at peak strains less than 0.001%. It is suggested by Dobry et al. (1981) that shear strain remain under 0.01%. These thresholds are summarized in Table 2.

Table 2: Reported Liquefaction and Residual Pore Pressure Thresholds for peak strain (Charlie et al., 2013)

Peak Strain (%)[b]	Density	Reference
Liquefaction (field explosive tests)		
>-0.09[c]	loose	Charlie et al. (2013)
>0.04	very dense	Charlie et al. (2013)
>0.03	dense	Charlie et al. (2013)
>0.03	loose	Charlie et al. (2013)
>0.04	loose	Al-Qassimi et al. (2005)[a]
>0.06[c]	loose	Pathirage (2000)[a]
>0.01	dense	Charlie et al. (1992)
Liquefaction (one-dimensional laboratory shock tests)		
>0.01	loose	Hubert (1986)
>0.03	loose	Veyera (1985)
Significant residual pore pressure: PPR >0.1 (field explosive tests)		
>-0.01[c]	loose-dense	Charlie et al. (2013)
>0.004	loose-dense	Charlie et al. (2013)
>0.001	loose	Al-Qassimi et al. (2005)[a]
>0.02[d]	loose	Gohl et al. (2001)
>0.01[d]	loose	Pathirage (2000)[a]
>0.002	dense	Charlie et al. (1992)
Significant residual pore pressure: PPR >0.1 (one-dimensional laboratory shock tests)		
>0.005		Veyera (1985) and Hubert (1986)

Note: All values are for single detonations unless where noted.

[a]Multiple millisecond-delayed detonations

[b]Peak radial compressive strain at peak stress (ε_{peak})

[c]Peak tangential tensile strain at peak displacement (ε_{peakd})

[d]Peak shear strain (γ_{peak})

3.1.3 Scaled Distance

For level deposits of loose saturated sand, Ivanov (1967) reported liquefaction occurring up to a cubed-root scaled distance of 6-8 m/kg$^{1/3}$ for loose sandy tailings, and for level deposits of dense saturated sand liquefaction was reported up to a cubed-root scaled distance of 6 m/kg$^{1/3}$. Studer and Kok (1980) reported

liquefaction occurring up to scaled distances of 2.8 m/kg$^{1/3}$ in loose sands. In alluvial sands of relative density between 70 and 90%, Charlie et al. (1992) reported liquefaction at scaled distances less than 3 m/kg$^{1/3}$. Al-Qassimi et al. (2005) reported liquefaction of loose sand tailings at less than 6.5 m/kg$^{1/3}$. Similarly, Pathirage (2000) reported liquefaction of loose sand tailings up to 6.75 m/kg$^{1/3}$. Charlie et al. (1992), reported no significant residual pore pressure (PPR < 0.1) increase at scaled distances greater than 16 m/kg$^{1/3}$ in dense alluvial sand. According to Al-Qassimi et al. (2005) and Pathirage (2000) no significant residual pore pressure occurs at scaled distances greater than 42 and 30 m/kg$^{1/3}$ respectively in loose sand tailings. A summary by Eller (2011) reports that no significant residual pore pressure occurred at scaled distances greater than 20 m/kg$^{1/3}$. Charlie et al. (2013) reported liquefaction at scaled distances of 8.8, 9.8, and 8.2 m/kg$^{1/3}$ and no significant residual pore pressures at scaled distances of 38, 37, and 27 m/kg$^{1/3}$ for loose, dense, and very dense, angular, poorly graded sands, respectively. A caution to Charlie et al.'s (2013) values are that the blasts were detonated in water above these oversaturated sands likely causing the larger scaled distances than those scaled distances from tests with detonations in a saturated matrix. These thresholds are summarized in Table 3.

Table 3: Reported Liquefaction and Residual Pore Pressure Thresholds for scaled distances (Charlie et al., 2013)

Scaled Distance (m/kg^⅓)	Density	Reference
Liquefaction (field explosive tests)		
<8.2	loose	Charlie et al. (2013)
<9.8	very dense	Charlie et al. (2013)
<8.8	dense	Charlie et al. (2013)
<8.2	loose	Charlie et al. (2013)
<6.3	loose	Al-Qassimi et al. (2005)[a]
<6.7	loose	Pathirage (2000)[a]
<3	dense	Charlie et al. (1992)
<2.8	-	Studer and Kok (1980)
<6-8	very loose	Ivanov (1967)
<5	very loose	Puchkov (1962)
<4.3	-	Kummeneje and Eide (1961)
Significant residual pore pressure: PPR >0.1 (field explosive tests)		
<38	loose-dense	Charlie et al. (2013)
<38	loose-dense	Charlie et al. (2013)
<20	loose-medium dense	Eller (2011)
<42	loose	Al-Qassimi et al. (2005)[a]
<30	loose	Pathirage (2000)[a]
<16	dense	Charlie et al. (1992)
<11.3	-	Studer and Kok (1980)
<12	-	Kummeneje and Eide (1961)

Note: All values are for single detonations unless where noted.

[a]Multiple millisecond-delayed detonations

3.2 Existing Empirical Equations for Liquefaction and Pore Pressures

As mentioned previously, multiple detonations can lower the PPV and peak strain thresholds of liquefaction and liquefaction may occur at greater scaled distances. A study by Al-Qassimi et al. (2005) utilizing multiple detonations with millisecond delays shown liquefaction at PPVs exceeding 0.13 m/s (5.1 in/s) and peak radial strains exceeding 0.008% at scaled distances less than 12.5 m/kg$^{1/3}$. The blasts

in Al-Qassimi's (2005) study were detonated in level deposits of tailings 10 to 50 m away from an 8 m high, clay, test impoundment, and utilized between 1.5 and 4.5 kg of POWERMITE™ by Dyno Novel, Inc. Pore pressures were measured at depths of 2 and 6 m. PPVs were calculated from accelerations measured at 6 m depth.

The results from a study by Charlie et al. (2013) also suggests that blasts resulting in nonplanar (spherical and cylindrical) stress waves may result in higher residual pore pressures than those blasts generating planar stress waves. The study by Charlie et al. (2013) utilized charges suspended in water 0.6 m from the surface and 1.8 m above a saturated, unconsolidated material sample surrounded by saturated clay. Charges consisted of blasting caps by Dupont, Primacord by Ensign-Brickford, and Tovex 800 by Dupont. Test charge weights ranged from 0.00044 kg to 7.02 kg. Figure 13 depicts a summary of existing empirical equations found to relate PPV in saturated conditions to scaled distance of several soil types.

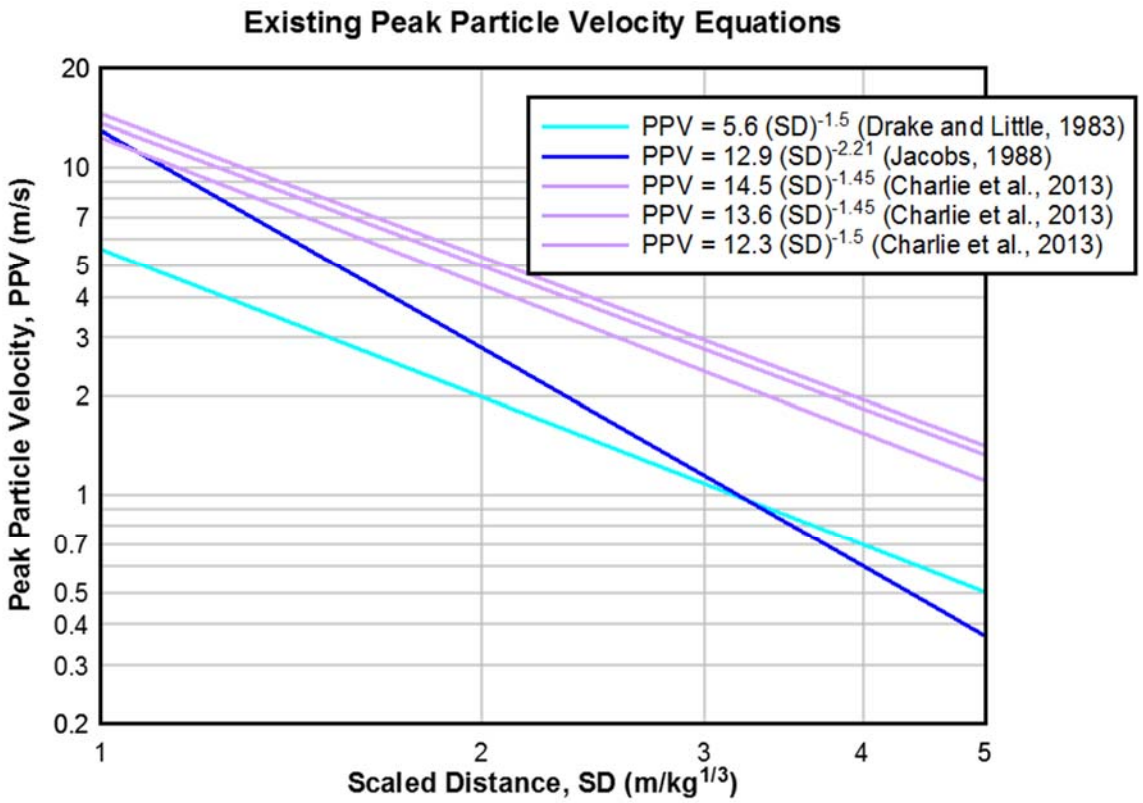

Figure 13: Existing empirical equations for PPV versus scaled distance for saturated soils; where the Drake and Little (1983) equation is for saturated clays and clay shales, the Jacobs (1988) equation is for dense alluvial sand, and the Charlie et al. (2013) equations are for loose, dense, and very dense sands, respectively.

Because the main driving factor behind impoundment failures is the increase of residual pore pressures of those saturated soils, there have been empirical attempts to relate pore pressure ratio, PPR, to these other easily measured factors. (Note: PPR is equal to the change in residual pore pressure divided by the initial effective stress; $\mathrm{PPR} = \frac{\Delta u_{res}}{\sigma'_0}$.) A study by Veyera (1985) produced the following equations through a multivariate regression analysis of the data:

$$PPR = 16.3\left(\varepsilon_{peak}\right)^{0.33}(\sigma'_0)^{-0.31}(D_r)^{-0.179} \quad (24)$$

$$PPR = 6.67\,(PPV)^{0.33}(\sigma'_0)^{-0.31}(D_r)^{-0.179} \quad (25)$$

Where, D_r is the relative density in percent, ε_{peak} is the peak strain in percent, the initial effective stress, σ'_0, is in kPa, and PPV is the peak particle velocity in m/s. This study was done with tests having effective stresses ranging from 86 to 690 kPa and relative densities from 20 to 80 percent (Charlie et al., 2013). Another study by Charlie et al. (1992) produced an empirical equation from tests done in dense sand and having an initial effective vertical stress of 38 kPa:

$$PPR = 3.90\,(SD)^{-1.41} = 1.02\,(PPV)^{0.72} \quad (26)$$

Where, SD is the cube-root scaled distance in m/kg, and PPV is the peak particle velocity in (m/s). In a study by Charlie et al. (2001), a 2.25 m high prototype dam made from poorly graded, subrounded to subangular sand was subject to single-detonation tests and resulted in a residual pore pressure equation as follows:

$$PPR = 4{,}025\,(SD)^{-2.08}(\sigma'_0)^{-1.56} \quad (27)$$

$$PPR = 520{,}000\,(PPV)^{3.01}\,(\sigma'_0)^{-1.56} \quad (28)$$

Where SD is the cube-root scaled distance in m/kg$^{1/3}$, σ'_0 is the initial effective stress in kPa, and PPV is the peak particle velocity in m/s. A couple of studies by Veyera (1985) and Veyera and Charlie's (1990) done with saturated Monterey No. 0/30 sand found the following empirical equations:

$$PPR = 16.00\left(\varepsilon_{peak}\right)^{0.33}\,(\sigma'_0)^{-0.31}\,(D_r)^{-0.18} \quad (29)$$

$$PPR = 16.00\left(\frac{100PPV}{V_c}\right)^{0.33}(\sigma'_0)^{-0.31}(D_r)^{-0.18} \quad (30)$$

Where ε_{peak} is the peak strain in percent, σ'_0 is the initial effective stress in kPa, D_r is the relative density in percent, PPV is the peak particle velocity in m/s, and V_c is the compressional wave velocity in m/s. A one-dimensional study done in saturated Poudre Valley sand by Hubert (1986) produced these empirical equations:

$$PPR = 10.59\left(\varepsilon_{peak}\right)^{0.43}(\sigma'_0)^{-0.17}(D_r)^{-0.18} \quad (31)$$

$$PPR = 10.59\left(\frac{100PPV}{V_c}\right)^{0.43}(\sigma'_0)^{-0.17}(D_r)^{-0.18} \quad (32)$$

A study done by Charlie et al. (2013) with angular, poorly graded, Poudre Valley sand where explosives were detonated suspended in water above the samples produced the following equations for residual pore pressures in loose, dense, and very dense sands respectively, Figure 14:

$$PPR = 30\,(SD)^{-1.6} \quad (33)$$

$$PPR = 51\,(SD)^{-1.7} \quad (34)$$

$$PPR = 60\,(SD)^{-1.9} \quad (35)$$

Where PPR is the residual excess pore pressure ratio and SD is the cube-root scaled distance of equivalent TNT in m/kg$^{1/3}$. The study by Charlie et al. (2013) also gave the following peak transient excess pore pressure equations in loose, dense, and very dense sands, respectively:

$$u_{peak} = 47{,}900\ (SD)^{-1.45} \quad (36)$$

$$u_{peak} = 47{,}400\ (SD)^{-1.45} \quad (37)$$

$$u_{peak} = 47{,}200\ (SD)^{-1.5} \quad (38)$$

Where u_{peak} is the peak transient excess pore pressure in kPa, and SD is the cube-root scaled distance of equivalent TNT in m/kg$^{1/3}$. A graphical summary of the existing peak transient excess pore pressure equations relating to scaled distance is depicted in Figure 15. The study by Charlie et al. (2013) also examined the relationship between PPV and PPR deriving the following equations for loose, dense, and very dense sand, respectively, Figure 16:

$$PPR = 2.6\ (PPV)^{1.3} \quad (39)$$

$$PPR = 2.2\ (PPV)^{1.2} \quad (40)$$

$$PPR = 1.4\ (PPV)^{1.0} \quad (41)$$

Where PPR is the residual pore pressure ratio, and PPV is the peak particle velocity in m/s. A significant observation from the study done by Charlie et al. (2013) was that the PPR in the very dense, dilative sand increased with decreasing scaled distance up to a liquefaction point (PPR = 1) and then decreased at a scaled distance of 2.8 m/kg$^{1/3}$ or less, at PPVs larger than 3 m/s, or at a peak strain of 0.2 % (Charlie et al., 2013); an observation not reported in other literature.

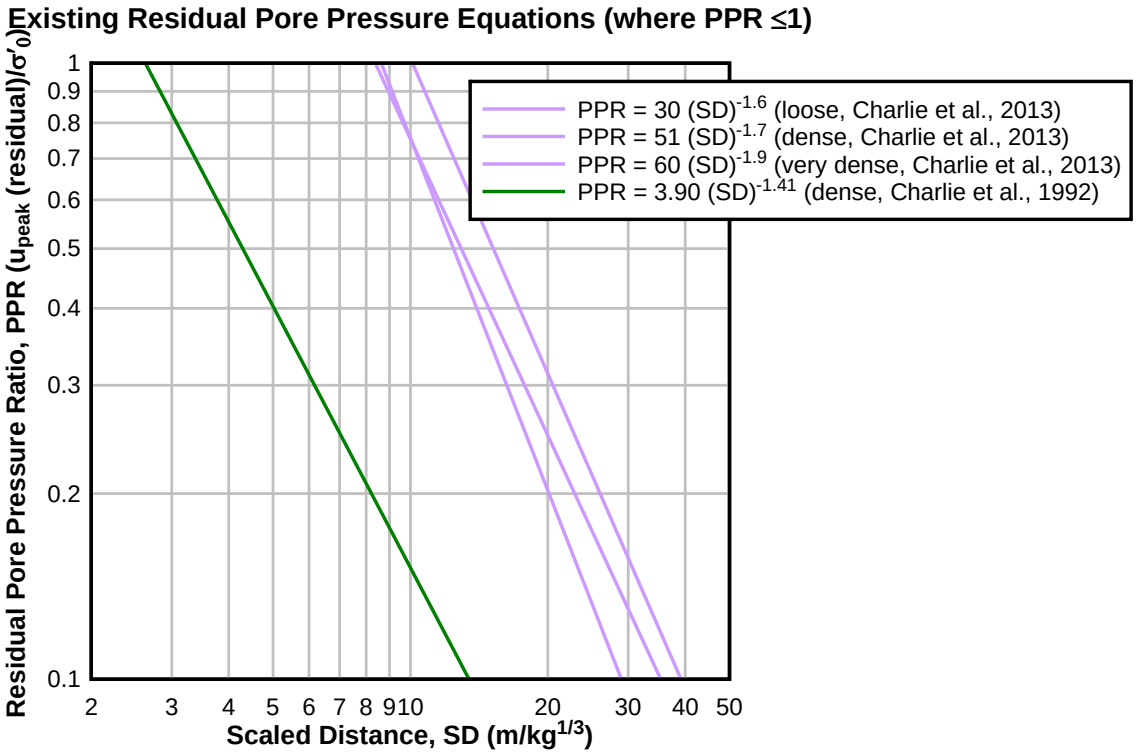

Figure 14: Existing empirical equations for PPR versus scaled distance in saturated sands

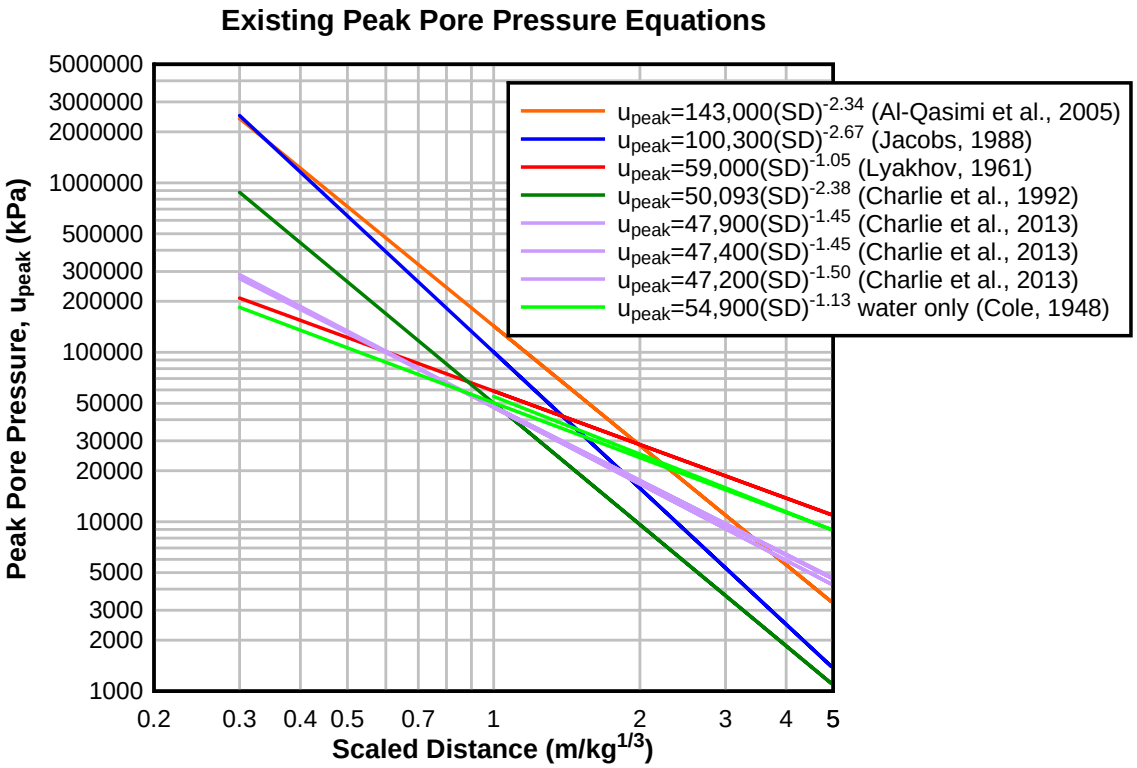

Figure 15: Existing empirical equations for peak transient excess pore pressure versus scaled distance

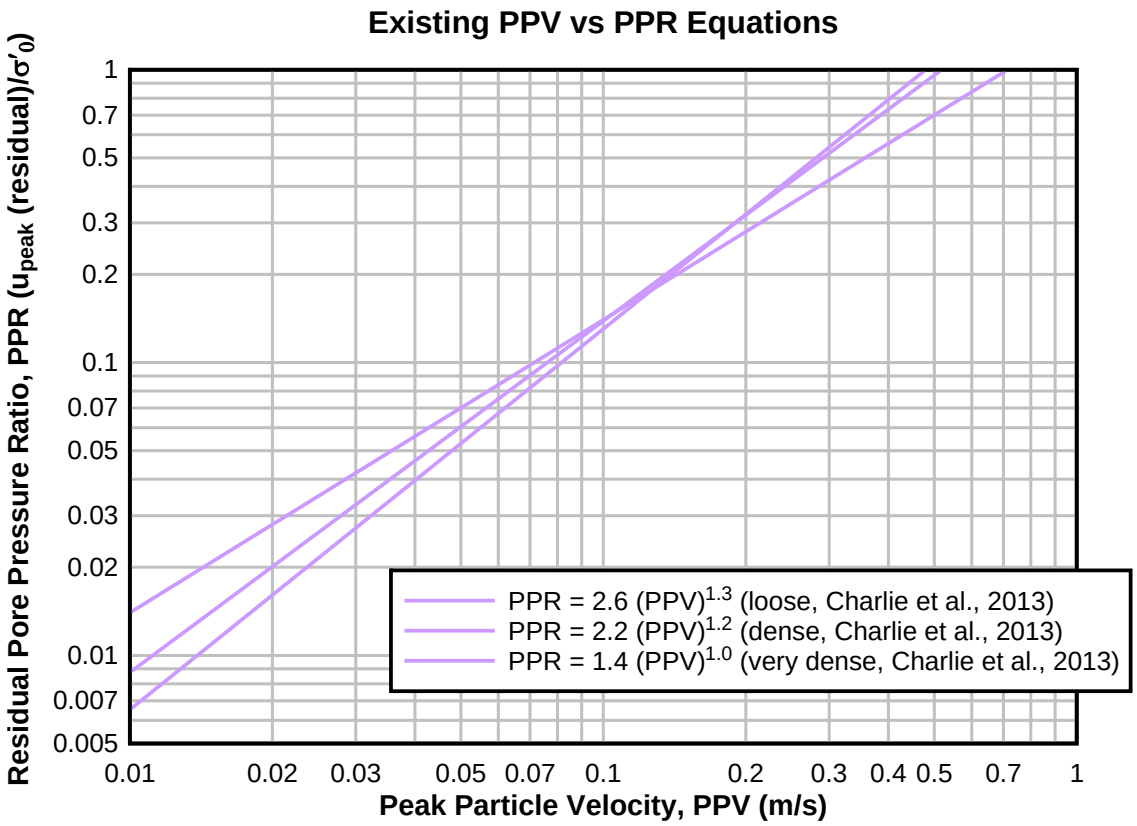

Figure 16: Existing empirical equations for PPR versus PPV for PPR <1

CHAPTER 4: EXPERIMENTAL METHODS

4.1 Experimental Setup

These tests were conducted at the University of Kentucky Explosives Research Team (UKERT) lab facility within the Nally & Gibson Georgetown, LLC limestone mine, within a Galfab gasketed tailgate open top container (2048F), Figure 17. The interior of the container measures 7 ft (2.1 m) wide, 20 ft (6.1 m) long, and 4 ft (1.2 m) deep with no internal obstructions. Prior to each blasting test, the sand material was compacted using a soil tamper to maintain consistent density between tests. A dry density and dry unit weight of the compacted sand were determined to be approximately 113.4 lb_m/ft^3 (1816 kg/m^3) and 0.1134 kip/ft^3 (17810 N/m^3), respectively, using the Standard Method for Density and Unit Weight of Soil in Place by the Sand-Cone Method (ASTM D1556).

The charges were set off from a depth of 18 inches (0.46 m) below the sand surface and 3.5 ft (1.1 m) from the end and sides of the tank. Standard geophones were set at 2.5 ft (0.76 m), 4.5 ft (1.4 m), and 14.5 ft (4.4 m) from the charge and buried 12 inches (0.30 m) below the sand surface. All instruments were centered 3.5 ft (1.1 m) from either side of the tank. Figures 18 and 19 show cross-sectional and plan view diagrams of the instrumentation and charge setup within the container. The closest seismograph, unit 1746, at 2.5 ft (0.76 m) from the charge was a NOMIS Mini-Graph® 7000. The middle seismograph, unit 5595, was a White Mini-Seis™, Figure 20. The furthest seismograph at 14.5 ft (4.4 m) from the charge was another NOMIS Mini-Graph® 7000. The seismographs were used in conjunction with a MREL DataTrap II for data recording. Seismograph

microphones were also placed 12 inches (0.30 m) above the sand at these locations.

Figure 17: Galfab gasketed tailgate open top container

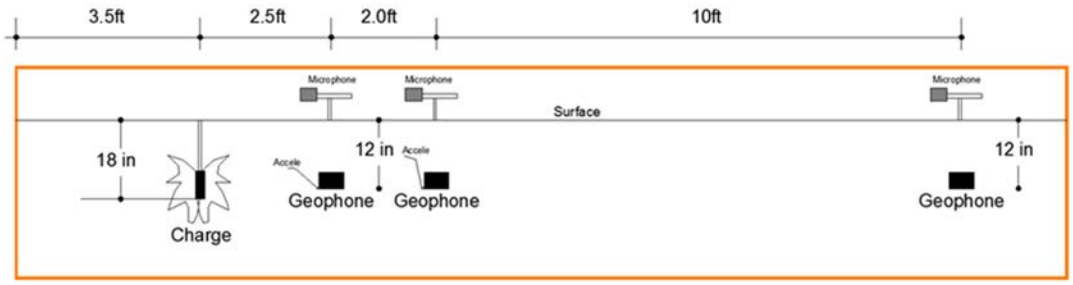

Figure 18: Cross sectional view of the container with instrumentation setup

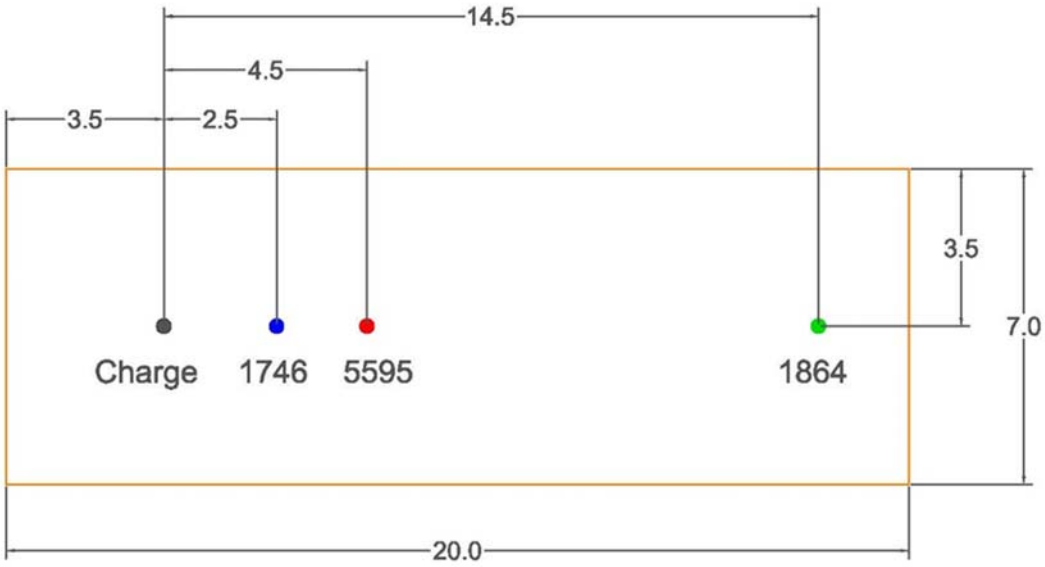

Figure 19: Plan view of the container with seismograph locations, distances in ft.

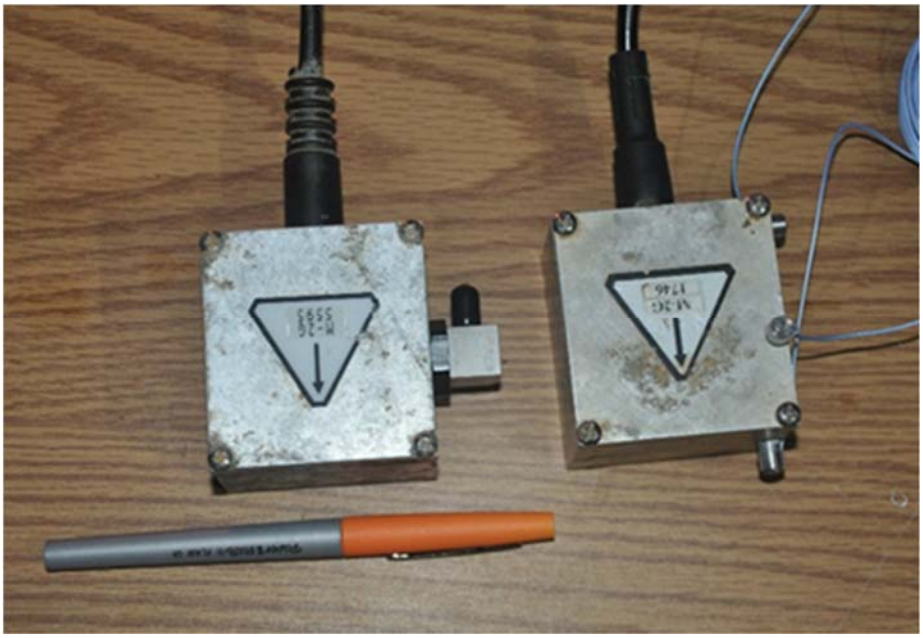

Figure 20: Seismographs 5595 (left) and 1749 (right)

To pursue the collection of pore pressure data, the sand tank was filled with water from the mine sump. To collect excess pore pressure data, several tests were

performed using strain gauge piezometers. It was found that conventional piezometer sampling rates are not frequent enough to record changes in pore pressure under dynamic conditions (typical sampling rates for conventional piezometers used in the attempts were between 10 to 100 samples per second). If it is considered that typical sampling rates between 1024 and 2048 samples per second are used to measure vibration from blasting, the conventional piezometers used in the first attempt were far from the adequate sampling rate. A study on typical piezometers with high sampling rates was performed without any success.

After abandoning the use of typical piezometers, tests were ran comparing the tourmaline pressure sensors and a piezoresistive strain gauge for airblasts. A PCB Piezoelectric airblast pressure sensor was modified with a metal shield casing and #230 mesh (Figure 21) (Sainato, 2016), much like factory retrofitting. However, waveform and pressures were not consistent with the other sensors in side by side tests, and the modified airblast pressure sensor was also abandoned.

Figure 21: Encased PCB piezoelectric airblast pressure sensor

Three tourmaline pressure sensors (PCB) W138A were acquired for this research; two having a maximum threshold of 1000 psi (6895 kPa) and a third having a maximum threshold of 50 psi (345 kPa). It was thought that using a tourmaline sensor directly in the saturated medium would produce values of total stress experienced by loading, since the effective membrane would be exposed to the sand particles and pore water. A casing of a steel, capped pipe with drilled holes on all sides covered in a fine wire mesh would allow the tourmaline sensor to measure pore pressures only, Figure 22. Side by side comparisons of the encased tourmaline results and those results collected from the uncased tourmaline proved the difference to be not statistically significant. Similarly, Veyera et al. (2002), Charlie et al. (2001), and Lyakhov (1961) state the peak transient increase in pore pressure is approximately equal to the peak total stress.

Figure 22: Uncased PCB tourmaline sensor (left) and cased PCB tourmaline sensor (right)

4.2 Material Tested

Prior to the blast tests, the geotechnical properties of the sand tank material were determined with lab tests. Grain size analysis was done according to ASTM D422 and ASTM D1140 and the material was classified using the Unified Soil Classification System resulting in a poorly-graded sand with 1.2% gravel, 97.7% sand, and 1.1% silt and clay, Figure 23. The moisture content of the material was assumed to be constant over the duration of the test series as the sand tank was housed underground. The initial moisture content of the “dry” sand was determined according to ASTM D2216 to be 3.87%. Direct Shear tests were run using a ShearTrac-II Direct Shear Apparatus by Geocomp, Figure 24, according to ASTM D3080 in both unsaturated and saturated conditions. Creating a Mohr-Coulomb failure envelope of these tests, and assuming a cohesionless material, the friction angle of the material unsaturated was determined to be 38.8°, Figure 25. The moisture content of the material during the unsaturated direct shear tests was 5.7%. The saturated tests resulted in a friction angle of 56.7°, assuming a cohesionless material, Figure 26. Although standard and modified Proctor tests (ASTM D698 and ASTM D1557) were done to determine an optimum water content, the results proved erroneous given the low amount of fines and the non-cohesiveness of the material.

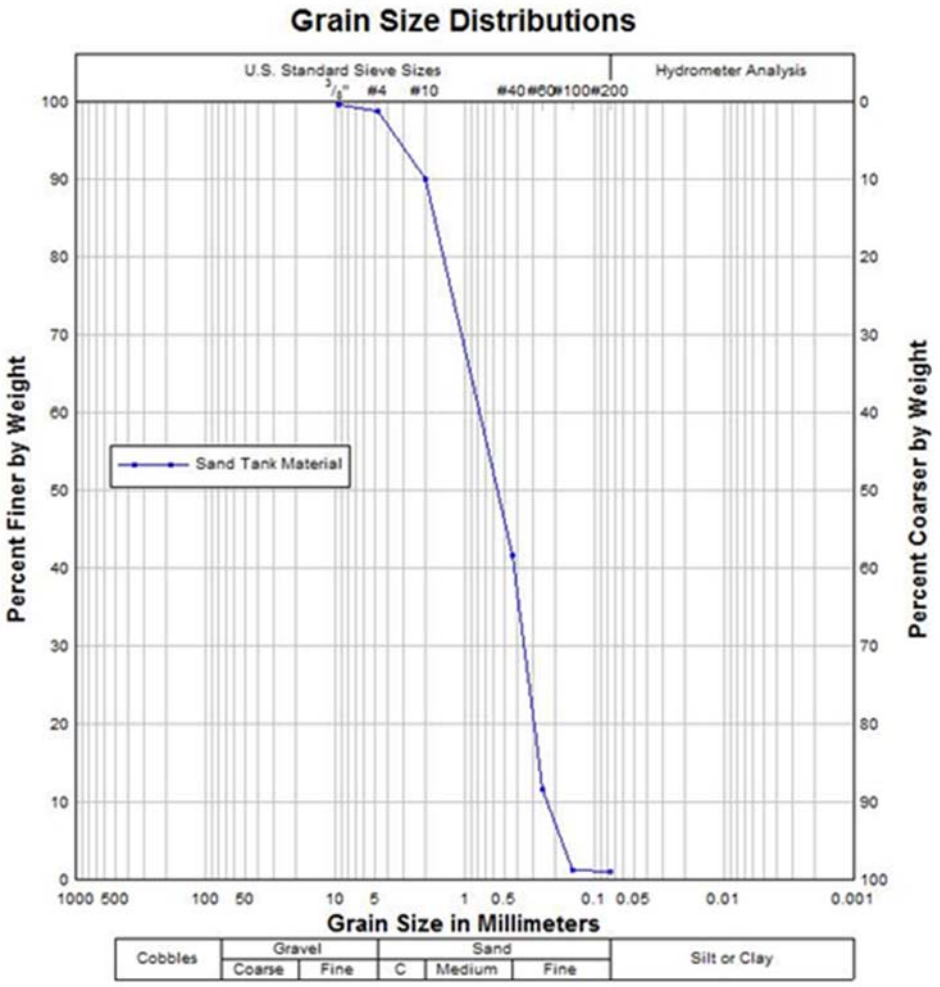

Figure 23: Results from the grain size distribution analysis

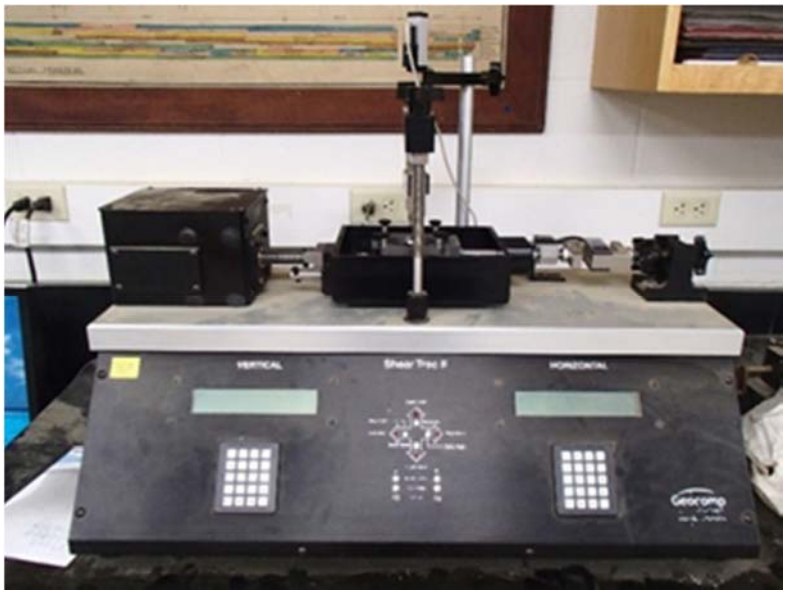

Figure 24: ShearTrac-II Direct Shear Apparatus by Geocomp

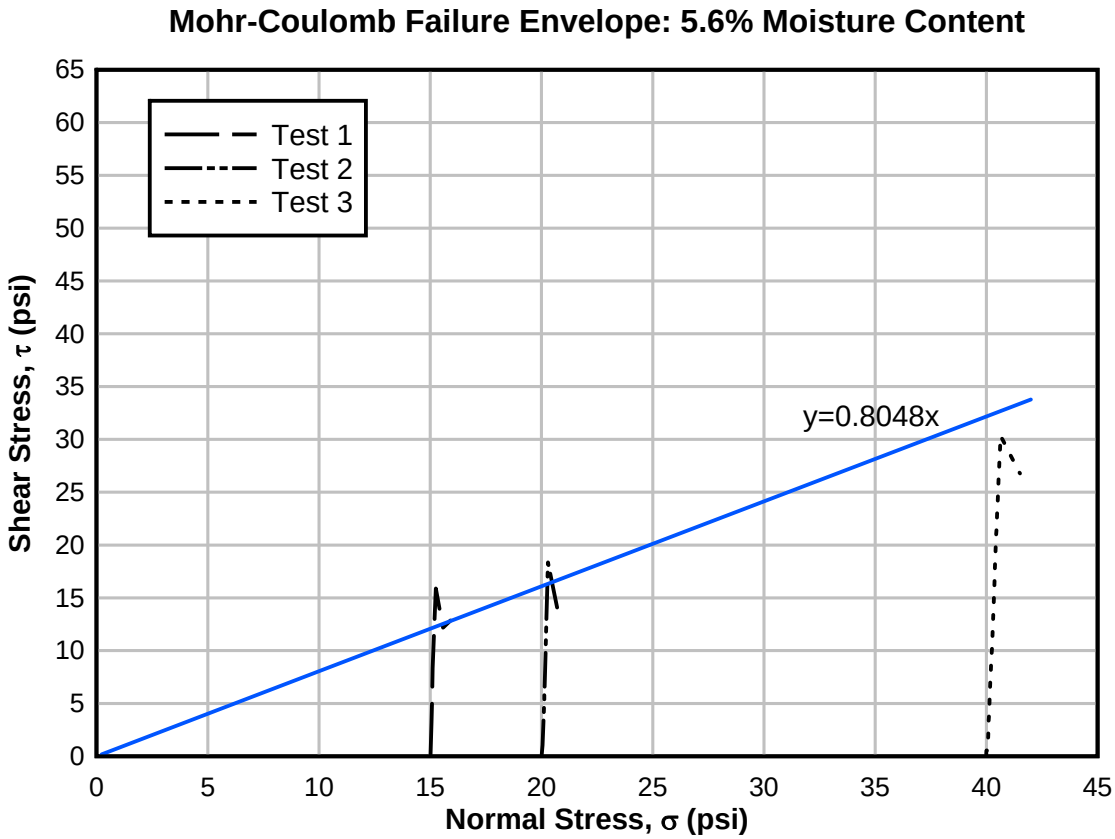

Figure 25: Mohr-Coulomb failure envelope of unsaturated sand

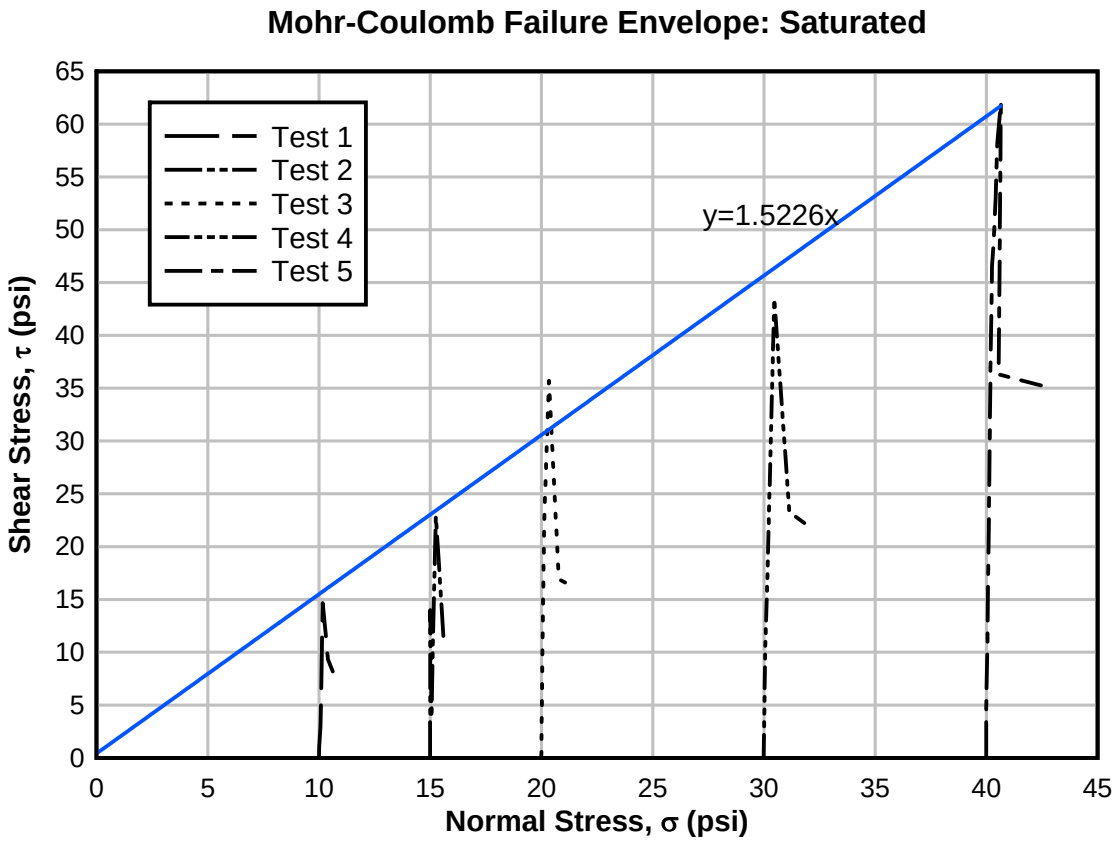

Figure 26: Mohr-Coulomb failure envelope of saturated sand

4.3 Explosive Charge

Tests used Austin DC 20g Cast Boosters, Diamond Nuggets, which are comprised of a combination of mainly Pentaerythritol tetranitrate (PETN) and Trinitrotoluene (TNT). These were chosen due to their high resistance to water and cylindrical detonation, Figure 27. These boosters were initiated using an electric detonator. Using multiple boosters with a single detonator to allow for a larger charge was experimented with, but ultimately proved unnecessary. Each test consisted of a single detonation and empirical relations do not consider the effects of a cyclic load

of multiple charge detonations. The cast boosters are composed mainly of pentaerythritol tetranitrite (PETN), which detonates at over 24,000 ft/s (7,380 m/s). The energy rating of PETN is 6,280 J/g which is equivalent to 150% of TNT (Charlie et al., 2013). Equations and analysis were done using TNT-equivalency, as is common practice.

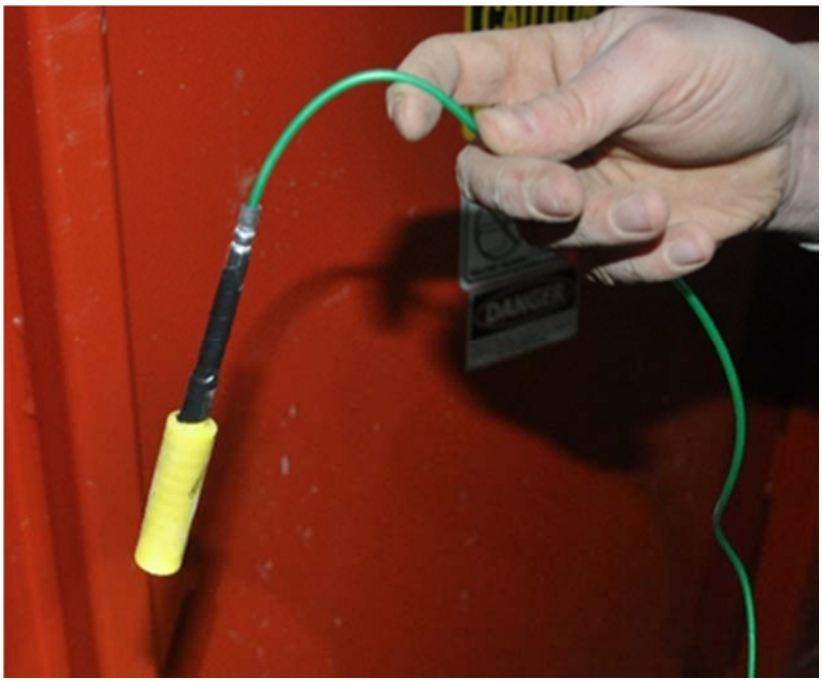

Figure 27: Austin DC 20g Diamond Nugget Cast Booster

All charges were detonated at a depth of 18 inches (0.46 m). According to Charlie et al. (2013) detonations are fully contained at scaled depths of at least 0.55 m/kg$^{1/3}$ of TNT-equivalent mass. With a raw mass of 20 g (30 g TNT-equivalent mass) this is equivalent to a depth of approximately 0.17 m, or 6.7 inches. Thus a depth of 18 inches (0.46 m) is sufficiently large to consider these tests fully contained. For dry conditions the charge was buried in the sand by driving a hollow steel pipe into the sand and removing it to produce a “drill hole”. The charge was lowered

into the hole and sand was poured and tamped into the hole to couple the charge to the surround material.

One challenge faced in the study under saturated conditions was getting a consistent blast. Due to saturation a “drill hole” would not remain open long enough to place a charge at a great enough depth. Digging a pit deep enough to bury a charge required a greater width resulting in the overlying material to be less dense and thus most energy was released vertically rather than laterally. A first attempt to solve this issue, and the setup used in the saturated tests of the seismographs, was to drive a capped ¾ inch (1.9 cm) wide 14 inch (0.36 m) long PVC pipe into the sand within a small hole, Figure 28. The charge was then placed at the bottom of the PVC pipe and stemmed properly with sand. The PVP pipe was then capped with the charge thread through. The PVC pipe was then buried the additional 4 inches that remained to equal a depth of 18 inches (0.46 m). This allowed the surrounding sand to remain compacted resulting in a more lateral energy transfer. A simpler solution was utilized in the tests collecting the pore pressure data from the tourmalines. For these tests the charge was buried in the sand by driving a narrow, square, wooden rod with the booster taped to the end with a mallet to the desired depth of 18 inches (0.46 m), Figure 29.

Figure 28: PVC pipe solution for charge burial in saturated conditions.

Figure 29: Test setup with wooden rods for charge burial and sensor measurements featuring Dr. Braden Lusk.

4.4 Experimental Results

4.4.1 Unsaturated Conditions

All data was analyzed using DPlot software. All equations relating PPV, PPR and other variables were derived in this program using the least squares curve fit to the data sets. Prior to testing saturated conditions in the container, the test setup was defined and run in unsaturated conditions for comparison. Figures 30, 31, and 32 show the typical particle velocity vs. time waveforms obtained from the geophones in the radially, vertically, and transverse components at close, mid, and far scaled distances, respectively in unsaturated conditions. All test waveforms and tables of raw test data and calculations for unsaturated tests can be found in Appendix A.

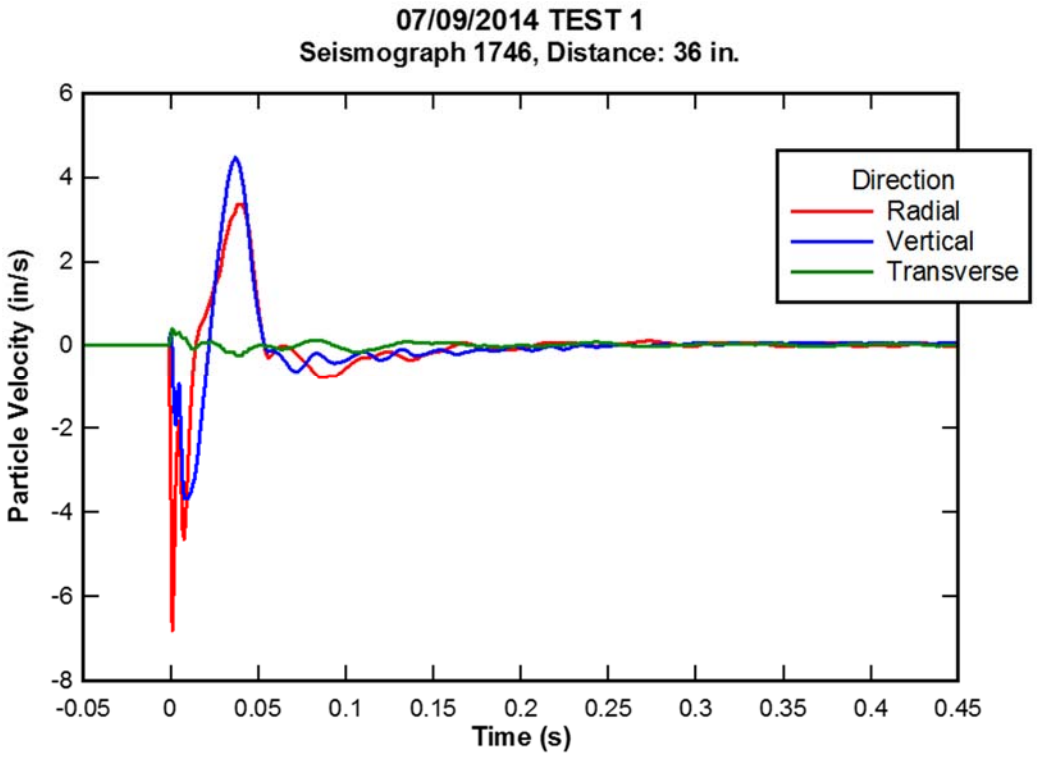

Figure 30: Typical waveform for particle velocity in unsaturated conditions at close scaled distances

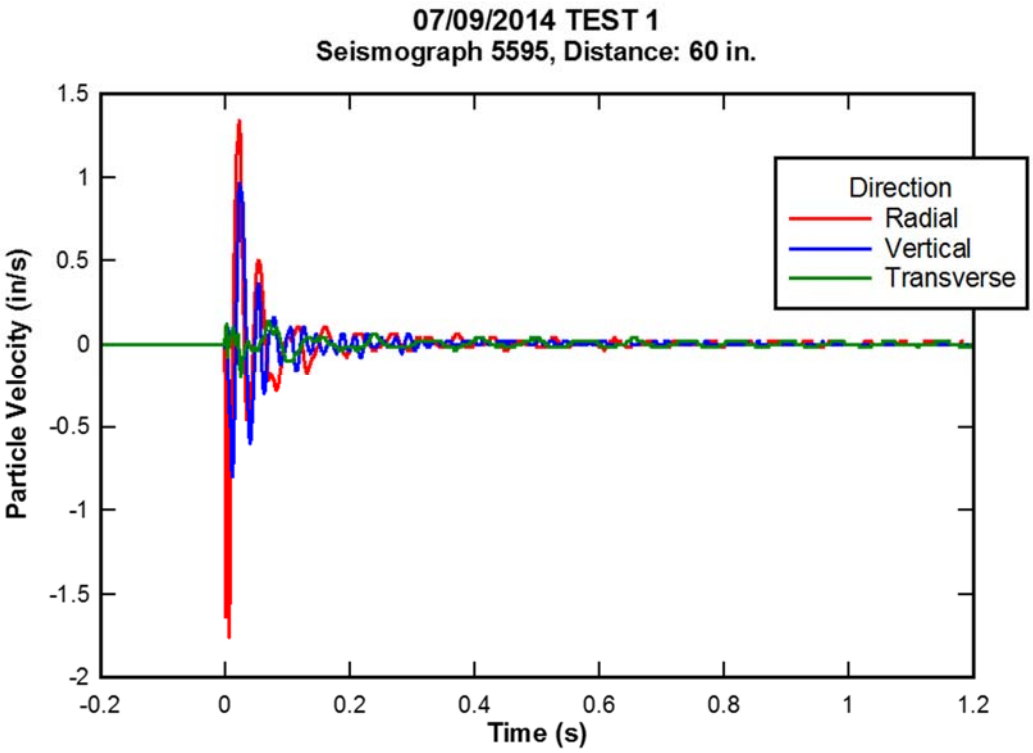

Figure 31: Typical waveform for particle velocity in unsaturated conditions at mid scaled distances

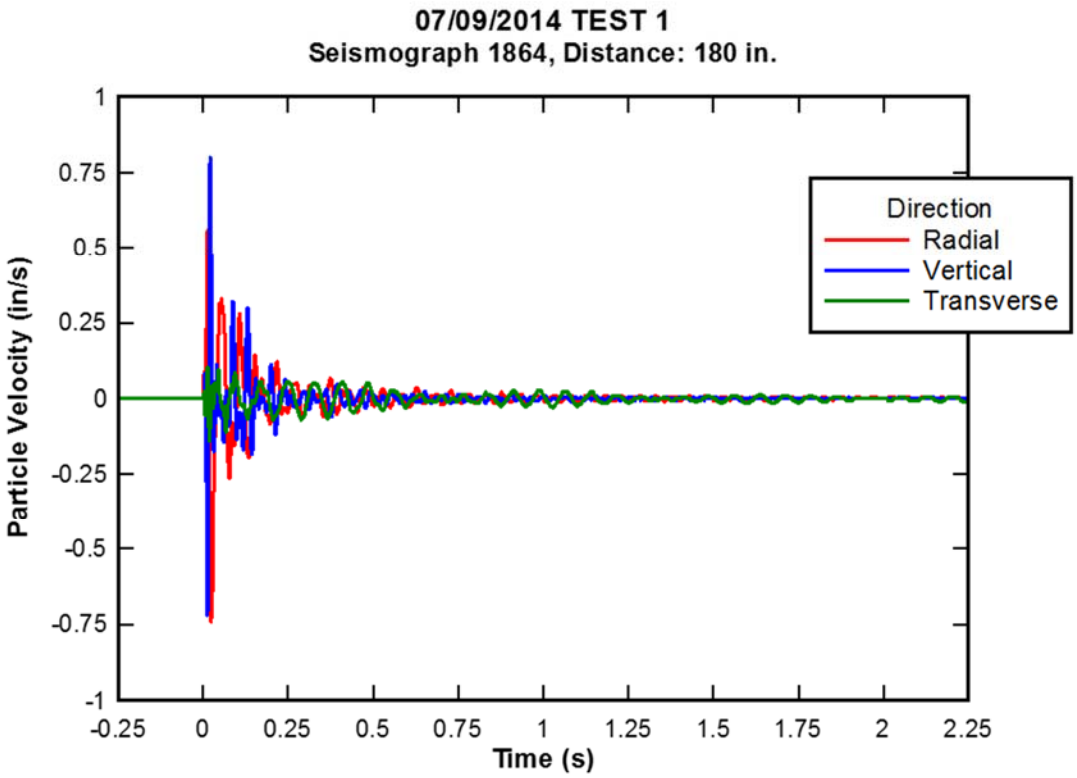

Figure 32: Typical waveform for particle velocity in unsaturated conditions at far scaled distances

To calculate scaled distances, the cube root scaling method using TNT-equivalency mass was chosen, as the model simulates a point charge buried at depth. Due to the controlled conditions of the setup, it is possible to assess the equation of peak particle velocity vs scaled distance for dry conditions in the radial, vertical and transverse components, respectively as:

$$PPV_{radial} = 98.6\,(SD)^{-1.48}\ in/s = 121.3\,(SD)^{-1.49}\ m/s \qquad (42)$$

$$PPV_{vertical} = 40.1\,(SD)^{-1.22}\ in/s = 67.1\,(SD)^{-1.21}\ m/s \qquad (43)$$

$$PPV_{transverse} = 3.6\,(SD)^{-0.94}\ in/s = 8.3\,(SD)^{-0.96}\ m/s \qquad (44)$$

These equations and the seismograph data points are graphically represented in the peak particle velocity versus scaled distance graph, Figures 33 and 34.

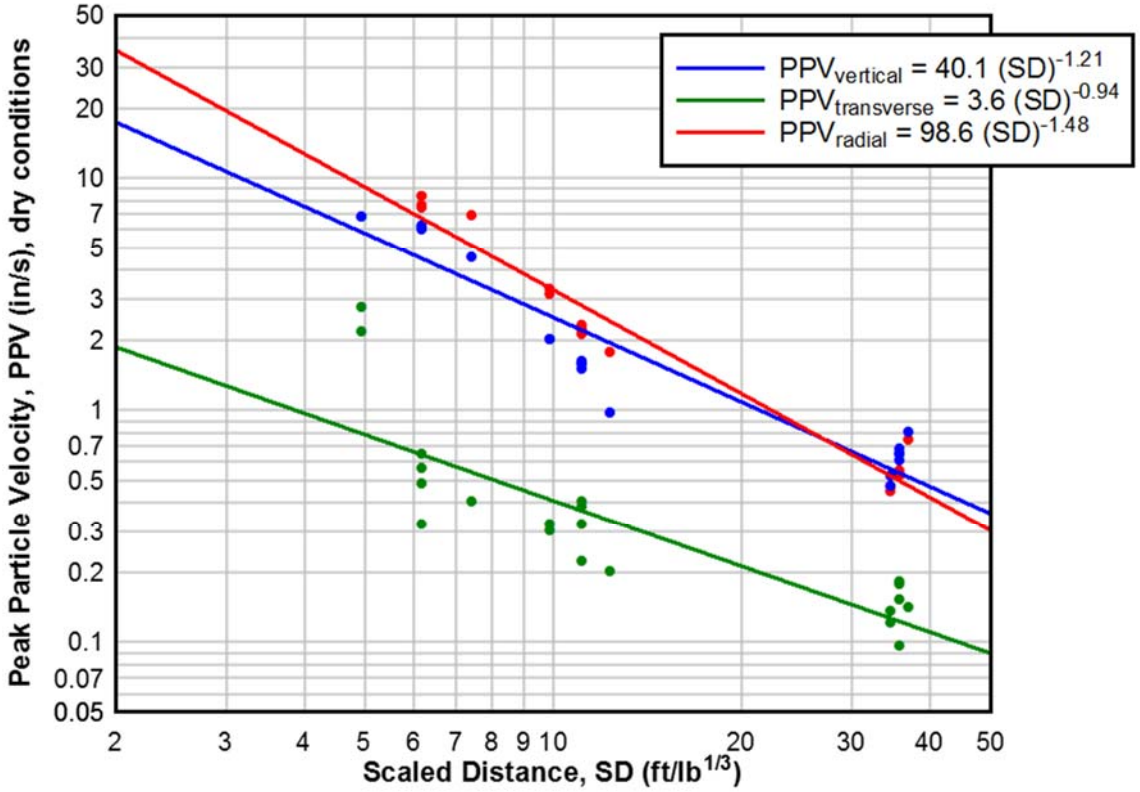

Figure 33: PPV versus scaled distance graph of unsaturated conditions in imperial units

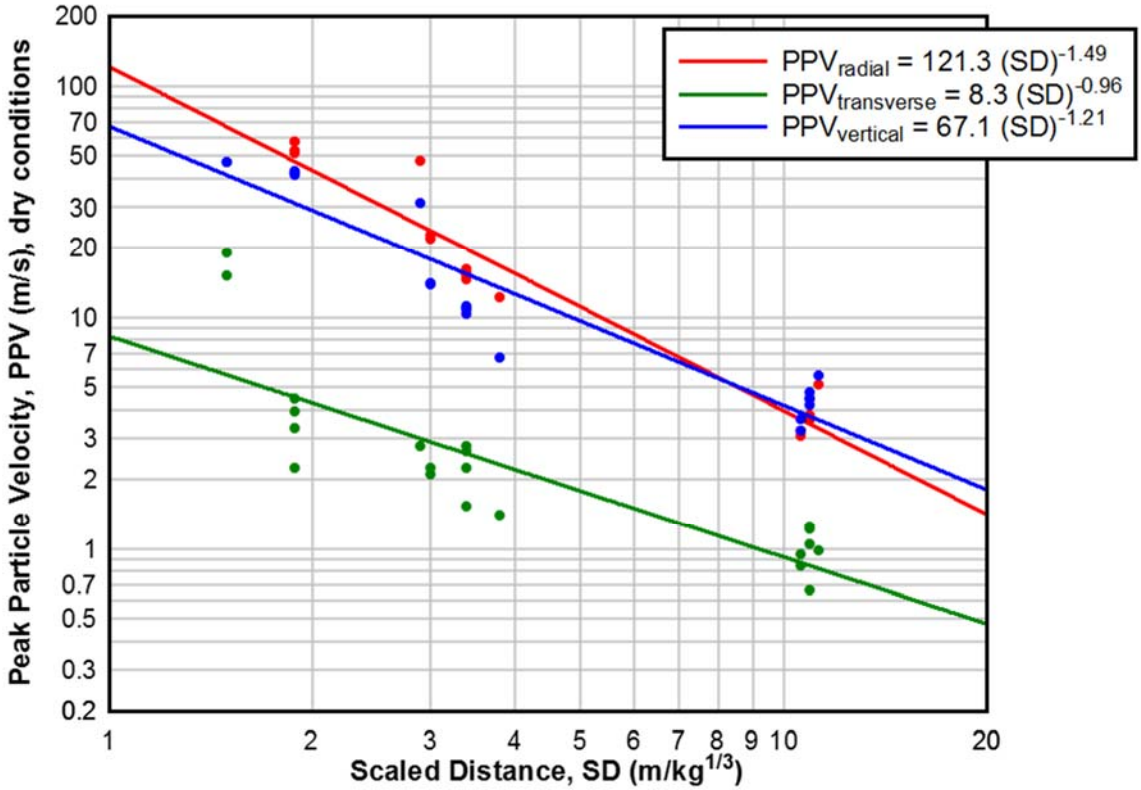

Figure 34: PPV versus scaled distance graph of unsaturated conditions in metric units

4.4.2 Saturated Conditions

Upon completion of the unsaturated tests, the container was filled up to a water level of 6 inches from the top of the leveled sand. A standing slotted pvc pipe was put into one end of the container to visualize the water table. Prior to conducting tests, the container was allowed several days to de-air and settle after filling. The seismograph tests done in the unsaturated conditions were then duplicated. Figures 35, 36, and 37 show the typical particle velocity vs. time waveforms obtained from the geophones in the radially, vertically, and transverse components at close, mid, and far scaled distances, respectively in saturated conditions. All test

waveforms and tables of raw test data and calculations for saturated tests can be found in Appendix B.

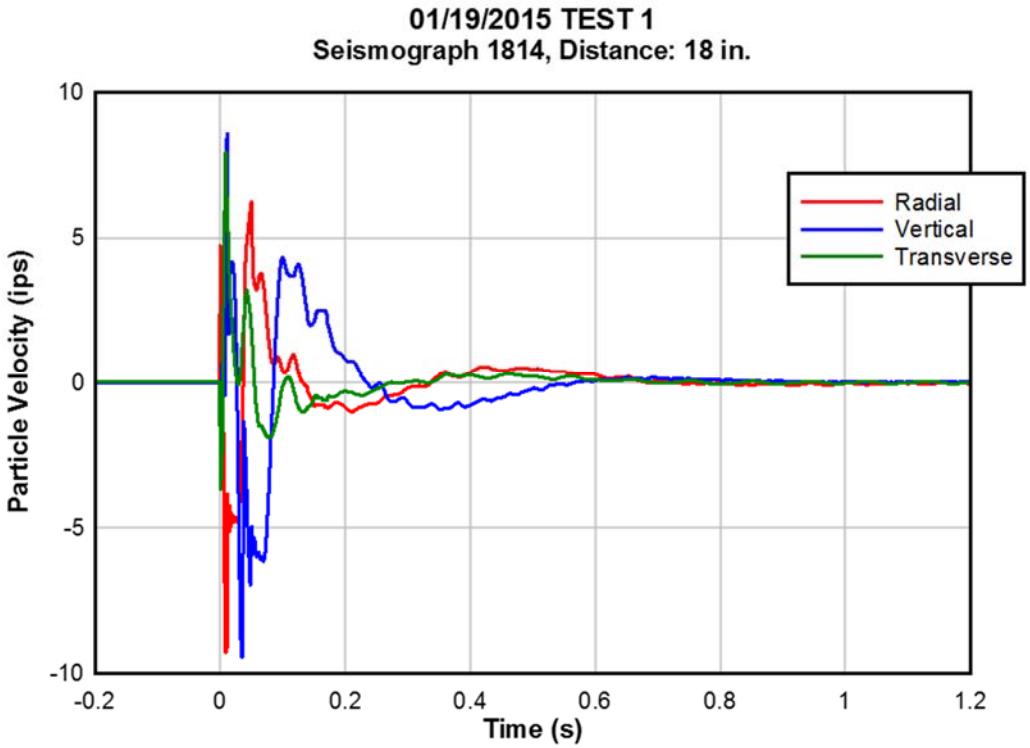

Figure 35: Typical waveform for particle velocity in saturated conditions at close scaled distances

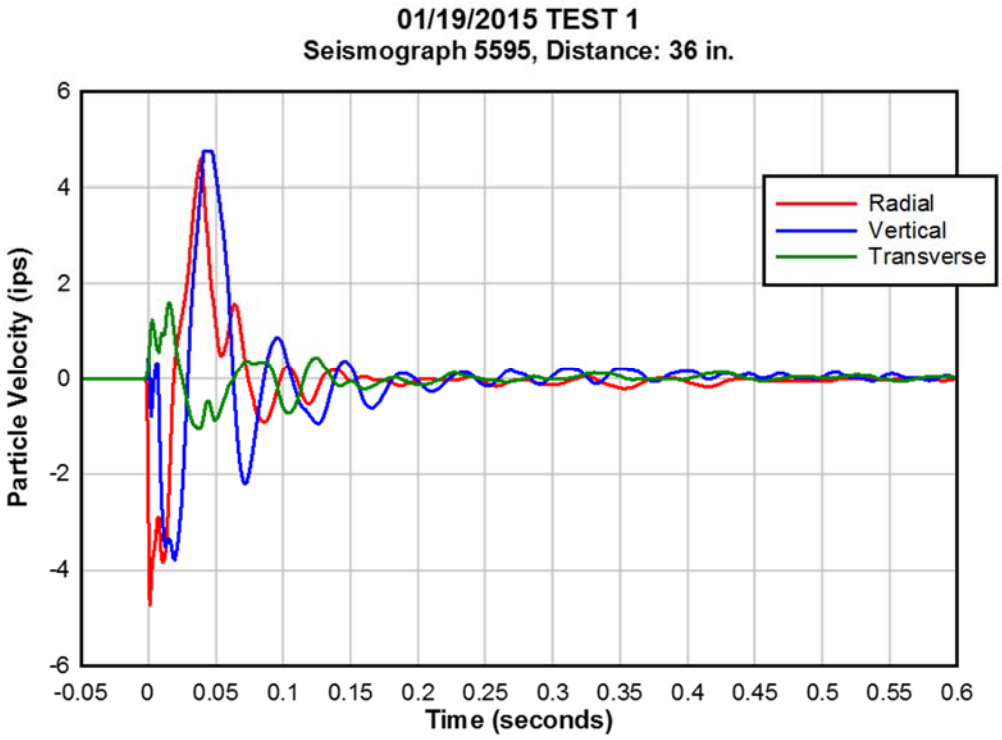

Figure 36: Typical waveform for particle velocity in saturated conditions at mid scaled distances

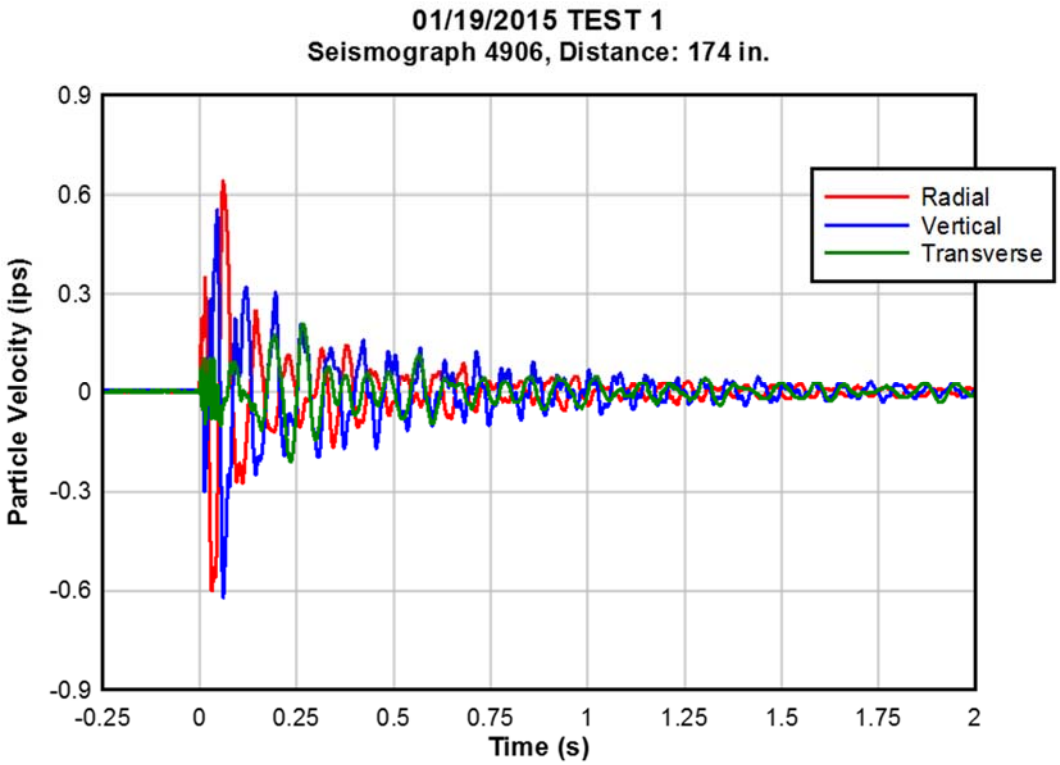

Figure 37: Typical waveform for particle velocity in saturated conditions at far scaled distances

To calculate scaled distances, the cube root scaling method using TNT-equivalency mass was chosen, as the model simulates a point charge buried at depth. Due to the controlled conditions of the setup, it is possible to assess the equation of peak particle velocity vs scaled distance for the saturated conditions in the radial, vertical and transverse components, respectively as:

$$PPV_{radial} = 35.1\ (SD)^{-1.00} in/s = 96.6\ (SD)^{-1.12}\ m/s \quad (45)$$

$$PPV_{vertical} = 31.8\ (SD)^{-1.00} in/s = 83.6\ (SD)^{-1.10}\ m/s \quad (46)$$

$$PPV_{transverse} = 23.3\ (SD)^{-1.13} in/s = 46.3\ (SD)^{-1.17}\ m/s \quad (47)$$

These equations and the seismograph data points are graphically represented in the peak particle velocity versus scaled distance graph, Figures 38 and 39.

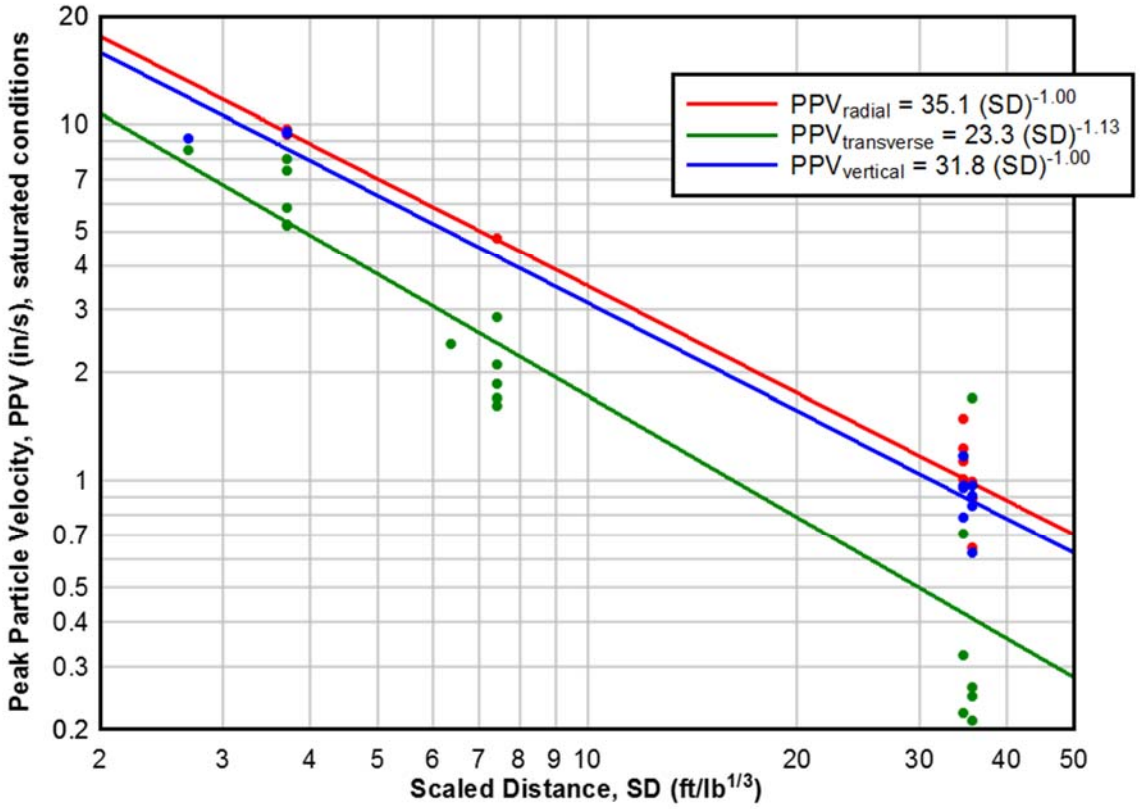

Figure 38: PPV versus scaled distance graph of saturated conditions in imperial units

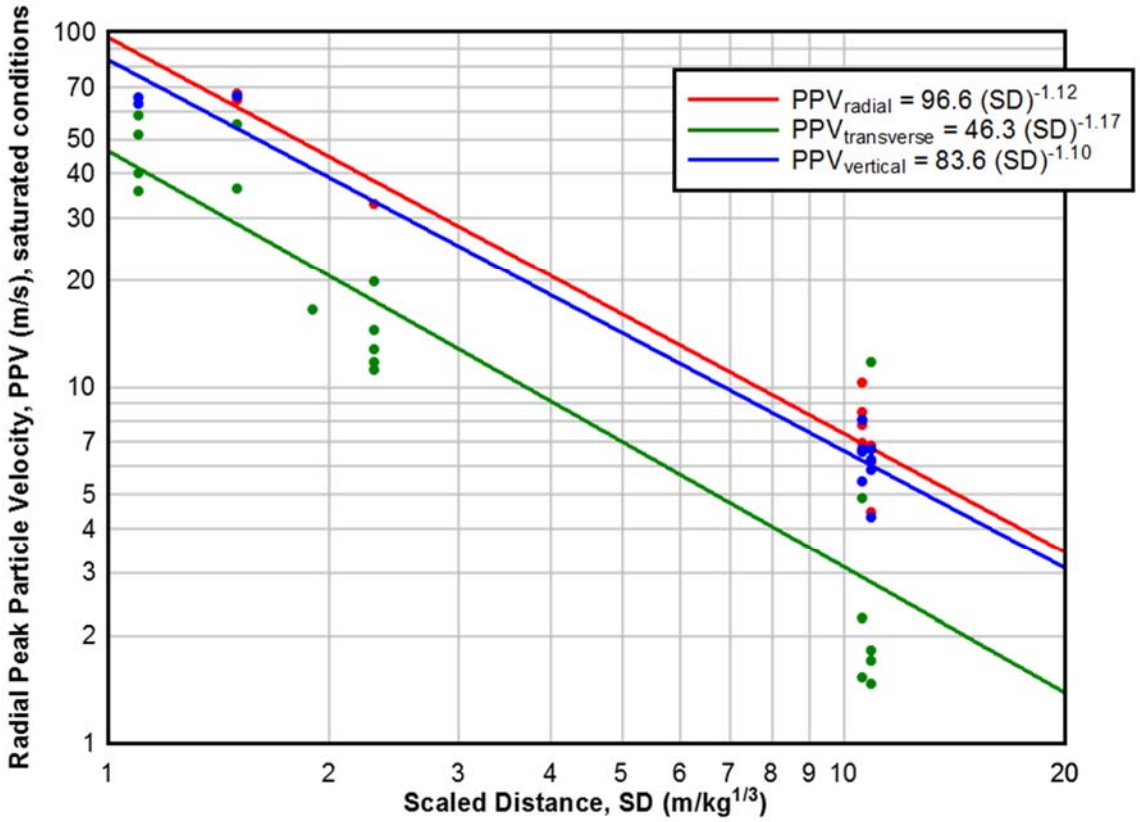

Figure 39: PPV versus scaled distance graph of saturated conditions in metric units

When comparing the PPV radial components in saturated versus dry conditions the PPV in the dry condition is more critical for ground vibrations close to the source (values lower than a SD < 9 ft/lb$^{1/3}$). At scaled distances greater than 9 ft/lb$^{1/3}$, this behavior inverts, Figure 40. The ground motion advances to further scaled distances in saturated soil rather than in dry soil.

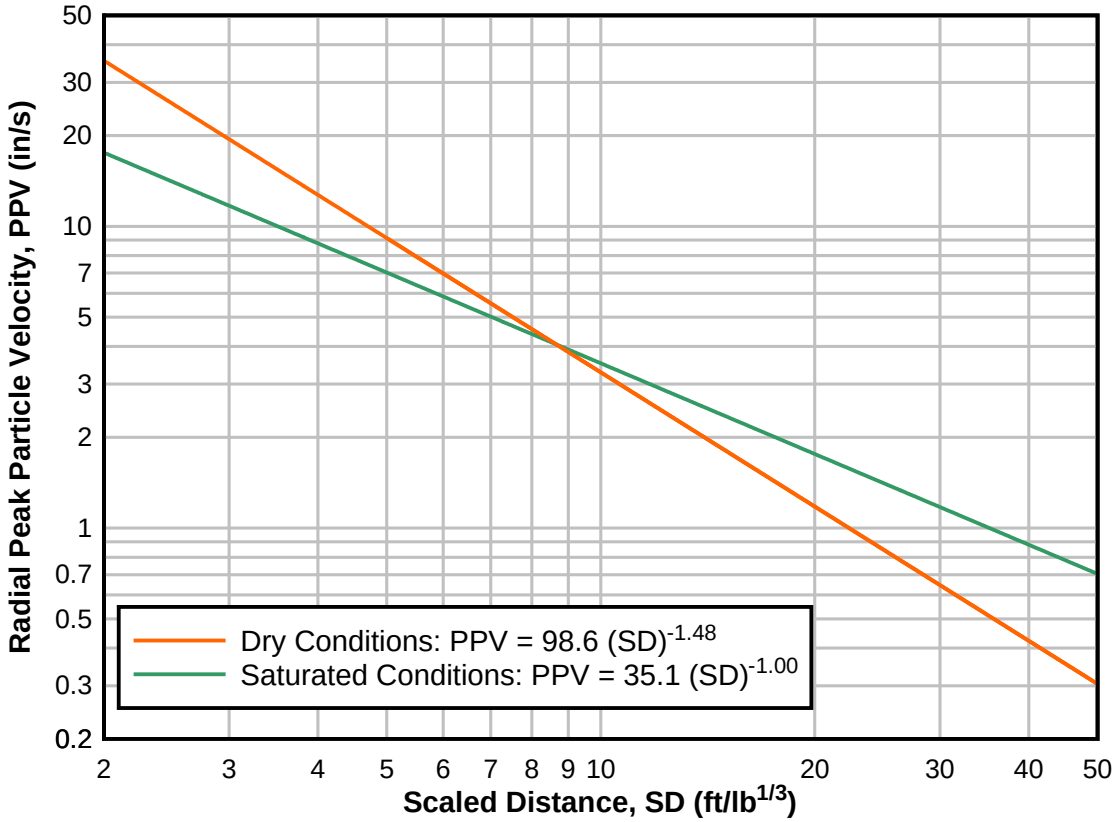

Figure 40: Comparison of radial PPV in saturated and unsaturated conditions

4.4.3 Tourmaline Results

The tourmaline pressure sensors proved to be difficult instruments requiring much involvement with the manufacturers and department faculty. After several tests utilizing the tourmaline pressure sensors to gather data, it was determined that the data being collected was not the desired pore pressure, but rather the total compressive stress due to the contact between the sensor's pressure membrane and the sand matrix and pore water. At this point, it was necessary to encase the tourmaline sensor to isolate it from the matrix but have it remain susceptible to

water conditions in order to get the desired pore pressure data. This was solved by dilling holes all around a capped, steel pipe and covering with a fine wire mesh; another hole was drilled in the top to input the tourmaline sensor. Table 4 shows the peak compressive stress data aquired from the uncased tourmalines and the calculated scaled distances for each saturated test used to create the peak compressive stress versus scaled distance graph, Figure 41 and 42. Again, the cube root scaling method was chosen using TNT-equivalent mass. The uncased data points resulted in a peak compressive stress equation of:

$$\sigma_{peak} = 3690\ (SD)^{-3.42}\ psi = 511.7\ (SD)^{-3.57}\ kPa \qquad (48)$$

Table 4: Peak compressive stress data collected with uncased tourmaline sensors

PEAK COMPRESSIVE STRESS, σpeak														
Date	Test	Tourmaline No.	Charge (g)	Charge (kg)	Charge (lb)	TNT Equivalency (kg)	TNT Equivalency (lb)	Distance to charge (in)	Distance to charge (ft)	Distance to charge (m)	TNT Eq. SD (m/kg^⅓)	TNT Eq. SD (ft/lb^⅓)	Peak stress (psi)	Peak stress (kPa)
1/19/2015	1	7259	20	0.020	0.044	0.030	0.066	18	1.5	0.46	1.47	3.71	29.87	205.94
1/19/2015	1	10205	20	0.020	0.044	0.030	0.066	36	3.0	0.91	2.26	7.42	4.42	30.49
1/19/2015	2	7259	20	0.020	0.044	0.030	0.066	18	1.5	0.46	1.13	3.71	52.86	364.45
1/19/2015	2	10205	20	0.020	0.044	0.030	0.066	36	3.0	0.91	2.26	7.42	5.50	37.96
1/19/2015	3	7259	20	0.020	0.044	0.030	0.066	18	1.5	0.46	1.13	3.71	47.44	327.10
1/19/2015	3	10205	20	0.020	0.044	0.030	0.066	36	3.0	0.91	2.26	7.42	5.15	35.53
1/19/2015	4	7259	20	0.020	0.044	0.030	0.066	18	1.5	0.46	1.13	3.71	59.02	406.91
1/19/2015	4	10205	20	0.020	0.044	0.030	0.066	36	3.0	0.91	2.26	7.42	4.26	29.37
1/19/2015	5	7259	20	0.020	0.044	0.030	0.066	18	1.5	0.46	1.13	3.71	61.10	421.29
1/19/2015	5	10205	20	0.020	0.044	0.030	0.066	36	3.0	0.91	2.26	7.42	4.95	34.16
1/22/2015	1	7259	20	0.020	0.044	0.030	0.066	13	1.1	0.33	1.06	2.68	133.06	917.41
1/22/2015	1	10205	20	0.020	0.044	0.030	0.066	31	2.6	0.79	1.95	6.39	5.89	40.60
1/22/2015	2	7259	20	0.020	0.044	0.030	0.066	13	1.1	0.33	0.82	2.68	141.30	974.26
1/22/2015	2	10205	20	0.020	0.044	0.030	0.066	31	2.6	0.79	1.95	6.39	7.05	48.62
1/22/2015	3	7259	20	0.020	0.044	0.030	0.066	13	1.1	0.33	0.82	2.68	135.89	936.91
1/22/2015	3	10205	20	0.020	0.044	0.030	0.066	31	2.6	0.79	1.95	6.39	8.81	60.73
1/22/2015	4	7259	20	0.020	0.044	0.030	0.066	13	1.1	0.33	0.82	2.68	119.78	825.85
1/22/2015	4	10205	20	0.020	0.044	0.030	0.066	31	2.6	0.79	1.95	6.39	NO DATA	NO DATA
6/26/2015	1	7259	20	0.020	0.044	0.030	0.066	28	2.3	0.71	1.76	5.77	7.68	52.99
6/26/2015	1	29169	20	0.020	0.044	0.030	0.066	28	2.3	0.71	1.76	5.77	5.42	37.35
6/26/2015	1	10226	20	0.020	0.044	0.030	0.066	28	2.3	0.71	2.29	5.77	NO DATA	NO DATA
6/26/2015	2	7259	20	0.020	0.044	0.030	0.066	28	2.3	0.71	1.76	5.77	7.21	49.70
6/26/2015	2	29169	20	0.020	0.044	0.030	0.066	28	2.3	0.71	1.76	5.77	7.98	55.01
6/26/2015	2	10226	20	0.020	0.044	0.030	0.066	28	2.3	0.71	1.76	5.77	7.50	51.73
6/26/2015	3	7259	20	0.020	0.044	0.030	0.066	28	2.3	0.71	1.76	5.77	7.55	52.07
6/26/2015	3	29169	20	0.020	0.044	0.030	0.066	28	2.3	0.71	1.76	5.77	9.22	63.59
6/26/2015	3	10226	20	0.020	0.044	0.030	0.066	28	2.3	0.71	1.76	5.77	8.12	56.02
8/13/2015	1	7259	20	0.020	0.044	0.030	0.066	20.25	1.7	0.51	1.27	4.17	16.61	114.52
8/13/2015	2	7259	20	0.020	0.044	0.030	0.066	31.25	2.6	0.79	1.96	6.44	5.91	40.76
8/13/2015	3	7259	20	0.020	0.044	0.030	0.066	43	3.6	1.09	2.70	8.86	NO DATA	NO DATA

Table 5 shows the peak transient pore pressure data aquired from the cased tourmalines and the calculated scaled distances for each saturated test used to

create the peak transient pore pressure versus scaled distance graph, Figure 41 and 42. Again, the cube root scaling method was chosen using TNT-equivalent mass. The cased data points resulted in a peak transient pore pressure equation of:

$$u_{peak} = 5224\ (SD)^{-3.76}\ psi = 405.5\ (SD)^{-3.70}\ kPa \qquad (49)$$

Table 5: Peak transient pore pressure data collected with cased tourmaline sensors

PEAK TRANSIENT PORE PRESSURE, upeak														
Date	Test	Tourmaline No.	Charge (g)	Charge (kg)	Charge (lb)	TNT Equivalency (kg)	TNT Equivalency (lb)	Distance to charge (in)	Distance to charge (ft)	Distance to charge (m)	TNT Eq. SD (m/kg^⅓)	TNT Eq. SD (ft/lb^⅓)	Peak transient pore pressure (psi)	Peak transient pore pressure (kPa)
8/13/2015	1	10226	20	0.020	0.044	0.030	0.066	21	1.8	0.53	1.32	4.33	10.35	71.34
8/13/2015	1	29169	20	0.020	0.044	0.030	0.066	19.5	1.6	0.50	1.59	4.02	21.03	144.99
8/13/2015	2	10226	20	0.020	0.044	0.030	0.066	32	2.7	0.81	2.01	6.59	2.19	15.07
8/13/2015	2	29169	20	0.020	0.044	0.030	0.066	30.5	2.5	0.77	1.92	6.28	4.62	31.87
8/13/2015	3	10226	20	0.020	0.044	0.030	0.066	44	3.7	1.12	2.76	9.07	NO DATA	NO DATA
8/13/2015	3	29169	20	0.020	0.044	0.030	0.066	42.5	3.5	1.08	2.67	8.76	NO DATA	NO DATA
3/15/2016	1	7259	20	0.020	0.044	0.030	0.066	25	2.1	0.64	1.57	5.15	7.68	52.99
3/15/2016	1	10226	20	0.020	0.044	0.030	0.066	30.75	2.6	0.78	1.93	6.34	7.08	48.82
3/15/2016	2	7259	20	0.020	0.044	0.030	0.066	16.5	1.4	0.42	1.04	3.40	103.93	716.56
3/15/2016	2	10226	20	0.020	0.044	0.030	0.066	22.5	1.9	0.57	1.41	4.64	21.26	146.61
3/15/2016	3	7259	20	0.020	0.044	0.030	0.066	18	1.5	0.46	1.13	3.71	96.43	664.89
3/15/2016	3	10226	20	0.020	0.044	0.030	0.066	24	2.0	0.61	1.51	4.95	18.19	125.45
3/15/2016	4	7259	20	0.020	0.044	0.030	0.066	24.5	2.0	0.62	1.54	5.05	8.87	61.14
3/15/2016	4	10226	20	0.020	0.044	0.030	0.066	30.25	2.5	0.77	1.90	6.23	5.86	40.39
3/15/2016	6	7259	20	0.020	0.044	0.030	0.066	20.25	1.7	0.51	1.27	4.17	68.84	474.64
3/15/2016	6	10226	20	0.020	0.044	0.030	0.066	26	2.2	0.66	1.63	5.36	13.86	95.57
3/15/2016	7	7259	20	0.020	0.044	0.030	0.066	14.75	1.2	0.37	0.93	3.04	106.27	732.73
3/15/2016	7	10226	20	0.020	0.044	0.030	0.066	20.5	1.7	0.52	1.29	4.22	28.91	199.30
3/15/2016	8	7259	20	0.020	0.044	0.030	0.066	12	1.0	0.30	0.75	2.47	225.08	1551.85
3/15/2016	8	10226	20	0.020	0.044	0.030	0.066	18	1.5	0.46	1.13	3.71	55.91	385.47
3/15/2016	9	7259	20	0.020	0.044	0.030	0.066	10.25	0.9	0.26	0.64	2.11	336.52	2320.21
3/15/2016	9	10226	20	0.020	0.044	0.030	0.066	16	1.3	0.41	1.00	3.30	94.86	654.07
3/15/2016	10	7259	20	0.020	0.044	0.030	0.066	8.5	0.7	0.22	0.53	1.75	509.00	3509.44
3/15/2016	10	10226	20	0.020	0.044	0.030	0.066	14.5	1.2	0.37	0.91	2.99	135.07	931.24
3/15/2016	11	7259	20	0.020	0.044	0.030	0.066	10.125	0.8	0.26	0.64	2.09	148.84	1026.19
3/15/2016	11	10226	20	0.020	0.044	0.030	0.066	16	1.3	0.41	1.00	3.30	93.88	647.29
3/15/2016	12	7259	20	0.020	0.044	0.030	0.066	19.75	1.6	0.50	1.24	4.07	34.94	240.87
3/15/2016	12	10226	20	0.020	0.044	0.030	0.066	25.75	2.1	0.65	1.62	5.31	5.98	41.22
3/15/2016	13	7259	20	0.020	0.044	0.030	0.066	8.25	0.7	0.21	0.52	1.70	272.20	1876.73
3/15/2016	13	10226	20	0.020	0.044	0.030	0.066	14	1.2	0.36	0.88	2.88	173.40	1195.55
3/15/2016	14	7259	20	0.020	0.044	0.030	0.066	5.875	0.5	0.15	0.37	1.21	957.48	6601.56
3/15/2016	14	10226	20	0.020	0.044	0.030	0.066	11.75	1.0	0.30	0.74	2.42	298.29	2056.67
3/15/2016	15	7259	40	0.040	0.088	0.060	0.132	42.25	3.5	1.07	2.11	6.91	1.14	7.89
3/15/2016	15	10226	40	0.040	0.088	0.060	0.132	48.375	4.0	1.23	2.41	7.91	1.16	8.02
3/15/2016	16	7259	60	0.060	0.132	0.090	0.198	52.75	4.4	1.34	2.30	7.54	1.60	11.04
3/15/2016	16	10226	60	0.060	0.132	0.090	0.198	59.75	5.0	1.52	2.60	8.54	2.03	13.97

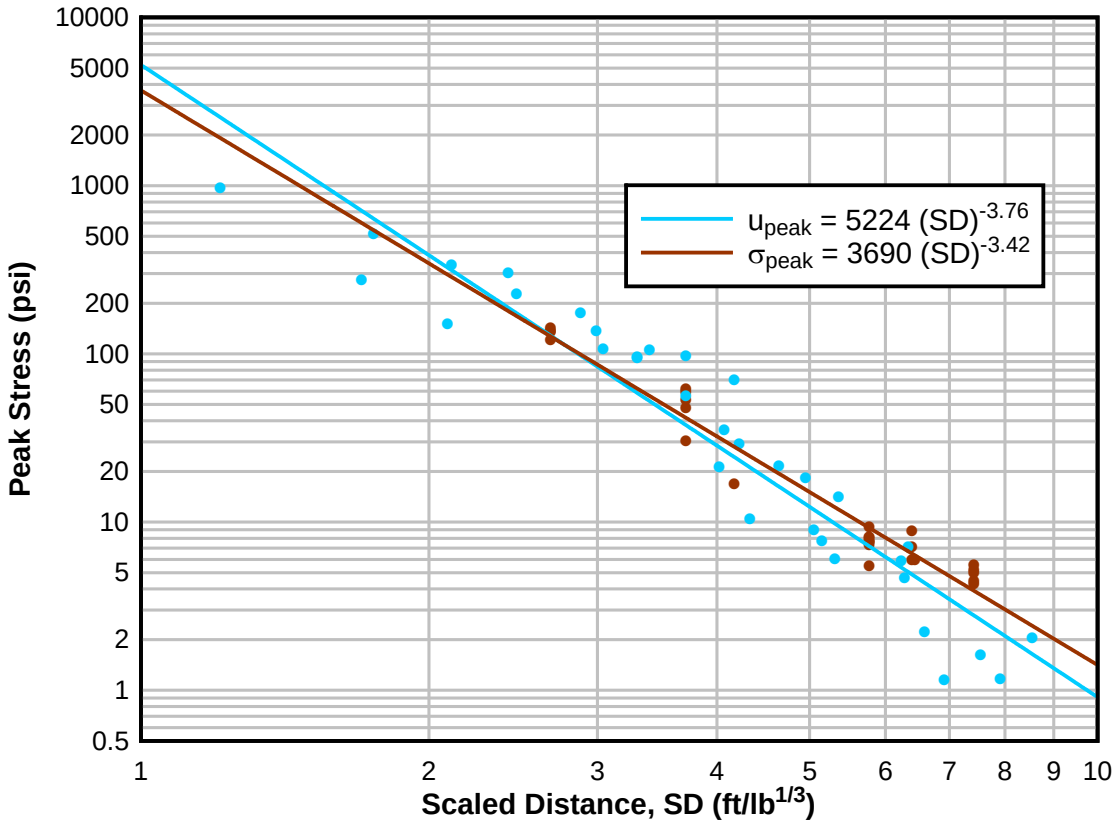

Figure 41: Peak compressive stress and transient pore pressure versus scaled distance graph in imperial units

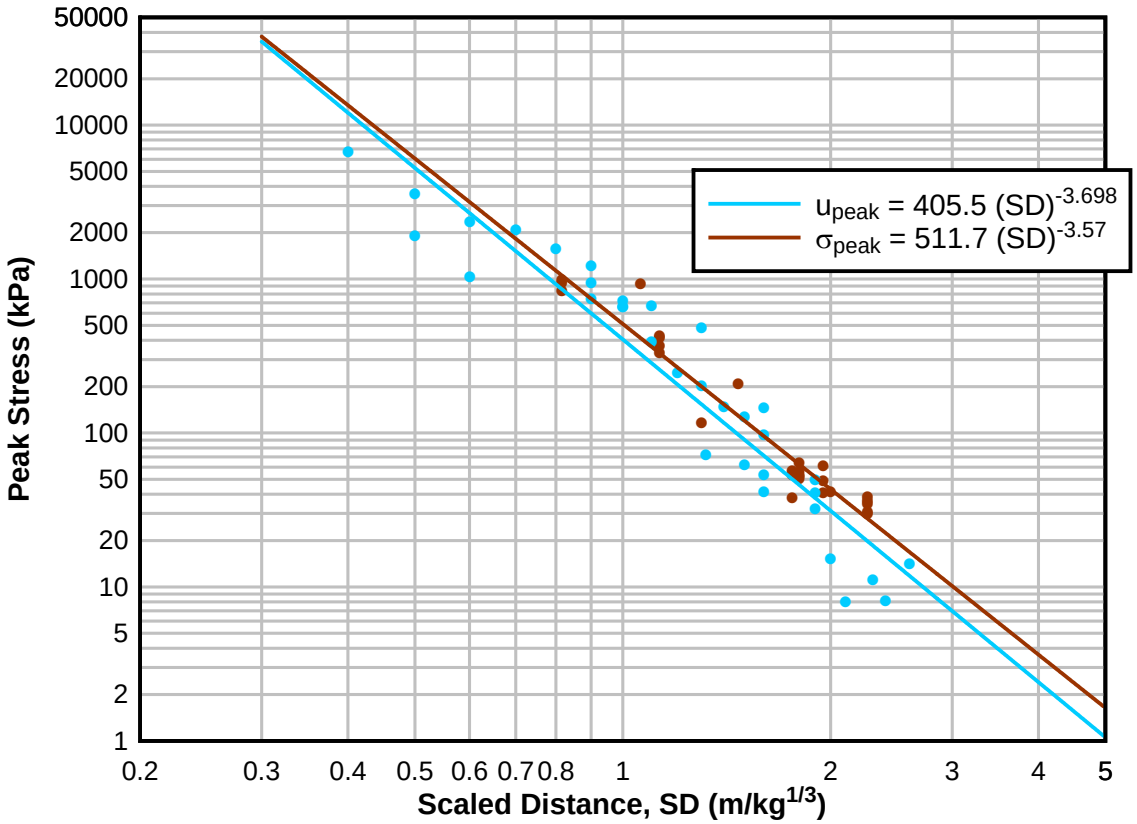

Figure 42: Peak compressive stress and transient pore pressure versus scaled distance graph in metric units

CHAPTER 5: DISCUSSION

If we examine the cube-root modeled scaled distance peak transient pore pressure equations from previous studies, as shown in Table 6, the experimental results are one to two orders of magnitude different with a significantly steeper decline, Figure 43. This may be due to our experimental setup of a near-by detonation within the saturated test medium rather than detonation occuring in water or a medium outside of the test material. The square-root modeled scaled distance was explored, but did not produce better regression models.

Table 6: Existing empirical peak excess pore pressure equations

Empirical Peak Pore Pressure Equation	Density	Reference
u_{peak} = 143,000 (SD)^(-2.34) kPa	loose	Al-Qasimi et al. (2005)
u_{peak} = 100,300 (SD)^(-2.67) kPa		Jacobs (1988)
u_{peak} = 59,000 (SD)^(-1.05) kPa	very loose	Lyakhov (1961)
u_{peak} = 50,093 (SD)^(-2.38) kPa	dense	Charlie et al. (1992)
u_{peak} = 47,900 (SD)^(-1.45) kPa	loose	Charlie et al. (2013)
u_{peak} = 47,400 (SD)^(-1.45) kPa	dense	Charlie et al. (2013)
u_{peak} = 47,200 (SD)^(-1.50) kPa	very dense	Charlie et al. (2013)
u_{peak} = 443.6 (SD)^(-3.57) kPa		Larson-Robl (2016)

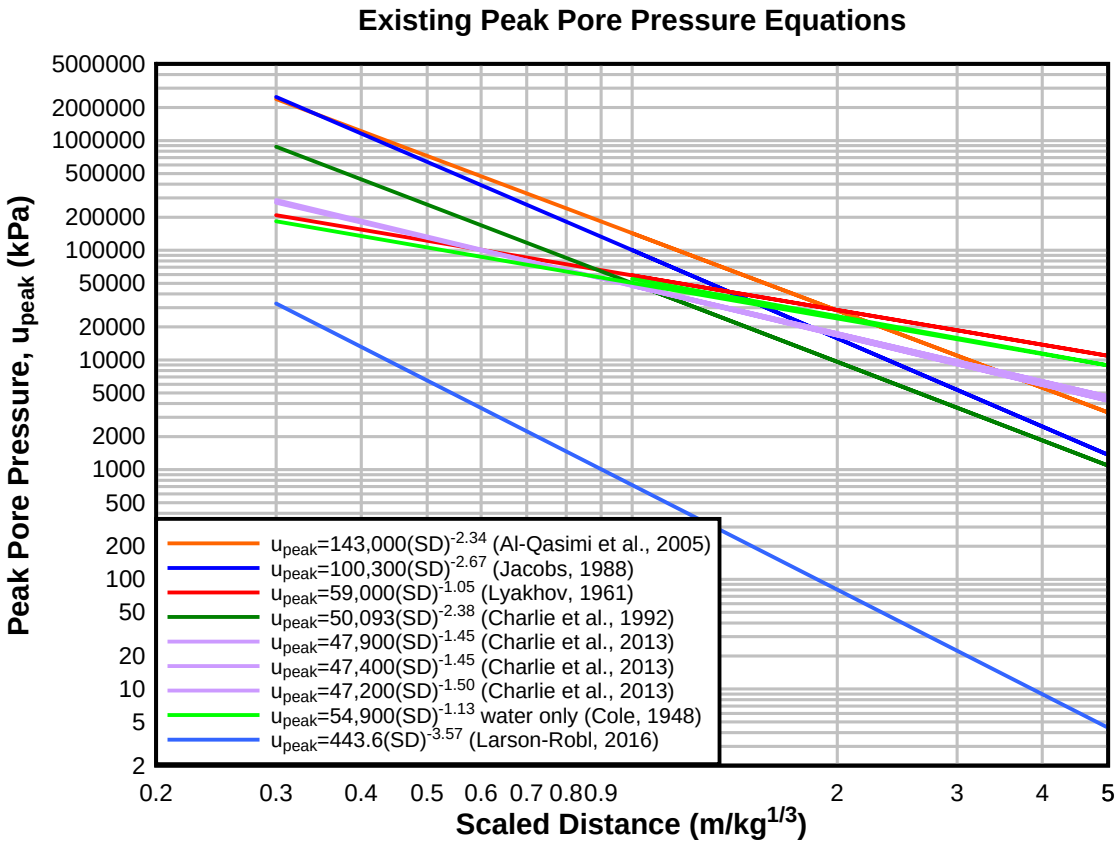

Figure 43: Comparison of existing empirical equations for peak transient pore pressure and the empirical equation from the data of this study

According to Lyakhov (1961), increased residual pore pressure resulting in liquefaction does not occur in horizontal deposits of water-saturated sands with dry densities greater than 1600 kg/m^3 (99.9 lb$_m$/ft^3). This supports the lack of significant residual pore pressures seen in these tests with a calculated dry density of approximately 1816 kg/m^3 (113.4 lb$_m$/ft^3) for this experimental setup.

At this point, it was determined that the difference between the results measured with the uncased tourmaline (total compressive stress) and the results measured with the encased tourmaline (pore pressure) was not statistically significant. These

results were analyzed together (Figures 44 and 45) to produce the following peak transient pore pressure equation:

$$u_{peak} = 4529\ (SD)^{-3.60}\ psi = 443.6\ (SD)^{-3.57}\ kPa \qquad (50)$$

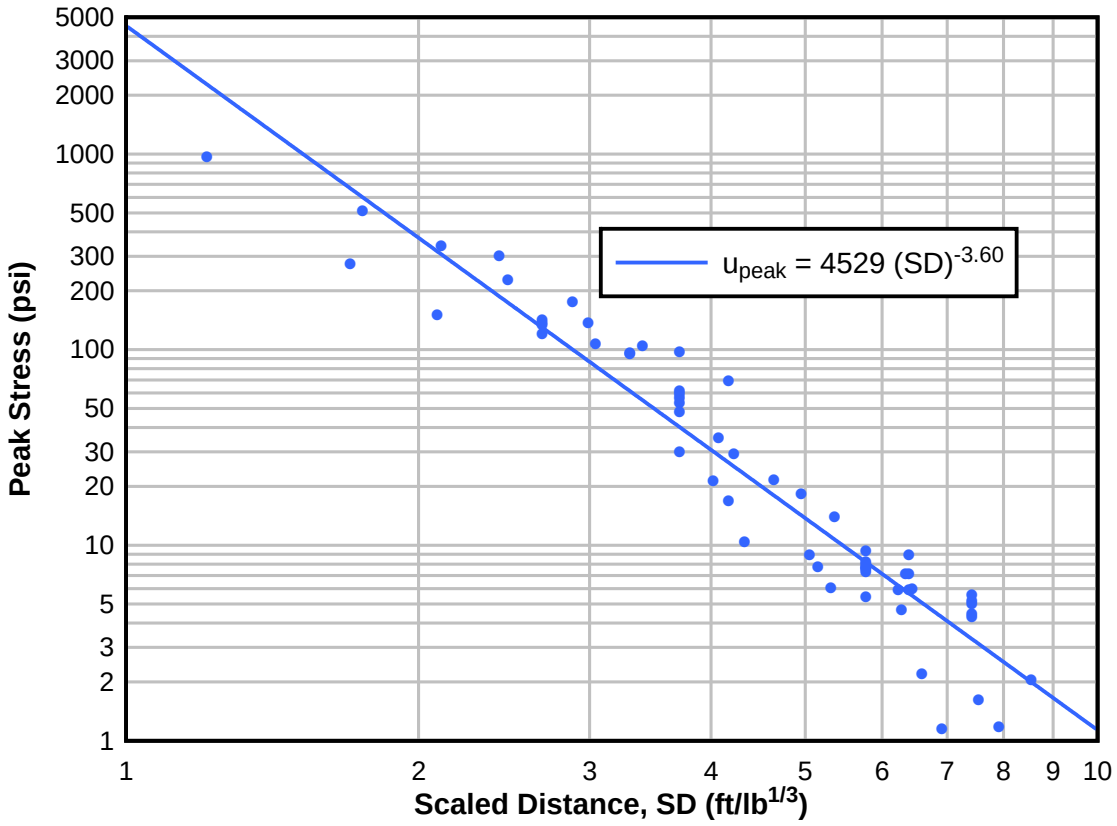

Figure 44: Peak transient pore pressure versus scaled distance graph of combined data in imperial units

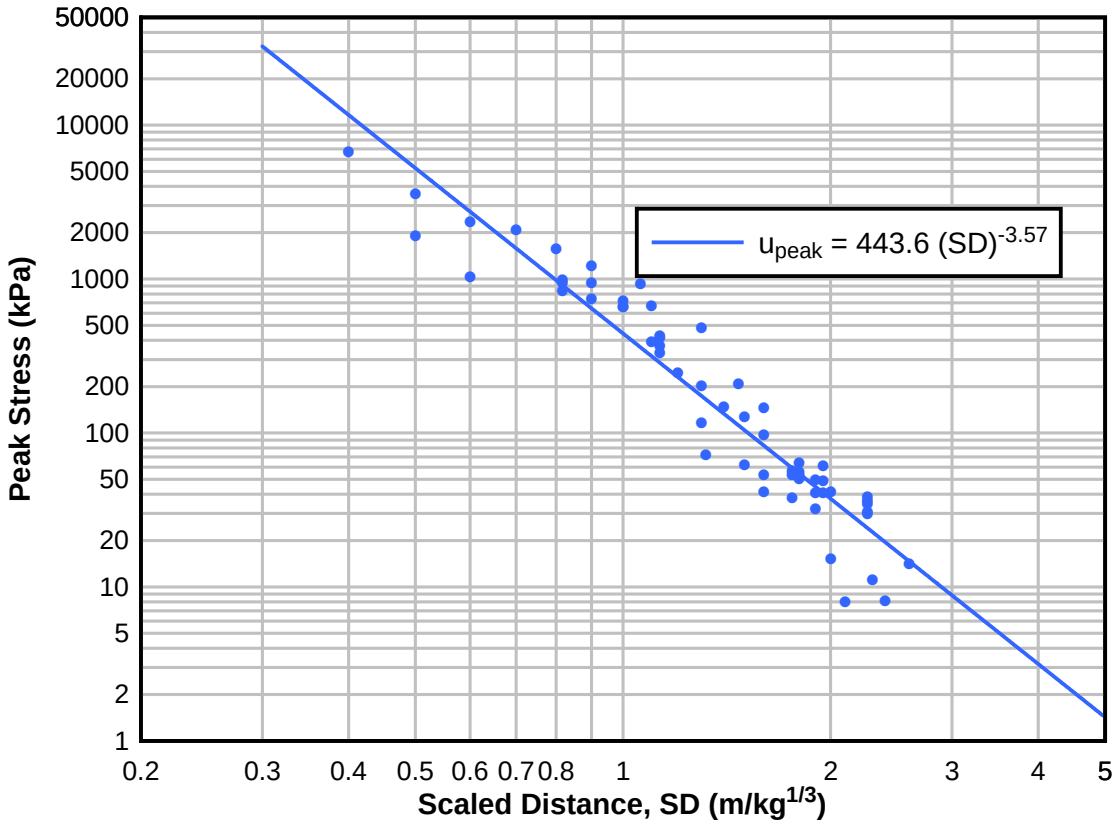

Figure 45: Peak transient pore pressure versus scaled distance graph of combined data in metric units

5.1 Charateristic Scaled Distance Vs Peak Excess Pore Pressure Curves

When comparing the decay lines of the peak transient excess pore pressure results and the peak particle velocity (radial direction) results, the peak transient excess pore pressure is more critical close to the source (values lower than a SD < 6.5 ft/lb$^{1/3}$ (1.8 m/kg$^{1/3}$)). At scaled distances greater than 6.5 ft/lb$^{1/3}$ (1.8 m/kg$^{1/3}$), the peak particle velocity becomes more critical, Figure 46. As observed by the slopes of these decay lines excess transient pore pressures

dissipate approximately three times as fast as the peak particle velocities. From Figure 46, the peak transient pore pressure goes to zero within a scaled distance of 20 ft/lb$^{1/3}$, and the peak particle velocity continues past a scaled distance of 20 ft/lb$^{1/3}$. Although full-scale impoundment dams would need to be examined on a site-specific basis, the knowledge that significant particle velocities exist in impoundment dams subject to near-by blasting does not give substance to the presence of excess pore pressure as they may dissipate at much faster rates.

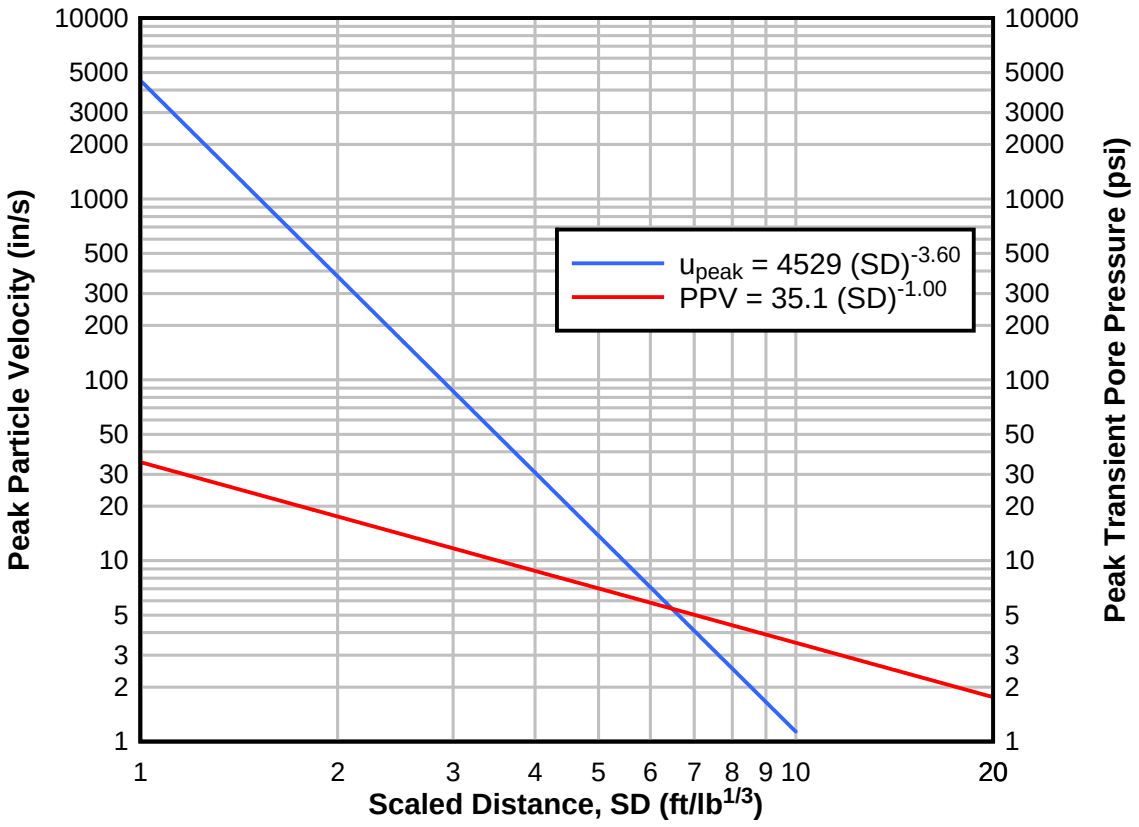

Figure 46: u_{peak} and PPV decay line comparison in imperial units

For the purpose of comparing dissipation slopes, the empirical equation for peak transient excess pore pressure was recalculated using square-root scaled

distance and is compared to the typical ground vibrations from mine blasting in rock, Figure 47. From the slopes of these lines, pore pressure dissipates approximately 2.3 times faster than typical ground vibrations from mine productions blasts.

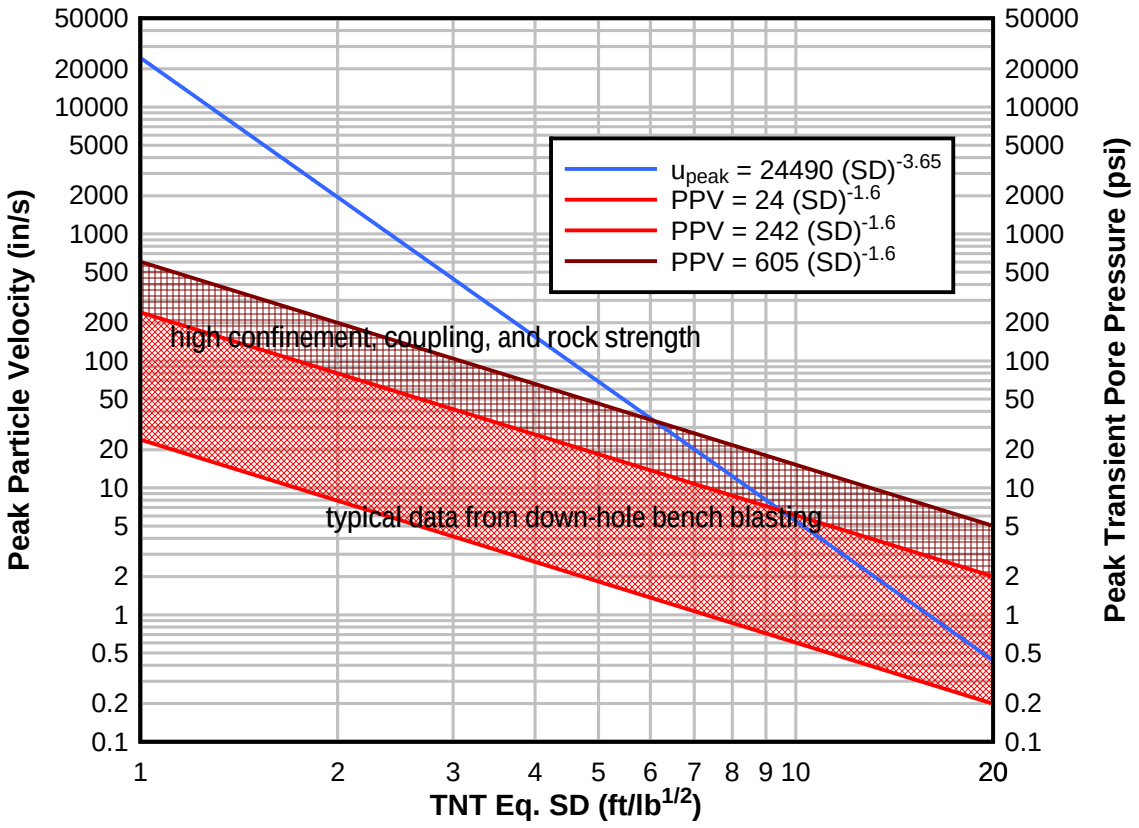

Figure 47: Ground vibrations from blasting and empirical equation for peak transient excess pore pressure (ISEE Blasters' Handbook, 2011).

5.2 Characteristic Waveform for Saturated Soils Under Dynamic Shock Waves

Comparing this study's typical residual pore pressure waveform with those from previous studies, similar waveform shapes emerge. For those tests close to the detonation (less than approximate SD of 4.2 ft/lb$^{1/3}$ or 1.3 m/kg$^{1/3}$) the typical waveform for the excess pore pressure includes a nearly instantaneous transient excess pore pressure followed by a more gradual residual excess pore pressure, Figure 48. Al-Qasimi et al. (2005) utilized cyclic loading of multiple detonations with approximately 500 ms delays. Figure 49 shows an example of an excess pore pressure waveform from Al-Qasimi et al.'s (2005) study. With each detonation there is a similar instantaneous transient excess pore pressure followed by the more gradual residual excess pore pressure increase. Similarly, Charlie et al.'s (2013) excess pore pressure measurements from a retro-fitted piezoresistive strain gauge pressure tranducer show additional excess pore pressure after the initial peak transient excess pore pressure (Figure 50).

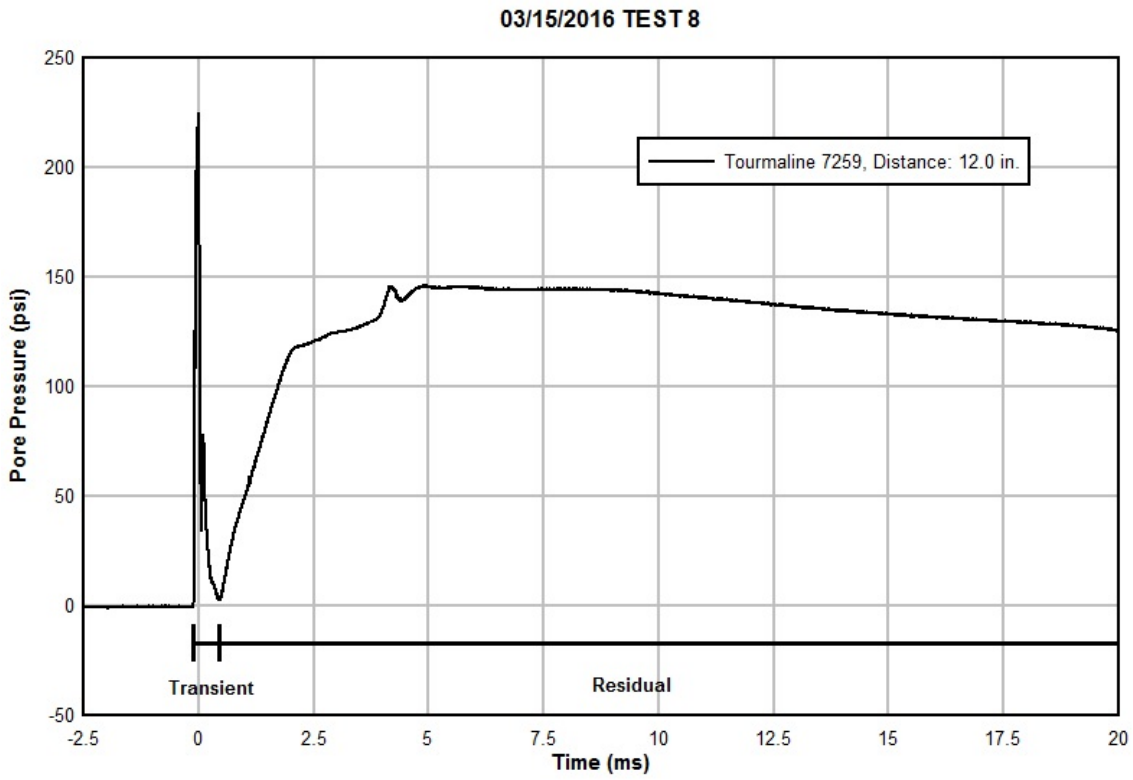

Figure 48: Characteristic excess pore pressure waveform for close distances

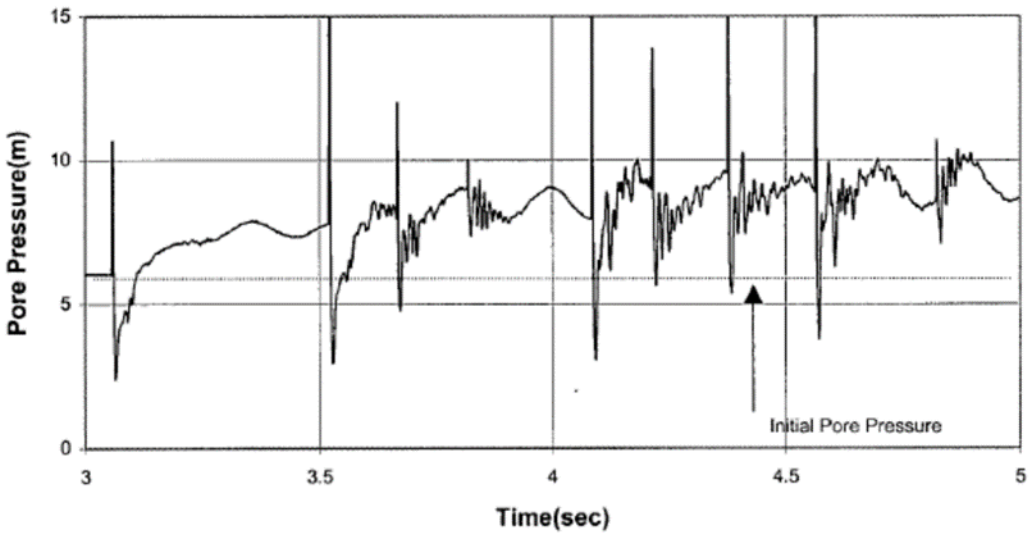

Figure 49: Excess pore pressure waveform from Al-Qasimi et al. (2005) blast 6 at a 30 m distance with multiple detonations

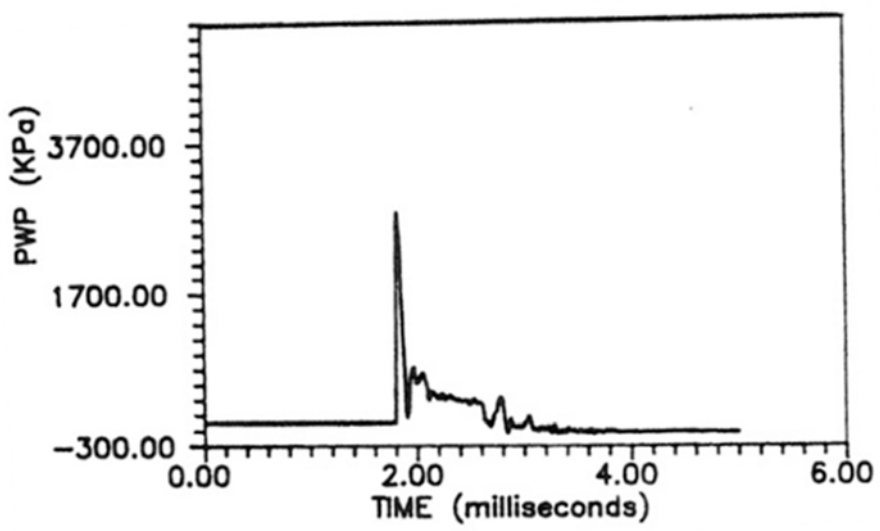

Figure 50: Excess pore pressure waveform from Charlie et al. (2013) test D5 at a 2.72 m distance using 0.028 kg of PETN

These typical excess pore pressure waveforms in saturated unconsolidated medium and those pressure waveforms from air (Figure 51) or water alone (Figure 52) differ significantly.

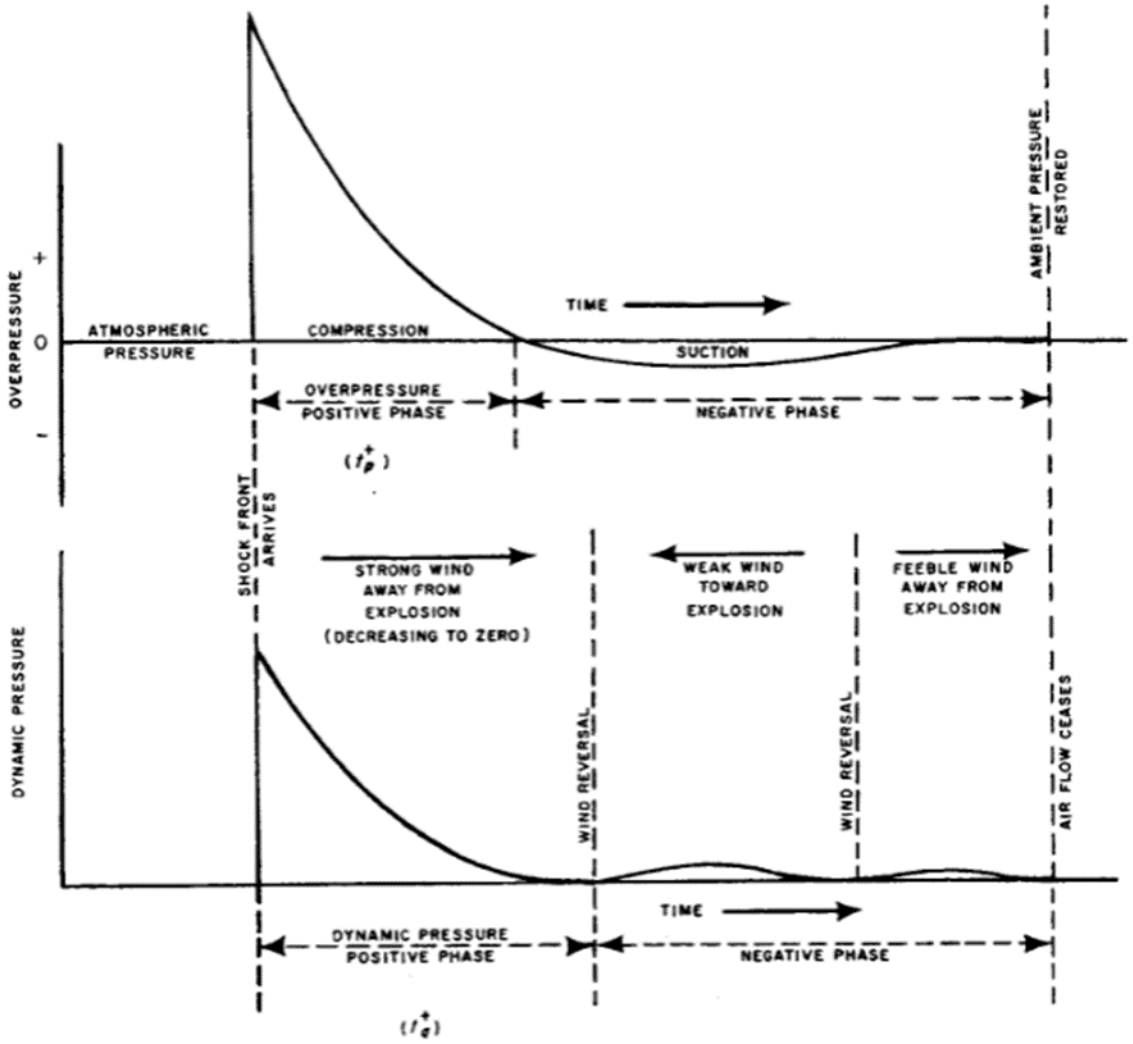

Figure 51: Typical dynamic pressure waveform through air as a medium from an explosive detonation

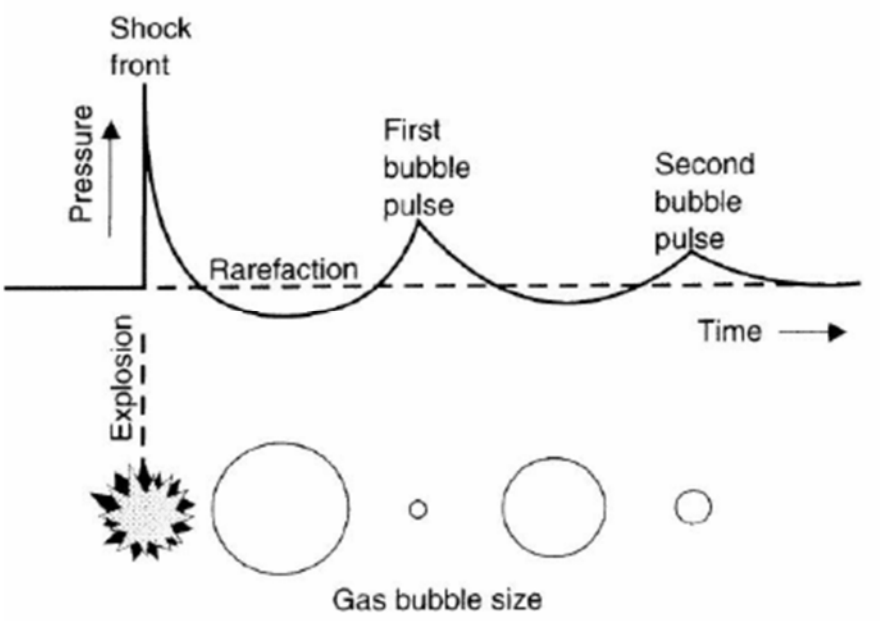

Figure 52: Typical dynamic pressure waveform through water alone as a medium from an explosive detonation, where the dashed line is the static water pressure (Simmonds and MacLennan, 2005)

Examining the typical waveform responses of particle velocity and excess pore pressures from close and far distances (Figure 53), it can be seen that the particle velocity waveform for the far distances look like the typical particle velocity waveform to a dynamic cyclic loading event such as an earthquake. Typically, residual excess pore pressures rather than transient excess pore pressures are a result from these waveforms.

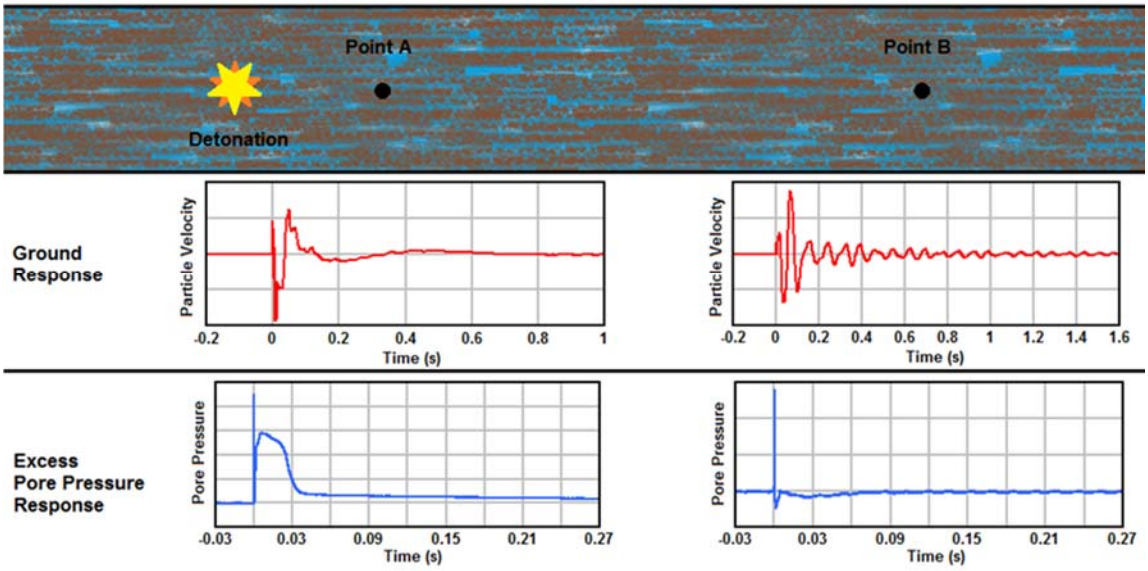

Figure 53: Schematic of typical waveform responses of particle velocity and excess pore pressures from close distances and far distances

In this study both transient and residual excess pore pressures were only shown up to an approximate scaled distance of 4.2 ft/lb$^{1/3}$ or 1.3 m/kg$^{1/3}$ (Figure 54). It is possible that since the test sand is poorly graded and has a high density the separation of the two variant excess pore pressures do not exist at further scaled distances. It is suspected that at larger scaled distances this one variant of excess pore pressure is the residual excess pore pressure. This is suspected based on the relative rise and fall time of these experimental tests, and cyclic nature of the PPV waveforms. The time for the excess pore pressure to peak and fall back to zero for those waveforms exhibiting only one variant of excess pore pressure was typically longer than the time for the transient excess pore pressure to peak and fall back to zero of those waveforms exhibiting both variants of excess pore pressure. Previous literature has proven residual excess

pore pressures are produced by cyclic loading events causing oscillatory PPV waveforms. Similar oscillatory PPV waveforms are produced are large scaled distances. This may suggest that the only necessary pore pressure to measure in impoundment dams is the residual excess pore pressure, as typically such close scaled distances as those necessary to produce both variants of excess pore pressure are not seen in practice.

It is also important to note that, while not the majority, some tests (Figure 54, 20.25 in. (Test 6 Channel 1)) exhibited larger residual excess pore pressure peaks than the initial transient excess pore pressure peak. Those curves produced from the closest scaled distances (Test 8 Channel 1, Test 9 Channel 1, and Test 10 Channel 1) depict a spike from sidewall reflections several milliseconds after the initial transient peak.

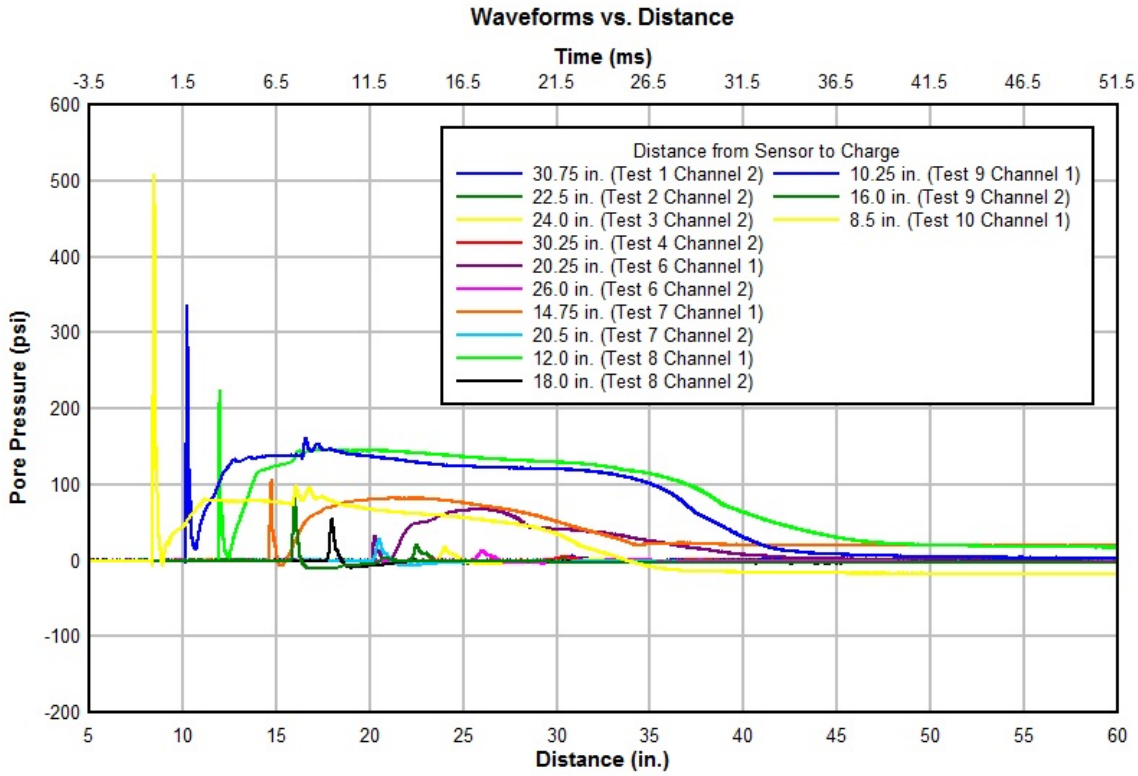

Figure 54: Excess pore pressure time-history waveforms plotted with their peak transient excess pore pressure at their distance from the detonation showing residual excess pore pressures up to a distance of 20.25 in.

CHAPTER 6: CONCLUSIONS

- Based on existing literature and the explosive testing done here there are two types of excess pore pressures; transient excess pore pressure and residual excess pore pressure. These are examined in previous literature as u_{peak} and PPR, respectively. The tourmaline pressure sensor results from these tests appeared to depict both the transient excess pore pressure and a short-lasting residual excess pore pressure at close scaled distances. At far scaled distances, the tourmaline pressure sensors only measured one variant of excess pore pressure.
- The difference between total compressive stress and excess pore pressure measured by the tourmaline pressure sensors was not statistically significant. Their use directly into an impoundment medium or narrow standing pipe will produce equivalent data.
- Transient excess pore pressures dissipate very quickly with scaled distance; up to 3.2 times greater than the PPV of saturated material and up to 2.4 times greater than the PPV of unsaturated material. The pore pressure coefficients for the Skempton (1954) and Terzaghi (1996) equations developed for monotonic loading are difficult to constrain, and are further more difficult to attempt to apply to dynamic shock wave loading.
- Conditions for excess pore pressures under dynamic cyclic loading is difficult to apply to dynamic shock wave loading due to the difference in

ground vibration characteristics as seen in the peak particle velocity waveforms.

CHAPTER 7: FUTURE WORK

As mentioned previously, in this study transient and residual excess pore pressures were only shown up to an approximate scaled distance of 4.2 $ft/lb^{1/3}$ or 1.3 $m/kg^{1/3}$, continuation of this study would consider utilizing piezometers at further distances to determine if the variant of excess pore pressure at greater scaled distances is in fact residual excess pore pressure. It would be useful to duplicate these scaled experiments using coal refuse material in the container, as well as gather data from an active full-scale coal refuse impoundment for comparison; this would allow better constrained peak transient pore pressure, PPV, and PPR equations for refuse material aiding in the ultimate goal of blasting recommendations near these structures.

APPENDIX A – DRY CONDITION SEISMOGRAPH DATA

RADIAL PPV, DRY CONDITIONS

Date	Test	Seismograph No.	Charge (g)	Charge (kg)	Charge (lb)	TNT Equivalency (kg)	TNT Equivalency (lb)	Distance to charge (in)	Distance to charge (ft)	Distance to charge (m)	TNT Eq. SD (m/kg^⅓)	TNT Eq. SD (ft/lb^⅓)	PPV (in/s)	PPV (m/s)
7/9/2014	1	1746	20	0.020	0.044	0.030	0.066	36	3	0.91	2.94	7.42	6.80	46.88
7/9/2014	1	5595	20	0.020	0.044	0.030	0.066	60	5	1.52	3.77	12.36	1.76	12.13
7/9/2014	1	1864	20	0.020	0.044	0.030	0.066	180	15	4.57	11.31	37.09	0.74	5.10
7/9/2014	2	1746	20	0.020	0.044	0.030	0.066	24	2	0.61	1.51	4.95	MAXED	MAXED
7/9/2014	2	5595	20	0.020	0.044	0.030	0.066	48	4	1.22	3.01	9.89	3.28	22.61
7/9/2014	2	1864	20	0.020	0.044	0.030	0.066	168	14	4.27	10.55	34.62	0.45	3.07
7/9/2014	3	1746	20	0.020	0.044	0.030	0.066	24	2	0.61	1.51	4.95	MAXED	MAXED
7/9/2014	3	5595	20	0.020	0.044	0.030	0.066	48	4	1.22	3.01	9.89	3.12	21.51
7/9/2014	3	1864	20	0.020	0.044	0.030	0.066	168	14	4.27	10.55	34.62	0.47	3.21
7/9/2014	4	1746	20	0.020	0.044	0.030	0.066	30	2.5	0.76	1.88	6.18	7.60	52.40
7/9/2014	4	5595	20	0.020	0.044	0.030	0.066	54	4.5	1.37	3.39	11.13	2.30	15.86
7/9/2014	4	1864	20	0.020	0.044	0.030	0.066	174	14.5	4.42	10.93	35.85	0.54	3.72
7/10/2014	1	1746	20	0.020	0.044	0.030	0.066	30	2.5	0.76	1.88	6.18	8.24	56.81
7/10/2014	1	5595	20	0.020	0.044	0.030	0.066	54	4.5	1.37	3.39	11.13	2.10	14.48
7/10/2014	1	1864	20	0.020	0.044	0.030	0.066	174	14.5	4.42	10.93	35.85	0.52	3.55
7/10/2014	2	1746	20	0.020	0.044	0.030	0.066	30	2.5	0.76	1.88	6.18	8.24	56.81
7/10/2014	2	5595	20	0.020	0.044	0.030	0.066	54	4.5	1.37	3.39	11.13	2.24	15.44
7/10/2014	2	1864	20	0.020	0.044	0.030	0.066	174	14.5	4.42	10.93	35.85	0.52	3.59
7/10/2014	3	1746	20	0.020	0.044	0.030	0.066	30	2.5	0.76	1.88	6.18	7.36	50.75
7/10/2014	3	5595	20	0.020	0.044	0.030	0.066	54	4.5	1.37	3.39	11.13	2.18	15.03
7/10/2014	3	1864	20	0.020	0.044	0.030	0.066	174	14.5	4.42	10.93	35.85	0.55	3.76

VERTICAL PPV, DRY CONDITIONS

Date	Test	Seismograph No.	Charge (g)	Charge (kg)	Charge (lb)	TNT Equivalency (kg)	TNT Equivalency (lb)	Distance to charge (in)	Distance to charge (ft)	Distance to charge (m)	TNT Eq. SD (m/kg^⅓)	TNT Eq. SD (ft/lb^⅓)	PPV (in/s)	PPV (m/s)
7/9/2014	1	1746	20	0.020	0.044	0.030	0.066	36	3	0.91	2.94	7.42	4.48	30.89
7/9/2014	1	5595	20	0.020	0.044	0.030	0.066	60	5	1.52	3.77	12.36	0.96	6.62
7/9/2014	1	1864	20	0.020	0.044	0.030	0.066	180	15	4.57	11.31	37.09	0.80	5.52
7/9/2014	2	1746	20	0.020	0.044	0.030	0.066	24	2	0.61	1.51	4.95	6.72	46.33
7/9/2014	2	5595	20	0.020	0.044	0.030	0.066	48	4	1.22	3.01	9.89	1.98	13.65
7/9/2014	2	1864	20	0.020	0.044	0.030	0.066	168	14	4.27	10.55	34.62	0.47	3.21
7/9/2014	3	1746	20	0.020	0.044	0.030	0.066	24	2	0.61	1.51	4.95	6.72	46.33
7/9/2014	3	5595	20	0.020	0.044	0.030	0.066	48	4	1.22	3.01	9.89	2.00	13.79
7/9/2014	3	1864	20	0.020	0.044	0.030	0.066	168	14	4.27	10.55	34.62	0.52	3.59
7/9/2014	4	1746	20	0.020	0.044	0.030	0.066	30	2.5	0.76	1.88	6.18	5.92	40.82
7/9/2014	4	5595	20	0.020	0.044	0.030	0.066	54	4.5	1.37	3.39	11.13	1.48	10.20
7/9/2014	4	1864	20	0.020	0.044	0.030	0.066	174	14.5	4.42	10.93	35.85	0.68	4.69
7/10/2014	1	1746	20	0.020	0.044	0.030	0.066	30	2.5	0.76	1.88	6.18	6.00	41.37
7/10/2014	1	5595	20	0.020	0.044	0.030	0.066	54	4.5	1.37	3.39	11.13	1.56	10.76
7/10/2014	1	1864	20	0.020	0.044	0.030	0.066	174	14.5	4.42	10.93	35.85	0.64	4.41
7/10/2014	2	1746	20	0.020	0.044	0.030	0.066	30	2.5	0.76	1.88	6.18	6.16	42.47
7/10/2014	2	5595	20	0.020	0.044	0.030	0.066	54	4.5	1.37	3.39	11.13	1.60	11.03
7/10/2014	2	1864	20	0.020	0.044	0.030	0.066	174	14.5	4.42	10.93	35.85	0.64	4.41
7/10/2014	3	1746	20	0.020	0.044	0.030	0.066	30	2.5	0.76	1.88	6.18	6.08	41.92
7/10/2014	3	5595	20	0.020	0.044	0.030	0.066	54	4.5	1.37	3.39	11.13	1.56	10.76
7/10/2014	3	1864	20	0.020	0.044	0.030	0.066	174	14.5	4.42	10.93	35.85	0.60	4.14

TRANSVERSE PPV, DRY CONDITIONS														
Date	Test	Seismograph No.	Charge (g)	Charge (kg)	Charge (lb)	TNT Equivalency (kg)	TNT Equivalency (lb)	Distance to charge (in)	Distance to charge (ft)	Distance to charge (m)	TNT Eq. SD (m/kg^⅓)	TNT Eq. SD (ft/lb^⅓)	PPV (in/s)	PPV (m/s)
7/9/2014	1	1746	20	0.020	0.044	0.030	0.066	36	3	0.91	2.94	7.42	0.40	2.76
7/9/2014	1	5595	20	0.020	0.044	0.030	0.066	60	5	1.52	3.77	12.36	0.20	1.38
7/9/2014	1	1864	20	0.020	0.044	0.030	0.066	180	15	4.57	11.31	37.09	0.14	0.97
7/9/2014	2	1746	20	0.020	0.044	0.030	0.066	24	2	0.61	1.51	4.95	2.72	18.75
7/9/2014	2	5595	20	0.020	0.044	0.030	0.066	48	4	1.22	3.01	9.89	0.30	2.07
7/9/2014	2	1864	20	0.020	0.044	0.030	0.066	168	14	4.27	10.55	34.62	0.12	0.83
7/9/2014	3	1746	20	0.020	0.044	0.030	0.066	24	2	0.61	1.51	4.95	2.16	14.89
7/9/2014	3	5595	20	0.020	0.044	0.030	0.066	48	4	1.22	3.01	9.89	0.32	2.21
7/9/2014	3	1864	20	0.020	0.044	0.030	0.066	168	14	4.27	10.55	34.62	0.14	0.93
7/9/2014	4	1746	20	0.020	0.044	0.030	0.066	30	2.5	0.76	1.88	6.18	0.64	4.41
7/9/2014	4	5595	20	0.020	0.044	0.030	0.066	54	4.5	1.37	3.39	11.13	0.22	1.52
7/9/2014	4	1864	20	0.020	0.044	0.030	0.066	174	14.5	4.42	10.93	35.85	0.10	0.66
7/10/2014	1	1746	20	0.020	0.044	0.030	0.066	30	2.5	0.76	1.88	6.18	0.32	2.21
7/10/2014	1	5595	20	0.020	0.044	0.030	0.066	54	4.5	1.37	3.39	11.13	0.38	2.62
7/10/2014	1	1864	20	0.020	0.044	0.030	0.066	174	14.5	4.42	10.93	35.85	0.15	1.03
7/10/2014	2	1746	20	0.020	0.044	0.030	0.066	30	2.5	0.76	1.88	6.18	0.56	3.86
7/10/2014	2	5595	20	0.020	0.044	0.030	0.066	54	4.5	1.37	3.39	11.13	0.40	2.76
7/10/2014	2	1864	20	0.020	0.044	0.030	0.066	174	14.5	4.42	10.93	35.85	0.18	1.21
7/10/2014	3	1746	20	0.020	0.044	0.030	0.066	30	2.5	0.76	1.88	6.18	0.48	3.31
7/10/2014	3	5595	20	0.020	0.044	0.030	0.066	54	4.5	1.37	3.39	11.13	0.32	2.21
7/10/2014	3	1864	20	0.020	0.044	0.030	0.066	174	14.5	4.42	10.93	35.85	0.18	1.24

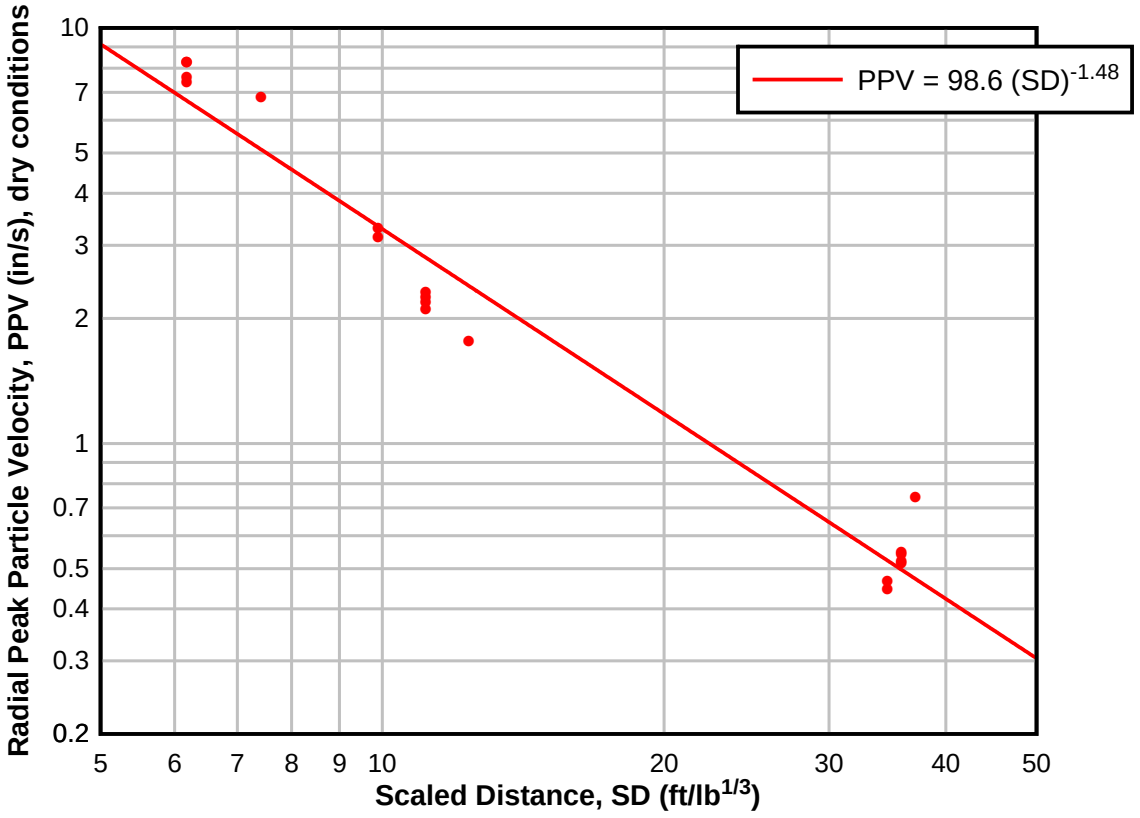

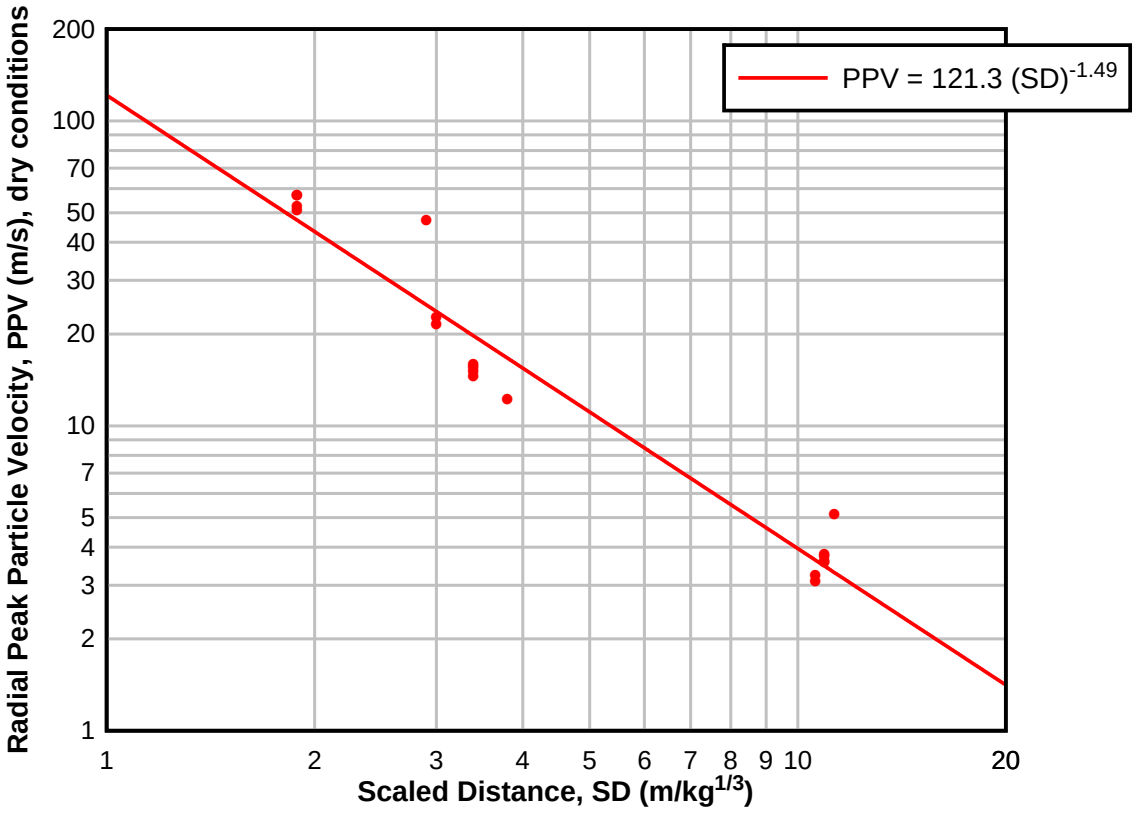
PPV = 121.3 (SD)-1.49
Radial Peak Particle Velocity, PPV (m/s), dry conditions
200
100
70
50
40
30
20
10
7
5
4
3
2
1
1
2
3
4
5
6
7
8
9
10
20
Scaled Distance, SD (m/kg1/3)

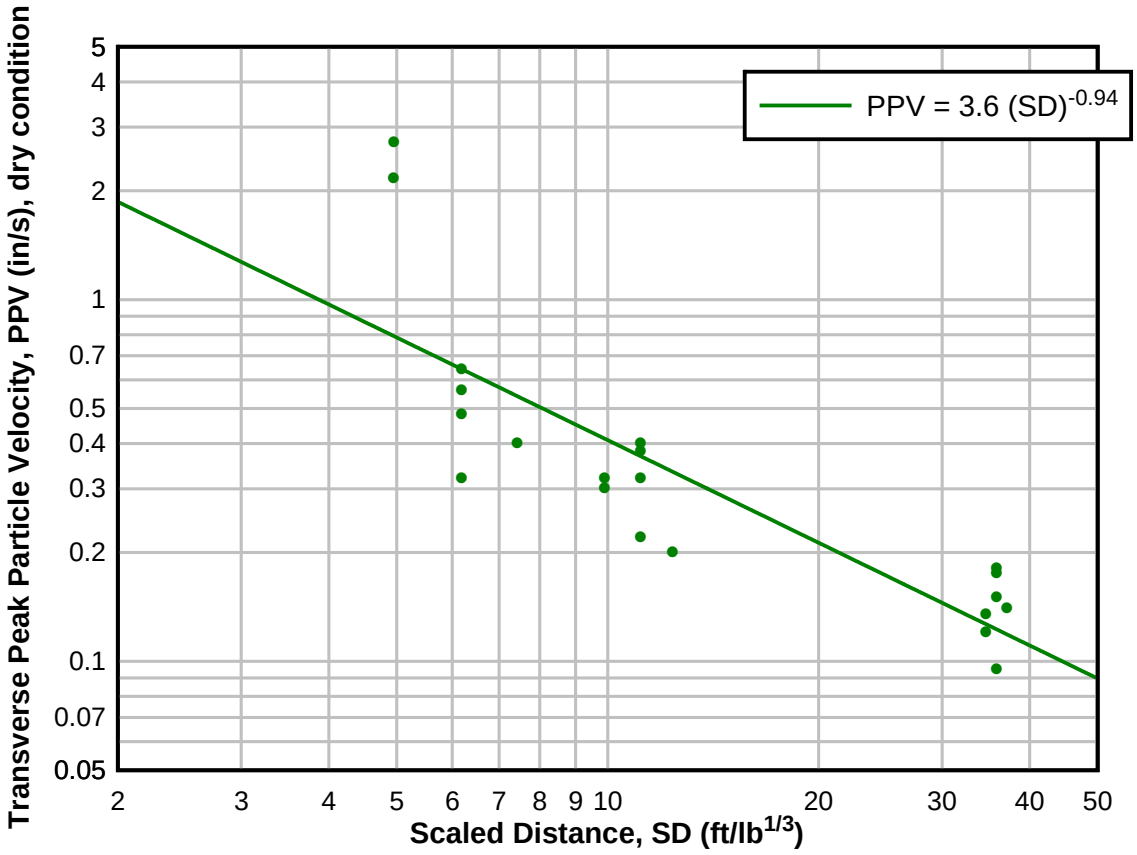
PPV = 3.6 (SD)-0.94
Transverse Peak Particle Velocity, PPV (in/s), dry condition
5
4
3
2
1
0.7
0.5
0.4
0.3
0.2
0.1
0.07
0.05
2
3
4
5
6
7
8
9
10
20
30
40
50
Scaled Distance, SD (ft/lb1/3)

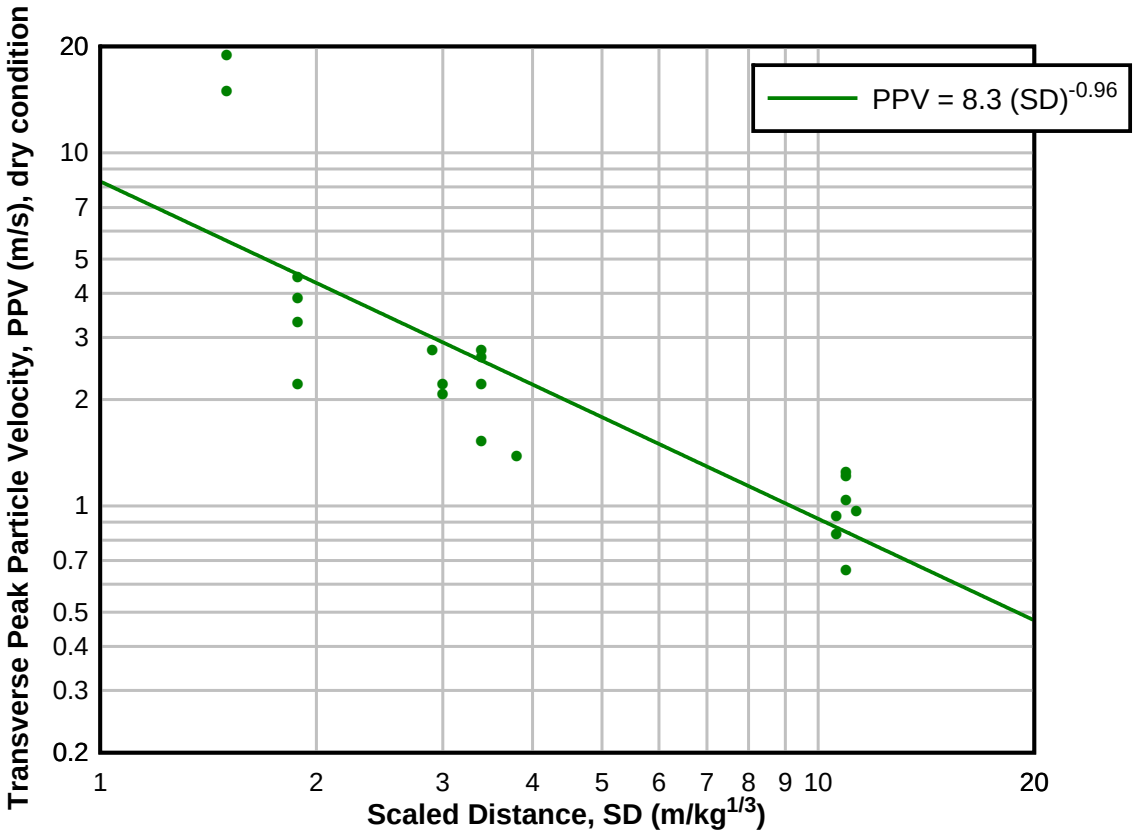
PPV = 8.3 (SD)-0.96
Transverse Peak Particle Velocity, PPV (m/s), dry condition
Scaled Distance, SD (m/kg1/3)
20
10
7
5
4
3
2
1
0.7
0.5
0.4
0.3
0.2
1
2
3
4
5
6
7
8
9
10
20

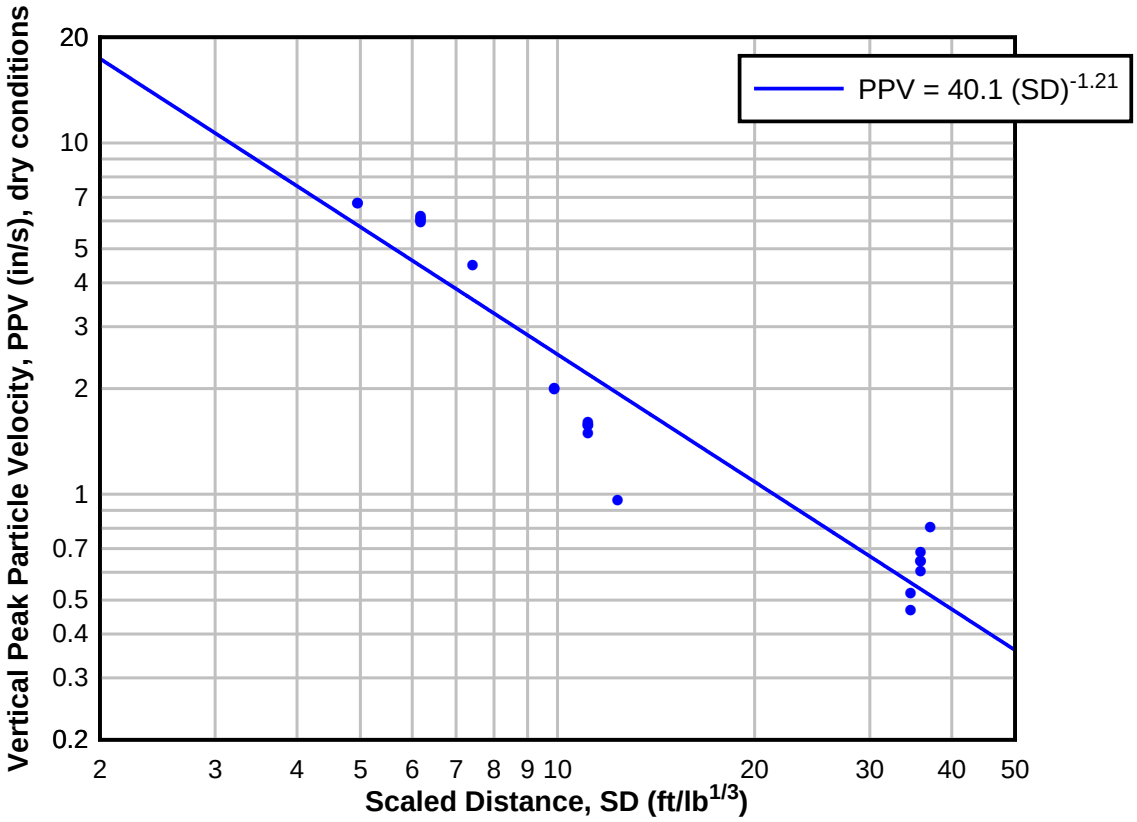
PPV = 40.1 (SD)-1.21
Vertical Peak Particle Velocity, PPV (in/s), dry conditions
Scaled Distance, SD (ft/lb1/3)
20
10
7
5
4
3
2
1
0.7
0.5
0.4
0.3
0.2
2
3
4
5
6
7
8
9
10
20
30
40
50

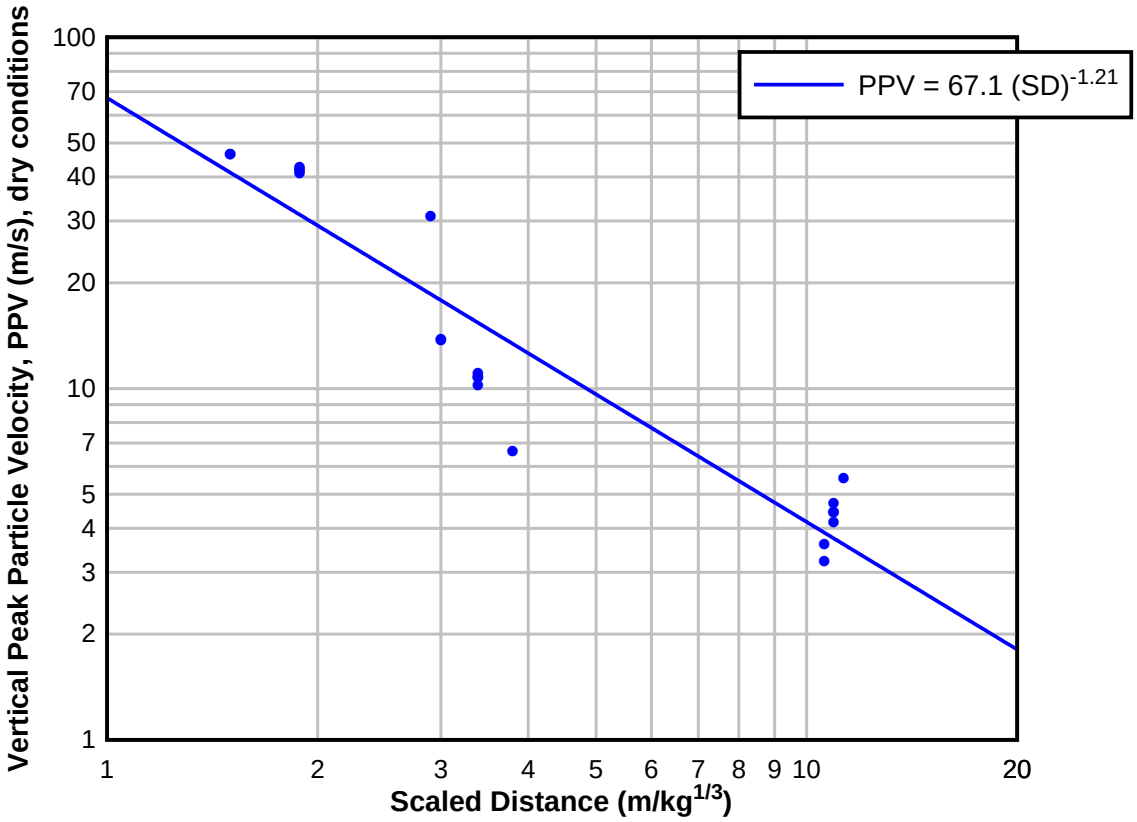
PPV = 67.1 (SD)-1.21
Vertical Peak Particle Velocity, PPV (m/s), dry conditions
Scaled Distance (m/kg1/3)
100
70
50
40
30
20
10
7
5
4
3
2
1
1
2
3
4
5
6
7
8
9
10
20

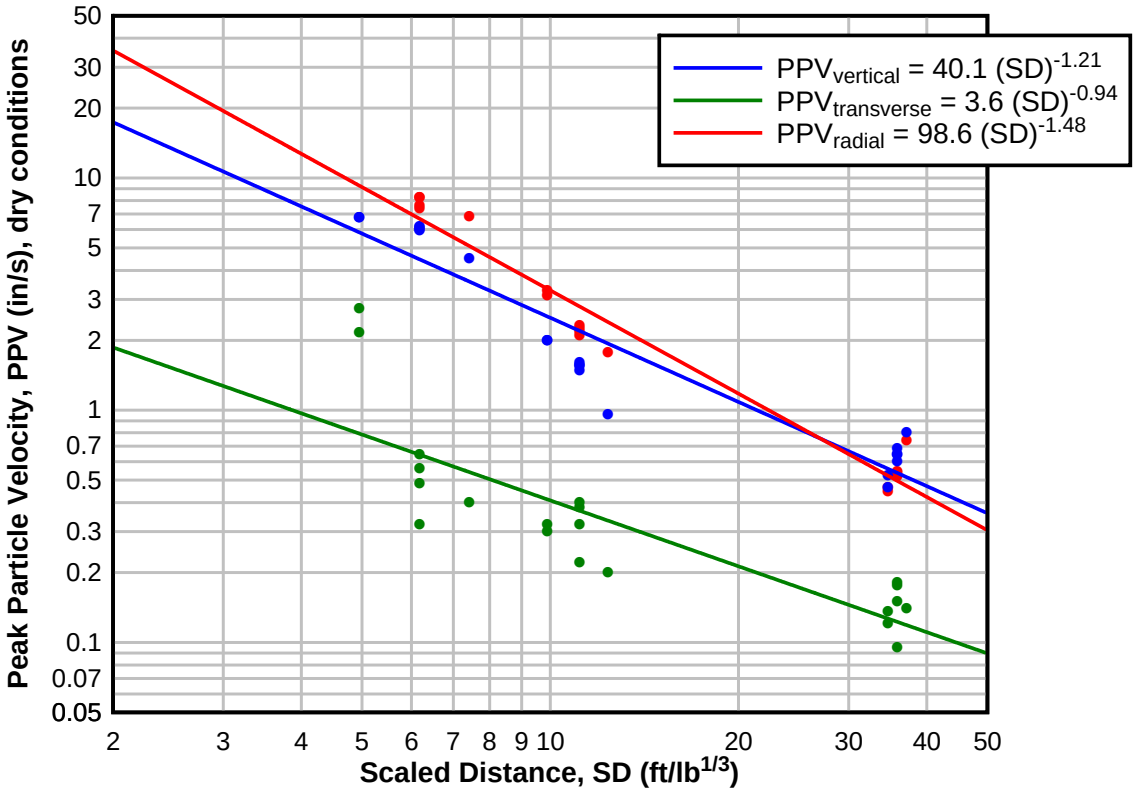
PPVvertical = 40.1 (SD)-1.21
PPVtransverse = 3.6 (SD)-0.94
PPVradial = 98.6 (SD)-1.48
Peak Particle Velocity, PPV (in/s), dry conditions
Scaled Distance, SD (ft/lb1/3)
50
30
20
10
7
5
3
2
1
0.7
0.5
0.3
0.2
0.1
0.07
0.05
2
3
4
5
6
7
8
9
10
20
30
40
50

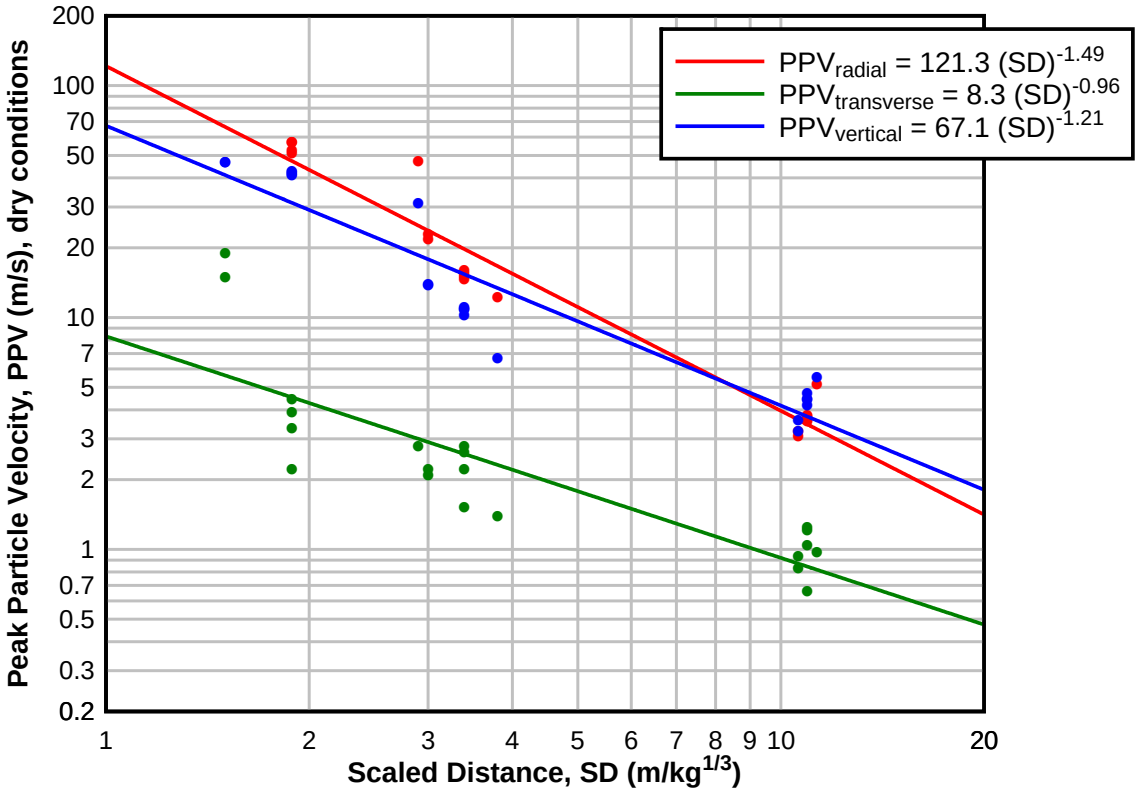

07/09/2014 TEST 1
Seismograph 1746, Distance: 36 in.

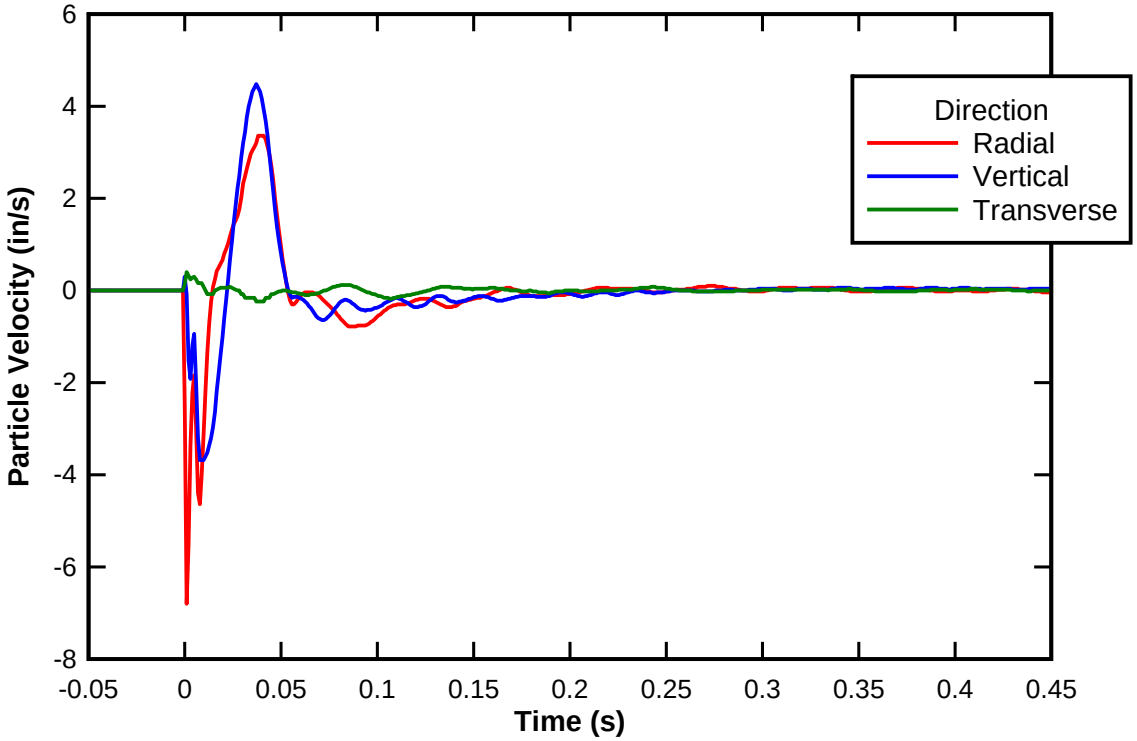

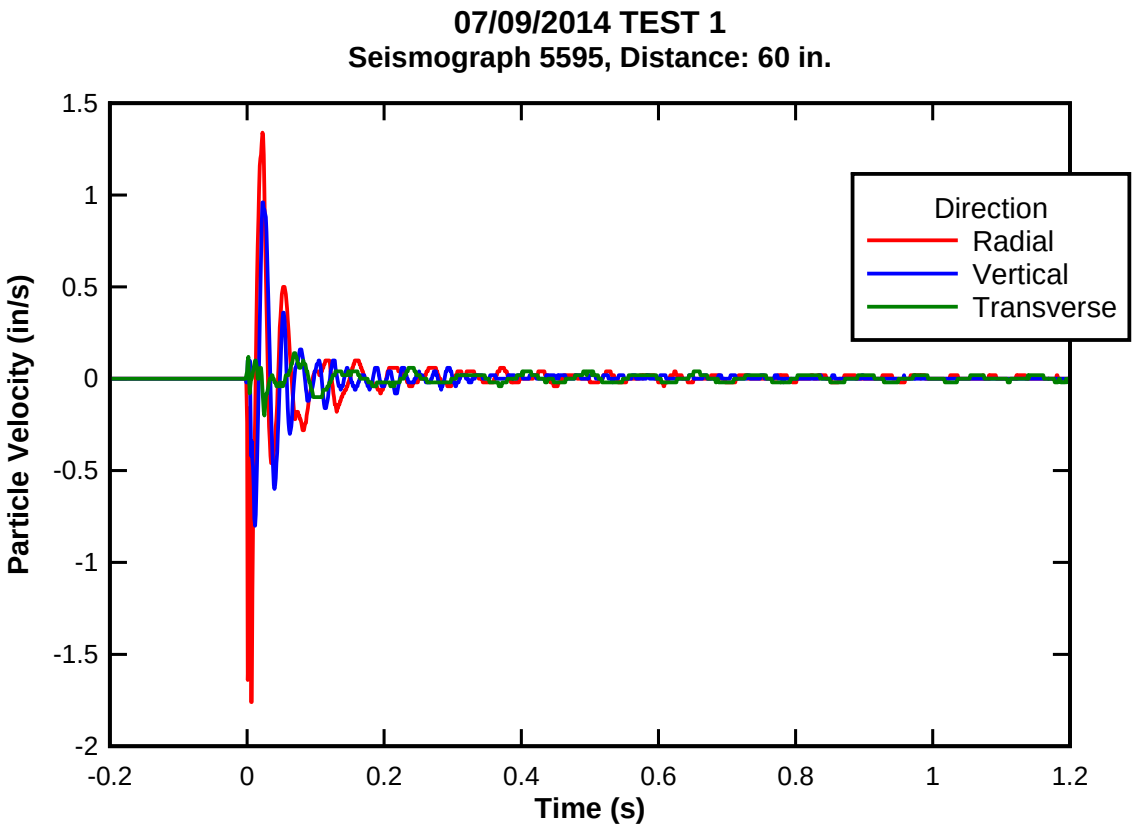
07/09/2014 TEST 1
Seismograph 5595, Distance: 60 in.
Particle Velocity (in/s)
Time (s)
Direction
Radial
Vertical
Transverse
1.5
1
0.5
0
-0.5
-1
-1.5
-2
-0.2
0
0.2
0.4
0.6
0.8
1
1.2

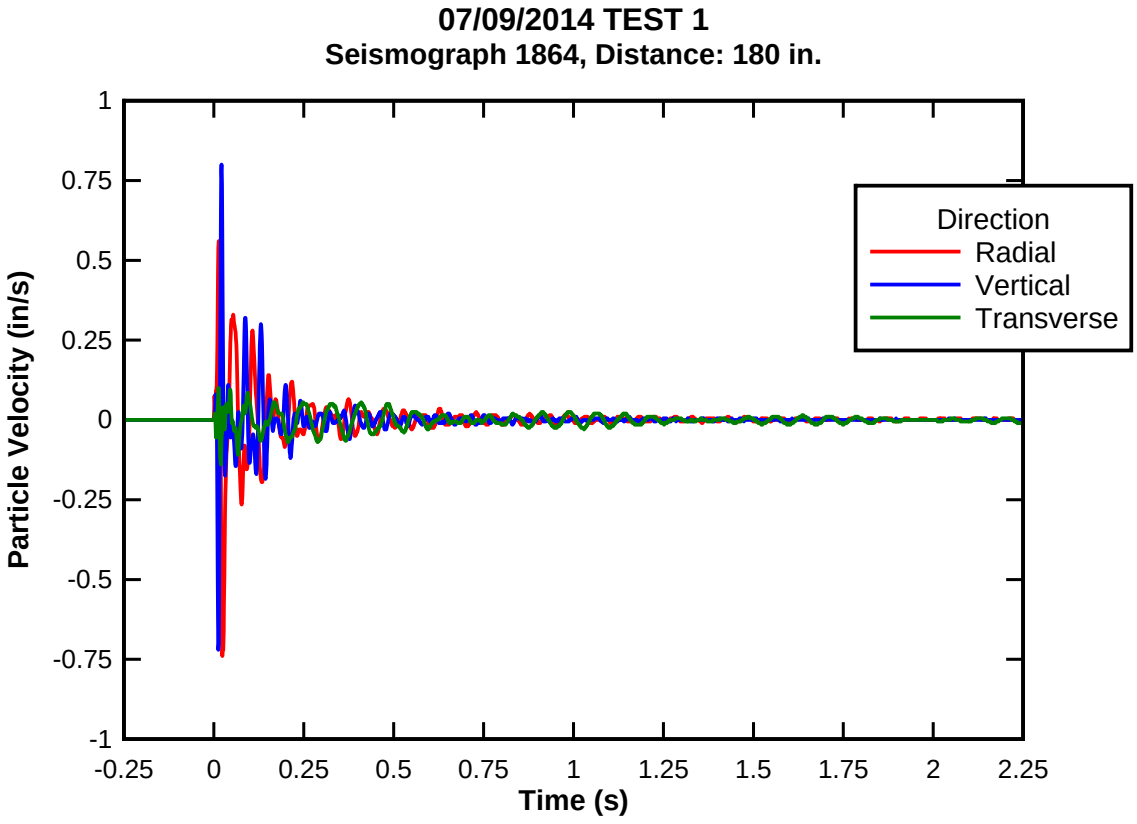
07/09/2014 TEST 1
Seismograph 1864, Distance: 180 in.
Particle Velocity (in/s)
Time (s)
Direction
Radial
Vertical
Transverse
1
0.75
0.5
0.25
0
-0.25
-0.5
-0.75
-1
-0.25
0
0.25
0.5
0.75
1
1.25
1.5
1.75
2
2.25

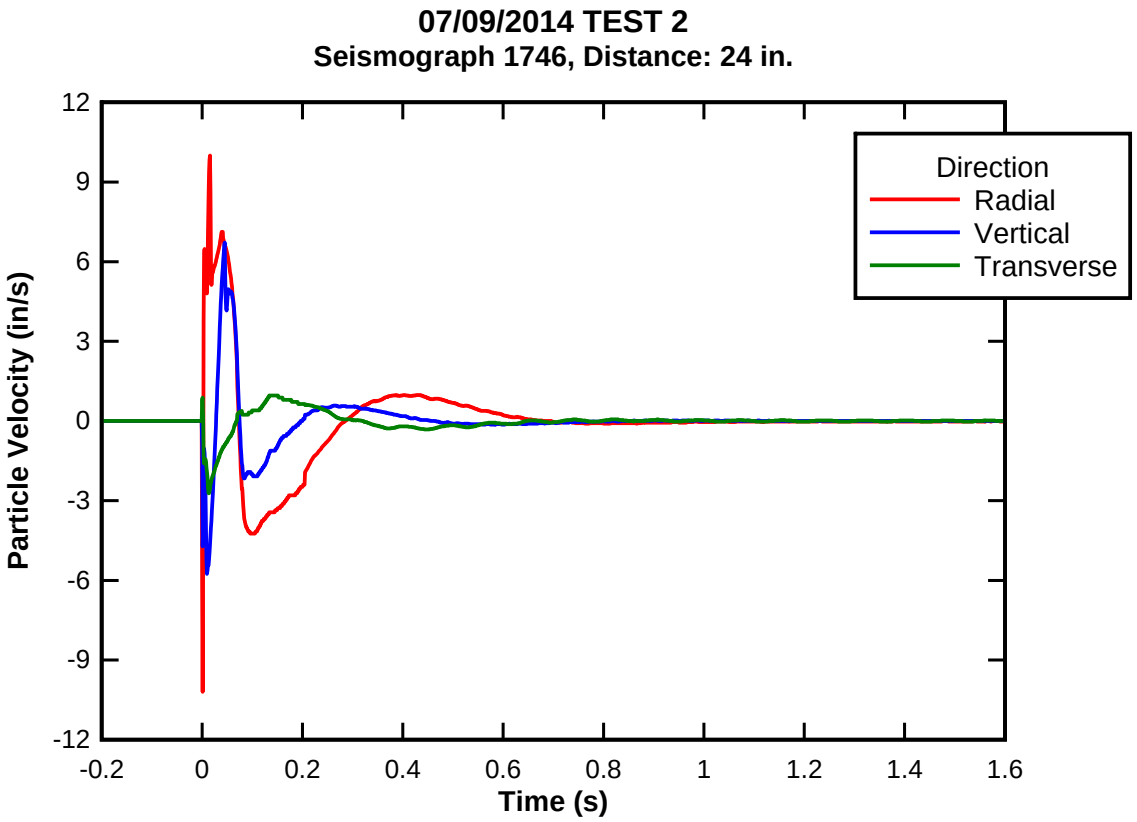
07/09/2014 TEST 2
Seismograph 1746, Distance: 24 in.
Particle Velocity (in/s)
Time (s)
Direction
Radial
Vertical
Transverse
12
9
6
3
0
-3
-6
-9
-12
-0.2
0
0.2
0.4
0.6
0.8
1
1.2
1.4
1.6

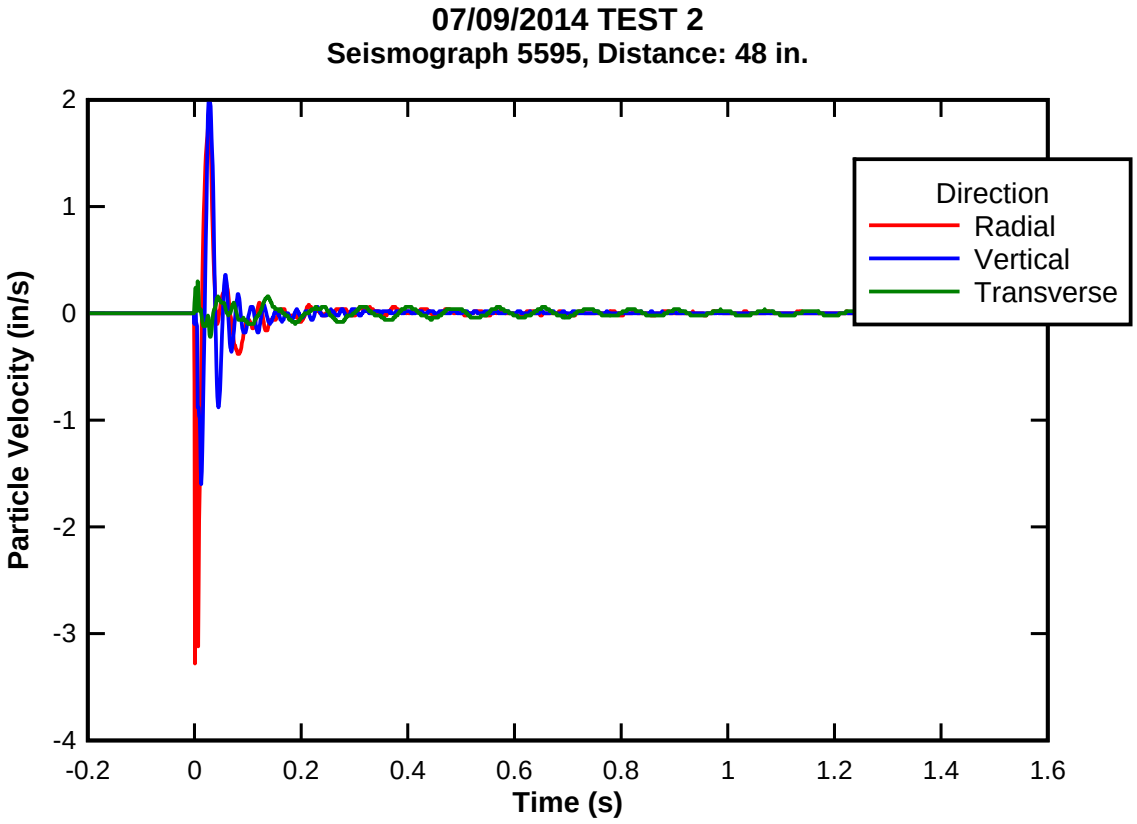
07/09/2014 TEST 2
Seismograph 5595, Distance: 48 in.
Particle Velocity (in/s)
Time (s)
Direction
Radial
Vertical
Transverse
2
1
0
-1
-2
-3
-4
-0.2
0
0.2
0.4
0.6
0.8
1
1.2
1.4
1.6

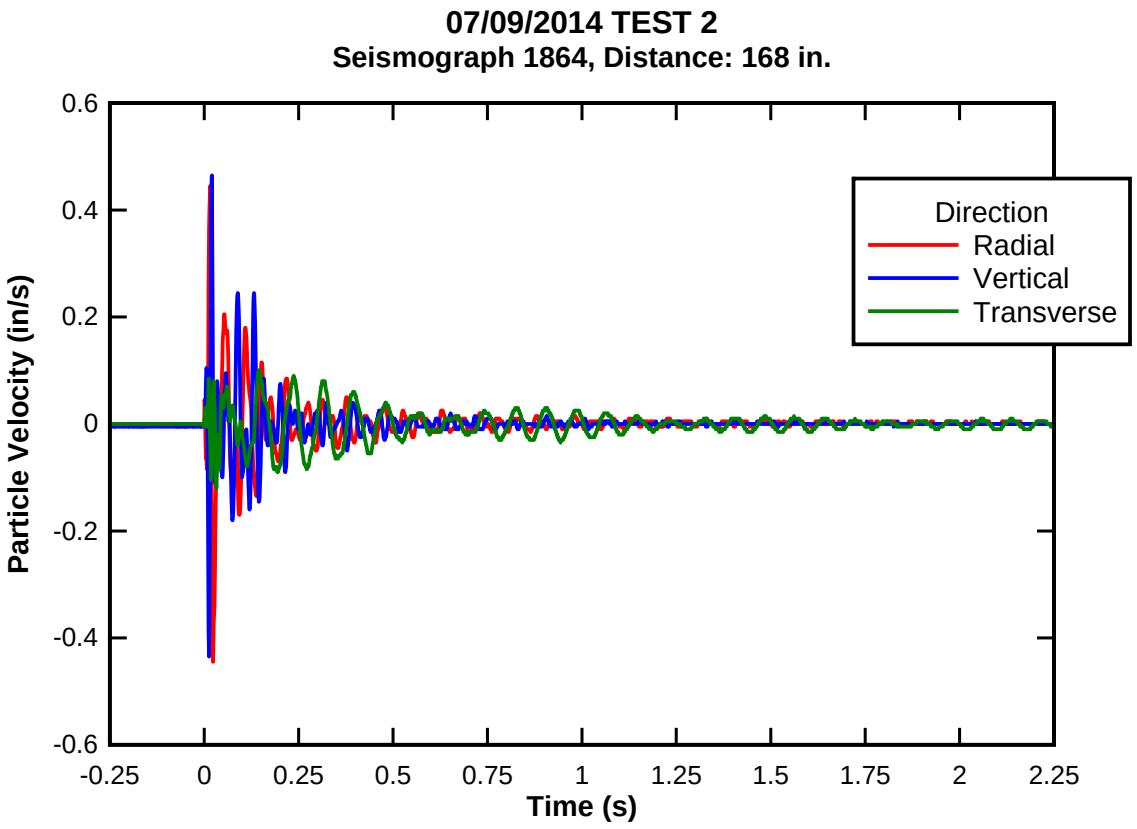
07/09/2014 TEST 2
Seismograph 1864, Distance: 168 in.
Particle Velocity (in/s)
Time (s)
Direction
Radial
Vertical
Transverse
0.6
0.4
0.2
0
-0.2
-0.4
-0.6
-0.25
0
0.25
0.5
0.75
1
1.25
1.5
1.75
2
2.25

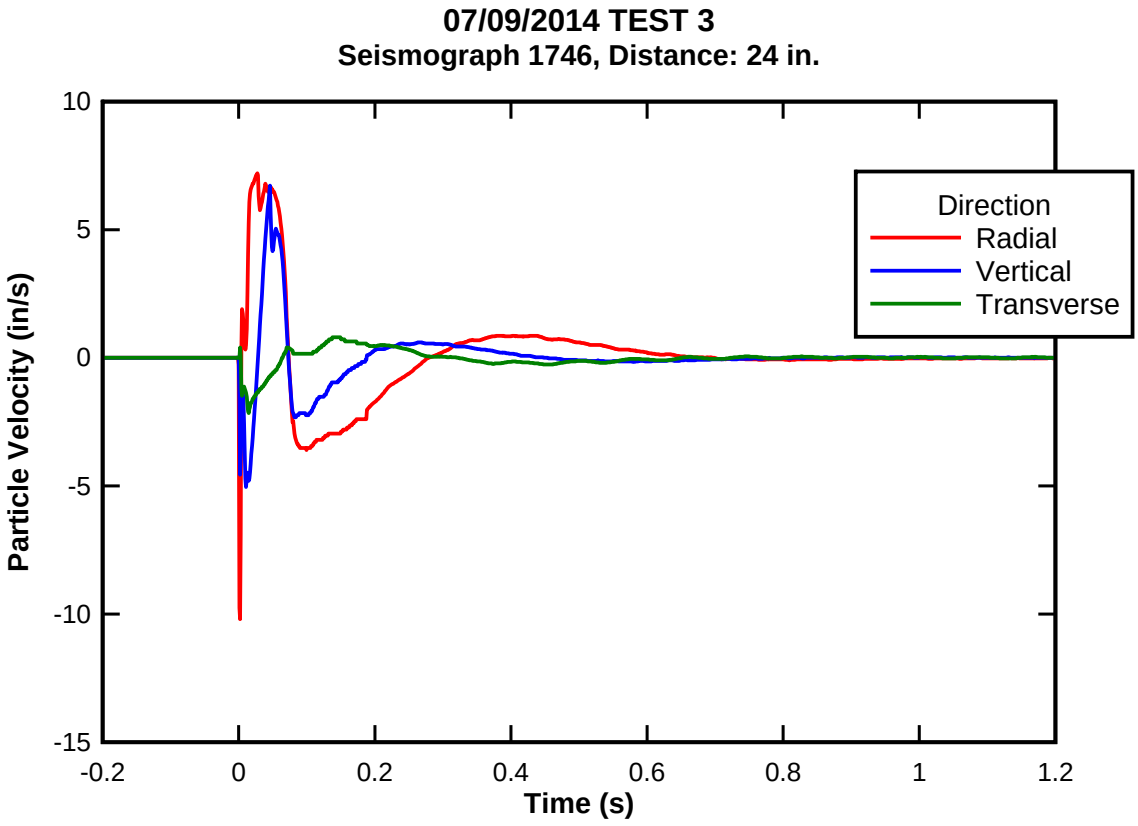
07/09/2014 TEST 3
Seismograph 1746, Distance: 24 in.
Particle Velocity (in/s)
Time (s)
Direction
Radial
Vertical
Transverse
10
5
0
-5
-10
-15
-0.2
0
0.2
0.4
0.6
0.8
1
1.2

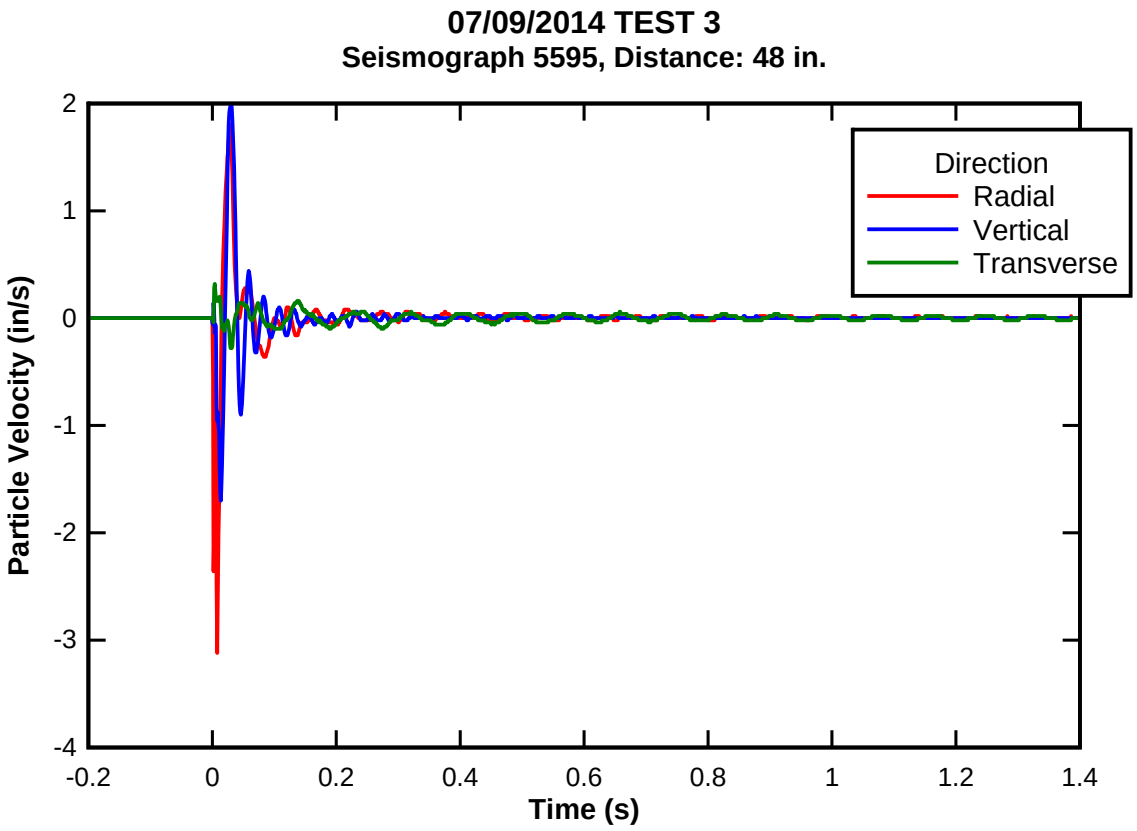
07/09/2014 TEST 3
Seismograph 5595, Distance: 48 in.
Particle Velocity (in/s)
Time (s)
Direction
Radial
Vertical
Transverse
2
1
0
-1
-2
-3
-4
-0.2
0
0.2
0.4
0.6
0.8
1
1.2
1.4

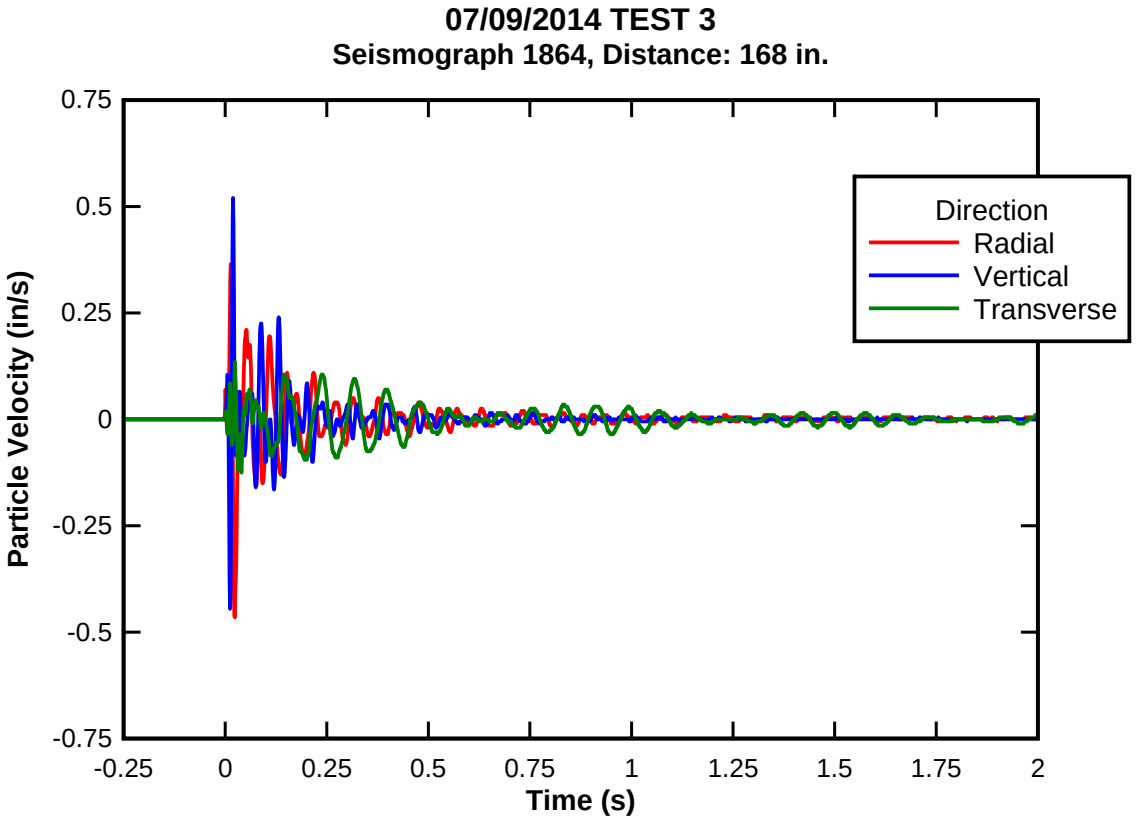
07/09/2014 TEST 3
Seismograph 1864, Distance: 168 in.
Particle Velocity (in/s)
Time (s)
Direction
Radial
Vertical
Transverse
0.75
0.5
0.25
0
-0.25
-0.5
-0.75
-0.25
0
0.25
0.5
0.75
1
1.25
1.5
1.75
2

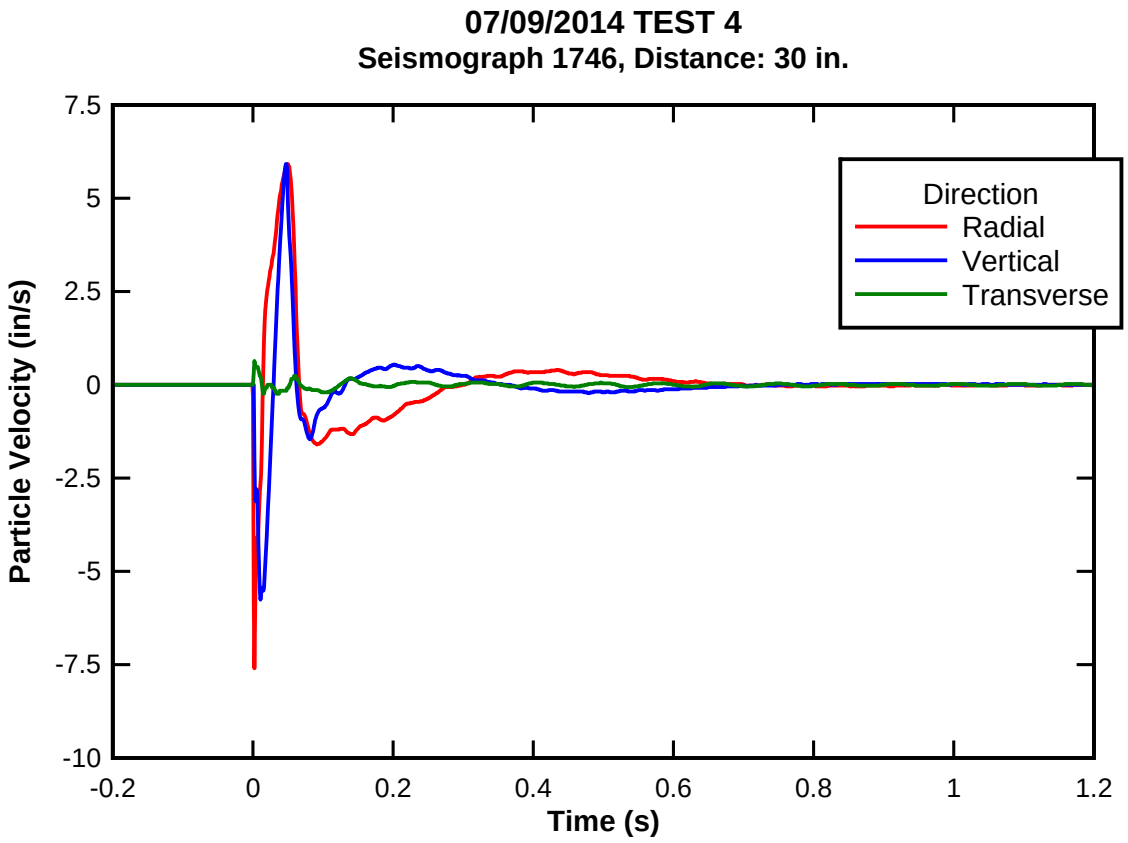
07/09/2014 TEST 4
Seismograph 1746, Distance: 30 in.
Particle Velocity (in/s)
Time (s)
Direction
Radial
Vertical
Transverse
7.5
5
2.5
0
-2.5
-5
-7.5
-10
-0.2
0
0.2
0.4
0.6
0.8
1
1.2

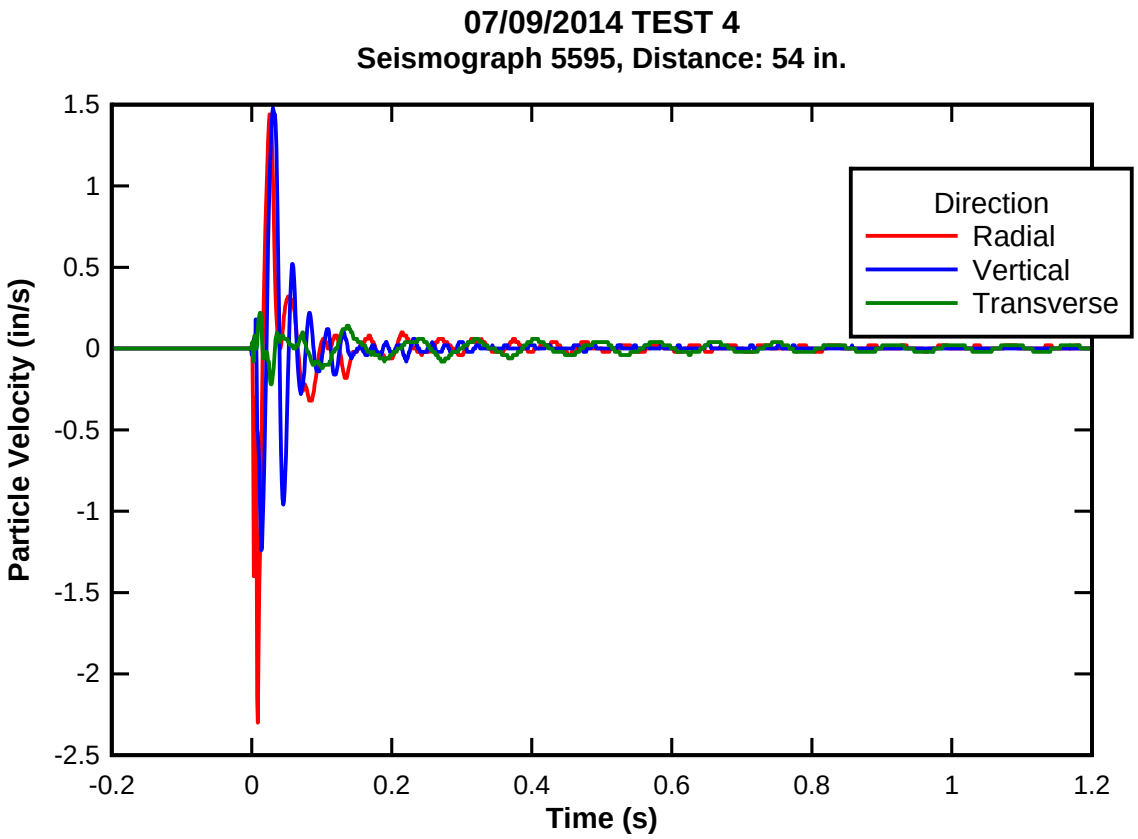
07/09/2014 TEST 4
Seismograph 5595, Distance: 54 in.
Particle Velocity (in/s)
Time (s)
Direction
Radial
Vertical
Transverse
1.5
1
0.5
0
-0.5
-1
-1.5
-2
-2.5
-0.2
0
0.2
0.4
0.6
0.8
1
1.2

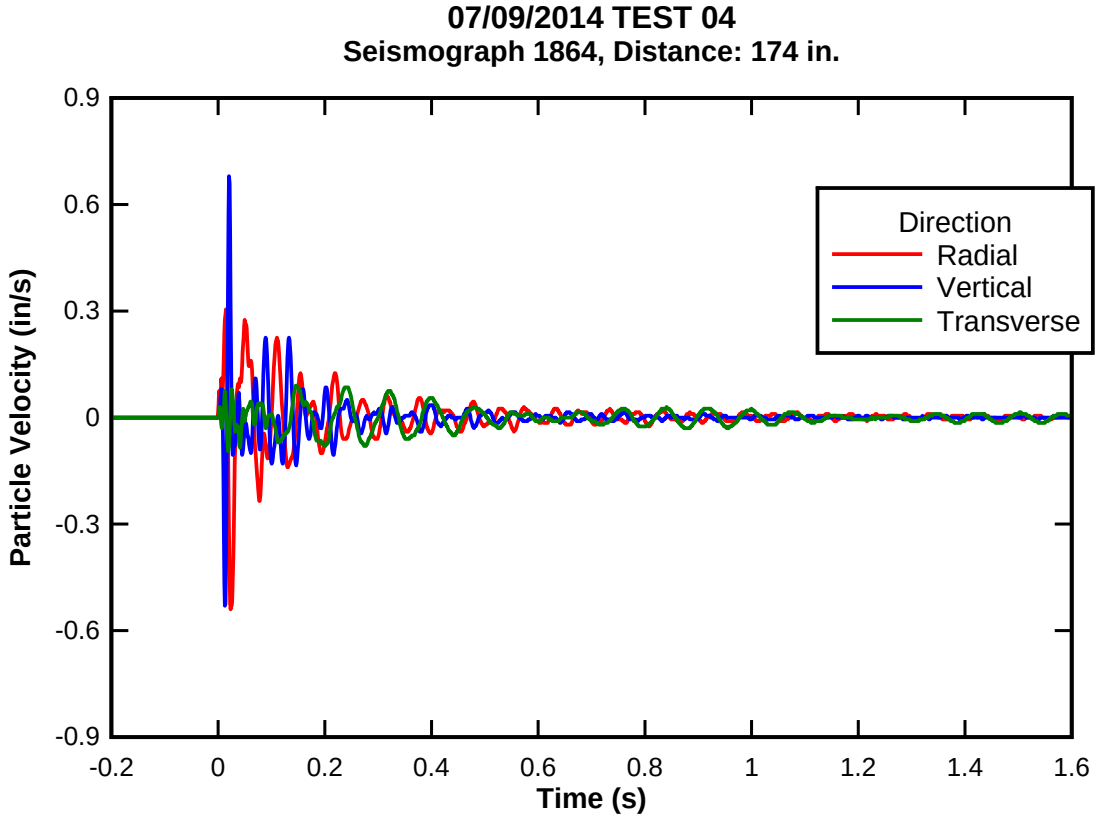
07/09/2014 TEST 04
Seismograph 1864, Distance: 174 in.
Particle Velocity (in/s)
Time (s)
Direction
Radial
Vertical
Transverse
0.9
0.6
0.3
0
-0.3
-0.6
-0.9
-0.2
0
0.2
0.4
0.6
0.8
1
1.2
1.4
1.6

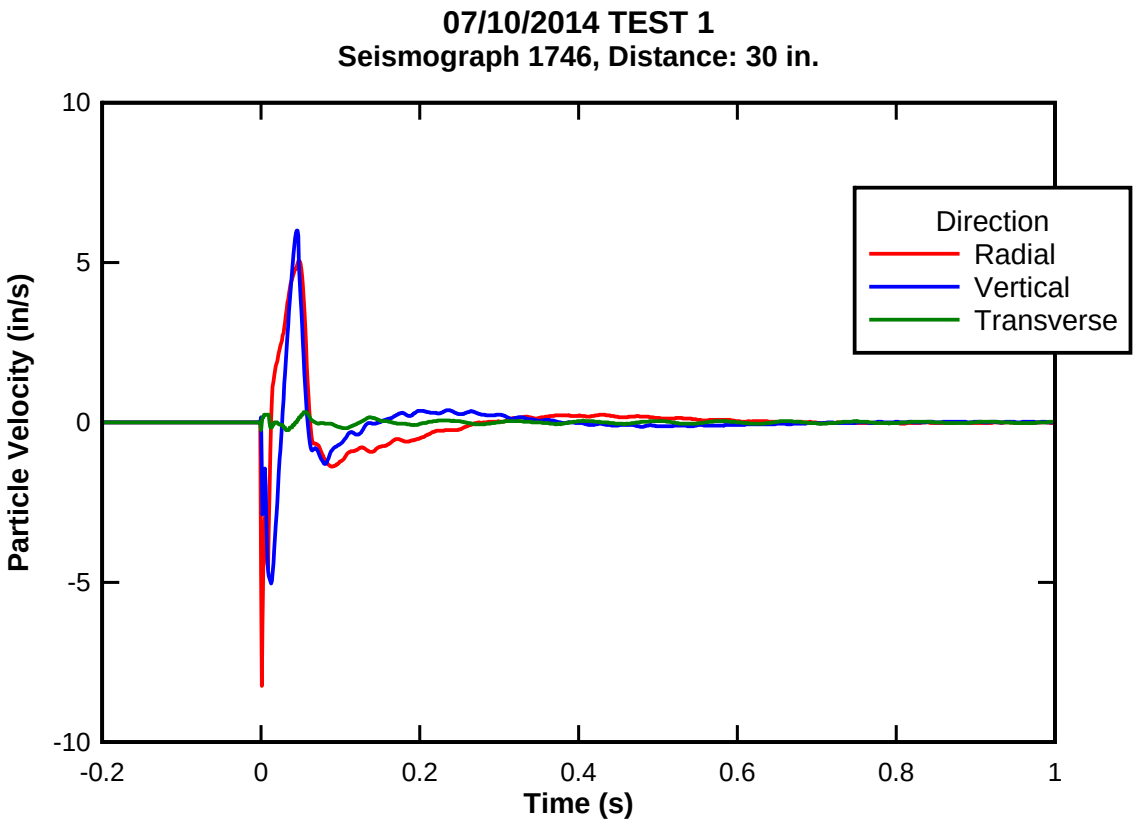
07/10/2014 TEST 1
Seismograph 1746, Distance: 30 in.
Particle Velocity (in/s)
Time (s)
Direction
Radial
Vertical
Transverse
10
5
0
-5
-10
-0.2
0
0.2
0.4
0.6
0.8
1

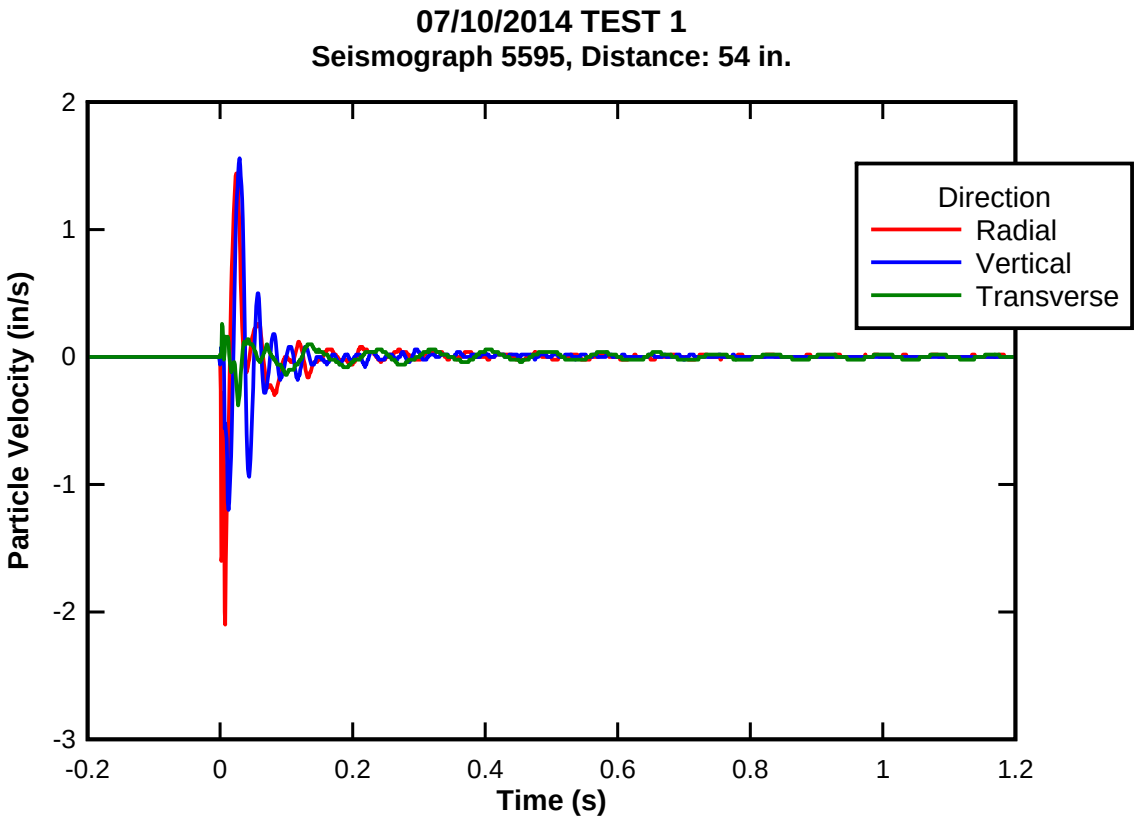
07/10/2014 TEST 1
Seismograph 5595, Distance: 54 in.
Particle Velocity (in/s)
Time (s)
Direction
Radial
Vertical
Transverse
2
1
0
-1
-2
-3
-0.2
0
0.2
0.4
0.6
0.8
1
1.2

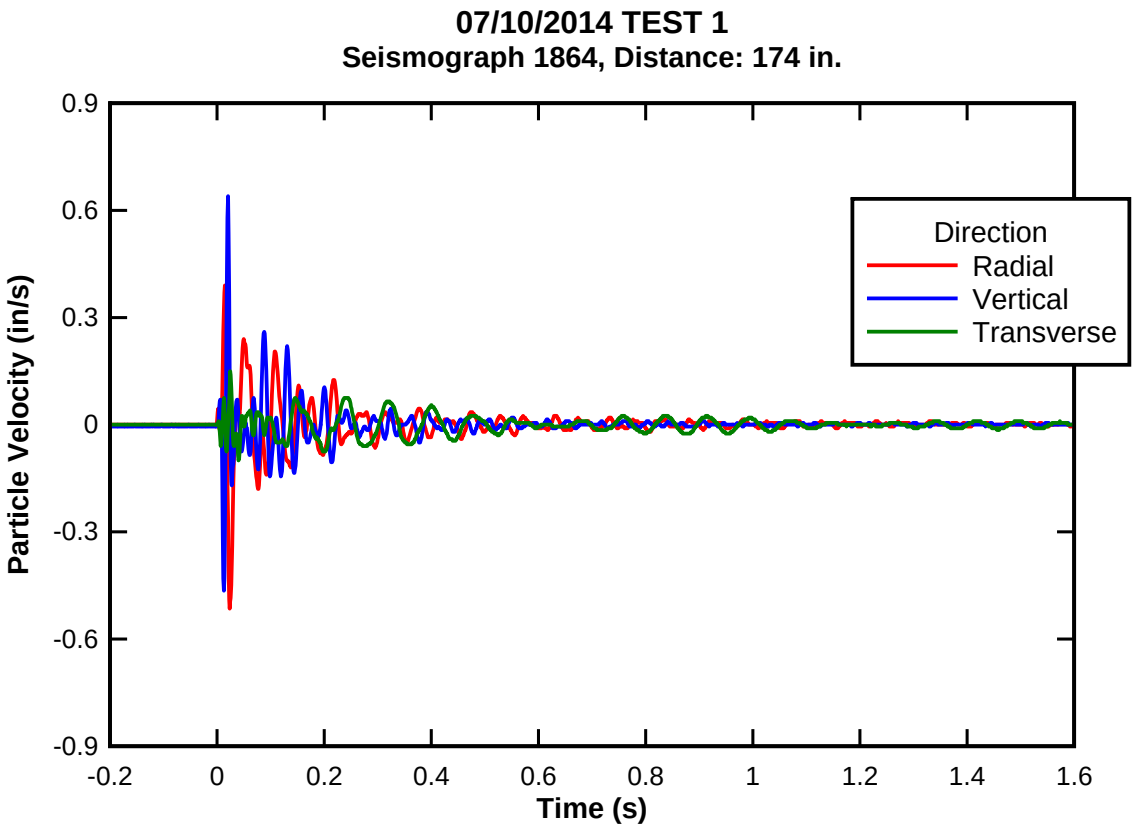
07/10/2014 TEST 1
Seismograph 1864, Distance: 174 in.
Particle Velocity (in/s)
Time (s)
Direction
Radial
Vertical
Transverse
0.9
0.6
0.3
0
-0.3
-0.6
-0.9
-0.2
0
0.2
0.4
0.6
0.8
1
1.2
1.4
1.6

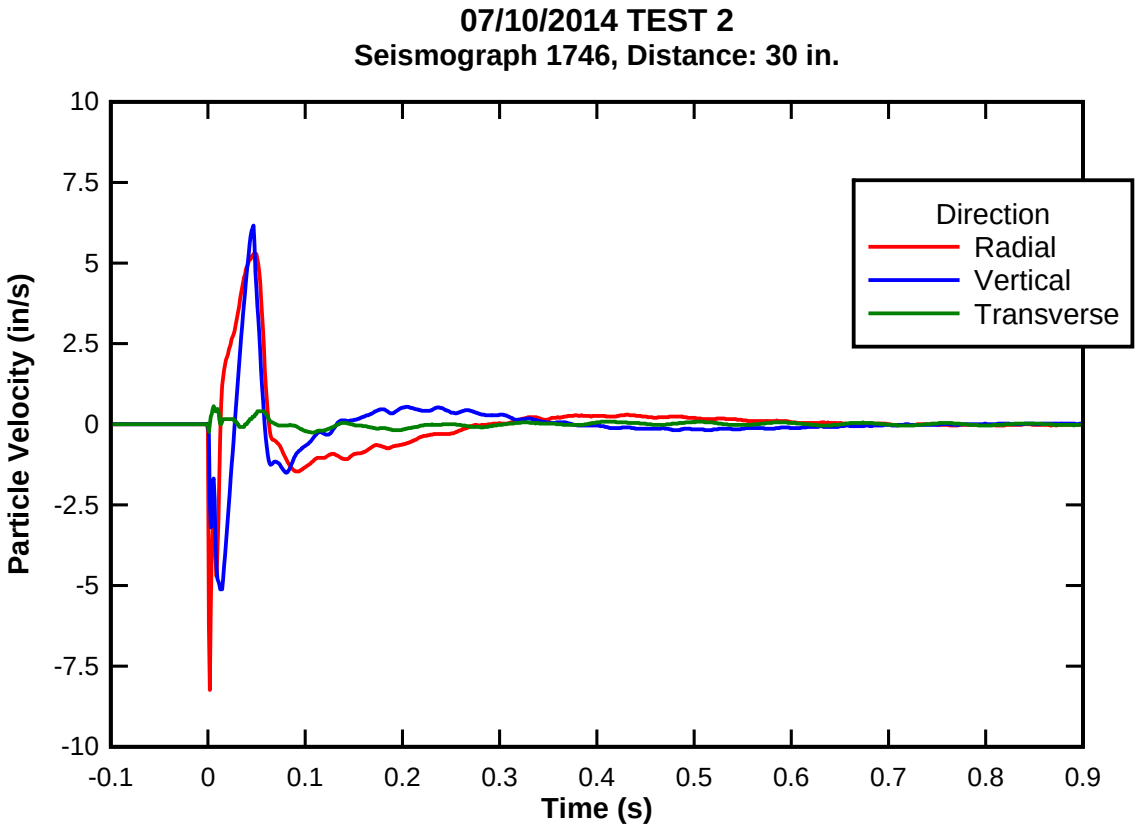
07/10/2014 TEST 2
Seismograph 1746, Distance: 30 in.
Particle Velocity (in/s)
Time (s)
Direction
Radial
Vertical
Transverse
10
7.5
5
2.5
0
-2.5
-5
-7.5
-10
-0.1
0
0.1
0.2
0.3
0.4
0.5
0.6
0.7
0.8
0.9

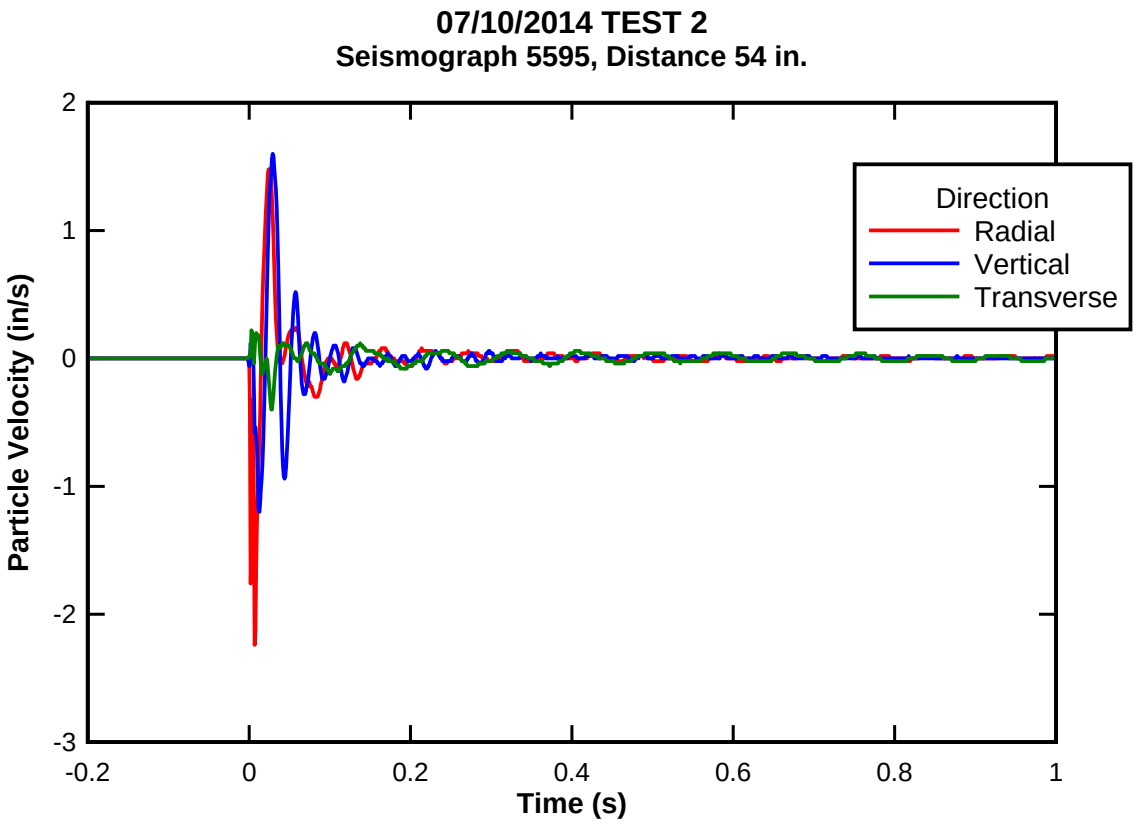
07/10/2014 TEST 2
Seismograph 5595, Distance 54 in.
Particle Velocity (in/s)
Time (s)
Direction
Radial
Vertical
Transverse
2
1
0
-1
-2
-3
-0.2
0
0.2
0.4
0.6
0.8
1

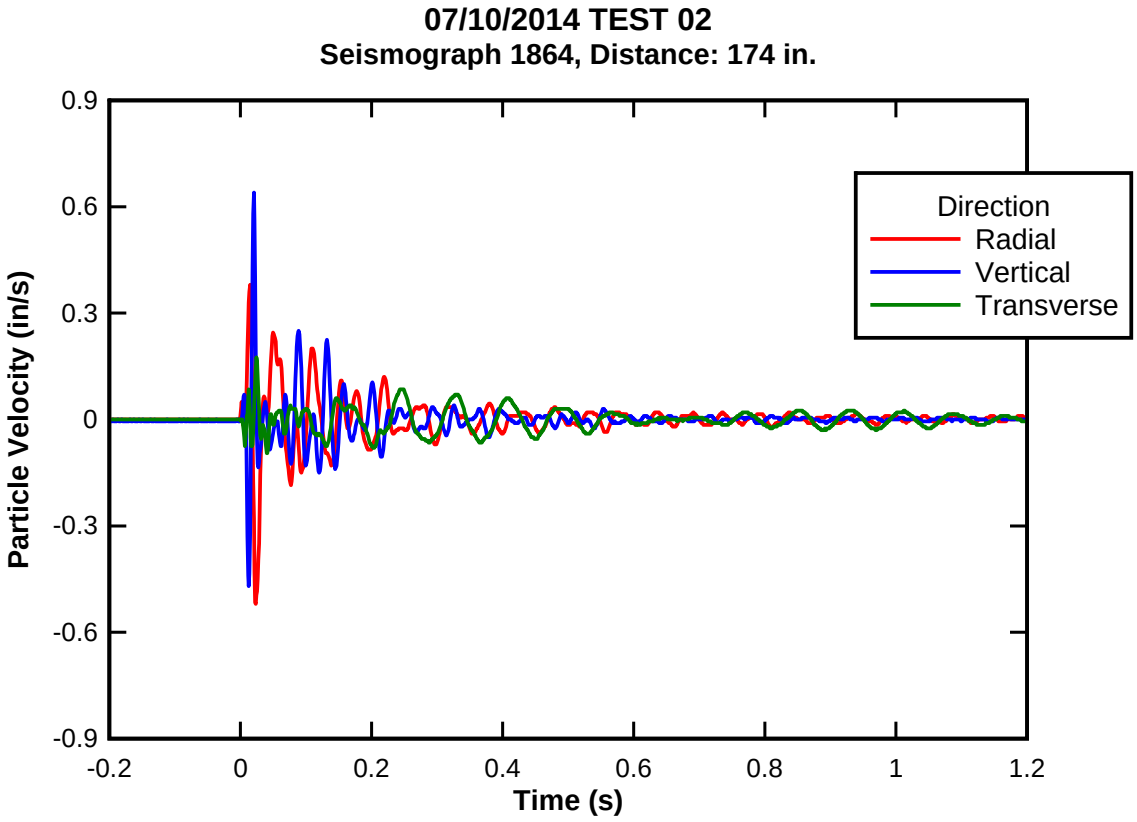
07/10/2014 TEST 02
Seismograph 1864, Distance: 174 in.
Particle Velocity (in/s)
Time (s)
Direction
Radial
Vertical
Transverse
0.9
0.6
0.3
0
-0.3
-0.6
-0.9
-0.2
0
0.2
0.4
0.6
0.8
1
1.2

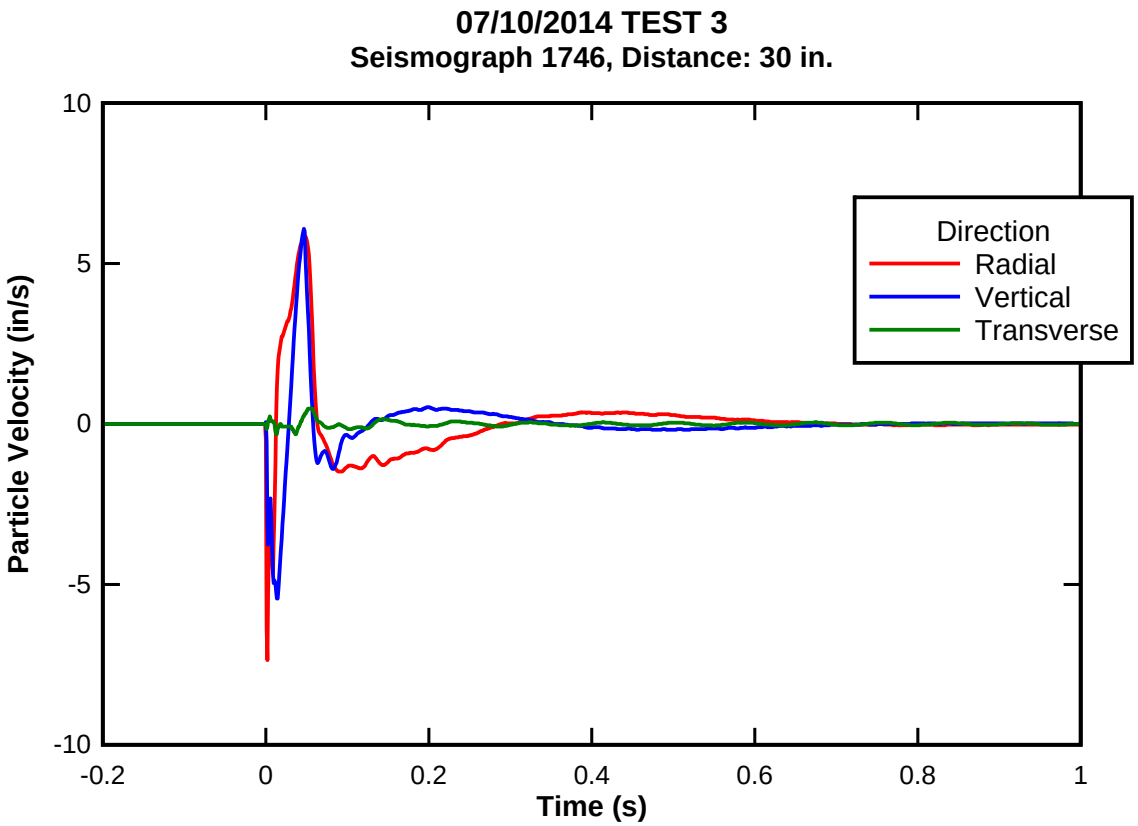
07/10/2014 TEST 3
Seismograph 1746, Distance: 30 in.
Particle Velocity (in/s)
Time (s)
Direction
Radial
Vertical
Transverse
10
5
0
-5
-10
-0.2
0
0.2
0.4
0.6
0.8
1

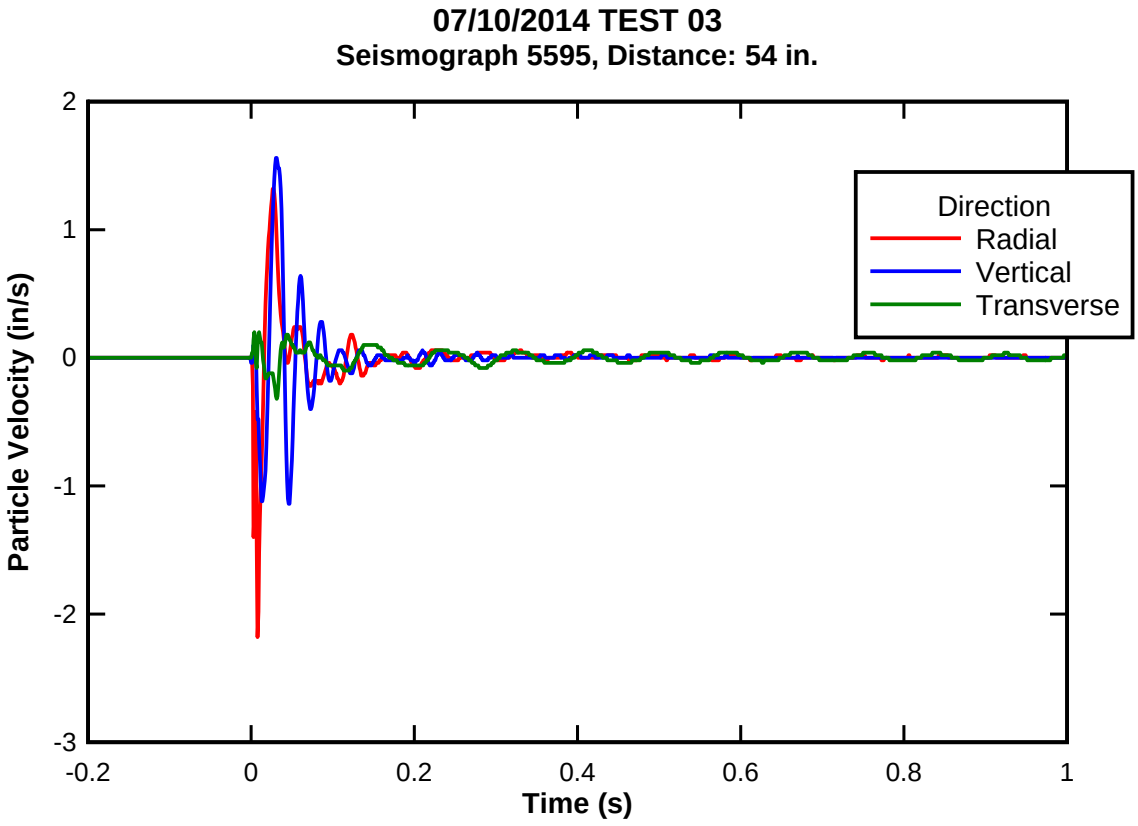
07/10/2014 TEST 03
Seismograph 5595, Distance: 54 in.
Particle Velocity (in/s)
Time (s)
Direction
Radial
Vertical
Transverse
2
1
0
-1
-2
-3
-0.2
0
0.2
0.4
0.6
0.8
1

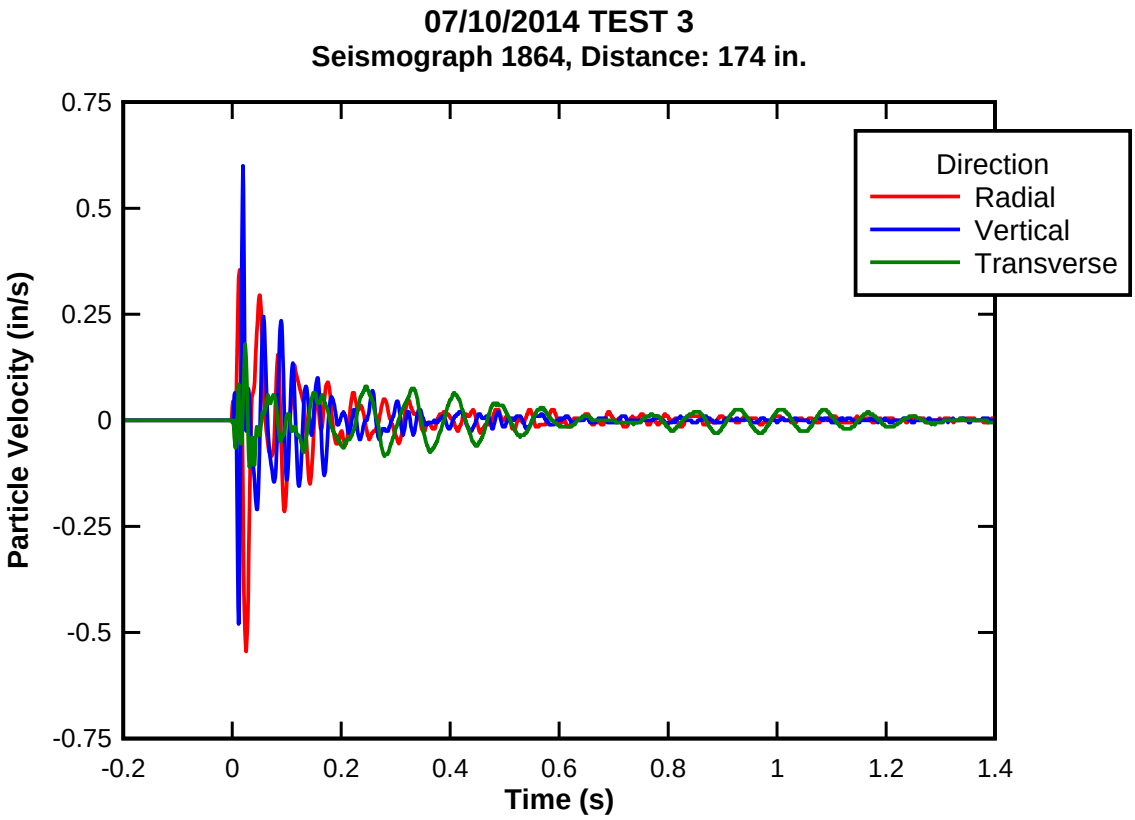
07/10/2014 TEST 3
Seismograph 1864, Distance: 174 in.
Particle Velocity (in/s)
Time (s)
Direction
Radial
Vertical
Transverse
0.75
0.5
0.25
0
-0.25
-0.5
-0.75
-0.2
0
0.2
0.4
0.6
0.8
1
1.2
1.4

APPENDIX B - SATURATED CONDITION SEISMOGRAPH DATA

RADIAL PPV, SATURATED CONDITIONS

Date	Test	Seismograph No.	Charge (g)	Charge (kg)	Charge (lb)	TNT Equivalency (kg)	TNT Equivalency (lb)	Distance to charge (in)	Distance to charge (ft)	Distance to charge (m)	TNT Eq. SD (m/kg^⅓)	TNT Eq. SD (ft/lb^⅓)	PPV (in/s)	PPV (m/s)
1/19/2015	1	1814	20	0.020	0.044	0.030	0.066	18	1.5	0.46	1.47	3.71	9.28	63.98
1/19/2015	1	5595	20	0.020	0.044	0.030	0.066	36	3.0	0.91	2.26	7.42	4.72	32.54
1/19/2015	1	4906	20	0.020	0.044	0.030	0.066	174	14.5	4.42	10.93	35.85	0.64	4.41
1/19/2015	2	1814	20	0.020	0.044	0.030	0.066	18	1.5	0.46	1.13	3.71	MAXED	MAXED
1/19/2015	2	5595	20	0.020	0.044	0.030	0.066	36	3.0	0.91	2.26	7.42	MAXED	MAXED
1/19/2015	2	4906	20	0.020	0.044	0.030	0.066	174	14.5	4.42	10.93	35.85	NO DATA	NO DATA
1/19/2015	3	1814	20	0.020	0.044	0.030	0.066	18	1.5	0.46	1.13	3.71	MAXED	MAXED
1/19/2015	3	5595	20	0.020	0.044	0.030	0.066	36	3.0	0.91	2.26	7.42	MAXED	MAXED
1/19/2015	3	4906	20	0.020	0.044	0.030	0.066	174	14.5	4.42	10.93	35.85	0.88	6.07
1/19/2015	4	1814	20	0.020	0.044	0.030	0.066	18	1.5	0.46	1.47	3.71	9.60	66.19
1/19/2015	4	5595	20	0.020	0.044	0.030	0.066	36	3.0	0.91	2.26	7.42	MAXED	MAXED
1/19/2015	4	4906	20	0.020	0.044	0.030	0.066	174	14.5	4.42	10.93	35.85	0.88	6.07
1/19/2015	5	1814	20	0.020	0.044	0.030	0.066	18	1.5	0.46	1.13	3.71	MAXED	MAXED
1/19/2015	5	5595	20	0.020	0.044	0.030	0.066	36	3.0	0.91	2.26	7.42	MAXED	MAXED
1/19/2015	5	4906	20	0.020	0.044	0.030	0.066	174	14.5	4.42	10.93	35.85	0.98	6.76
1/22/2015	1	1814	20	0.020	0.044	0.030	0.066	13	1.1	0.33	1.06	2.68	MAXED	MAXED
1/22/2015	1	4906	20	0.020	0.044	0.030	0.066	31	2.6	0.79	1.95	6.39	MAXED	MAXED
1/22/2015	1	5595	20	0.020	0.044	0.030	0.066	169	14.1	4.29	10.61	34.82	1.48	10.20
1/22/2015	2	5595	20	0.020	0.044	0.030	0.066	13	1.1	0.33	0.82	2.68	MAXED	MAXED
1/22/2015	2	4906	20	0.020	0.044	0.030	0.066	31	2.6	0.79	1.95	6.39	MAXED	MAXED
1/22/2015	2	1814	20	0.020	0.044	0.030	0.066	169	14.1	4.29	10.61	34.82	1.00	6.89
1/22/2015	3	5595	20	0.020	0.044	0.030	0.066	13	1.1	0.33	0.82	2.68	MAXED	MAXED
1/22/2015	3	4906	20	0.020	0.044	0.030	0.066	31	2.6	0.79	1.95	6.39	MAXED	MAXED
1/22/2015	3	1814	20	0.020	0.044	0.030	0.066	169	14.1	4.29	10.61	34.82	1.12	7.72
1/22/2015	4	5595	20	0.020	0.044	0.030	0.066	13	1.1	0.33	1.06	2.68	MAXED	MAXED
1/22/2015	4	4906	20	0.020	0.044	0.030	0.066	31	2.6	0.79	1.95	6.39	MAXED	MAXED
1/22/2015	4	1814	20	0.020	0.044	0.030	0.066	169	14.1	4.29	10.61	34.82	1.22	8.41

TRANSVERSE PPV, SATURATED CONDITIONS

Date	Test	Seismograph No.	Charge (g)	Charge (kg)	Charge (lb)	TNT Equivalency (kg)	TNT Equivalency (lb)	Distance to charge (in)	Distance to charge (ft)	Distance to charge (m)	TNT Eq. SD (m/kg^⅓)	TNT Eq. SD (ft/lb^⅓)	PPV (in/s)	PPV (m/s)
1/19/2015	1	1814	20	0.020	0.044	0.030	0.066	18	1.5	0.46	1.47	3.71	7.92	54.61
1/19/2015	1	5595	20	0.020	0.044	0.030	0.066	36	3.0	0.91	2.26	7.42	1.60	11.03
1/19/2015	1	4906	20	0.020	0.044	0.030	0.066	174	14.5	4.42	10.93	35.85	0.21	1.45
1/19/2015	2	1814	20	0.020	0.044	0.030	0.066	18	1.5	0.46	1.13	3.71	7.36	50.75
1/19/2015	2	5595	20	0.020	0.044	0.030	0.066	36	3.0	0.91	2.26	7.42	2.84	19.58
1/19/2015	2	4906	20	0.020	0.044	0.030	0.066	174	14.5	4.42	10.93	35.85	NO DATA	NO DATA
1/19/2015	3	1814	20	0.020	0.044	0.030	0.066	18	1.5	0.46	1.13	3.71	5.76	39.71
1/19/2015	3	5595	20	0.020	0.044	0.030	0.066	36	3.0	0.91	2.26	7.42	2.08	14.34
1/19/2015	3	4906	20	0.020	0.044	0.030	0.066	174	14.5	4.42	10.93	35.85	0.25	1.69
1/19/2015	4	1814	20	0.020	0.044	0.030	0.066	18	1.5	0.46	1.47	3.71	5.20	35.85
1/19/2015	4	5595	20	0.020	0.044	0.030	0.066	36	3.0	0.91	2.26	7.42	1.68	11.58
1/19/2015	4	4906	20	0.020	0.044	0.030	0.066	174	14.5	4.42	10.93	35.85	1.68	11.58
1/19/2015	5	1814	20	0.020	0.044	0.030	0.066	18	1.5	0.46	1.13	3.71	5.12	35.30
1/19/2015	5	5595	20	0.020	0.044	0.030	0.066	36	3.0	0.91	2.26	7.42	1.84	12.69
1/19/2015	5	4906	20	0.020	0.044	0.030	0.066	174	14.5	4.42	10.93	35.85	0.26	1.79
1/22/2015	1	1814	20	0.020	0.044	0.030	0.066	13	1.1	0.33	1.06	2.68	8.40	57.92
1/22/2015	1	4906	20	0.020	0.044	0.030	0.066	31	2.6	0.79	1.95	6.39	2.38	16.41
1/22/2015	1	5595	20	0.020	0.044	0.030	0.066	169	14.1	4.29	10.61	34.82	1.16	8.00
1/22/2015	2	5595	20	0.020	0.044	0.030	0.066	13	1.1	0.33	0.82	2.68	MAXED	MAXED
1/22/2015	2	4906	20	0.020	0.044	0.030	0.066	31	2.6	0.79	1.95	6.39	MAXED	MAXED
1/22/2015	2	1814	20	0.020	0.044	0.030	0.066	169	14.1	4.29	10.61	34.82	0.22	1.52
1/22/2015	3	5595	20	0.020	0.044	0.030	0.066	13	1.1	0.33	0.82	2.68	MAXED	MAXED
1/22/2015	3	4906	20	0.020	0.044	0.030	0.066	31	2.6	0.79	1.95	6.39	MAXED	MAXED
1/22/2015	3	1814	20	0.020	0.044	0.030	0.066	169	14.1	4.29	10.61	34.82	0.32	2.21
1/22/2015	4	5595	20	0.020	0.044	0.030	0.066	13	1.1	0.33	1.06	2.68	MAXED	MAXED
1/22/2015	4	4906	20	0.020	0.044	0.030	0.066	31	2.6	0.79	1.95	6.39	MAXED	MAXED
1/22/2015	4	1814	20	0.020	0.044	0.030	0.066	169	14.1	4.29	10.61	34.82	0.70	4.83

VERTICAL PPV, SATURATED CONDITIONS														
Date	Test	Seismograph No.	Charge (g)	Charge (kg)	Charge (lb)	TNT Equivalency (kg)	TNT Equivalency (lb)	Distance to charge (in)	Distance to charge (ft)	Distance to charge (m)	TNT Eq. SD (m/kg^⅓)	TNT Eq. SD (ft/lb^⅓)	PPV (in/s)	PPV (m/s)
1/19/2015	1	1814	20	0.020	0.044	0.030	0.066	18	1.5	0.46	1.47	3.71	9.44	65.09
1/19/2015	1	5595	20	0.020	0.044	0.030	0.066	36	3.0	0.91	2.26	7.42	MAXED	MAXED
1/19/2015	1	4906	20	0.020	0.044	0.030	0.066	174	14.5	4.42	10.93	35.85	0.62	4.27
1/19/2015	2	1814	20	0.020	0.044	0.030	0.066	18	1.5	0.46	1.13	3.71	MAXED	MAXED
1/19/2015	2	5595	20	0.020	0.044	0.030	0.066	36	3.0	0.91	2.26	7.42	MAXED	MAXED
1/19/2015	2	4906	20	0.020	0.044	0.030	0.066	174	14.5	4.42	10.93	35.85	NO DATA	NO DATA
1/19/2015	3	1814	20	0.020	0.044	0.030	0.066	18	1.5	0.46	1.13	3.71	9.36	64.53
1/19/2015	3	5595	20	0.020	0.044	0.030	0.066	36	3.0	0.91	2.26	7.42	MAXED	MAXED
1/19/2015	3	4906	20	0.020	0.044	0.030	0.066	174	14.5	4.42	10.93	35.85	0.90	6.21
1/19/2015	4	1814	20	0.020	0.044	0.030	0.066	18	1.5	0.46	1.47	3.71	9.44	65.09
1/19/2015	4	5595	20	0.020	0.044	0.030	0.066	36	3.0	0.91	2.26	7.42	MAXED	MAXED
1/19/2015	4	4906	20	0.020	0.044	0.030	0.066	174	14.5	4.42	10.93	35.85	0.84	5.79
1/19/2015	5	1814	20	0.020	0.044	0.030	0.066	18	1.5	0.46	1.13	3.71	MAXED	MAXED
1/19/2015	5	5595	20	0.020	0.044	0.030	0.066	36	3.0	0.91	2.26	7.42	MAXED	MAXED
1/19/2015	5	4906	20	0.020	0.044	0.030	0.066	174	14.5	4.42	10.93	35.85	0.96	6.62
1/22/2015	1	1814	20	0.020	0.044	0.030	0.066	13	1.1	0.33	1.06	2.68	9.04	62.33
1/22/2015	1	4906	20	0.020	0.044	0.030	0.066	31	2.6	0.79	1.95	6.39	MAXED	MAXED
1/22/2015	1	5595	20	0.020	0.044	0.030	0.066	169	14.1	4.29	10.61	34.82	1.16	8.00
1/22/2015	2	5595	20	0.020	0.044	0.030	0.066	13	1.1	0.33	0.82	2.68	MAXED	MAXED
1/22/2015	2	4906	20	0.020	0.044	0.030	0.066	31	2.6	0.79	1.95	6.39	MAXED	MAXED
1/22/2015	2	1814	20	0.020	0.044	0.030	0.066	169	14.1	4.29	10.61	34.82	0.78	5.38
1/22/2015	3	5595	20	0.020	0.044	0.030	0.066	13	1.1	0.33	0.82	2.68	MAXED	MAXED
1/22/2015	3	4906	20	0.020	0.044	0.030	0.066	31	2.6	0.79	1.95	6.39	MAXED	MAXED
1/22/2015	3	1814	20	0.020	0.044	0.030	0.066	169	14.1	4.29	10.61	34.82	0.94	6.48
1/22/2015	4	5595	20	0.020	0.044	0.030	0.066	13	1.1	0.33	1.06	2.68	MAXED	MAXED
1/22/2015	4	4906	20	0.020	0.044	0.030	0.066	31	2.6	0.79	1.95	6.39	MAXED	MAXED
1/22/2015	4	1814	20	0.020	0.044	0.030	0.066	169	14.1	4.29	10.61	34.82	0.96	6.62

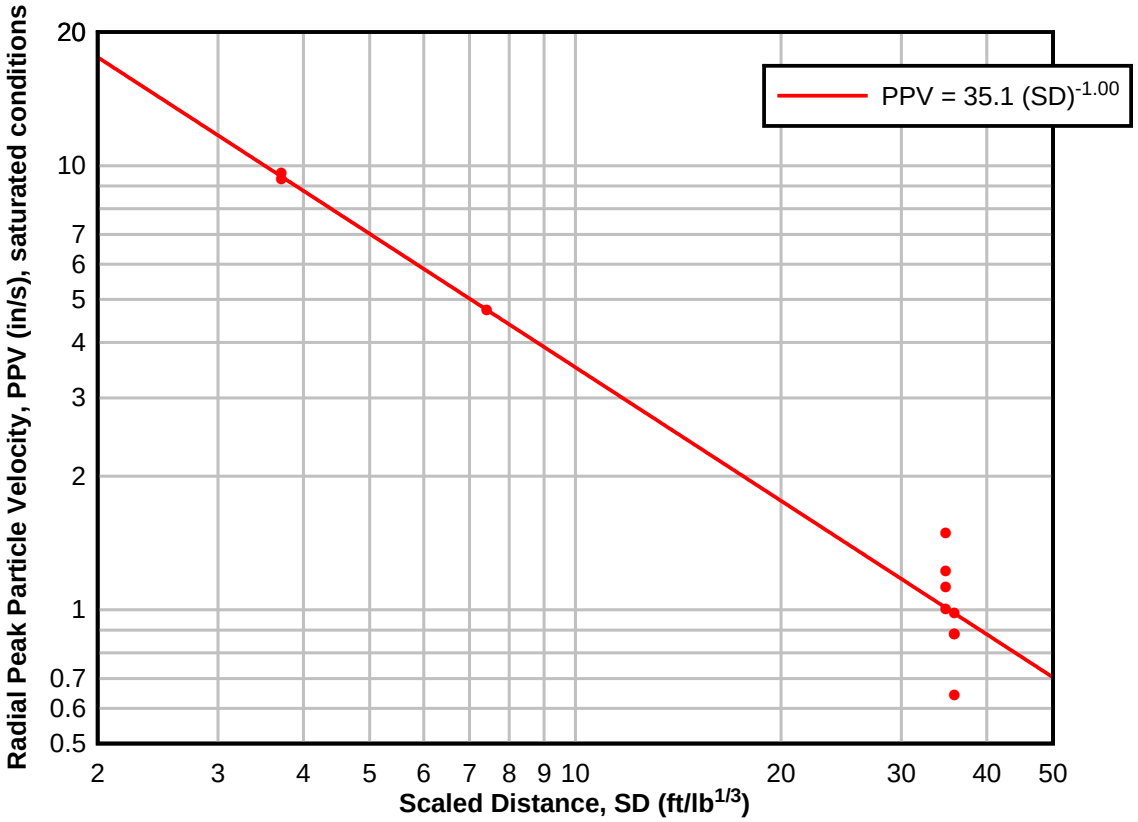

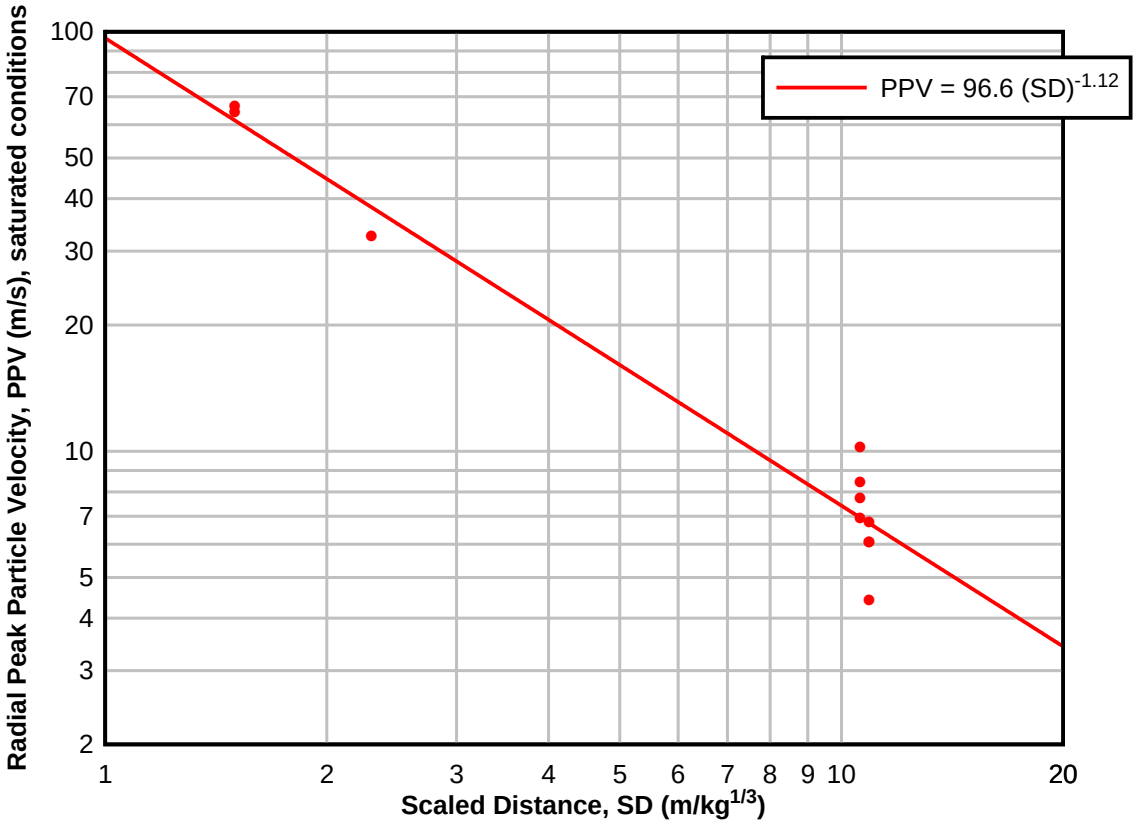
Radial Peak Particle Velocity, PPV (m/s), saturated conditions
100
70
50
40
30
20
10
7
5
4
3
2
1
2
3
4
5
6
7
8
9
10
20
Scaled Distance, SD (m/kg1/3)
PPV = 96.6 (SD)-1.12

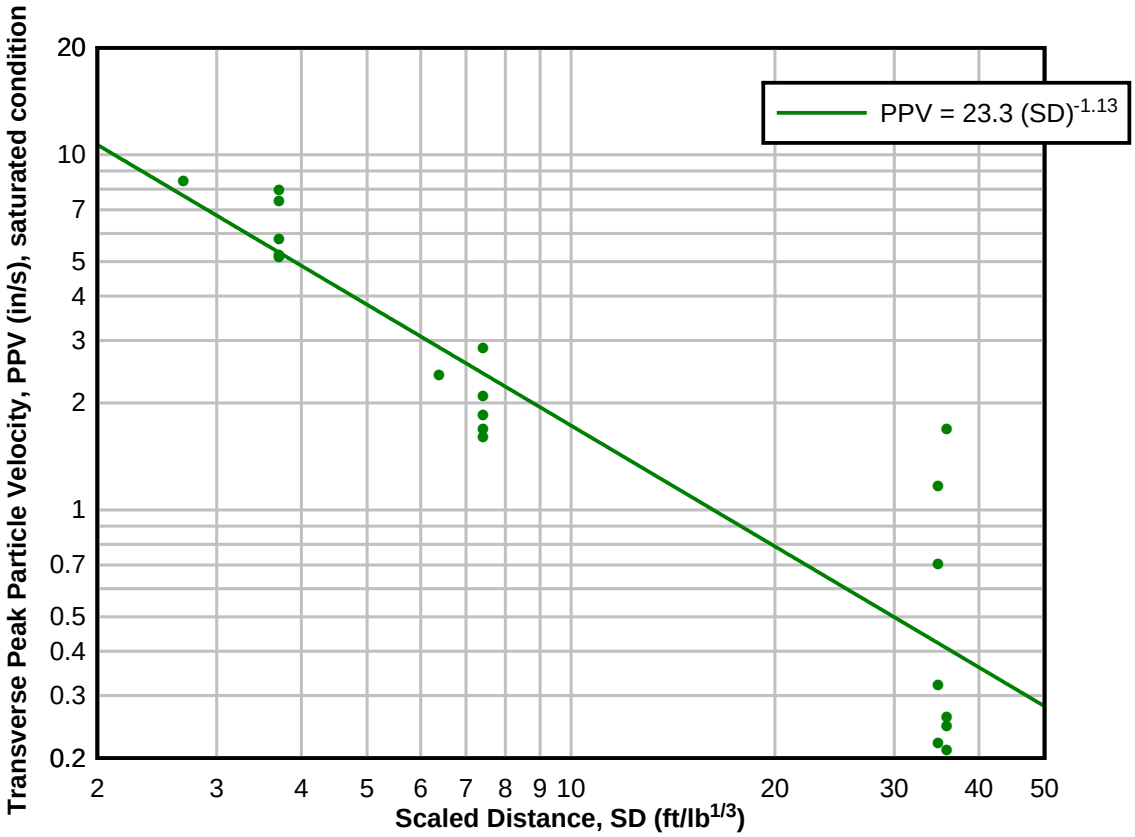
Transverse Peak Particle Velocity, PPV (in/s), saturated condition
20
10
7
5
4
3
2
1
0.7
0.5
0.4
0.3
0.2
2
3
4
5
6
7
8
9
10
20
30
40
50
Scaled Distance, SD (ft/lb1/3)
PPV = 23.3 (SD)-1.13

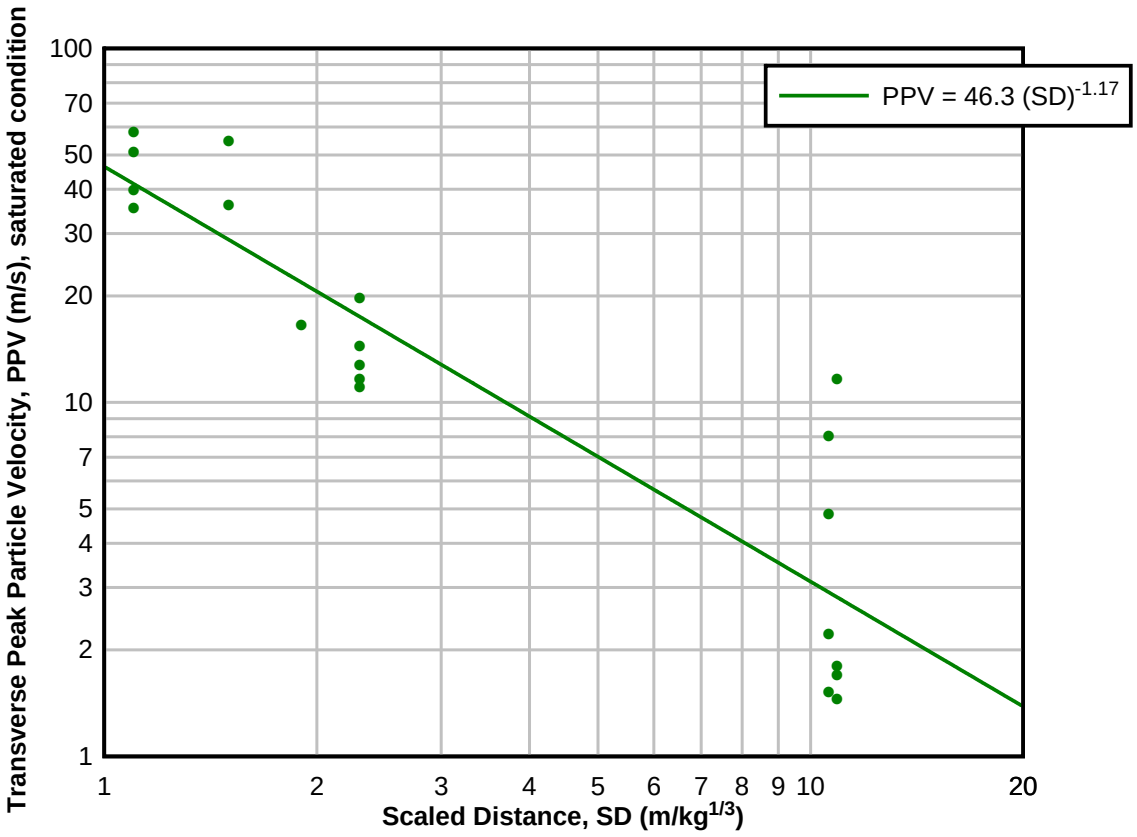
Transverse Peak Particle Velocity, PPV (m/s), saturated condition
100
70
50
40
30
20
10
7
5
4
3
2
1
1
2
3
4
5
6
7
8
9
10
20
Scaled Distance, SD (m/kg1/3)
PPV = 46.3 (SD)-1.17

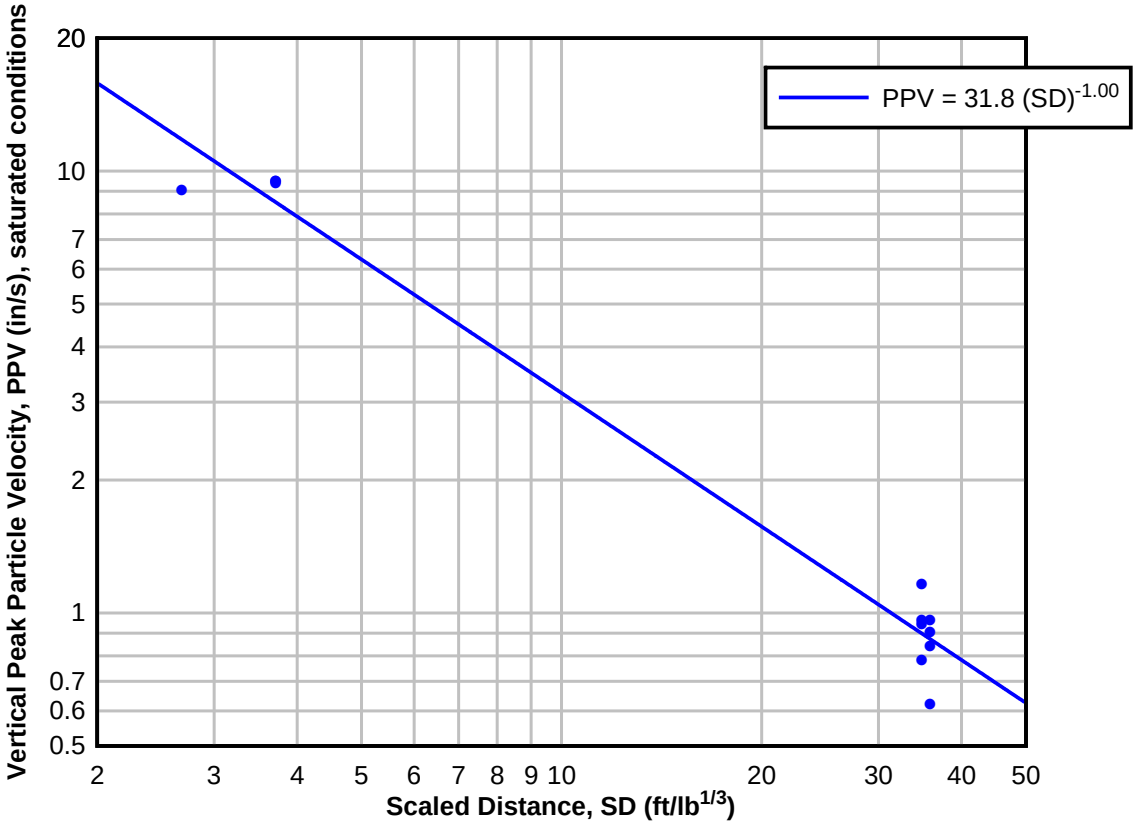
Vertical Peak Particle Velocity, PPV (in/s), saturated conditions
20
10
7
6
5
4
3
2
1
0.7
0.6
0.5
2
3
4
5
6
7
8
9
10
20
30
40
50
Scaled Distance, SD (ft/lb1/3)
PPV = 31.8 (SD)-1.00

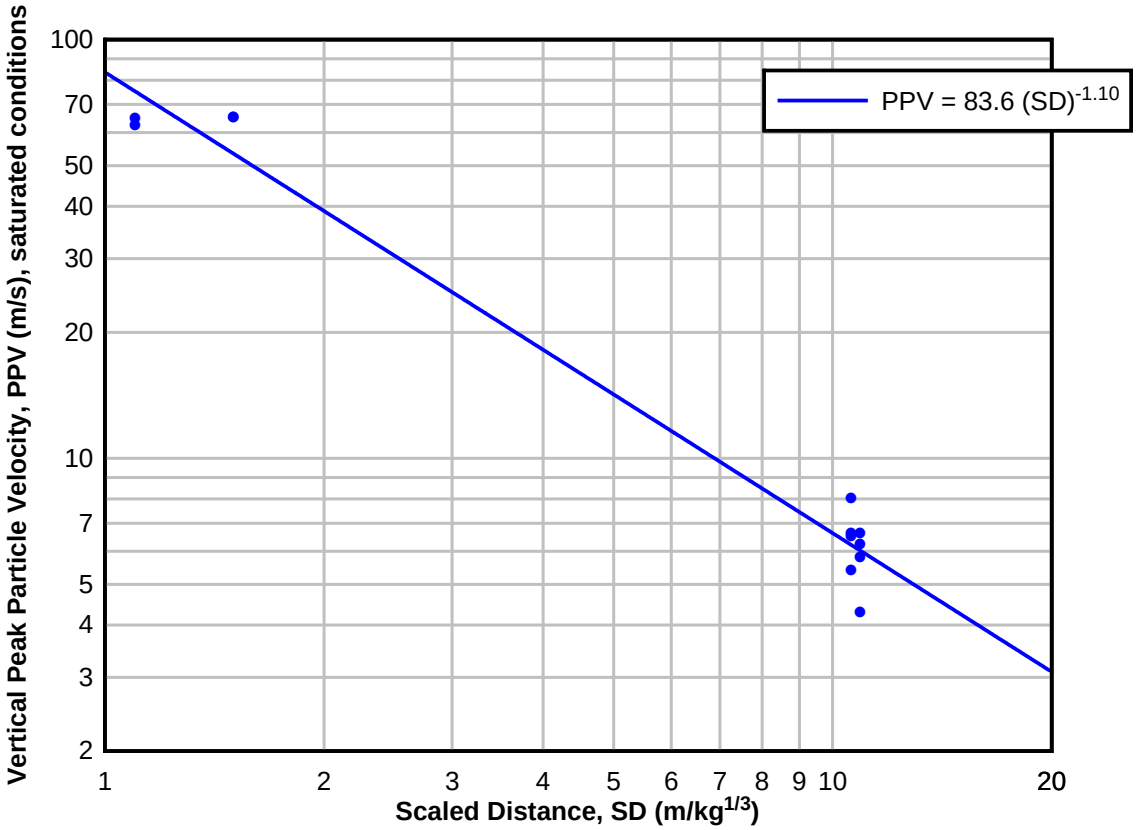
Vertical Peak Particle Velocity, PPV (m/s), saturated conditions
100
70
50
40
30
20
10
7
5
4
3
2
1
2
3
4
5
6
7
8
9
10
20
Scaled Distance, SD (m/kg1/3)
PPV = 83.6 (SD)-1.10

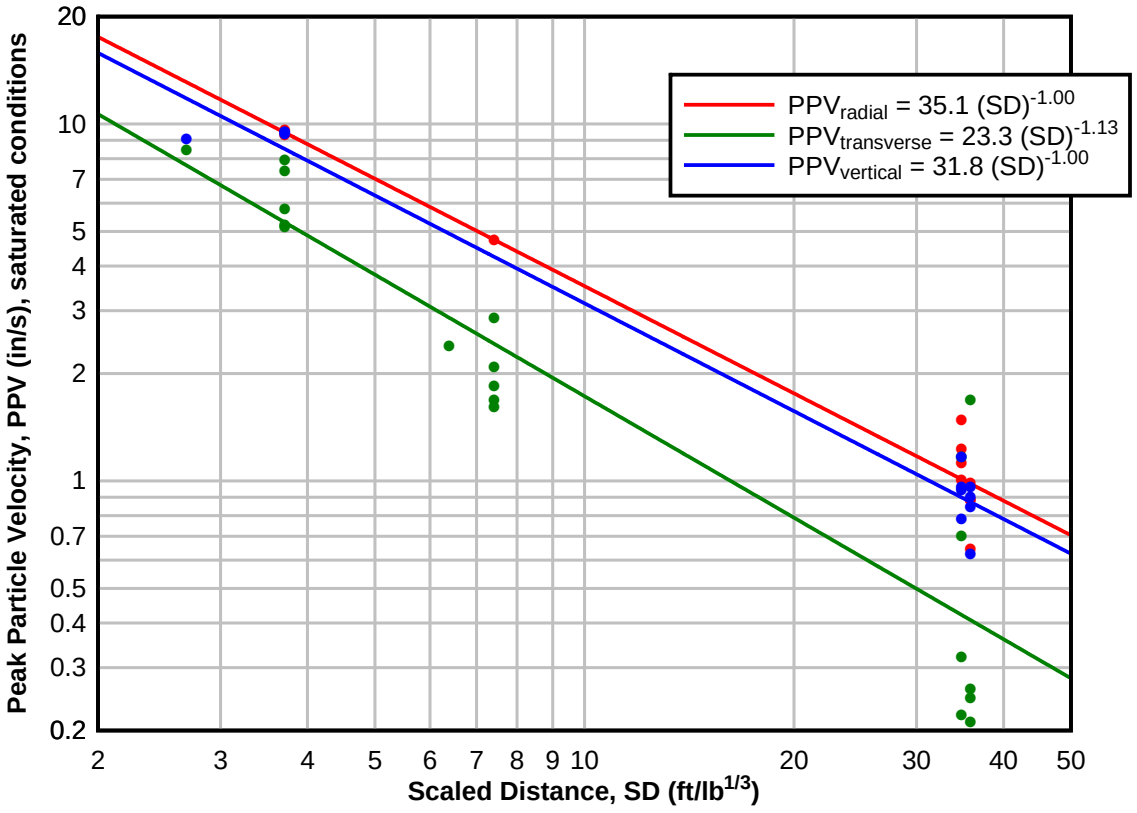
Peak Particle Velocity, PPV (in/s), saturated conditions
20
10
7
5
4
3
2
1
0.7
0.5
0.4
0.3
0.2
2
3
4
5
6
7
8
9
10
20
30
40
50
Scaled Distance, SD (ft/lb1/3)
PPVradial = 35.1 (SD)-1.00
PPVtransverse = 23.3 (SD)-1.13
PPVvertical = 31.8 (SD)-1.00

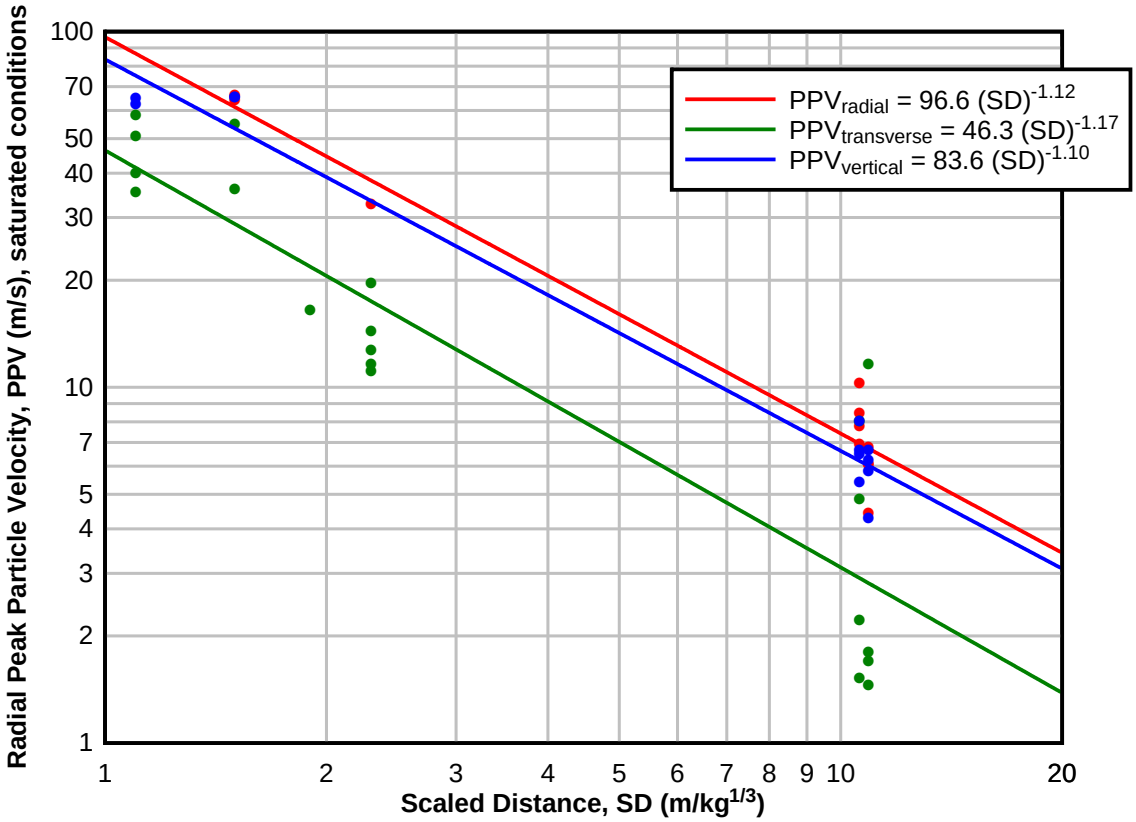

01/19/2015 TEST 1
Seismograph 1814, Distance: 18 in.

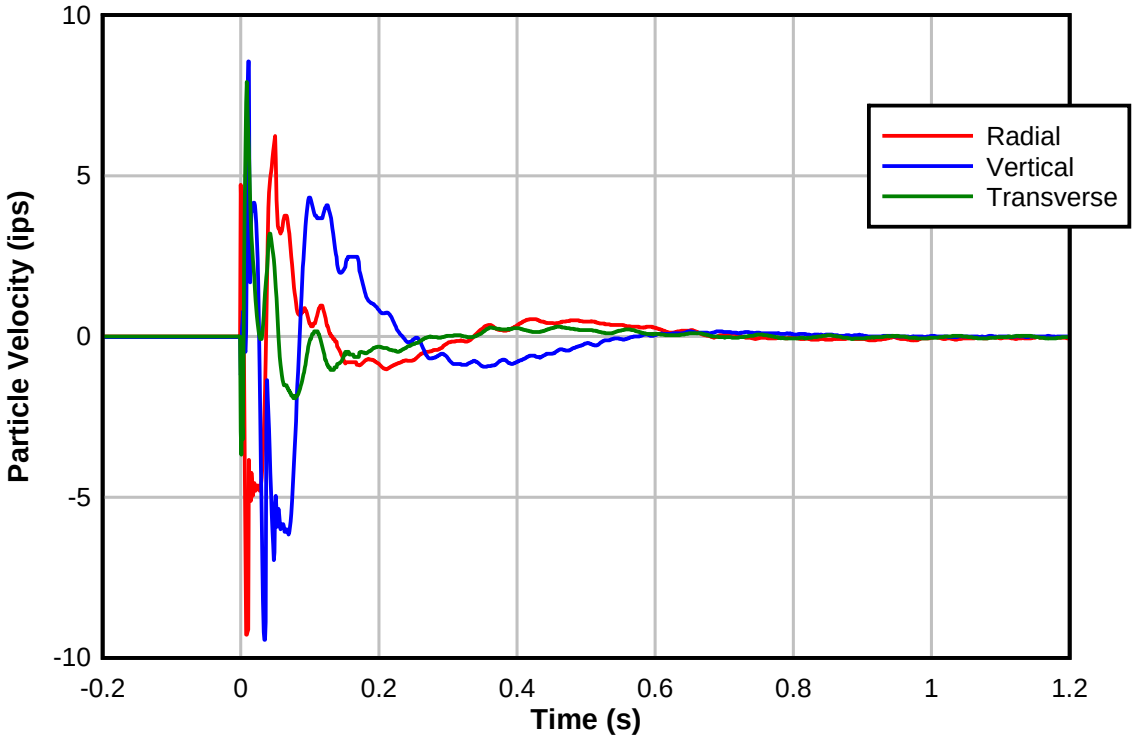

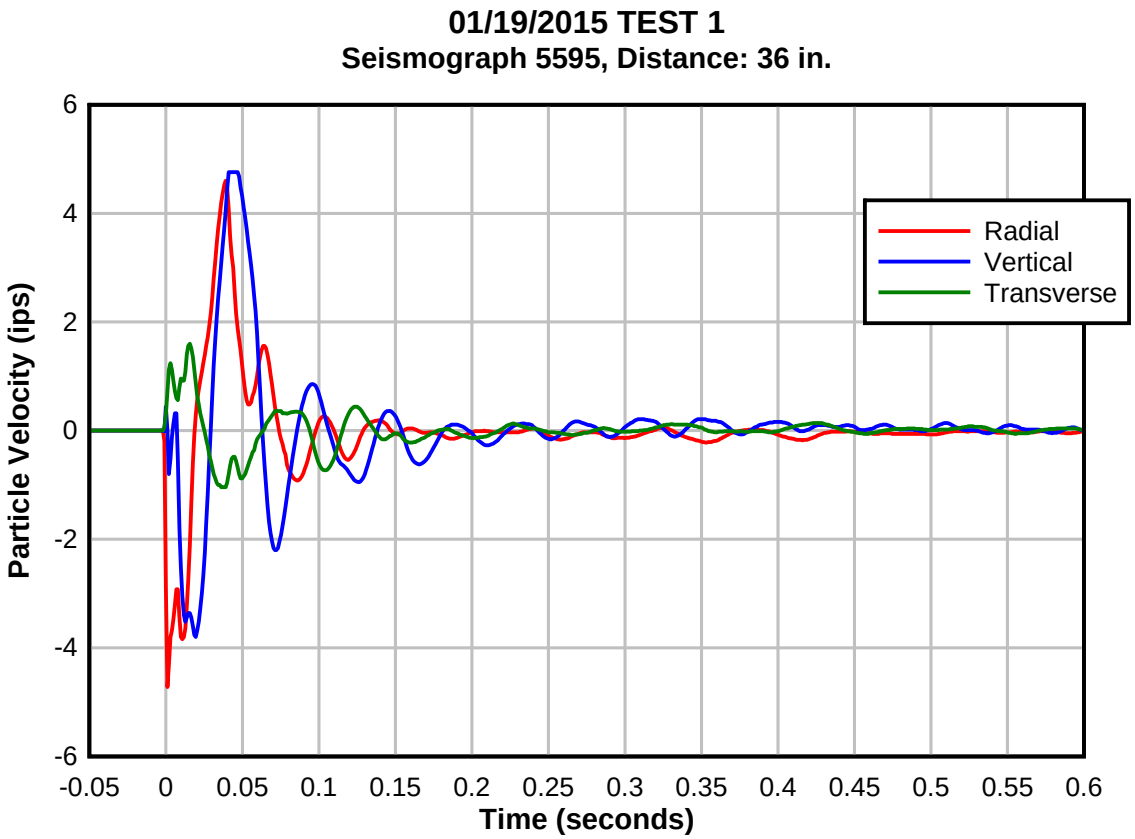
01/19/2015 TEST 1
Seismograph 5595, Distance: 36 in.
Particle Velocity (ips)
Time (seconds)
Radial
Vertical
Transverse
6
4
2
0
-2
-4
-6
-0.05
0
0.05
0.1
0.15
0.2
0.25
0.3
0.35
0.4
0.45
0.5
0.55
0.6

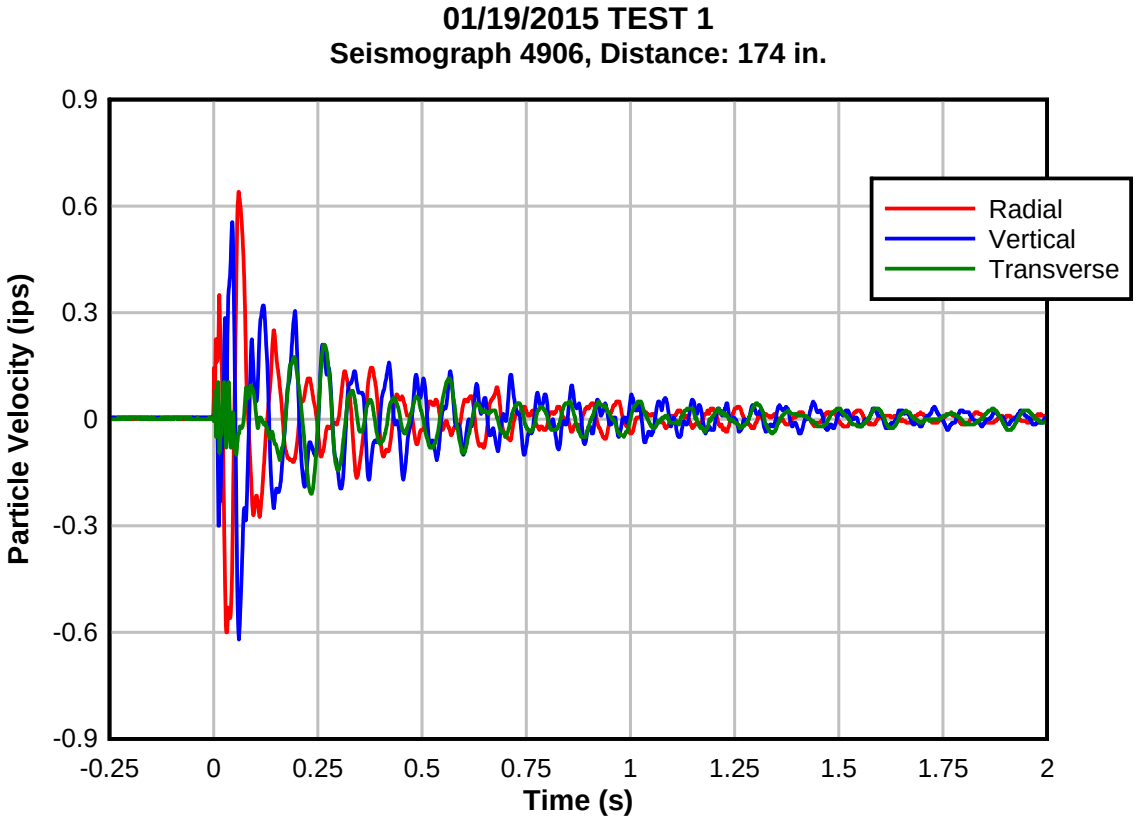
01/19/2015 TEST 1
Seismograph 4906, Distance: 174 in.
Particle Velocity (ips)
Time (s)
Radial
Vertical
Transverse
0.9
0.6
0.3
0
-0.3
-0.6
-0.9
-0.25
0
0.25
0.5
0.75
1
1.25
1.5
1.75
2

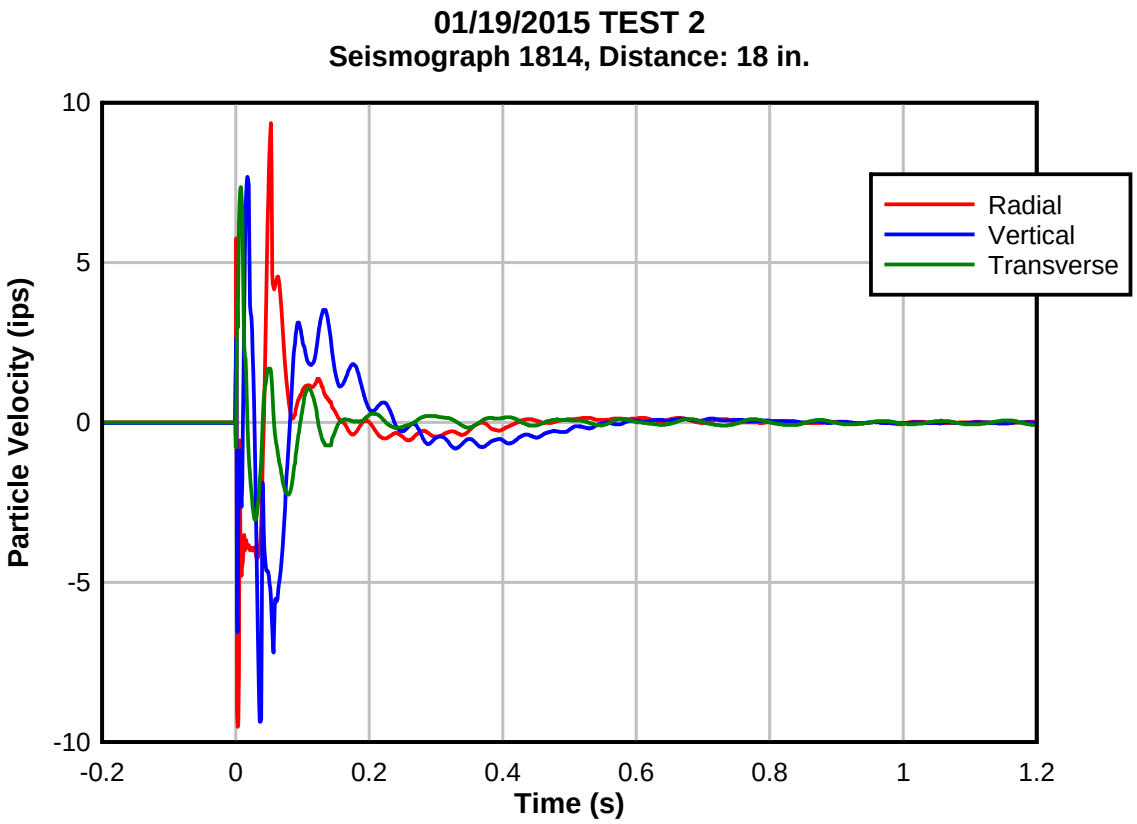
01/19/2015 TEST 2
Seismograph 1814, Distance: 18 in.
Particle Velocity (ips)
Time (s)
Radial
Vertical
Transverse
10
5
0
-5
-10
-0.2
0
0.2
0.4
0.6
0.8
1
1.2

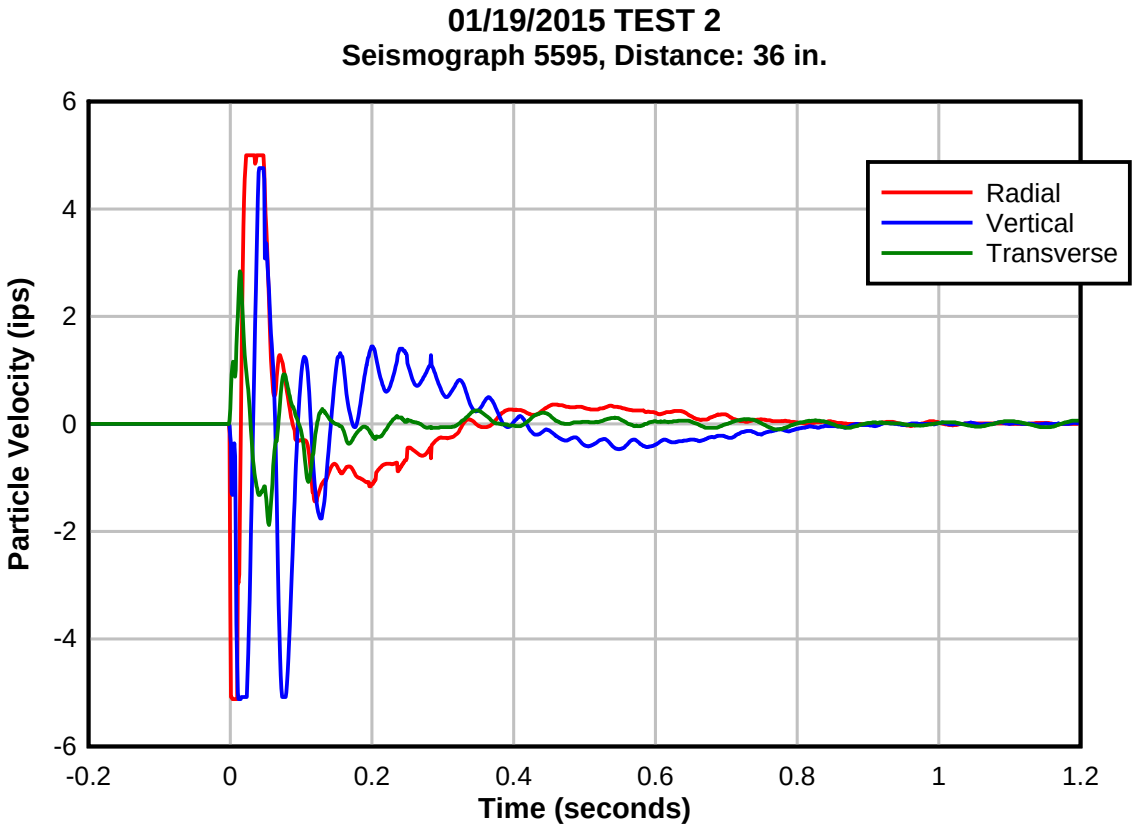
01/19/2015 TEST 2
Seismograph 5595, Distance: 36 in.
Particle Velocity (ips)
Time (seconds)
Radial
Vertical
Transverse
6
4
2
0
-2
-4
-6
-0.2
0
0.2
0.4
0.6
0.8
1
1.2

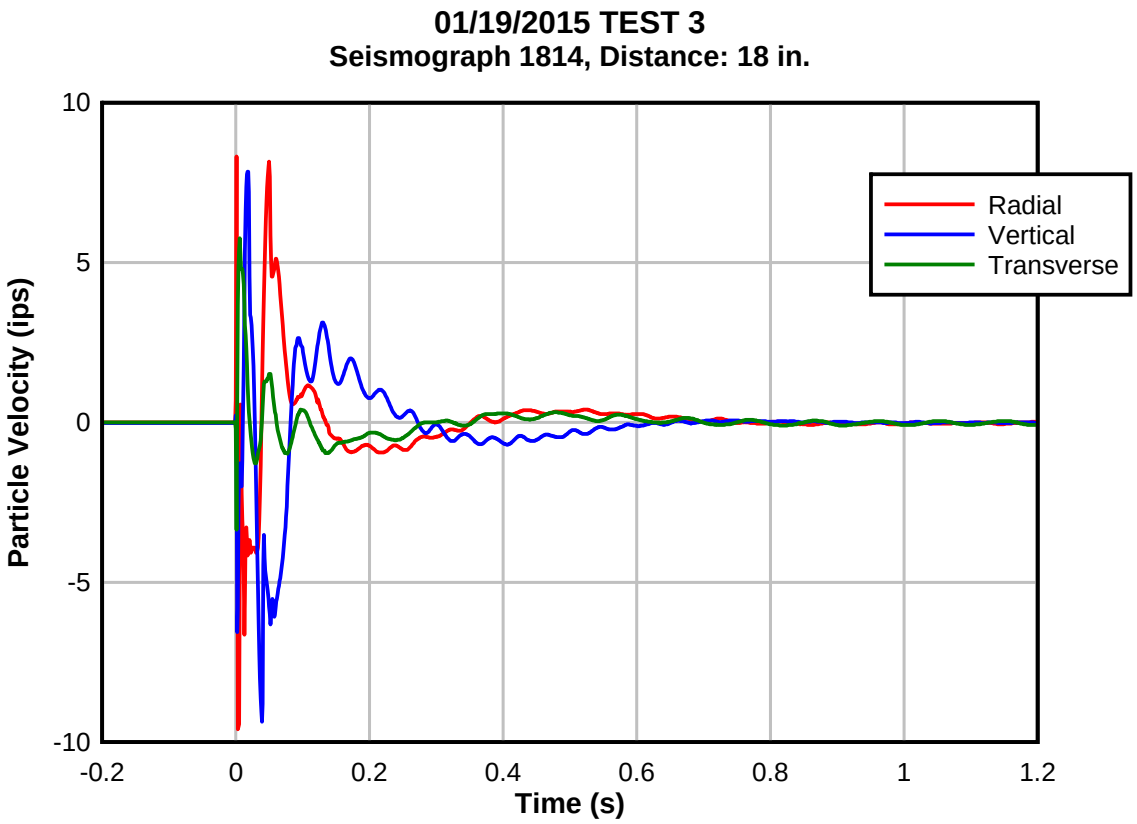
01/19/2015 TEST 3
Seismograph 1814, Distance: 18 in.
Particle Velocity (ips)
Time (s)
Radial
Vertical
Transverse
10
5
0
-5
-10
-0.2
0
0.2
0.4
0.6
0.8
1
1.2

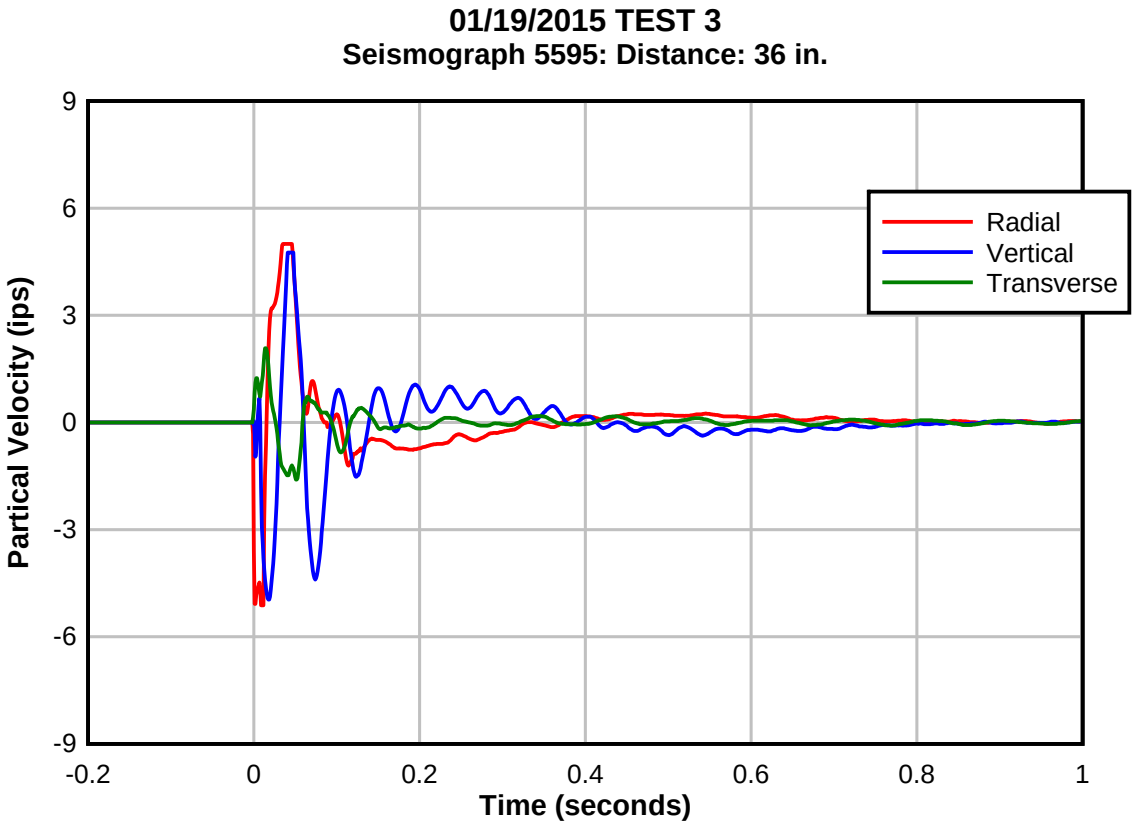
01/19/2015 TEST 3
Seismograph 5595: Distance: 36 in.
Partical Velocity (ips)
Time (seconds)
Radial
Vertical
Transverse
9
6
3
0
-3
-6
-9
-0.2
0
0.2
0.4
0.6
0.8
1

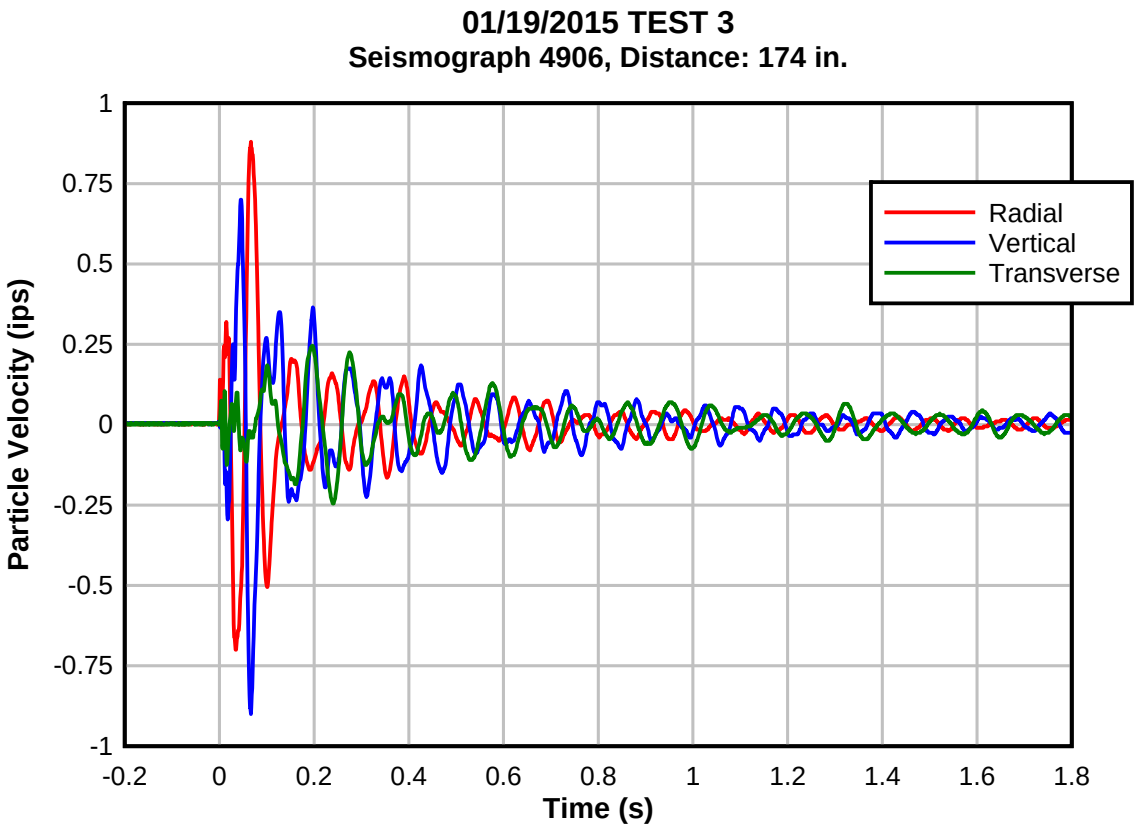
01/19/2015 TEST 3
Seismograph 4906, Distance: 174 in.
Particle Velocity (ips)
Time (s)
Radial
Vertical
Transverse
1
0.75
0.5
0.25
0
-0.25
-0.5
-0.75
-1
-0.2
0
0.2
0.4
0.6
0.8
1
1.2
1.4
1.6
1.8

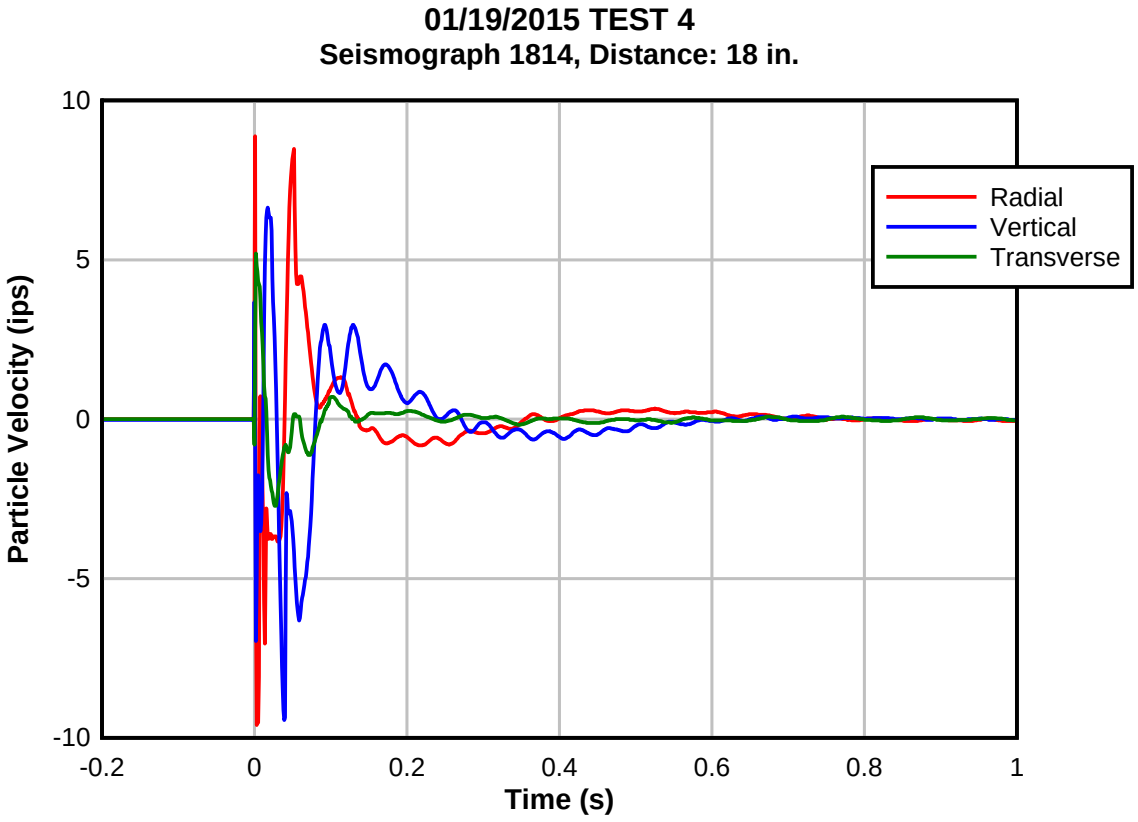
01/19/2015 TEST 4
Seismograph 1814, Distance: 18 in.
Particle Velocity (ips)
Time (s)
Radial
Vertical
Transverse
10
5
0
-5
-10
-0.2
0
0.2
0.4
0.6
0.8
1

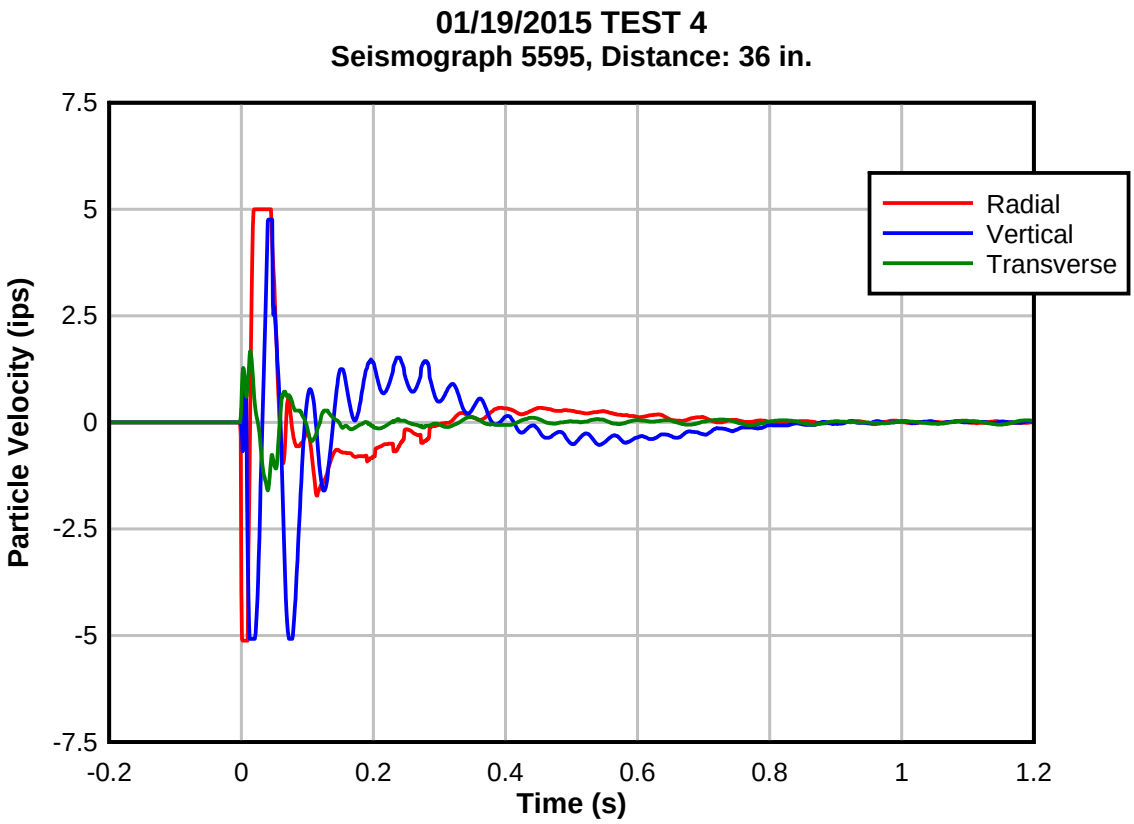
01/19/2015 TEST 4
Seismograph 5595, Distance: 36 in.
Particle Velocity (ips)
7.5
5
2.5
0
-2.5
-5
-7.5
-0.2
0
0.2
0.4
0.6
0.8
1
1.2
Time (s)
Radial
Vertical
Transverse

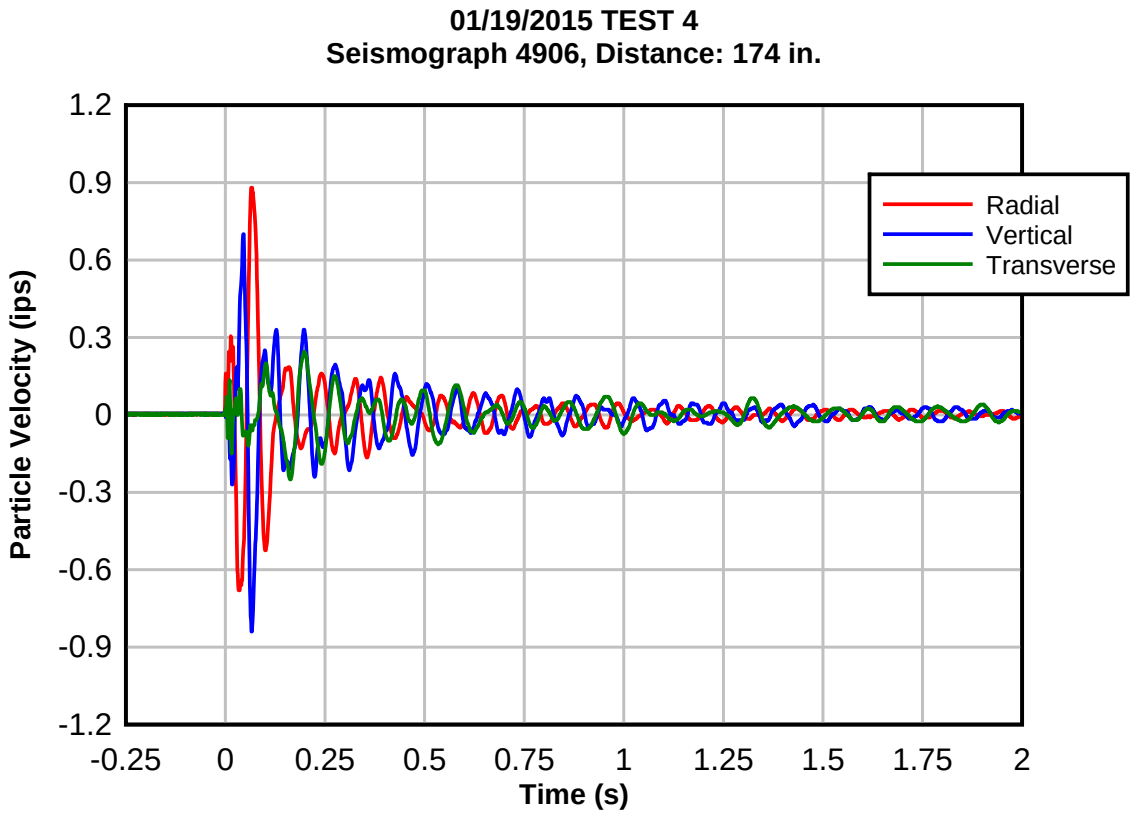
01/19/2015 TEST 4
Seismograph 4906, Distance: 174 in.
Particle Velocity (ips)
1.2
0.9
0.6
0.3
0
-0.3
-0.6
-0.9
-1.2
-0.25
0
0.25
0.5
0.75
1
1.25
1.5
1.75
2
Time (s)
Radial
Vertical
Transverse

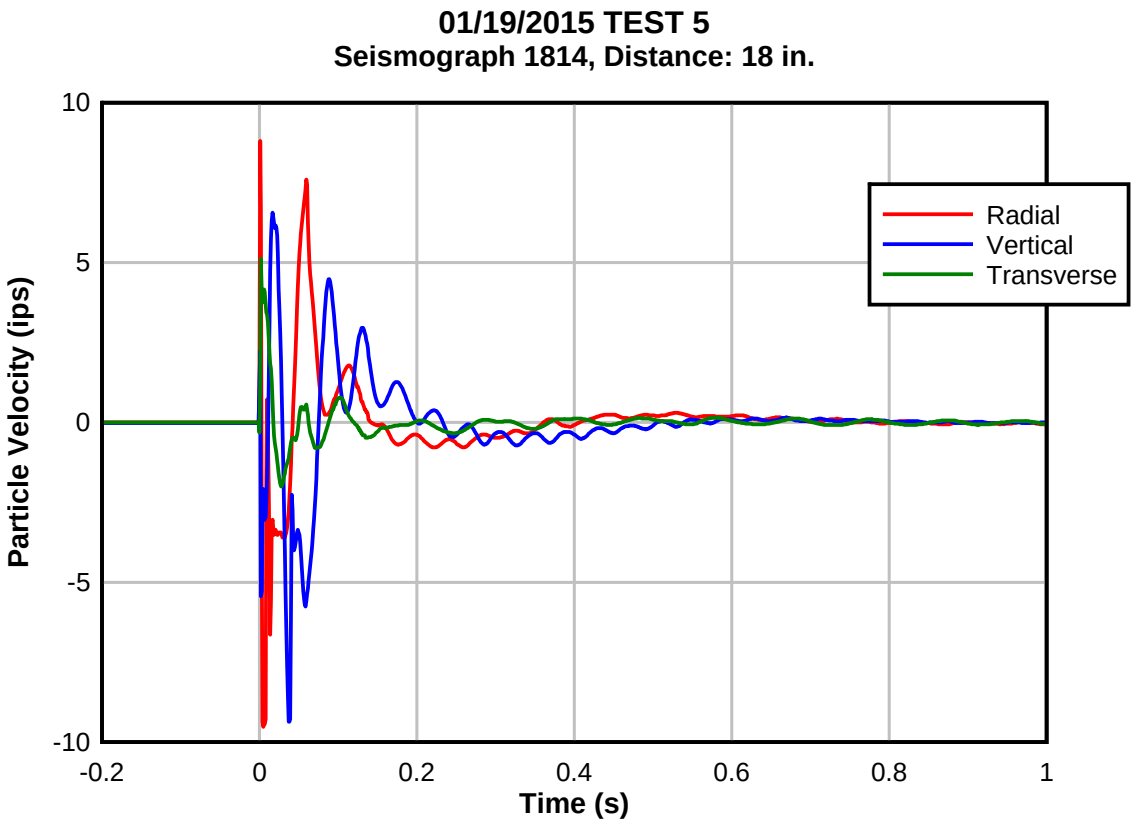
01/19/2015 TEST 5
Seismograph 1814, Distance: 18 in.
Particle Velocity (ips)
Time (s)
Radial
Vertical
Transverse
10
5
0
-5
-10
-0.2
0
0.2
0.4
0.6
0.8
1

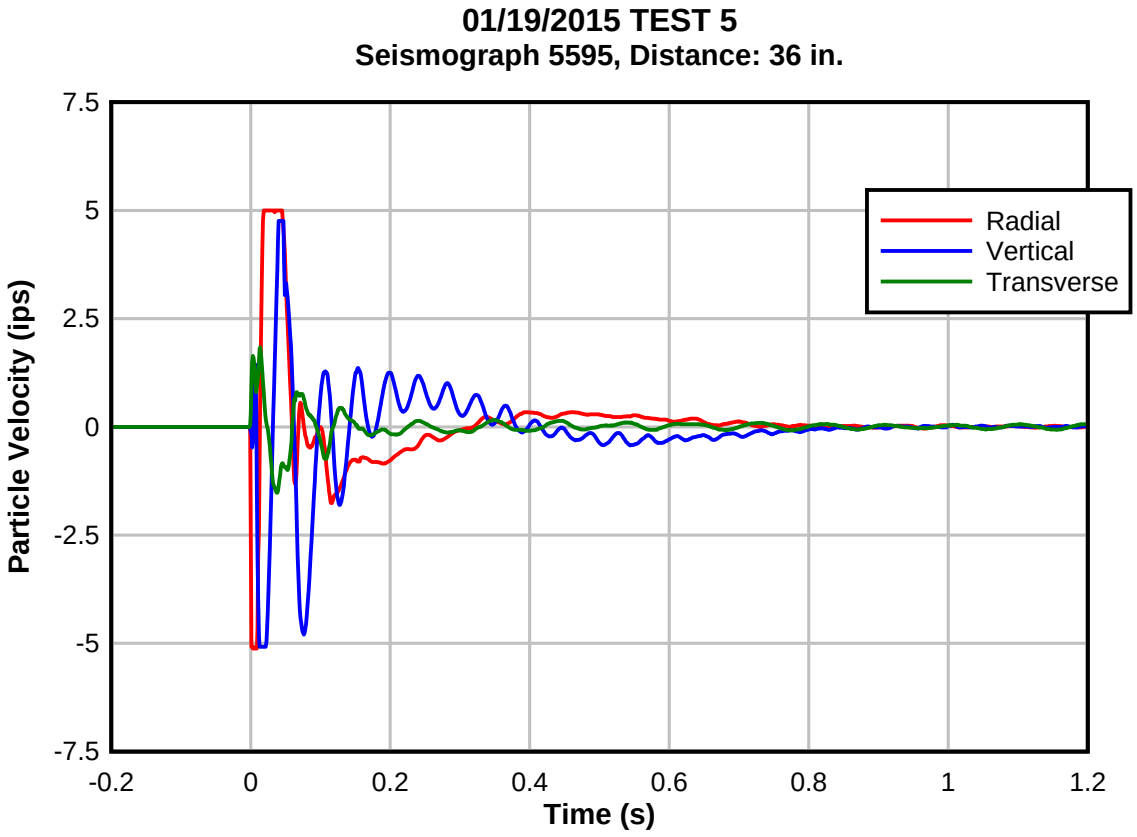
01/19/2015 TEST 5
Seismograph 5595, Distance: 36 in.
Particle Velocity (ips)
Time (s)
Radial
Vertical
Transverse
7.5
5
2.5
0
-2.5
-5
-7.5
-0.2
0
0.2
0.4
0.6
0.8
1
1.2

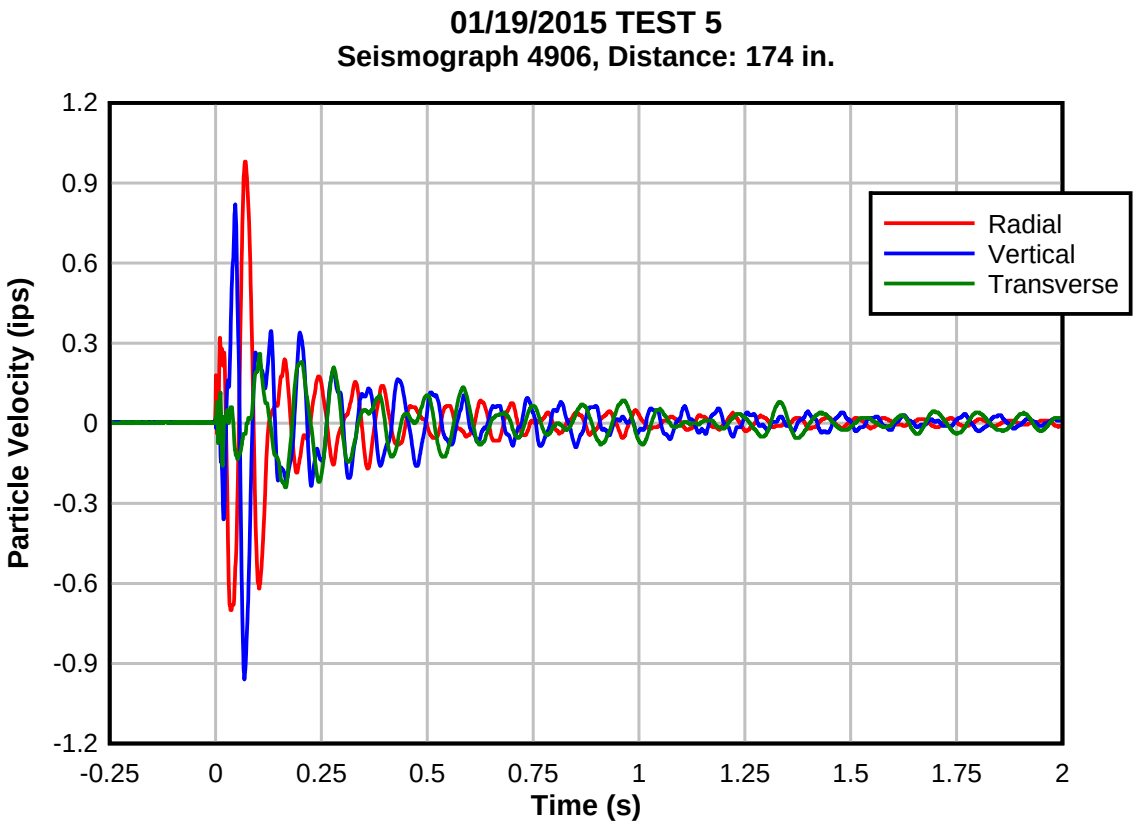
01/19/2015 TEST 5
Seismograph 4906, Distance: 174 in.
Particle Velocity (ips)
Time (s)
Radial
Vertical
Transverse
1.2
0.9
0.6
0.3
0
-0.3
-0.6
-0.9
-1.2
-0.25
0
0.25
0.5
0.75
1
1.25
1.5
1.75
2

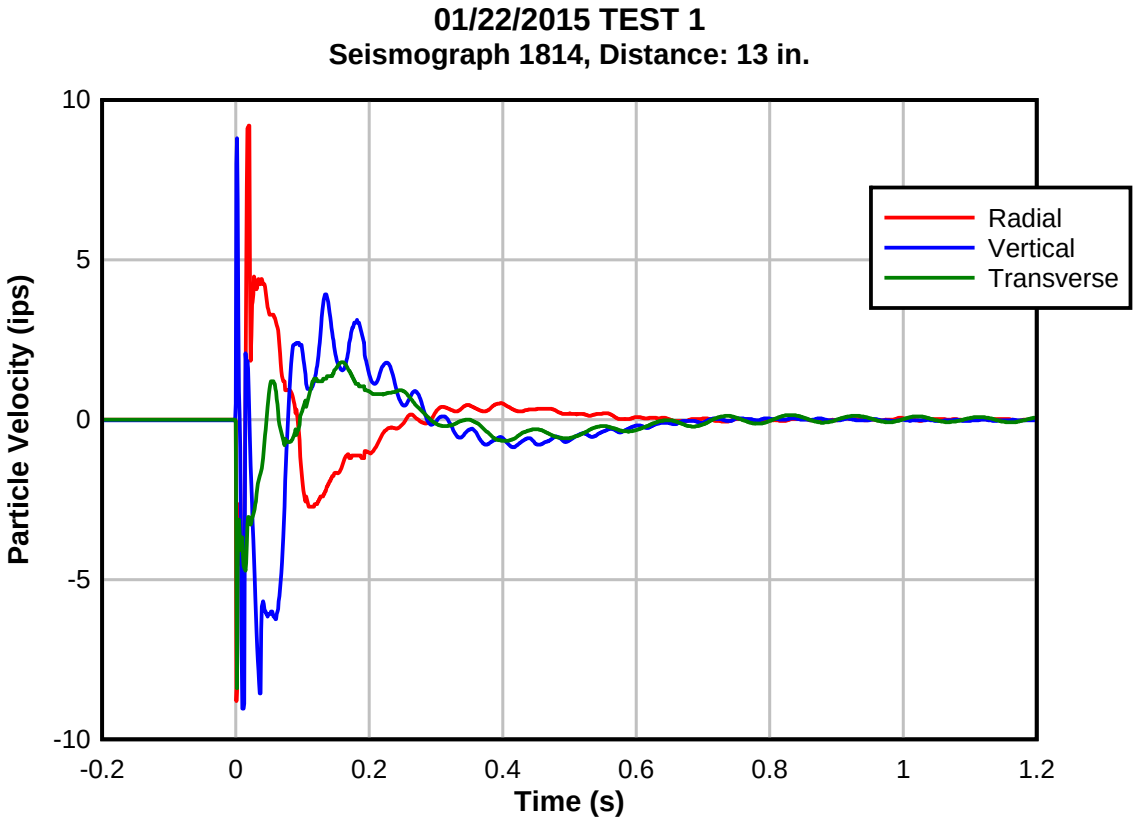
01/22/2015 TEST 1
Seismograph 1814, Distance: 13 in.
Particle Velocity (ips)
Time (s)
Radial
Vertical
Transverse
10
5
0
-5
-10
-0.2
0
0.2
0.4
0.6
0.8
1
1.2

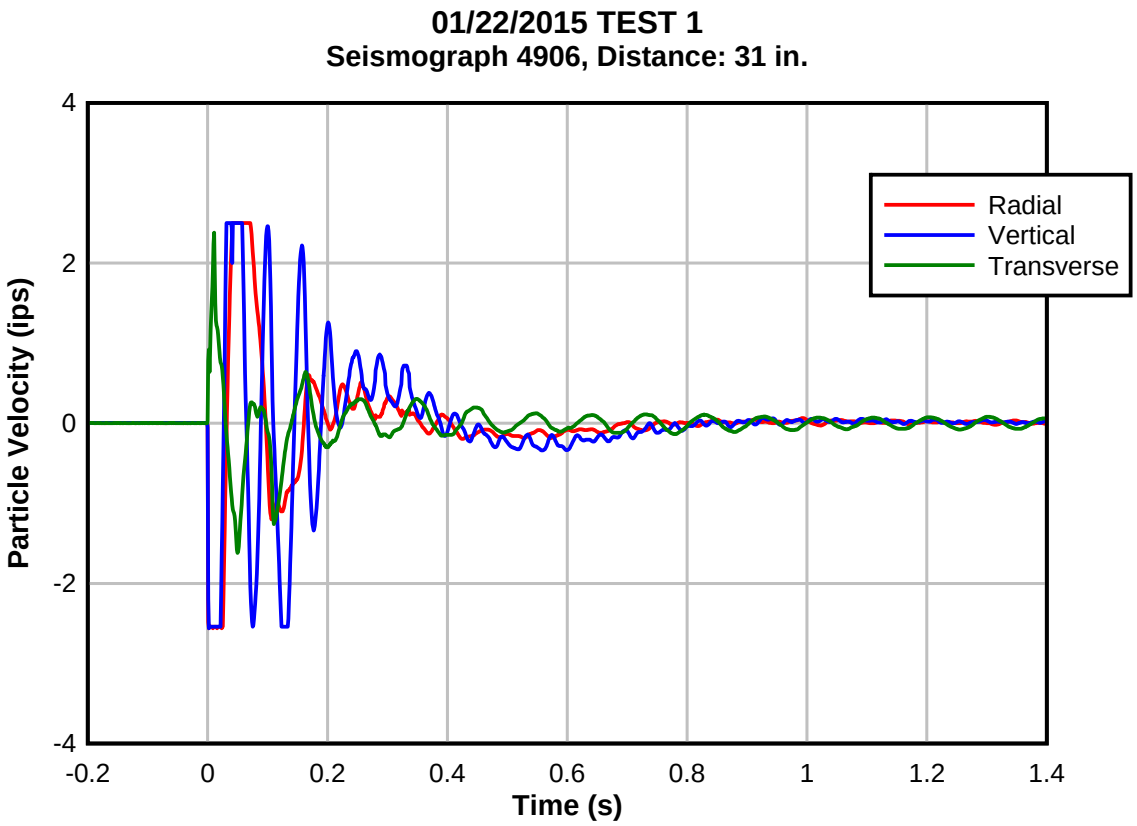
01/22/2015 TEST 1
Seismograph 4906, Distance: 31 in.
Particle Velocity (ips)
Time (s)
Radial
Vertical
Transverse
4
2
0
-2
-4
-0.2
0
0.2
0.4
0.6
0.8
1
1.2
1.4

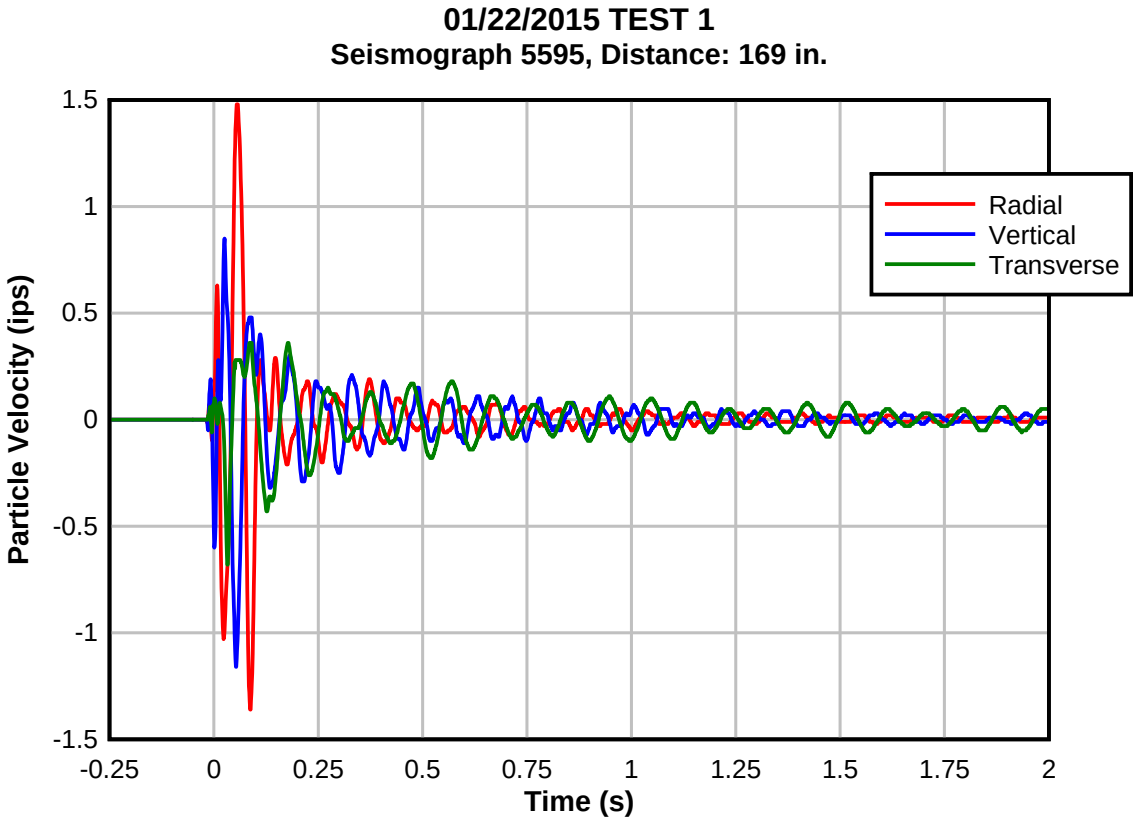
01/22/2015 TEST 1
Seismograph 5595, Distance: 169 in.
Particle Velocity (ips)
Time (s)
Radial
Vertical
Transverse
1.5
1
0.5
0
-0.5
-1
-1.5
-0.25
0
0.25
0.5
0.75
1
1.25
1.5
1.75
2

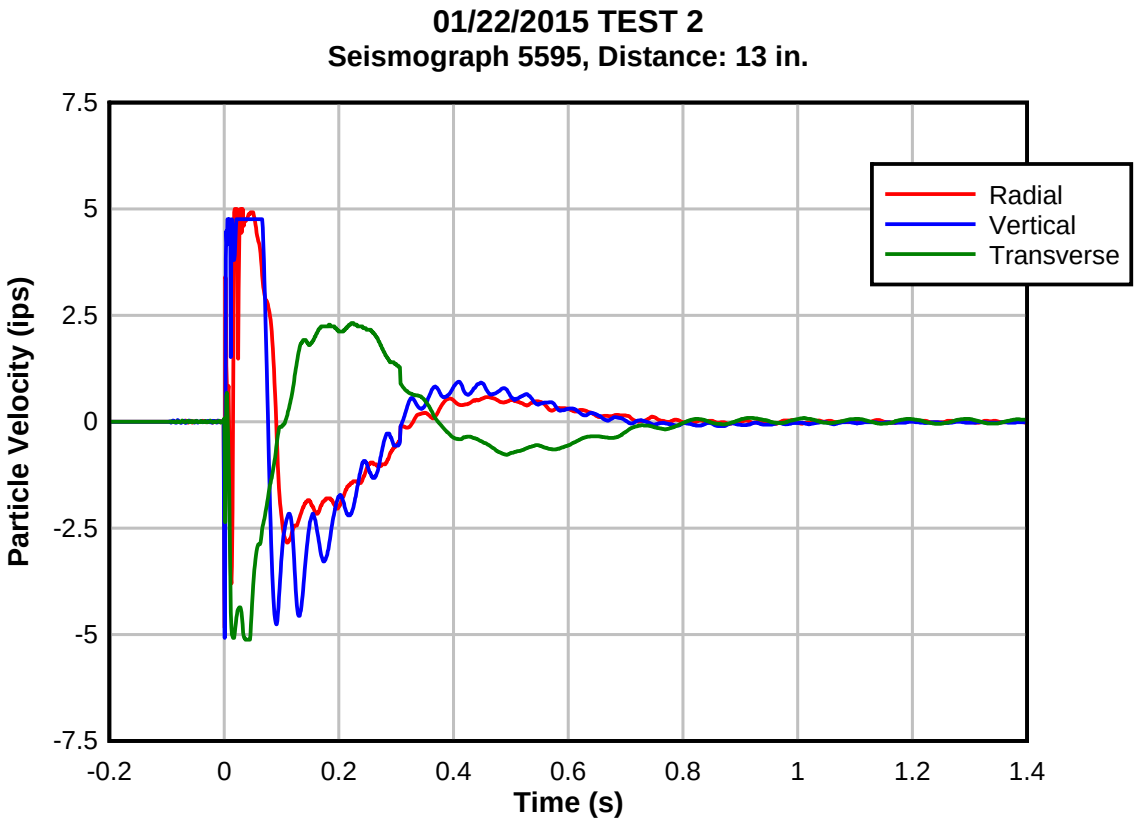
01/22/2015 TEST 2
Seismograph 5595, Distance: 13 in.
Particle Velocity (ips)
Time (s)
Radial
Vertical
Transverse
7.5
5
2.5
0
-2.5
-5
-7.5
-0.2
0
0.2
0.4
0.6
0.8
1
1.2
1.4

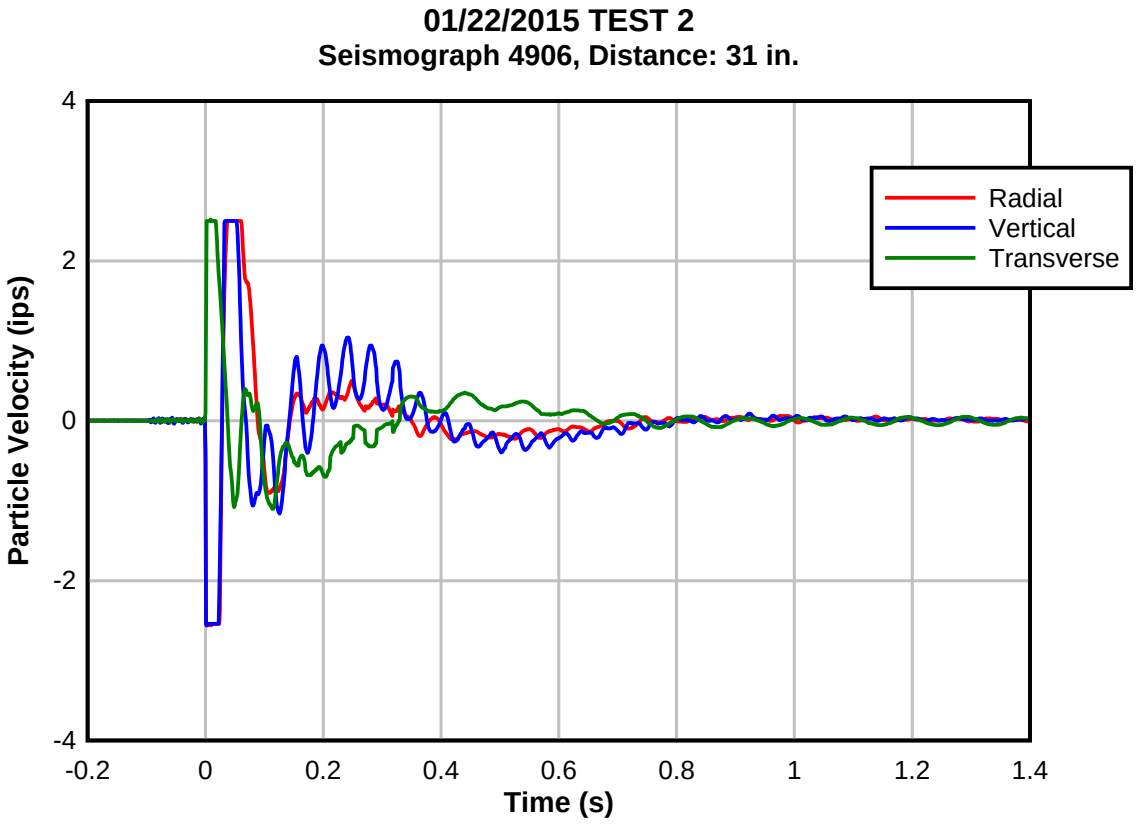
01/22/2015 TEST 2
Seismograph 4906, Distance: 31 in.
Particle Velocity (ips)
Time (s)
Radial
Vertical
Transverse
4
2
0
-2
-4
-0.2
0
0.2
0.4
0.6
0.8
1
1.2
1.4

01/22/2015 TEST 2
Seismograph 1814, Distance: 169 in.

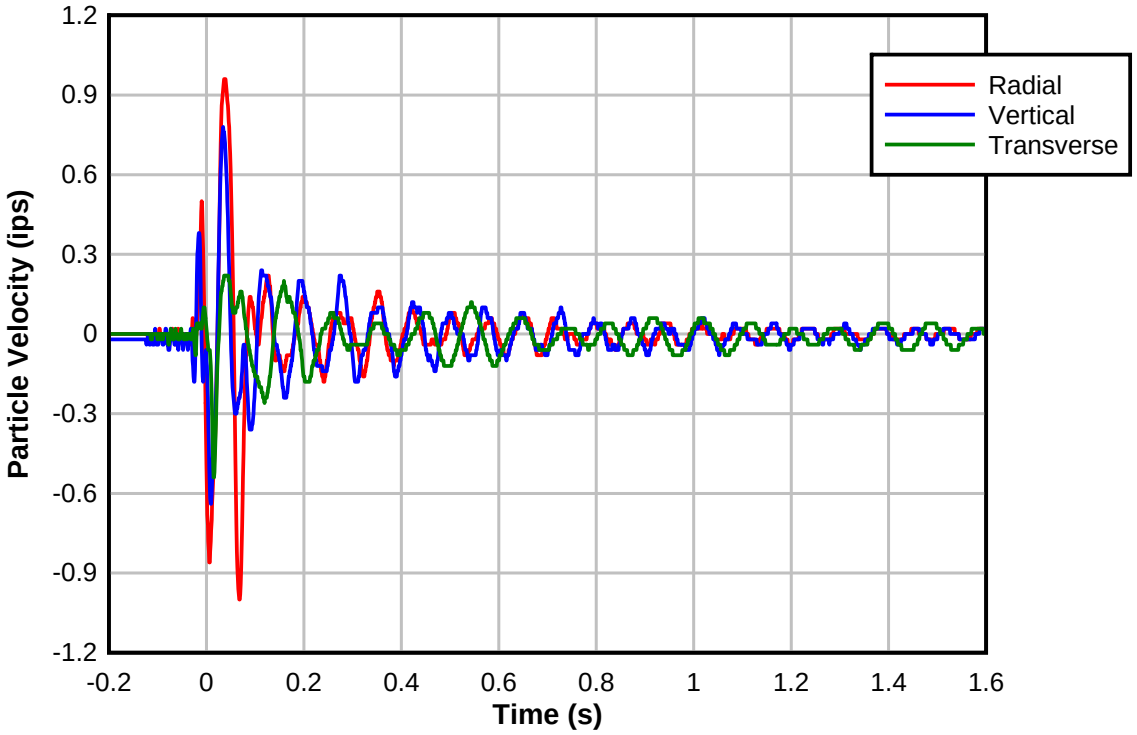

01/22/2015 TEST 3
Seismograph 5595, Distance: 13 in.

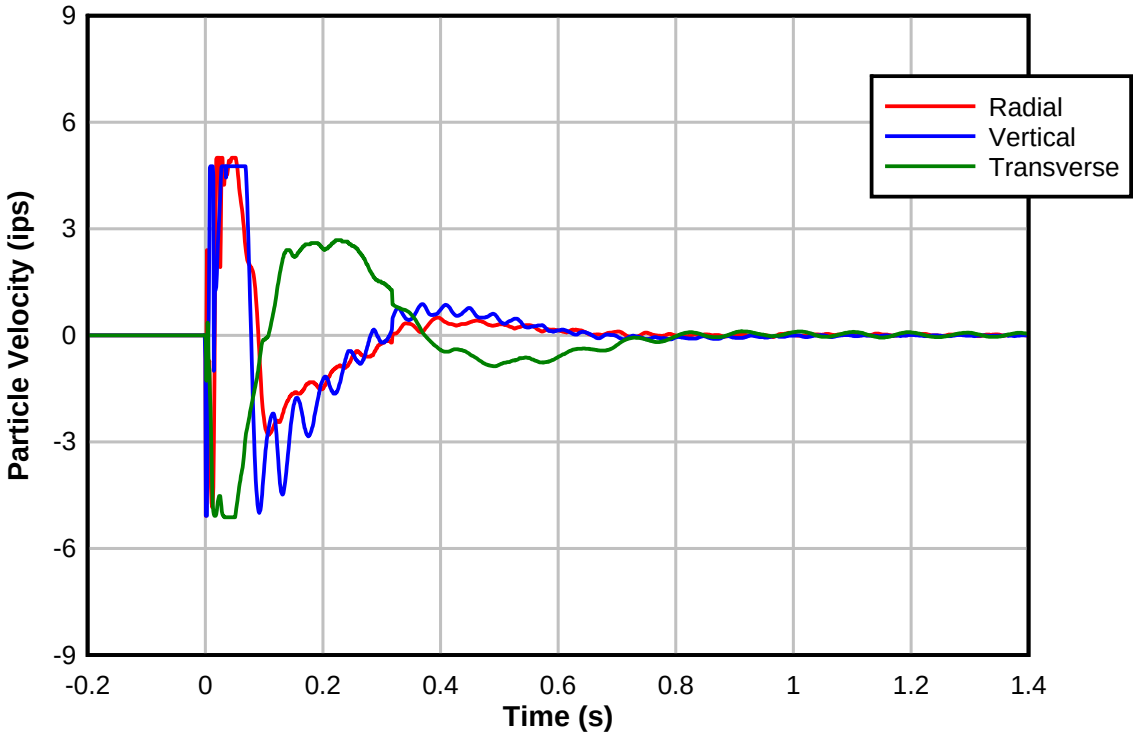

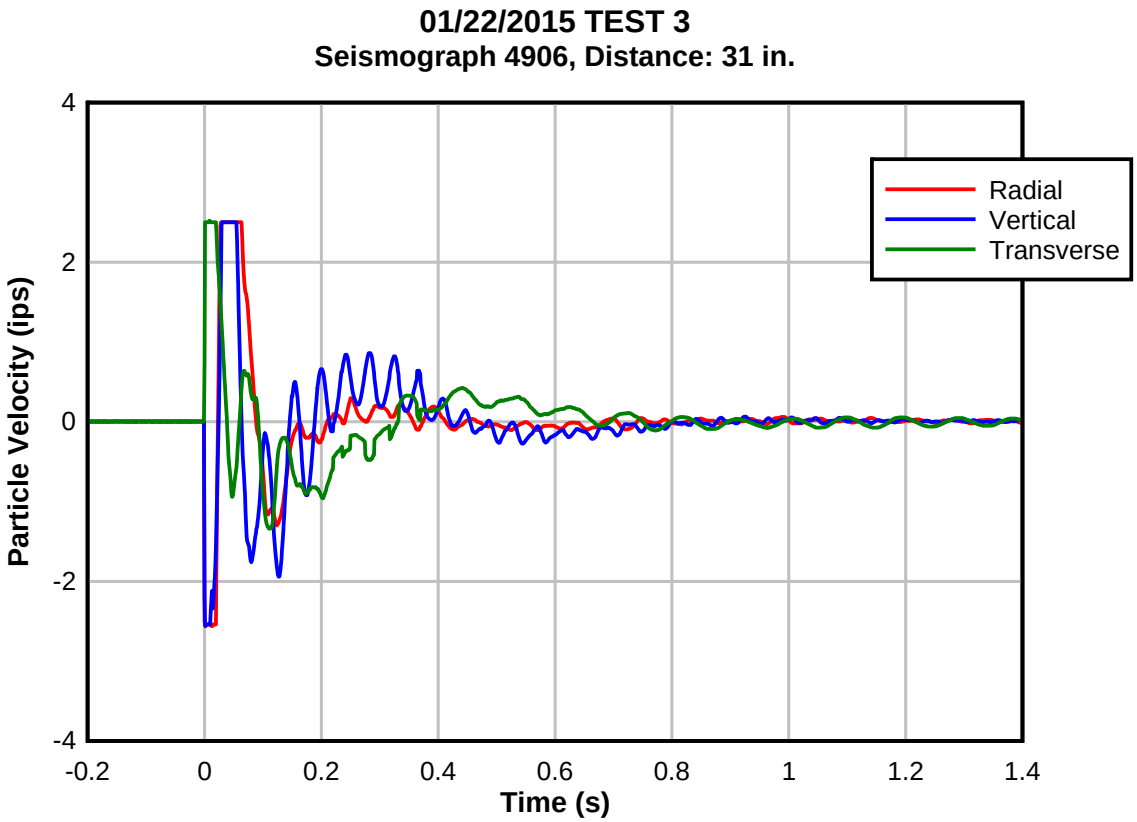
01/22/2015 TEST 3
Seismograph 4906, Distance: 31 in.
Particle Velocity (ips)
Time (s)
Radial
Vertical
Transverse
4
2
0
-2
-4
-0.2
0
0.2
0.4
0.6
0.8
1
1.2
1.4

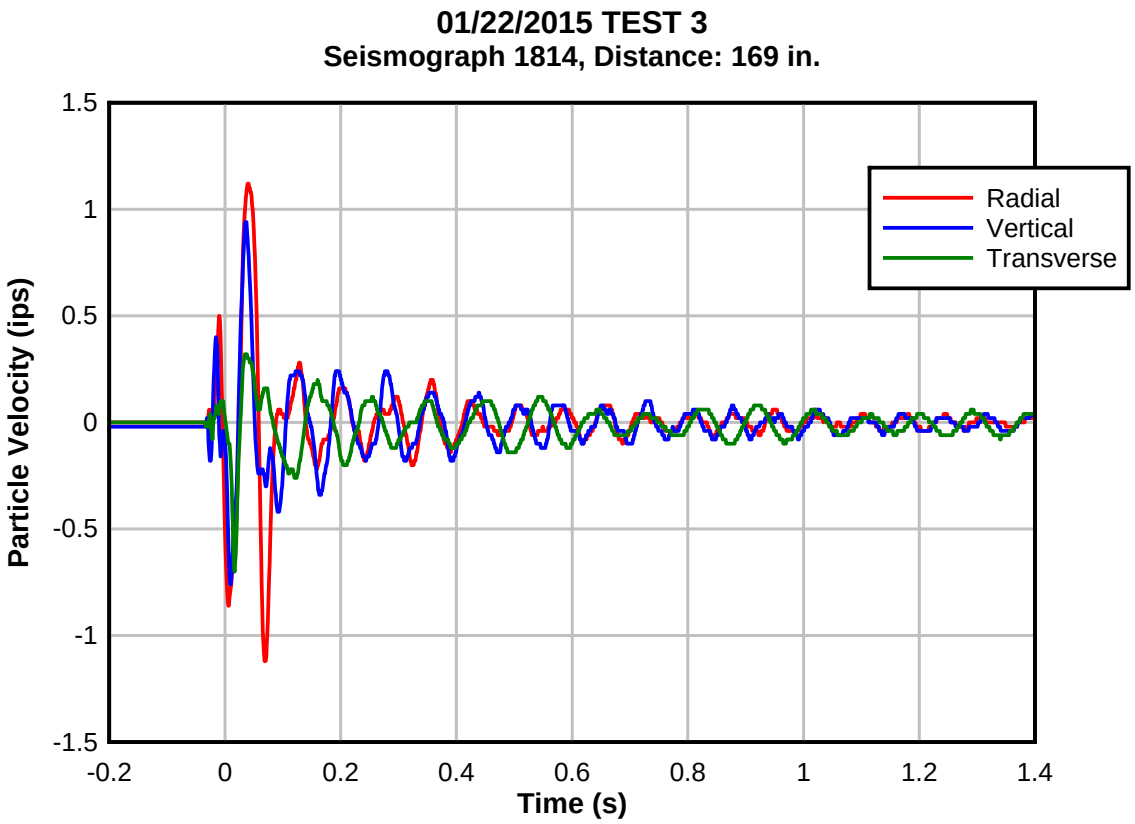
01/22/2015 TEST 3
Seismograph 1814, Distance: 169 in.
Particle Velocity (ips)
Time (s)
Radial
Vertical
Transverse
1.5
1
0.5
0
-0.5
-1
-1.5
-0.2
0
0.2
0.4
0.6
0.8
1
1.2
1.4

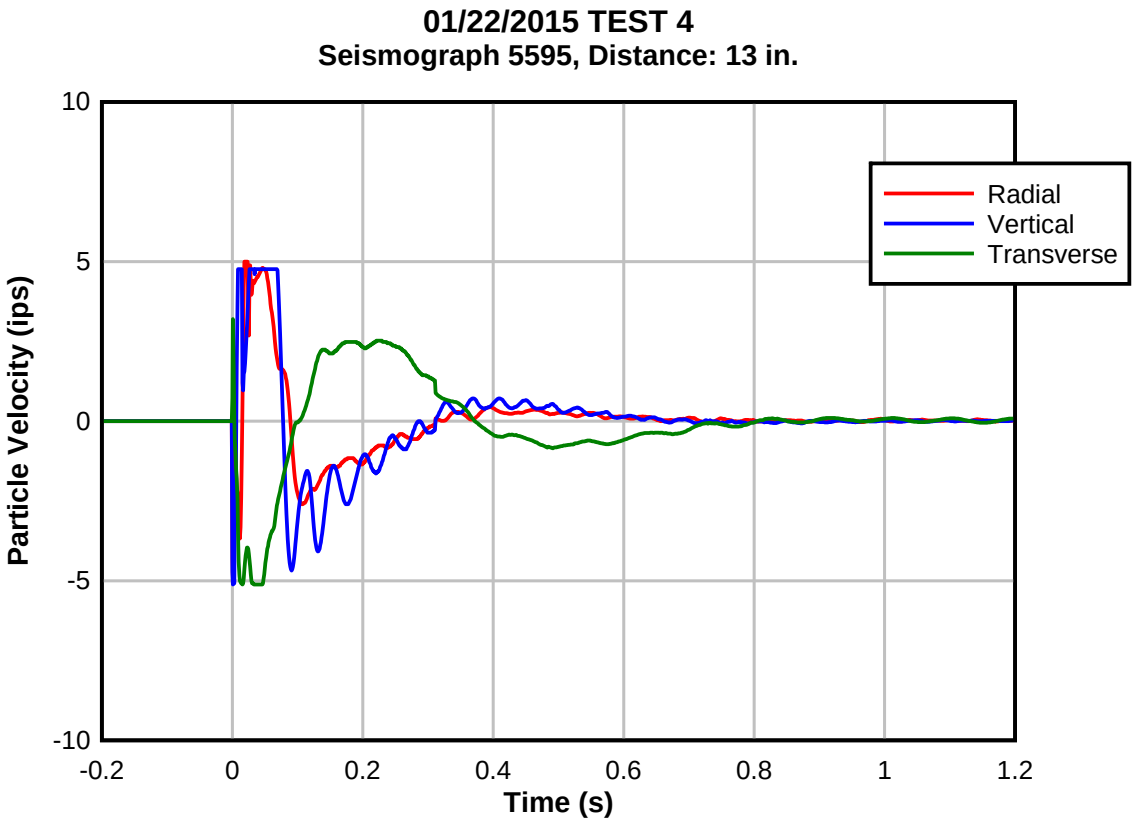
01/22/2015 TEST 4
Seismograph 5595, Distance: 13 in.
Particle Velocity (ips)
Time (s)
Radial
Vertical
Transverse
10
5
0
-5
-10
-0.2
0
0.2
0.4
0.6
0.8
1
1.2

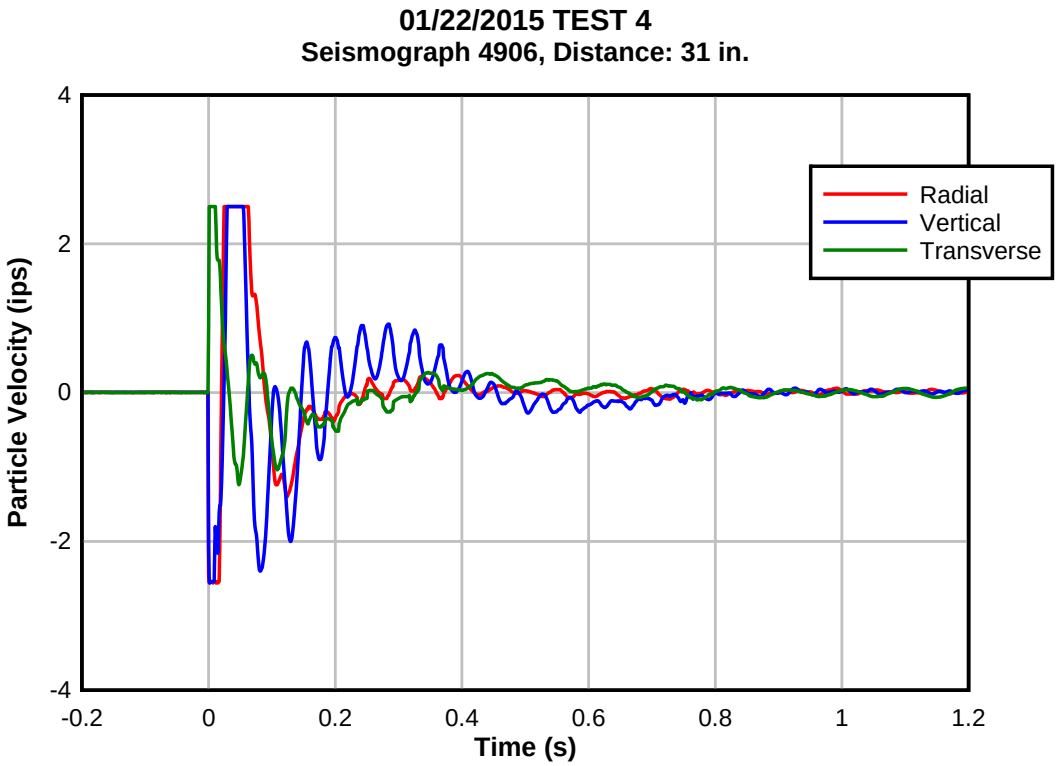
01/22/2015 TEST 4
Seismograph 4906, Distance: 31 in.
Particle Velocity (ips)
Time (s)
Radial
Vertical
Transverse
4
2
0
-2
-4
-0.2
0
0.2
0.4
0.6
0.8
1
1.2

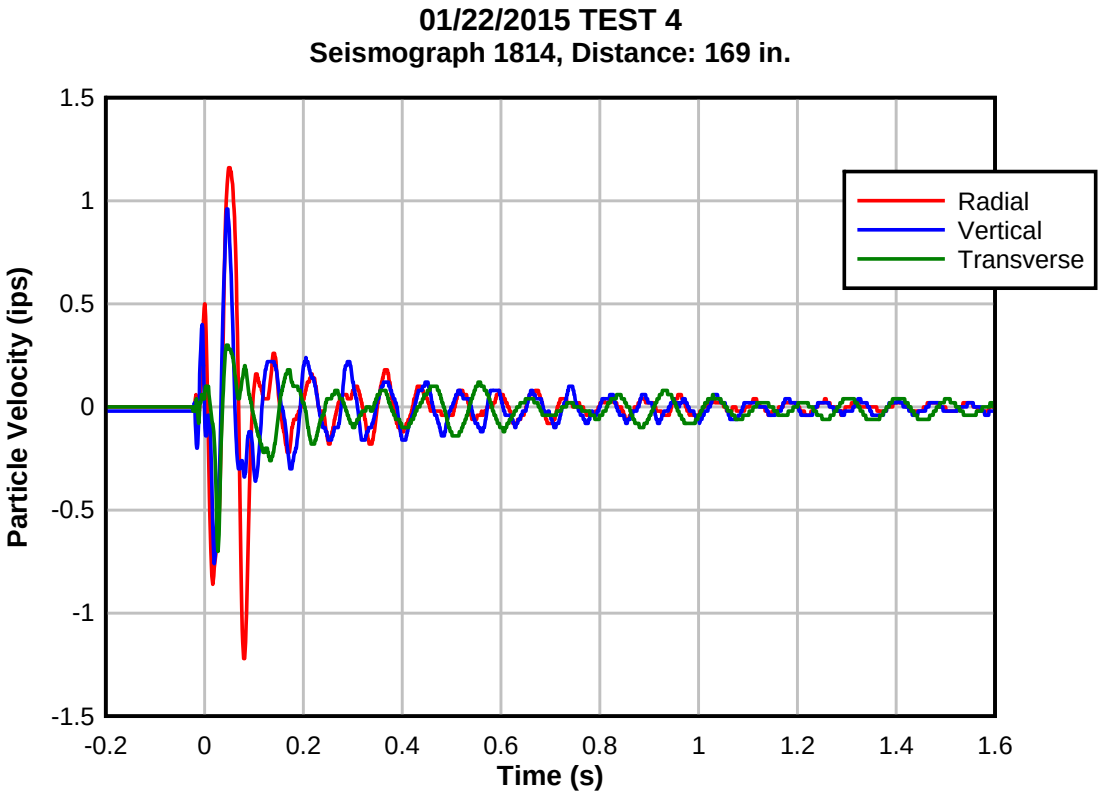
01/22/2015 TEST 4
Seismograph 1814, Distance: 169 in.
Particle Velocity (ips)
Time (s)
Radial
Vertical
Transverse
1.5
1
0.5
0
-0.5
-1
-1.5
-0.2
0
0.2
0.4
0.6
0.8
1
1.2
1.4
1.6

APPENDIX C – TOURMALINE DATA

PEAK COMPRESSIVE STRESS, σpeak

Date	Test	Tourmaline No.	Charge (g)	Charge (kg)	Charge (lb)	TNT Equivalency (kg)	TNT Equivalency (lb)	Distance to charge (in)	Distance to charge (ft)	Distance to charge (m)	TNT Eq. SD (m/kg^⅓)	TNT Eq. SD (ft/lb^⅓)	Peak stress (psi)	Peak stress (kPa)
1/19/2015	1	7259	20	0.020	0.044	0.030	0.066	18	1.5	0.46	1.47	3.71	29.87	205.94
1/19/2015	1	10205	20	0.020	0.044	0.030	0.066	36	3.0	0.91	2.26	7.42	4.42	30.49
1/19/2015	2	7259	20	0.020	0.044	0.030	0.066	18	1.5	0.46	1.13	3.71	52.86	364.45
1/19/2015	2	10205	20	0.020	0.044	0.030	0.066	36	3.0	0.91	2.26	7.42	5.50	37.96
1/19/2015	3	7259	20	0.020	0.044	0.030	0.066	18	1.5	0.46	1.13	3.71	47.44	327.10
1/19/2015	3	10205	20	0.020	0.044	0.030	0.066	36	3.0	0.91	2.26	7.42	5.15	35.53
1/19/2015	4	7259	20	0.020	0.044	0.030	0.066	18	1.5	0.46	1.13	3.71	59.02	406.91
1/19/2015	4	10205	20	0.020	0.044	0.030	0.066	36	3.0	0.91	2.26	7.42	4.26	29.37
1/19/2015	5	7259	20	0.020	0.044	0.030	0.066	18	1.5	0.46	1.13	3.71	61.10	421.29
1/19/2015	5	10205	20	0.020	0.044	0.030	0.066	36	3.0	0.91	2.26	7.42	4.95	34.16
1/22/2015	1	7259	20	0.020	0.044	0.030	0.066	13	1.1	0.33	1.06	2.68	133.06	917.41
1/22/2015	1	10205	20	0.020	0.044	0.030	0.066	31	2.6	0.79	1.95	6.39	5.89	40.60
1/22/2015	2	7259	20	0.020	0.044	0.030	0.066	13	1.1	0.33	0.82	2.68	141.30	974.26
1/22/2015	2	10205	20	0.020	0.044	0.030	0.066	31	2.6	0.79	1.95	6.39	7.05	48.62
1/22/2015	3	7259	20	0.020	0.044	0.030	0.066	13	1.1	0.33	0.82	2.68	135.89	936.91
1/22/2015	3	10205	20	0.020	0.044	0.030	0.066	31	2.6	0.79	1.95	6.39	8.81	60.73
1/22/2015	4	7259	20	0.020	0.044	0.030	0.066	13	1.1	0.33	0.82	2.68	119.78	825.85
1/22/2015	4	10205	20	0.020	0.044	0.030	0.066	31	2.6	0.79	1.95	6.39	NO DATA	NO DATA
6/26/2015	1	7259	20	0.020	0.044	0.030	0.066	28	2.3	0.71	1.76	5.77	7.68	52.99
6/26/2015	1	29169	20	0.020	0.044	0.030	0.066	28	2.3	0.71	1.76	5.77	5.42	37.35
6/26/2015	1	10226	20	0.020	0.044	0.030	0.066	28	2.3	0.71	2.29	5.77	NO DATA	NO DATA
6/26/2015	2	7259	20	0.020	0.044	0.030	0.066	28	2.3	0.71	1.76	5.77	7.21	49.70
6/26/2015	2	29169	20	0.020	0.044	0.030	0.066	28	2.3	0.71	1.76	5.77	7.98	55.01
6/26/2015	2	10226	20	0.020	0.044	0.030	0.066	28	2.3	0.71	1.76	5.77	7.50	51.73
6/26/2015	3	7259	20	0.020	0.044	0.030	0.066	28	2.3	0.71	1.76	5.77	7.55	52.07
6/26/2015	3	29169	20	0.020	0.044	0.030	0.066	28	2.3	0.71	1.76	5.77	9.22	63.59
6/26/2015	3	10226	20	0.020	0.044	0.030	0.066	28	2.3	0.71	1.76	5.77	8.12	56.02
8/13/2015	1	7259	20	0.020	0.044	0.030	0.066	20.25	1.7	0.51	1.27	4.17	16.61	114.52
8/13/2015	2	7259	20	0.020	0.044	0.030	0.066	31.25	2.6	0.79	1.96	6.44	5.91	40.76
8/13/2015	3	7259	20	0.020	0.044	0.030	0.066	43	3.6	1.09	2.70	8.86	NO DATA	NO DATA

PEAK TRANSIENT PORE PRESSURE, upeak

Date	Test	Tourmaline No.	Charge (g)	Charge (kg)	Charge (lb)	TNT Equivalency (kg)	TNT Equivalency (lb)	Distance to charge (in)	Distance to charge (ft)	Distance to charge (m)	TNT Eq. SD (m/kg^⅓)	TNT Eq. SD (ft/lb^⅓)	Peak transient pore pressure (psi)	Peak transient pore pressure (kPa)
8/13/2015	1	10226	20	0.020	0.044	0.030	0.066	21	1.8	0.53	1.32	4.33	10.35	71.34
8/13/2015	1	29169	20	0.020	0.044	0.030	0.066	19.5	1.6	0.50	1.59	4.02	21.03	144.99
8/13/2015	2	10226	20	0.020	0.044	0.030	0.066	32	2.7	0.81	2.01	6.59	2.19	15.07
8/13/2015	2	29169	20	0.020	0.044	0.030	0.066	30.5	2.5	0.77	1.92	6.28	4.62	31.87
8/13/2015	3	10226	20	0.020	0.044	0.030	0.066	44	3.7	1.12	2.76	9.07	NO DATA	NO DATA
8/13/2015	3	29169	20	0.020	0.044	0.030	0.066	42.5	3.5	1.08	2.67	8.76	NO DATA	NO DATA
3/15/2016	1	7259	20	0.020	0.044	0.030	0.066	25	2.1	0.64	1.57	5.15	7.68	52.99
3/15/2016	1	10226	20	0.020	0.044	0.030	0.066	30.75	2.6	0.78	1.93	6.34	7.08	48.82
3/15/2016	2	7259	20	0.020	0.044	0.030	0.066	16.5	1.4	0.42	1.04	3.40	103.93	716.56
3/15/2016	2	10226	20	0.020	0.044	0.030	0.066	22.5	1.9	0.57	1.41	4.64	21.26	146.61
3/15/2016	3	7259	20	0.020	0.044	0.030	0.066	18	1.5	0.46	1.13	3.71	96.43	664.89
3/15/2016	3	10226	20	0.020	0.044	0.030	0.066	24	2.0	0.61	1.51	4.95	18.19	125.45
3/15/2016	4	7259	20	0.020	0.044	0.030	0.066	24.5	2.0	0.62	1.54	5.05	8.87	61.14
3/15/2016	4	10226	20	0.020	0.044	0.030	0.066	30.25	2.5	0.77	1.90	6.23	5.86	40.39
3/15/2016	6	7259	20	0.020	0.044	0.030	0.066	20.25	1.7	0.51	1.27	4.17	68.84	474.64
3/15/2016	6	10226	20	0.020	0.044	0.030	0.066	26	2.2	0.66	1.63	5.36	13.86	95.57
3/15/2016	7	7259	20	0.020	0.044	0.030	0.066	14.75	1.2	0.37	0.93	3.04	106.27	732.73
3/15/2016	7	10226	20	0.020	0.044	0.030	0.066	20.5	1.7	0.52	1.29	4.22	28.91	199.30
3/15/2016	8	7259	20	0.020	0.044	0.030	0.066	12	1.0	0.30	0.75	2.47	225.08	1551.85
3/15/2016	8	10226	20	0.020	0.044	0.030	0.066	18	1.5	0.46	1.13	3.71	55.91	385.47
3/15/2016	9	7259	20	0.020	0.044	0.030	0.066	10.25	0.9	0.26	0.64	2.11	336.52	2320.21
3/15/2016	9	10226	20	0.020	0.044	0.030	0.066	16	1.3	0.41	1.00	3.30	94.86	654.07
3/15/2016	10	7259	20	0.020	0.044	0.030	0.066	8.5	0.7	0.22	0.53	1.75	509.00	3509.44
3/15/2016	10	10226	20	0.020	0.044	0.030	0.066	14.5	1.2	0.37	0.91	2.99	135.07	931.24
3/15/2016	11	7259	20	0.020	0.044	0.030	0.066	10.125	0.8	0.26	0.64	2.09	148.84	1026.19
3/15/2016	11	10226	20	0.020	0.044	0.030	0.066	16	1.3	0.41	1.00	3.30	93.88	647.29
3/15/2016	12	7259	20	0.020	0.044	0.030	0.066	19.75	1.6	0.50	1.24	4.07	34.94	240.87
3/15/2016	12	10226	20	0.020	0.044	0.030	0.066	25.75	2.1	0.65	1.62	5.31	5.98	41.22
3/15/2016	13	7259	20	0.020	0.044	0.030	0.066	8.25	0.7	0.21	0.52	1.70	272.20	1876.73
3/15/2016	13	10226	20	0.020	0.044	0.030	0.066	14	1.2	0.36	0.88	2.88	173.40	1195.55
3/15/2016	14	7259	20	0.020	0.044	0.030	0.066	5.875	0.5	0.15	0.37	1.21	957.48	6601.56
3/15/2016	14	10226	20	0.020	0.044	0.030	0.066	11.75	1.0	0.30	0.74	2.42	298.29	2056.67
3/15/2016	15	7259	40	0.040	0.088	0.060	0.132	42.25	3.5	1.07	2.11	6.91	1.14	7.89
3/15/2016	15	10226	40	0.040	0.088	0.060	0.132	48.375	4.0	1.23	2.41	7.91	1.16	8.02
3/15/2016	16	7259	60	0.060	0.132	0.090	0.198	52.75	4.4	1.34	2.30	7.54	1.60	11.04
3/15/2016	16	10226	60	0.060	0.132	0.090	0.198	59.75	5.0	1.52	2.60	8.54	2.03	13.97

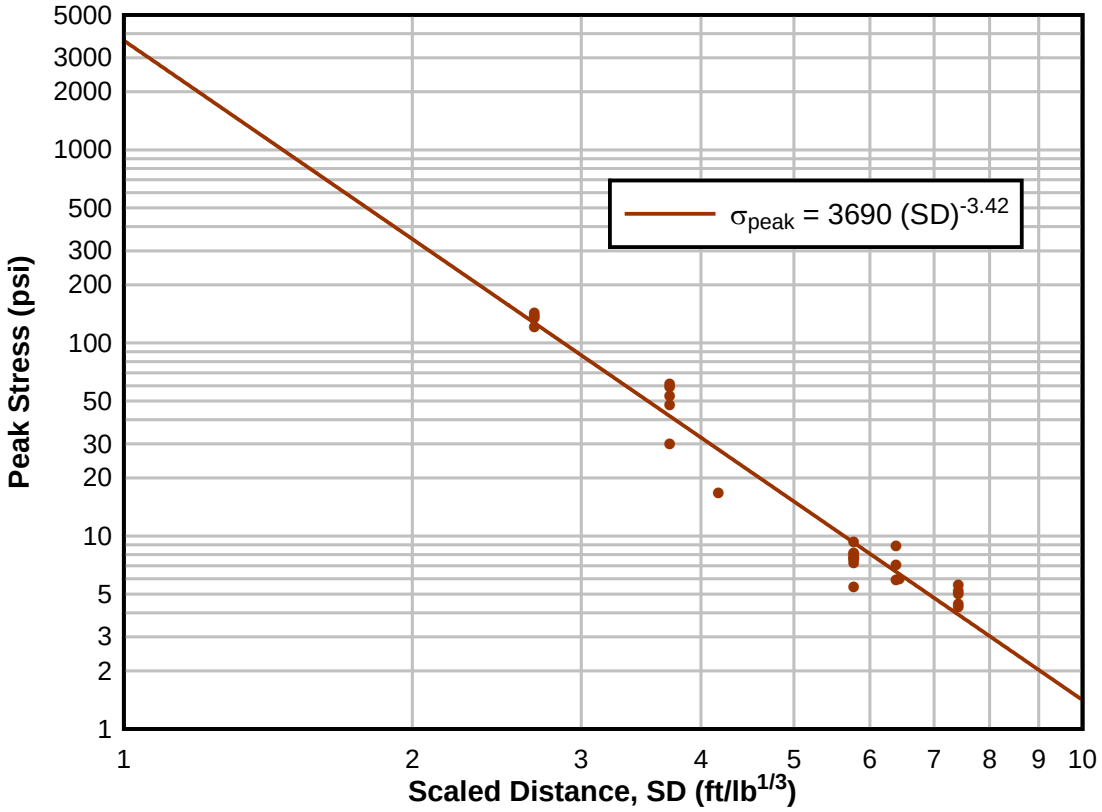
5000
3000
2000
1000
500
300
200
100
50
30
20
10
5
3
2
1
Peak Stress (psi)
σpeak = 3690 (SD)-3.42
1
2
3
4
5
6
7
8
9
10
Scaled Distance, SD (ft/lb1/3)

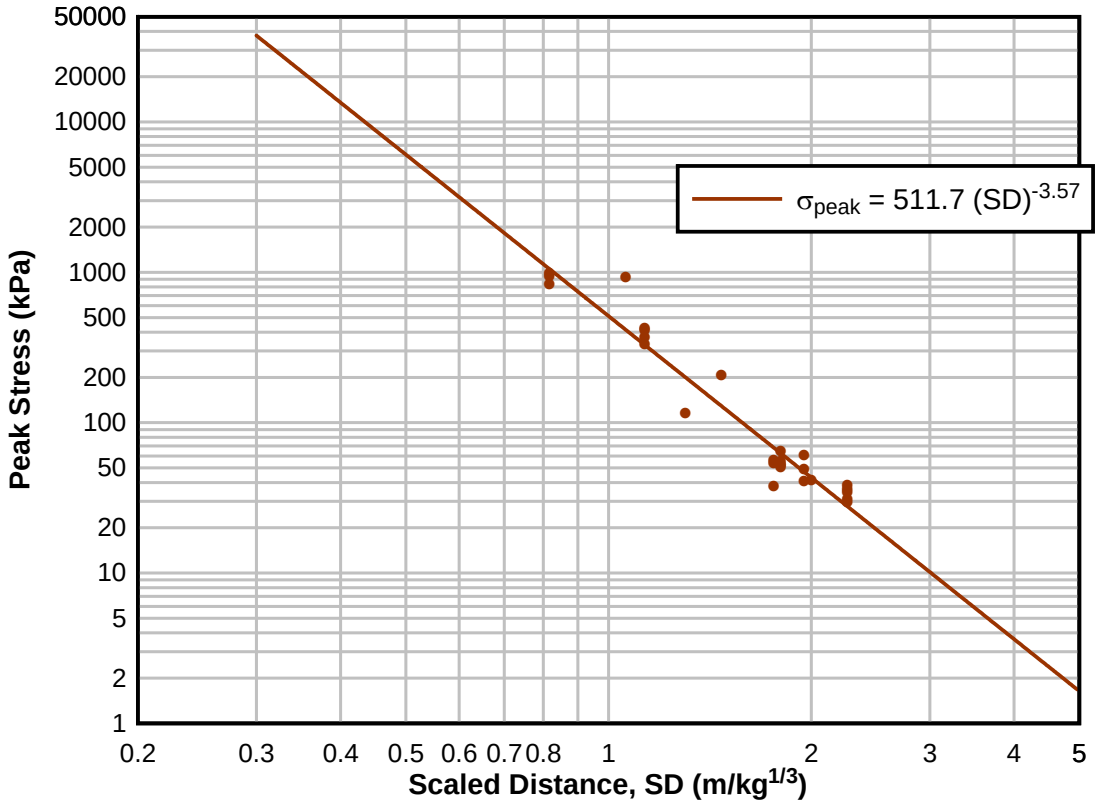
50000
20000
10000
5000
2000
1000
500
200
100
50
20
10
5
2
1
Peak Stress (kPa)
σpeak = 511.7 (SD)-3.57
0.2
0.3
0.4
0.5
0.6
0.7
0.8
1
2
3
4
5
Scaled Distance, SD (m/kg1/3)

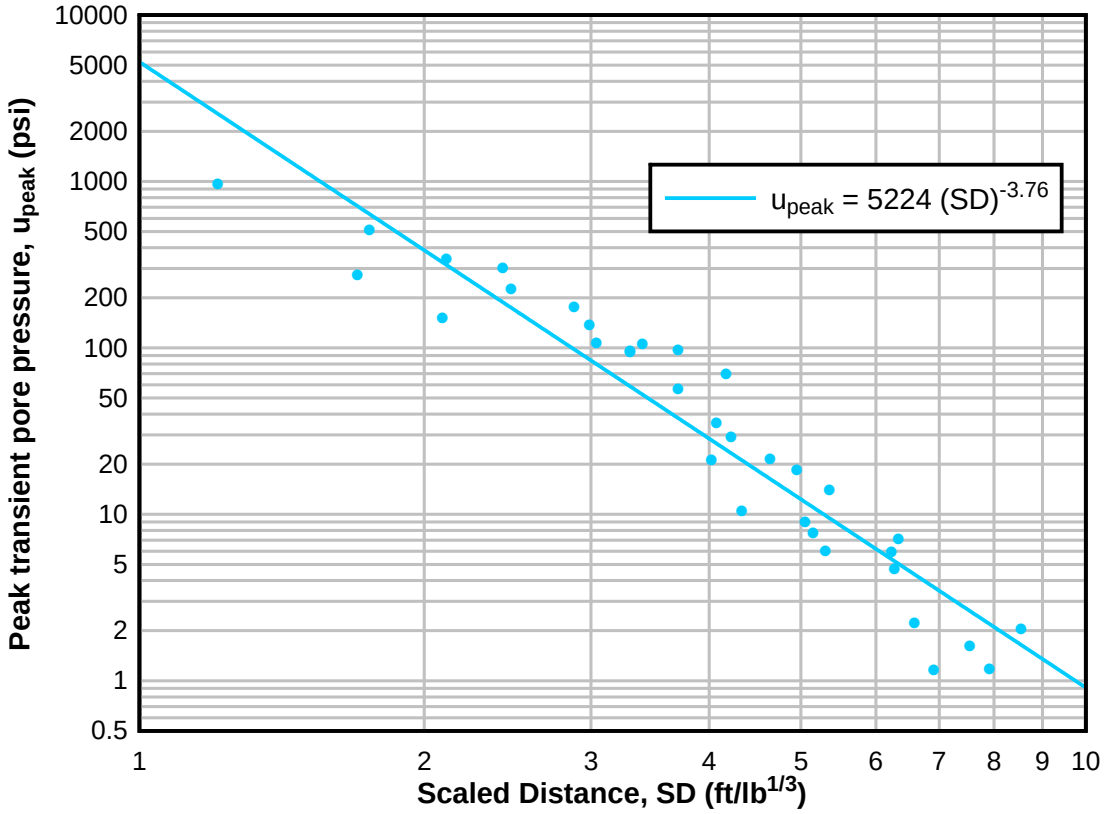
Peak transient pore pressure, u_{peak} (psi)
10000
5000
2000
1000
500
200
100
50
20
10
5
2
1
0.5
1
2
3
4
5
6
7
8
9
10
Scaled Distance, SD (ft/lb$^{1/3}$)
u_{peak} = 5224 (SD)$^{-3.76}$

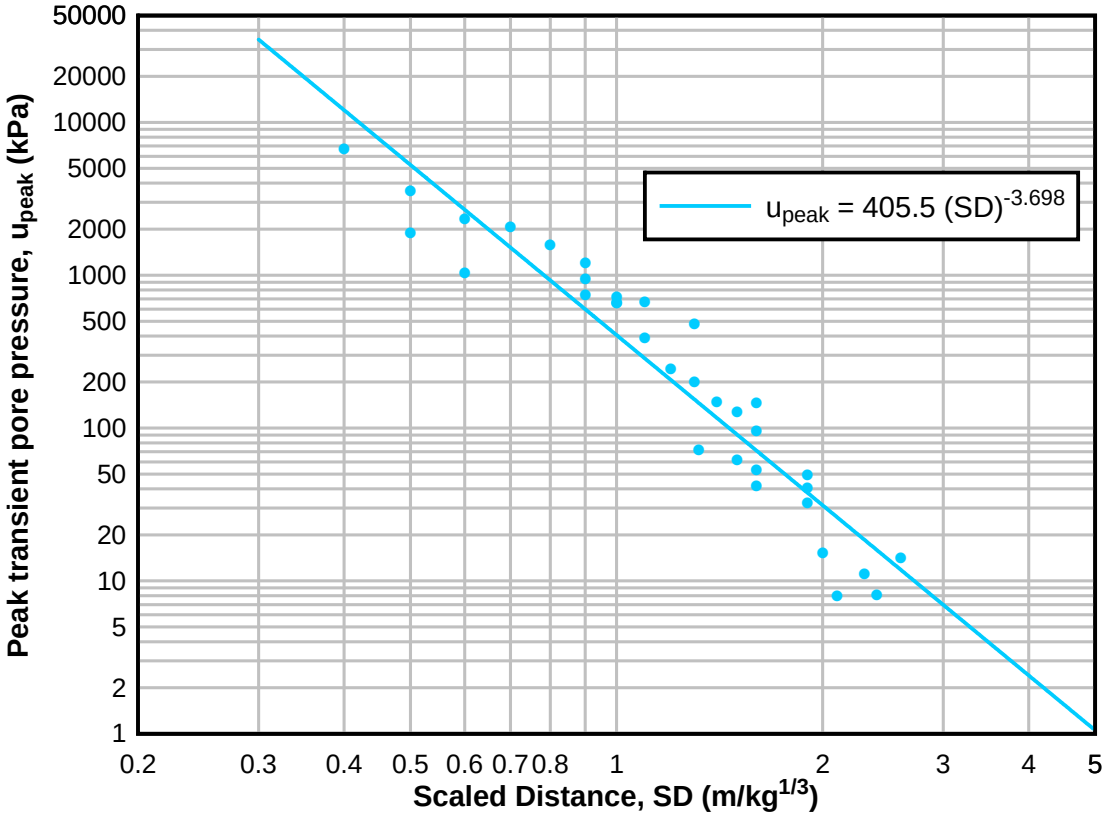
Peak transient pore pressure, u_{peak} (kPa)
50000
20000
10000
5000
2000
1000
500
200
100
50
20
10
5
2
1
0.2
0.3
0.4
0.5
0.6
0.7
0.8
1
2
3
4
5
Scaled Distance, SD (m/kg$^{1/3}$)
u_{peak} = 405.5 (SD)$^{-3.698}$

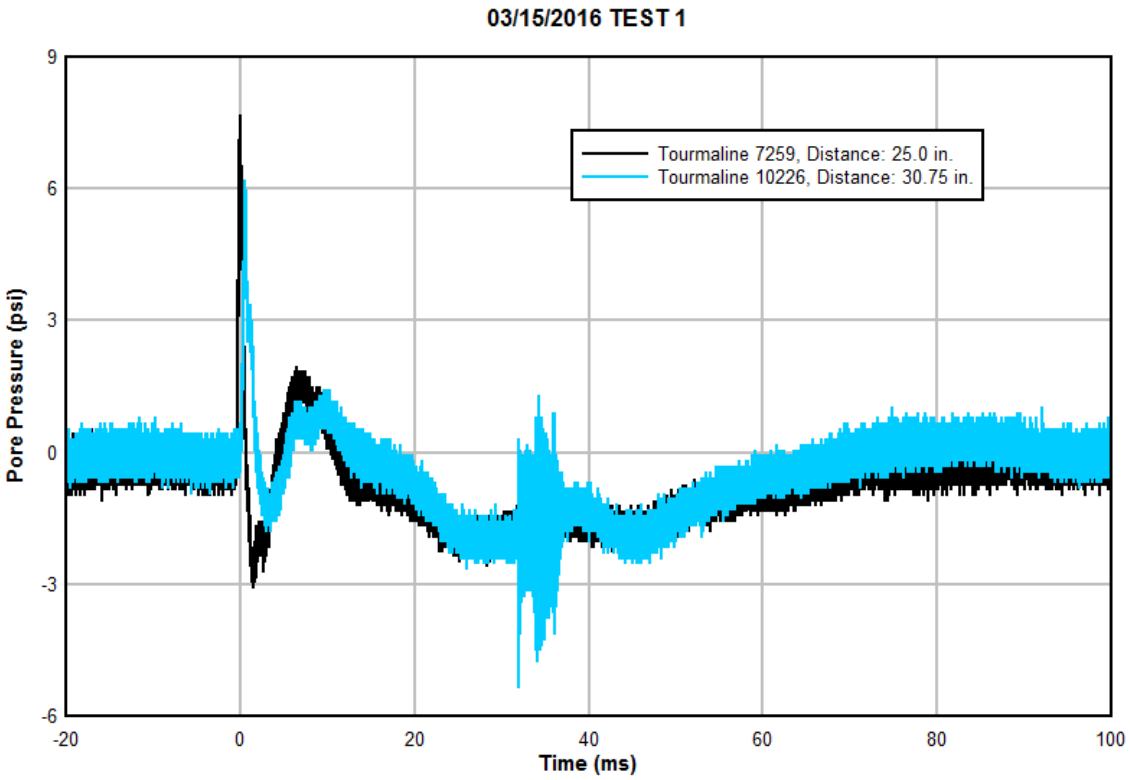
03/15/2016 TEST 1
Tourmaline 7259, Distance: 25.0 in.
Tourmaline 10226, Distance: 30.75 in.
Pore Pressure (psi)
Time (ms)
9
6
3
0
-3
-6
-20
0
20
40
60
80
100

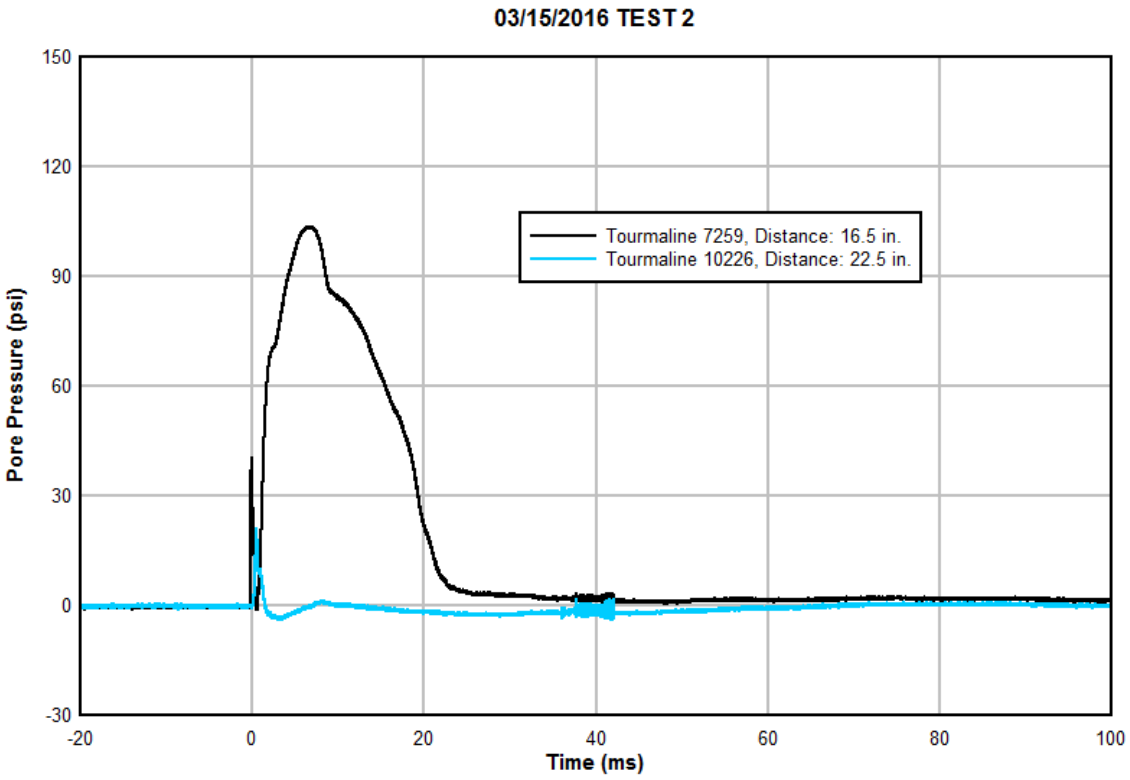
03/15/2016 TEST 2
Tourmaline 7259, Distance: 16.5 in.
Tourmaline 10226, Distance: 22.5 in.
Pore Pressure (psi)
Time (ms)
150
120
90
60
30
0
-30
-20
0
20
40
60
80
100

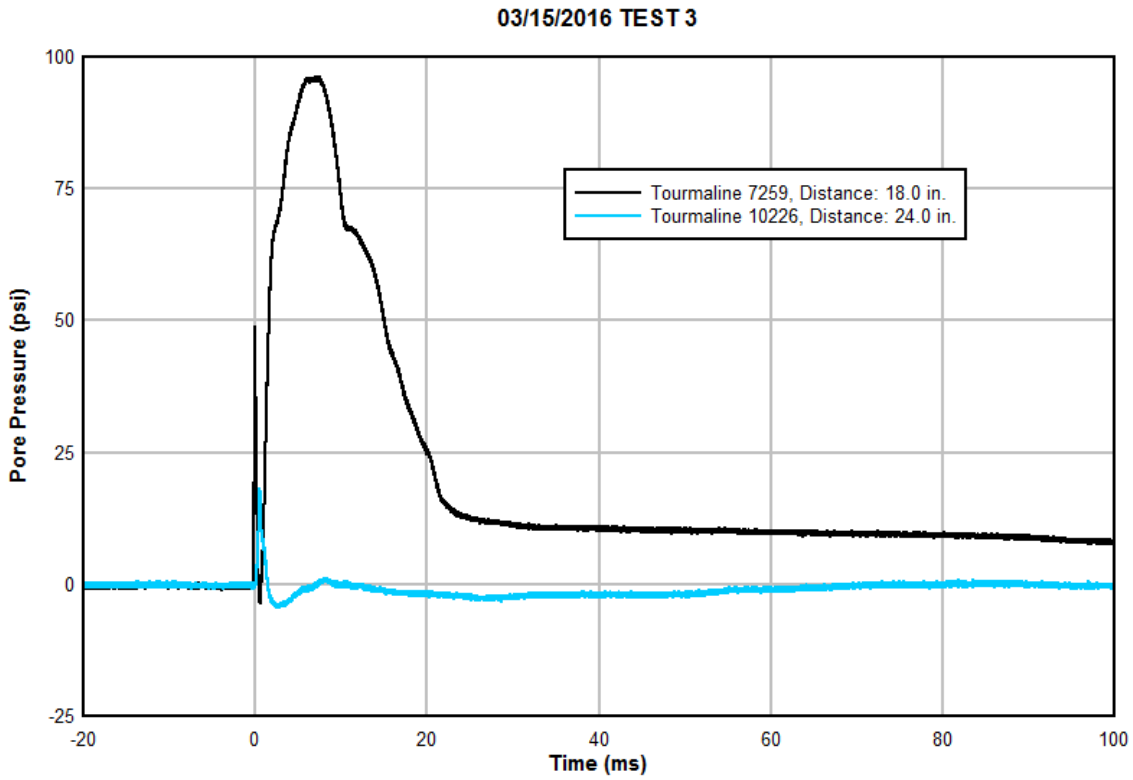
03/15/2016 TEST 3
Tourmaline 7259, Distance: 18.0 in.
Tourmaline 10226, Distance: 24.0 in.
Pore Pressure (psi)
Time (ms)
100
75
50
25
0
-25
-20
0
20
40
60
80
100

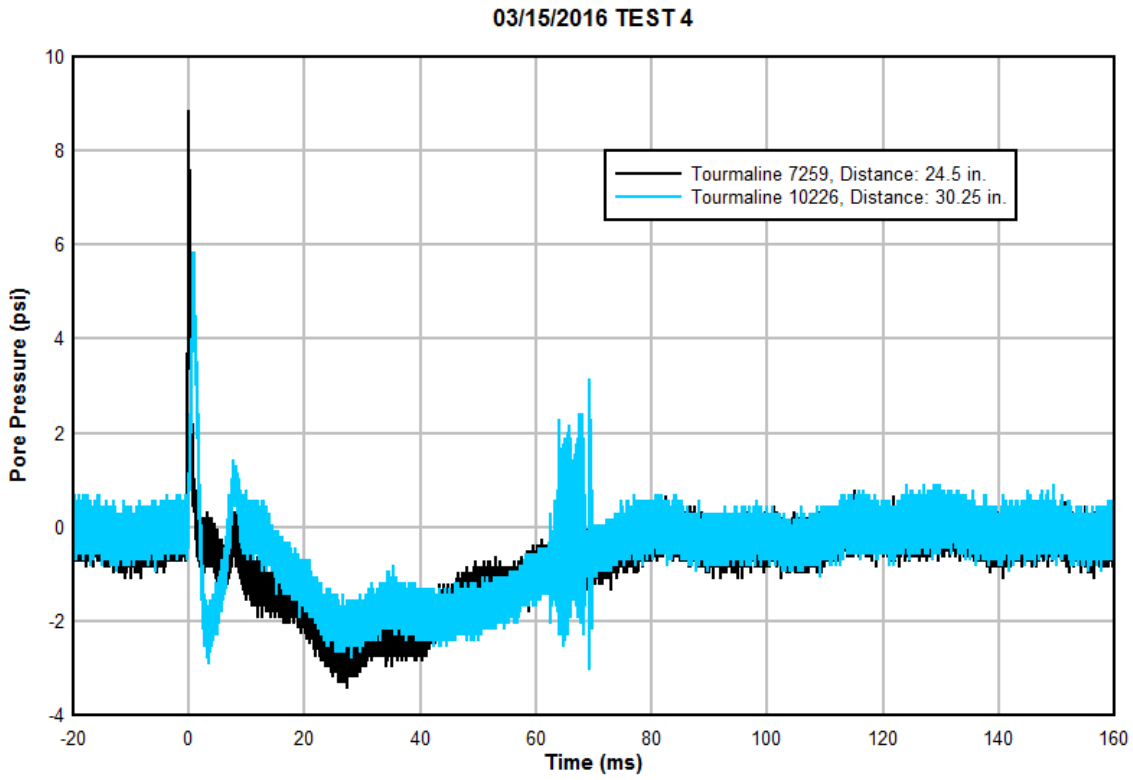
03/15/2016 TEST 4
Tourmaline 7259, Distance: 24.5 in.
Tourmaline 10226, Distance: 30.25 in.
Pore Pressure (psi)
Time (ms)
10
8
6
4
2
0
-2
-4
-20
0
20
40
60
80
100
120
140
160

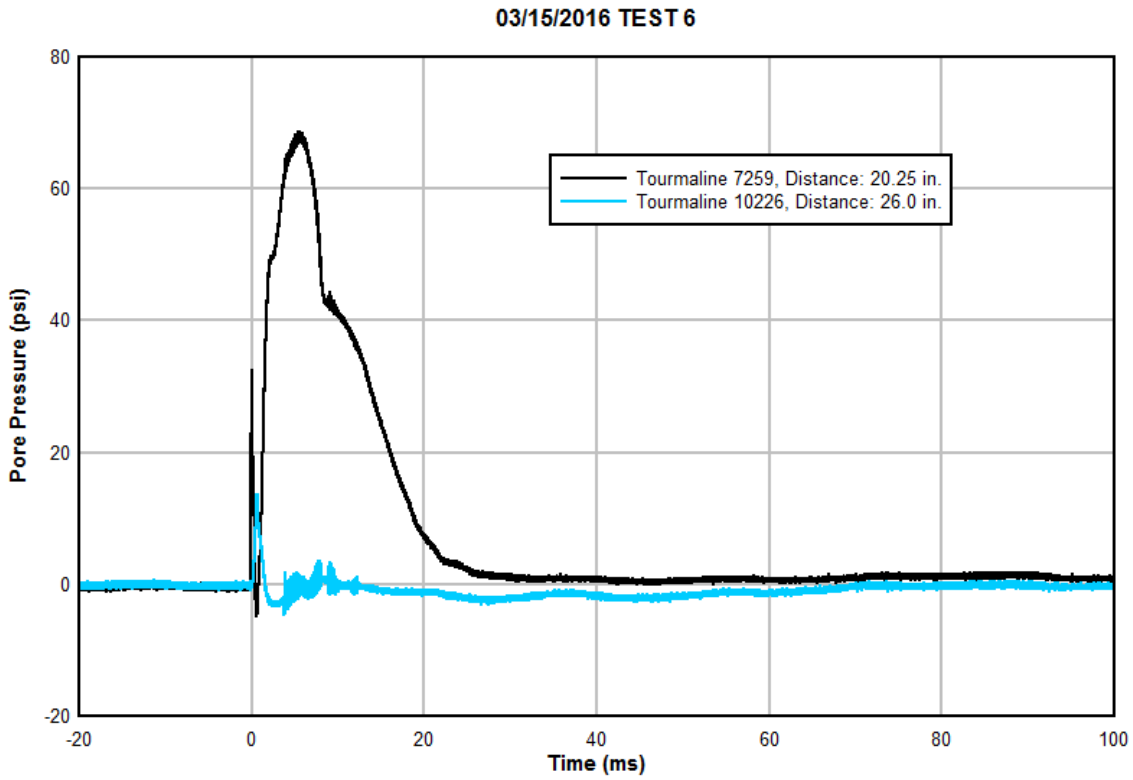
03/15/2016 TEST 6
Tourmaline 7259, Distance: 20.25 in.
Tourmaline 10226, Distance: 26.0 in.
Pore Pressure (psi)
Time (ms)
80
60
40
20
0
-20
-20
0
20
40
60
80
100

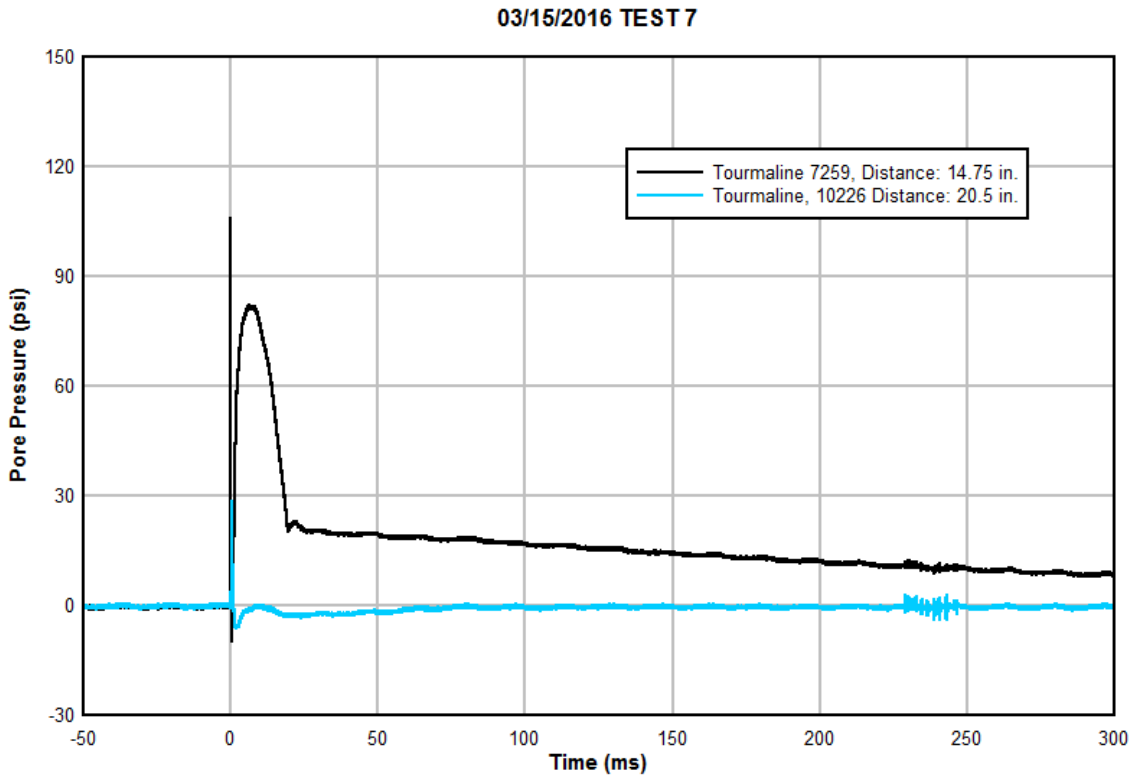
03/15/2016 TEST 7
Tourmaline 7259, Distance: 14.75 in.
Tourmaline, 10226 Distance: 20.5 in.
Pore Pressure (psi)
Time (ms)
150
120
90
60
30
0
-30
-50
0
50
100
150
200
250
300

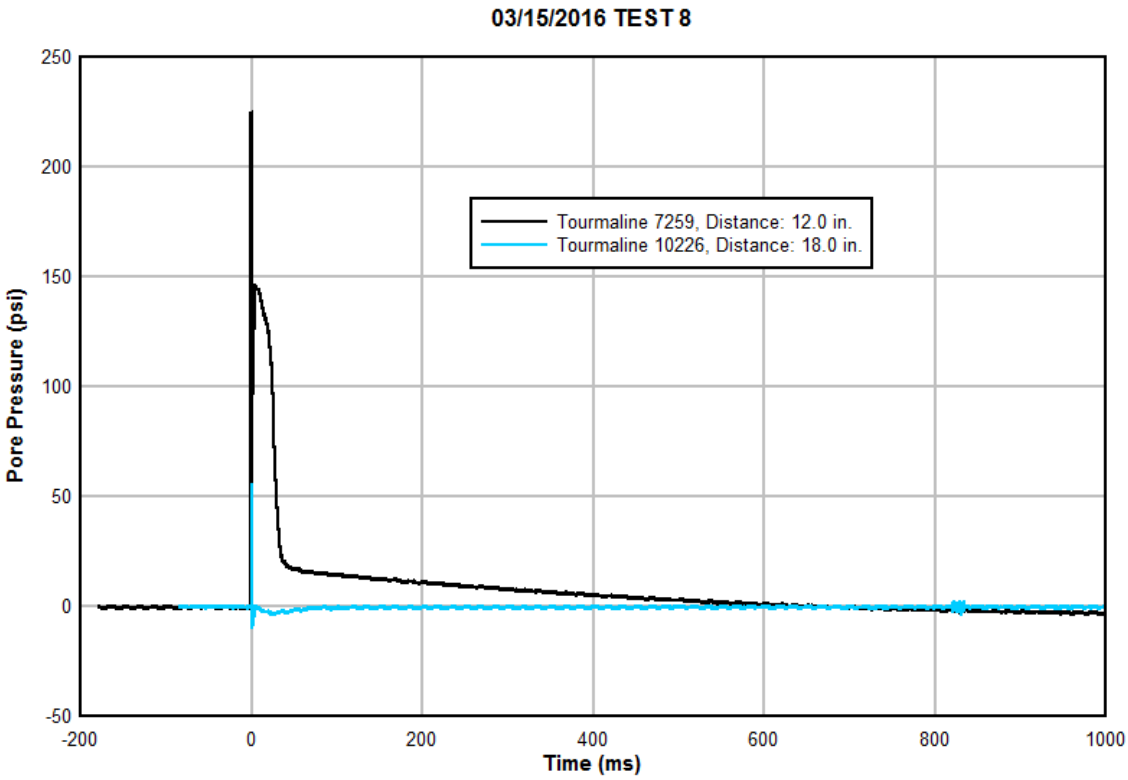
03/15/2016 TEST 8
Tourmaline 7259, Distance: 12.0 in.
Tourmaline 10226, Distance: 18.0 in.
Pore Pressure (psi)
Time (ms)
250
200
150
100
50
0
-50
-200
0
200
400
600
800
1000

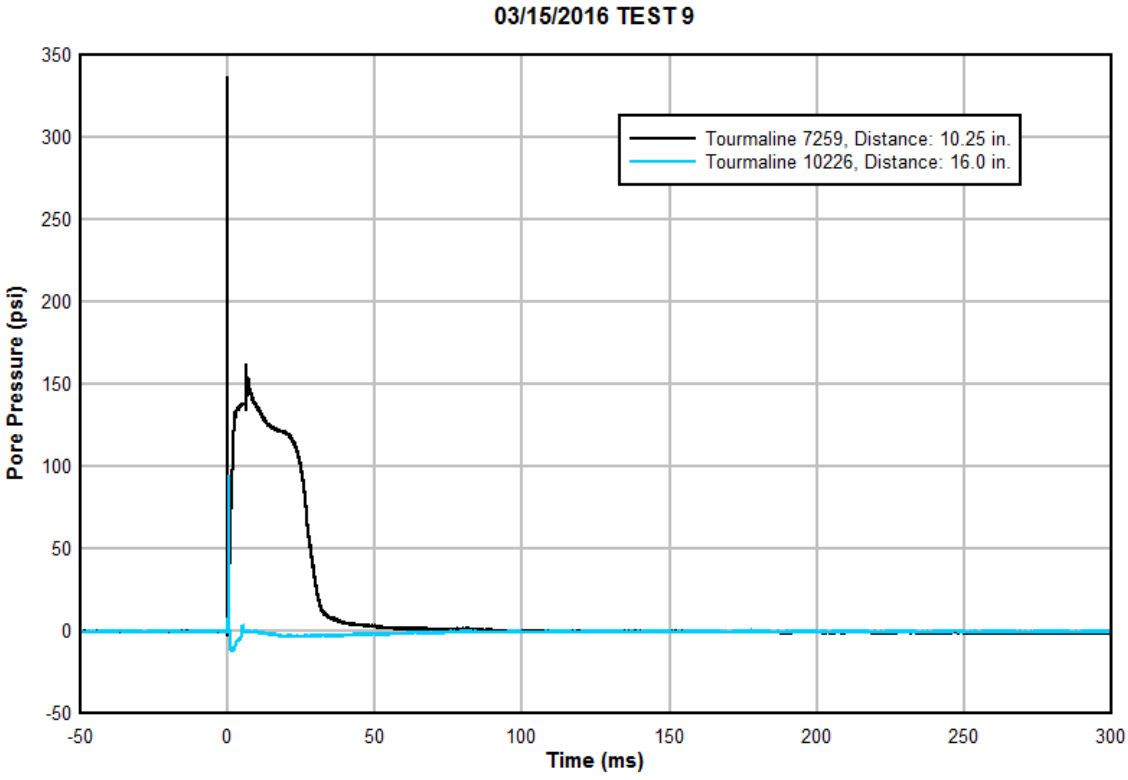
03/15/2016 TEST 9
Tourmaline 7259, Distance: 10.25 in.
Tourmaline 10226, Distance: 16.0 in.
Pore Pressure (psi)
Time (ms)
350
300
250
200
150
100
50
0
-50
-50
0
50
100
150
200
250
300

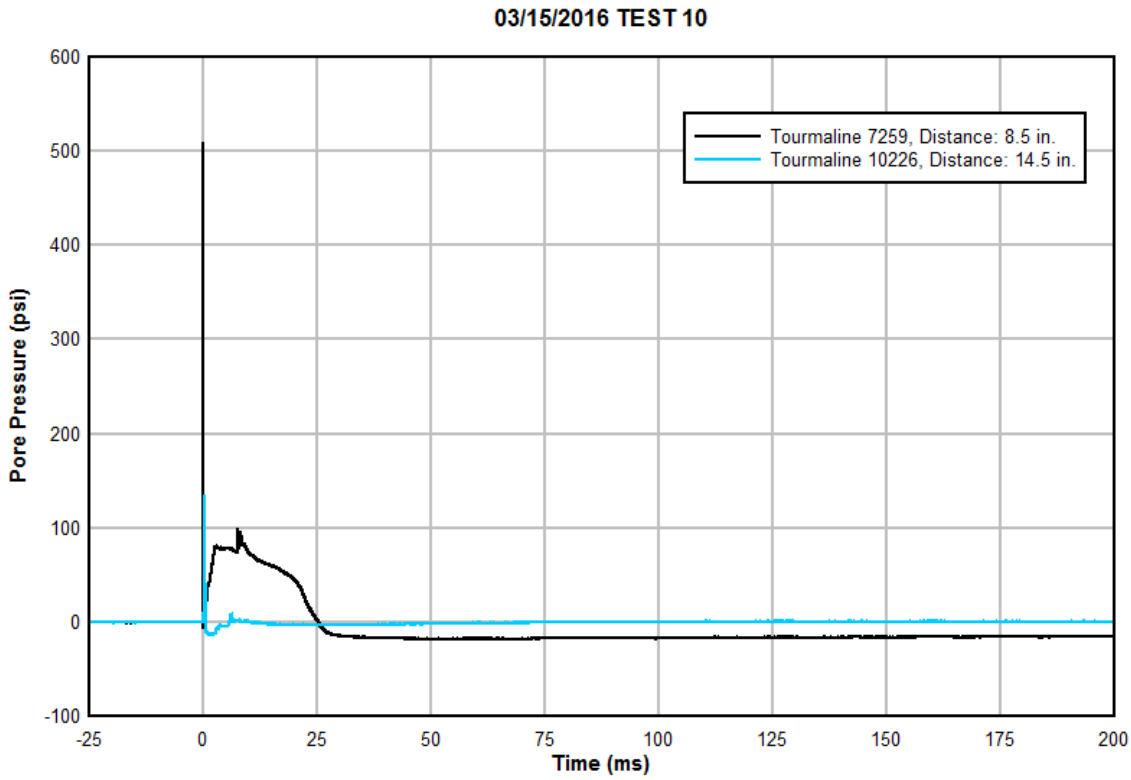
03/15/2016 TEST 10
Tourmaline 7259, Distance: 8.5 in.
Tourmaline 10226, Distance: 14.5 in.
Pore Pressure (psi)
600
500
400
300
200
100
0
-100
-25
0
25
50
75
100
125
150
175
200
Time (ms)

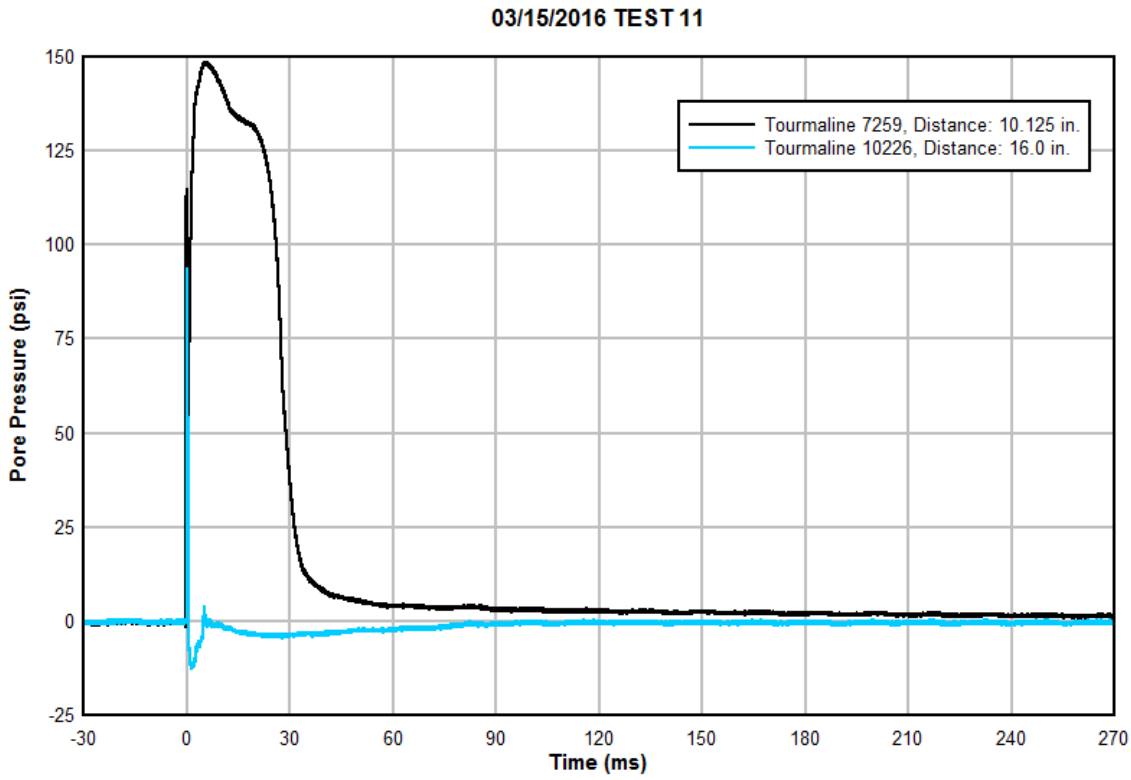
03/15/2016 TEST 11
Tourmaline 7259, Distance: 10.125 in.
Tourmaline 10226, Distance: 16.0 in.
Pore Pressure (psi)
150
125
100
75
50
25
0
-25
-30
0
30
60
90
120
150
180
210
240
270
Time (ms)

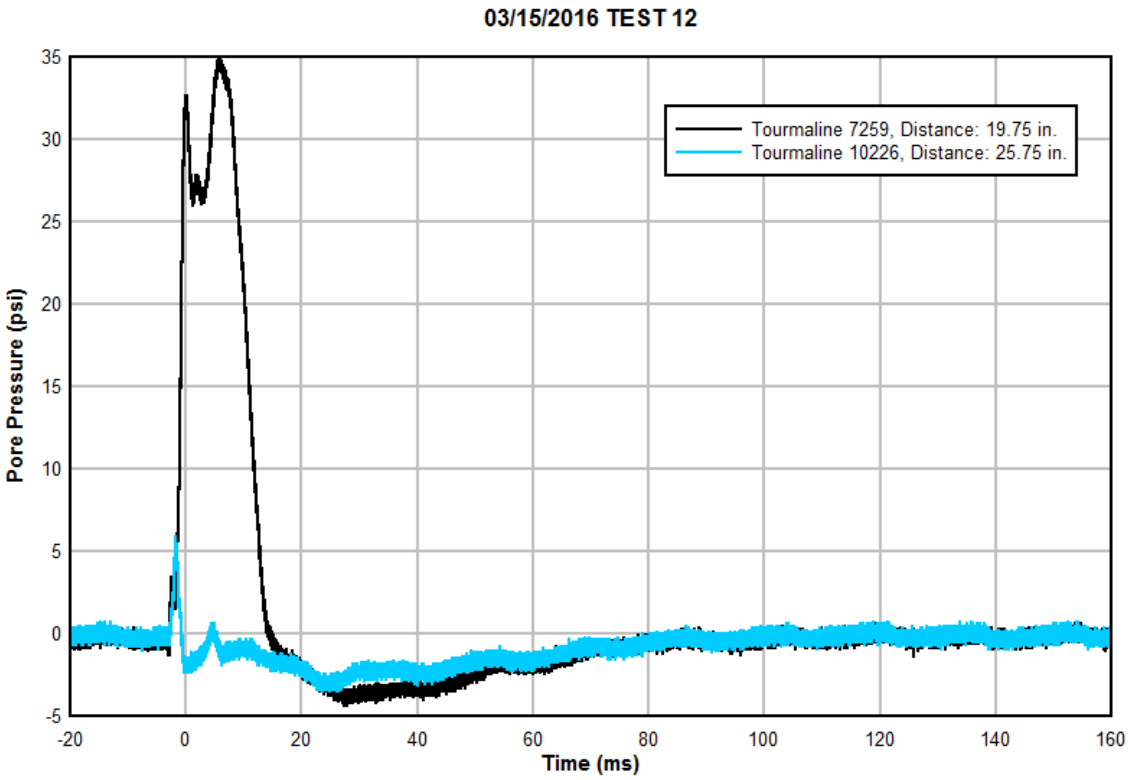
03/15/2016 TEST 12
Tourmaline 7259, Distance: 19.75 in.
Tourmaline 10226, Distance: 25.75 in.
Pore Pressure (psi)
Time (ms)
35
30
25
20
15
10
5
0
-5
-20
0
20
40
60
80
100
120
140
160

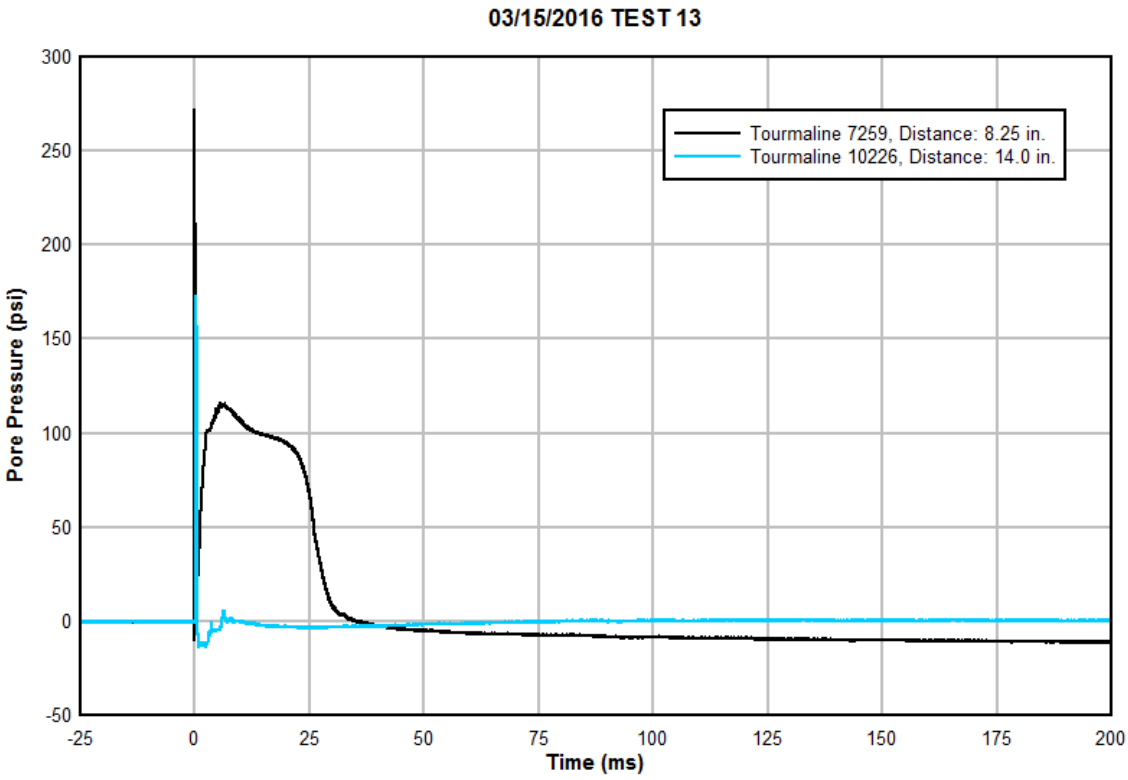
03/15/2016 TEST 13
Tourmaline 7259, Distance: 8.25 in.
Tourmaline 10226, Distance: 14.0 in.
Pore Pressure (psi)
Time (ms)
300
250
200
150
100
50
0
-50
-25
0
25
50
75
100
125
150
175
200

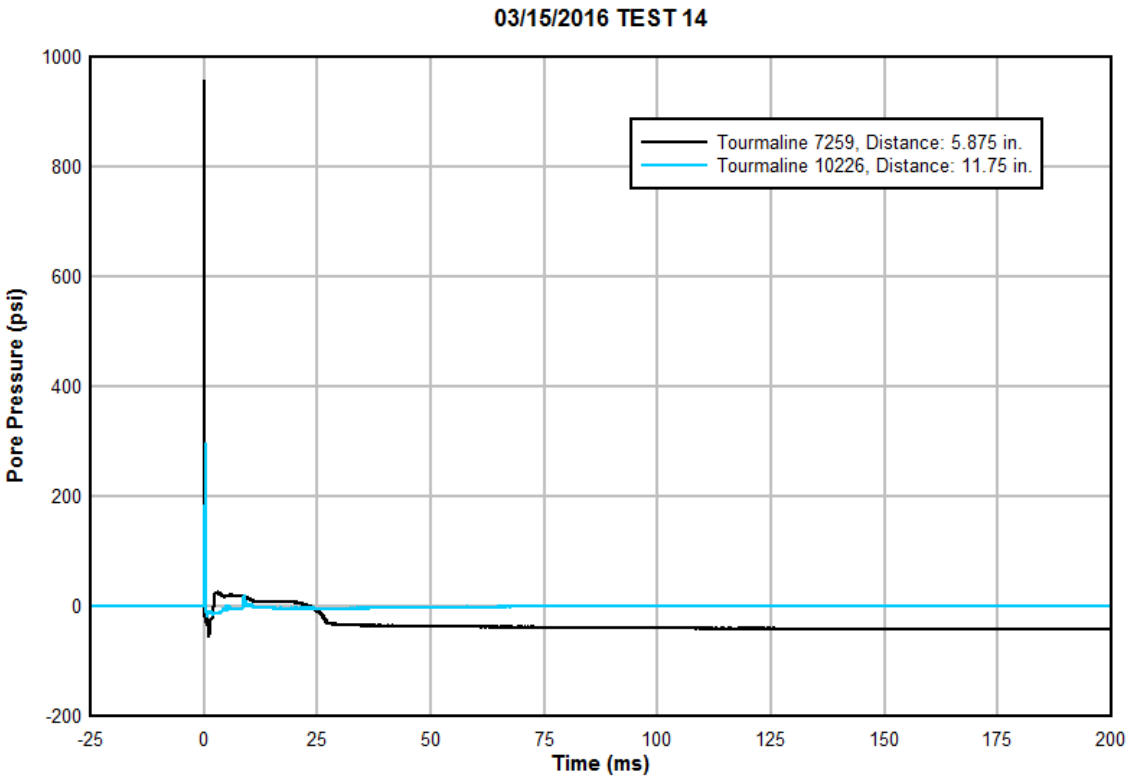
03/15/2016 TEST 14
Tourmaline 7259, Distance: 5.875 in.
Tourmaline 10226, Distance: 11.75 in.
Pore Pressure (psi)
Time (ms)
1000
800
600
400
200
0
-200
-25
0
25
50
75
100
125
150
175
200

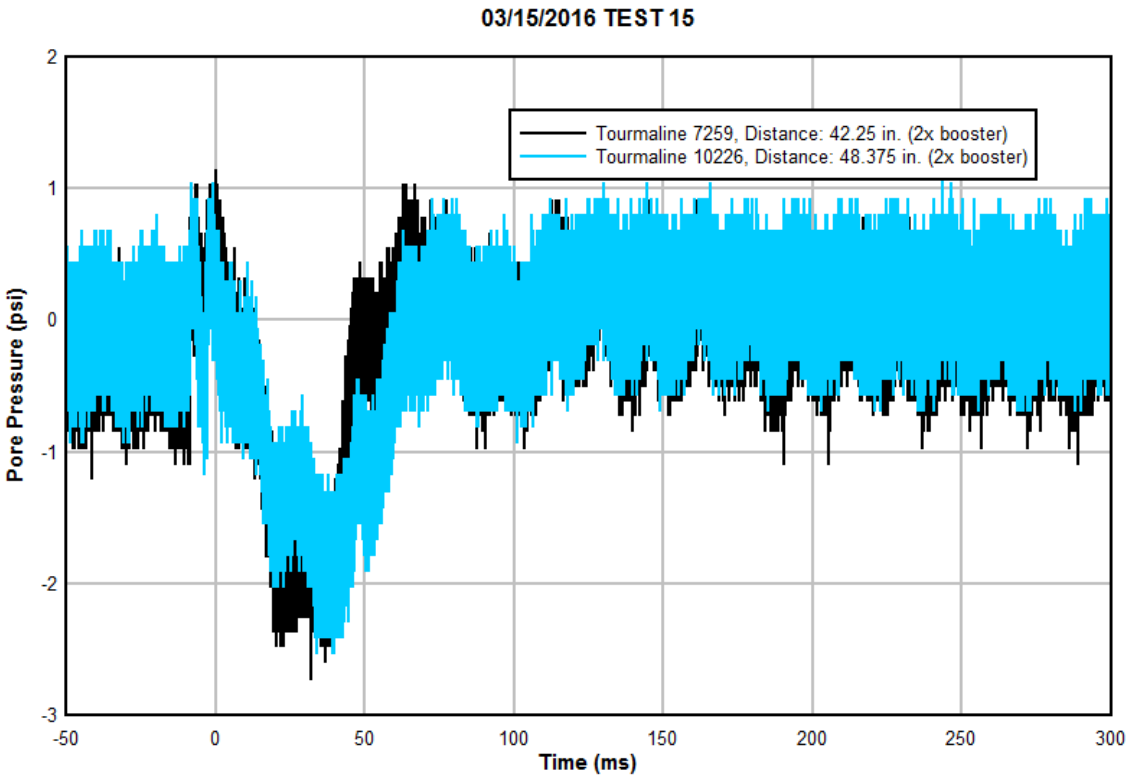
03/15/2016 TEST 15
Tourmaline 7259, Distance: 42.25 in. (2x booster)
Tourmaline 10226, Distance: 48.375 in. (2x booster)
Pore Pressure (psi)
Time (ms)
2
1
0
-1
-2
-3
-50
0
50
100
150
200
250
300

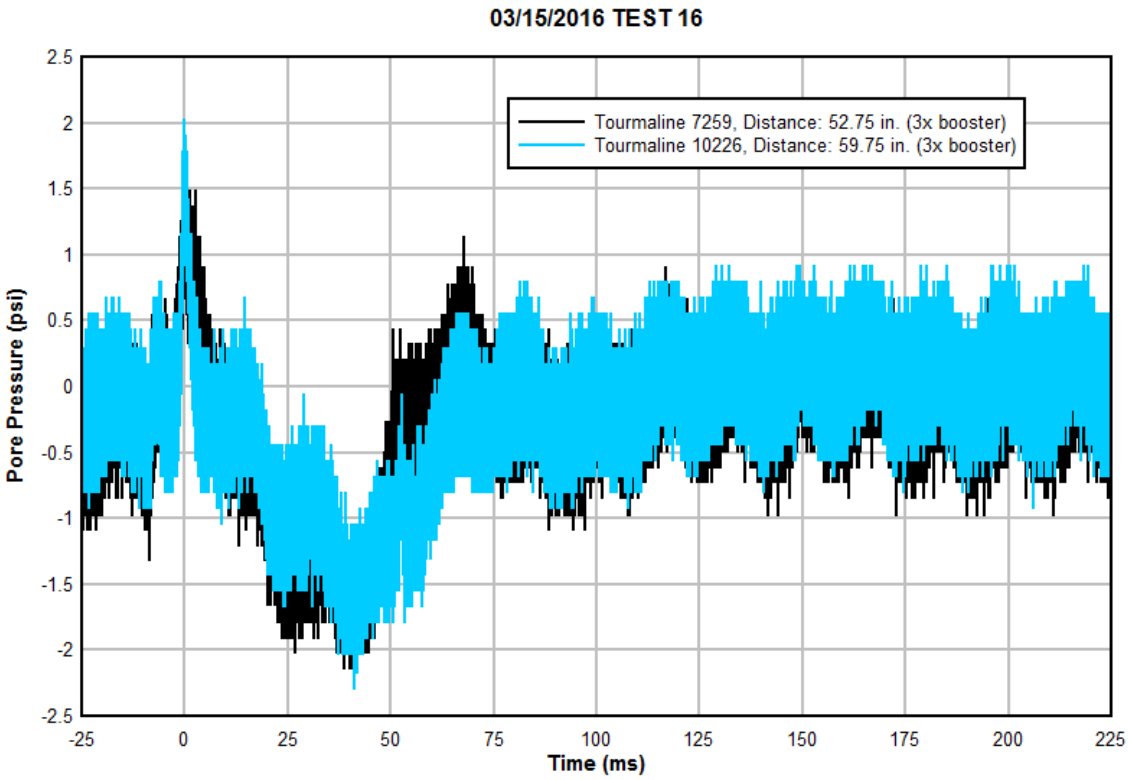
03/15/2016 TEST 16
Tourmaline 7259, Distance: 52.75 in. (3x booster)
Tourmaline 10226, Distance: 59.75 in. (3x booster)
Pore Pressure (psi)
Time (ms)
2.5
2
1.5
1
0.5
0
-0.5
-1
-1.5
-2
-2.5
-25
0
25
50
75
100
125
150
175
200
225

BIBLIOGRAPHY

Al-Qasimi, M.A. Erfan, Wayne A. Charlie, and David J. Woeller, “Canadian Liquefaction Experiment (CANLEX): Blast-Induced Ground Motion and Pore Pressure Experiments,” *Geotechnical Testing Journal*, Vol. 28, No. 1, January 2005.

ASTM Standard D1140, 2000 (2006), “Standard Test Methods for Amount of Material in Soils Finer than No. 200 (75-µm) Sieve,” *ASTM International*, West Conshohocken, PA, 2006, DOI: 10.1520/D1140-00R06.

ASTM Standard D1557, 2009, “Standard Test Methods for Laboratory Compaction Characteristics of Soil Using Modified Effort (56,000 ft-lbf/ft^3 (2,700 kN-m/m^3)),” *ASTM International*, West Conshohocken, PA, 2009, DOI: 10.1520/D1557-09.

ASTM Standard D3080, 2004, “Standard Test Methods for Direct Shear Test of Soils Under Consolidated Drained Conditions,” *ASTM International*, West Conshohocken, PA, 2004, DOI: 10.1520/D3080-04.

ASTM Standard D422, 2007, “Standard Test Method for Particle-Size Analysis of Soils,” *ASTM International*, West Conshohocken, PA, 2007, DOI: 10.1520/D0422-63R07.

ASTM Standard D698, 2007, “Standard Test Methods for Laboratory Compaction Characteristics of Soil Using Standard Effort (12 400 ft-lbf/ft^3 (600 kN-m/m^3)),” *ASTM International*, West Conshohocken, PA, 2007, DOI: 10.1520/D0698-07E01.

Charlie, W. A., “Review of Present Practices Used in Prediction of the Effects of Blasting on Pore Pressure,” U.S. Department of Interior, Bureau of Reclamation, Technical Report No. GR-85-9, Lakewood, CO, November 1985.

Charlie, W. A., P. J. Jacobs, and D. O. Doehring, “Blast-Induced Liquefaction of an Alluvial Sand Deposit,” *Geotechnical Testing Journal*, Vol. 15, No. 1, 1992, pp. 14-23.

Charlie, Wayne A., Wayne A. Lewis, and Donald O. Doehring, “Explosive Induced Pore Pressure in a Sandfill Dam,” *Geotechnical Testing Journal*, Vol. 24, No. 4, 2001, pp. 391-400

Charlie, Wayne A., Thomas E. Bretz, Lynne A. Schure (White), and Donald O. Doehring, “Blast-Induced Pore Pressure and Liquefaction of Saturated Sand,” *Journal of Geotechnical and Geoenvironmental Engineering,* Vol. 139, No. 8, August 2013, pp. 1308-1319.

Cole, R. H., “Underwater Explosions,” *Princeton University Press*, Princeton, NJ, 1948.

Crawford, R. E., C. J. Higgins, and E. A. Bultmann, “The Air Force manual for design and analysis of hardened structures,” *AFWL-TR-74-102*, Air Force Weapons Laboratory, Kirtland Air Force Base, NM, 1974.

Crenwelge, Jr., O. E., “Method for Determining Amplitude-frequency Components of Blast Induced Ground Vibrations,” *International Society of Explosives Engineers*, 1988R, 2000, pp. 73-88.

Davies, William E., James F. Bailey, and Donavan B. Kelly, “West Virginia’s Buffalo Creek Flood: A Study of the Hydrology and Engineering Geology”, *USGS Circular* 667. Reston, VA: U.S. Geological Survey, 1972.

Dobry, R. H., Ladd, R. S., Yokel, F. Y., Chung, R. M., and Powell, D., “Prediction of Porewater Pressure Buildup and Liquefaction of Sands during Earthquakes by Cyclic Strain Methods,” *Building Science Series 138*, National Bureau of Standards, U.S. Government Printing Office, Washington, D.C., 1982.

Drake, J. L. and C. D. Little, “Ground Shock from Penetrating Conventional Weapons,” *1st Symposium on Non-Nuclear Munitions with Structures, U.S. Air Force*, U.S. Air Force Academy, Colorado Springs, CO, May 1983, pp. 1-6.

Eller, J. M., “Predicting pore pressure response in in-situ liquefaction studies using controlled blasting,” *M.S. thesis*, School of Civil and Construction Engineering, Oregon State University, 2011.

FEMA, “Federal Guidelines for Dam Safety, Earthquake Analyses and Design of Dams,” May 2005, pp. 1-45.

Gohl, W. B., Howie, J. A., and C. E. Rea, “Use of controlled detonation of explosives for liquefaction testing,” *Proc., 4th International Conference on Recent Advances in Geotechnical Earthquake Engineering and Soil Dynamics and Symposium in Honor of Professor W.D. Liam Finn*, University of Missouri-Rolla, 2001, pp. 1-9.

Harp, Edwin L., Wade G. Wells II, and John G. Sarmiento, “Pore Pressure Response During Failure in Soils,” *Geologic Society of America Bulletin*, Vol. 102, April 1990, pp. 428-438.

Hubert, M. E., “Shock loading of water saturated Eniwetok coral sand,” *M.S. thesis*, Department of Civil Engineering, Colorado State University, 1986, pp. 145-154.

Itasca Consulting Group, Incorporated, “Dynamic Analysis,” *FLAC3D Version 5.01*.

ISEE Blasters’ Handbook, International Society of Explosives Engineers, 2011.

Ivano, P. L., “Compaction of noncohesive soils by explosions,” *Izdatel’stvor Literatury Po Stroitel’stvu*, 1967.

Jacobs, P. J., “Blast-Induced Liquefaction of an Alluvial Sand Deposit,” M. S. Thesis, Department of Civil Engineering, Colorado State University, 1988.

Joachim, Charles E., and Charles R. Welch, “Underwater Shocks From Blasting,” *International Society of Explosives Engineers*, 1997G, 2000, pp. 525-536.

Kalinski, Michael E., Soil Mechanics Lab Manual 2nd Edition, John Wiley & Sons, Incorporated, 2011.

Kolden, Kristen D., and Cathy Aimone-Martin, “Underwater Blast Pressure Monitoring for the Columbia River Channel Improvement Project,” *International Society of Explosives Engineers*, 2014G, 2014.

Kumar, Ranjan, Deepankar Choudhury, and Kapilesh Bhargava, “Prediction of Blast-Induced Vibration Parameters for Soil Sites,” *International Journal of Geomechanics*, Vol. 14, No. 3, 2013.

Kummeneje, D., and O. Eide, “Investigation of loose sand deposits by blasting,” *Proc., 5th ICSMFE*, ISSMFE, 1961, pp. 491-497.

Larson-Robl, Kylie, Jhon Silva-Castro, and Joshua Micah Hoffman, “Blasting Effects on Pore Pressure in Coal Impoundments (Dry Conditions – Part I),” *Proceedings of the 41st Annual Conference on Explosives & Blasting Technique,* February 2015.

Lee, Fook-Hou, “Frequency Response of Diaphragm Pore Pressure Transducers in Dynamic Centrifuge Model Tests,” *Geotechnical Testing Journal*, Vol. 13, No. 3, September 1990, pp. 201-207.

Long, J. H., Ries, E. R., and Michalopoulos, A. P. “Potential for Liquefaction Due to Construction Blasting,” *Proceedings, International Conference on Recent Advances in Geotechnical Engineering and Soil Dynamics*, University of Missouri – Rolla, 1981, pp. 191-194.

Lyakhov, G. M., “Shock Waves in the Ground and the Dilatency of Water Saturated Sand,” *Zhurnal Prikladony Mekhanik I Tekhnicheskoy Fiziki*, Moscow, USSR, No. 1, 1961, pp. 38-46.

Moore, Peter L., and Neal R. Iverson, “Slow Episodic Shear of Granular Materials Regulated by Dilatant Strengthening,” *Geology*, Vol. 30, No. 9, September 2002, pp. 843-846.

Moore, Walter I., “Role of Fluid Pressure in Overthrust Faulting: A Discussion,” *Geological Society of America Bulletin*, Vol. 72, October 1961, pp. 1581-1586.

Moses, Lynn J., “The Ross Point Landslide: An Instrumental Record of Landslide Reactivation,” *Reviews in Engineering Geology*, Vol. 20, 2008, pp. 167-181.

Nonveiller, Ervin, Josip Rupcic, and Zvonimir Sever, “War Damages and Reconstruction of Peruca Dam,” *Journal of Geotechnical and Geoenvironmental Engineering*, Vol. 125, No. 4, April 1999, pp. 280-288.

Obermeyer, J. R., “Monitoring Uranium Tailings Dams During Blasting Program,” *Symposium on Uranium Mill Tailings Management*, Colorado State University, November 1980, pp. 513-527.

Pampeyan, Earl H., Thomas L. Holzer, and Malcolm M. Clark, “Modern Ground Failure in the Garlock Fault Zone, Fremont Valley, California,” *Geological Society of America Bulletin,* Vol. 100, May 1988, pp. 677-691.

Pathirage, K. S., “Critical assessment of the CANLEX blast experiment to facilitate a development of an in-situ liquefaction methodology using explosives,” *M.S. thesis,* Department of Civil Engineering, University of British Colombia, 2000.

Puchkov, S. V., “Correlation between the Velocity of Seismic Oscillations of Particles and the Liquefaction Phenomenon of Water-Saturated Sand,” *Problems of Engineering Seismology*, Vol. 6, 1962.

Saharan, M. R., H.S. Mitri, and J. L. Jethwa, “Rock Fracturing by Explosive Energy: Review of State-of-the-Art,” *Fragblast*, Vol. 10, No.1-2, March- June 2006, pp. 61-81.

Sainato, Paul, “Blasting Effects on Coal Refuse Impoundment Structures,” Proposal for Dissertation Research, Department of Mining Engineering, Universty of Kentucky, 2016.

Salehian, Ali, “Predicting the Dynamic Behavior of Coal Mine Tailings Using State-of-Practice Geotechnical Field Methods,” *Theses and Dissertations—Civil Engineering*, Department of Civil Engineering, University of Kentucky, 2013.

Sanchidrian, Jose A., Pablo Segarra, and Lina M. Lopez, “Energy Components in Rock Blasting,” *International Journal of Rock Mechanics & Mining Sciences*, Vol. 44, No. 1, January 2007, pp. 130-147.

Simmonds, John, and David N. MacLennan, Fisheries Acoustics: *Theory and Practice, 2nd Edition*, Wiley-Blackwell, 2015.

Skempton, A. W., “The Pore-Pressure Coefficients A and B,” *Géotechnique*, Vol. 4, No. 4, 1954, pp. 143-147.

Studer, J., and L. Kok, “Blast-induced excess porewater pressure and liquefaction, experience and application,” *Proc., Int. Symposium on Soils Under Cyclic and Transient Loading*, 1980, pp. 581-593.

Taylor, L. C., W. L. Fourney, and H. U. Leiste, “Close-In Shockwave Characteristics in Saturated Sand,” *Blasting and Fragmentation,* Vol. 7, No. 3, 2013, pp. 183-195.

Terzaghi, K., R. B. Peck, and G. Mesri, “Article 17 Stress, Strain, and Failure in Soils,” *Soil Mechanics in Engineering Practice*, 3rd Edition, Wiley, 1996.

Veyera, G. E., “Transient porewater pressure response and liquefaction in a saturated sand,” Ph.D. dissertation*,* Department of Civil Engineering, Colorado State University, 1985.

Veyera, G. E., and W. A. Charlie, “An experimental laboratory facility for studying shock-induced liquefaction,” *Geotechnical Testing Journal*, Vol. 13, No. 6, 1990, pp. 291-300.

Veyera, G. E., W. A. Charlie, and M. E. Hubert, “One-Dimensional Shock-Induced Pore Pressure Response in Saturated Carbonate Sand,” *Geotechnical Testing Journal*, Vol. 25, No. 3, September 2002.

Woldeselassie, Bruck H., “The effect of blasting in layered soils, example from Finneidfjord, Norway,” Master thesis, Department of Civil and Transport Engineering, Norwegian University of Science and Technology, 2012.

VITA

Kylie M. Larson-Robl was born in Oshkosh, Wisconsin to Craig and Justine Larson. Kylie received a Bachelor of Science in Geology from the University of Wisconsin Oshkosh, where she also served as an undergraduate research assistant. During her time at the University of Kentucky, Kylie has been a graduate research assistant to Dr. Jhon Silva-Castro and a member of the University of Kentucky Explosives Research Team (UKERT). Kylie has also worked at Alliance Coal, LLC as an environmental compliance and permitting intern. She has been a member of GSA since 2012, a member of SME since 2013, and a member of ISEE and WIM since 2014. Kylie has a publication through ISEE, *Blasting Effects on Pore Pressure in Coal Impoundments (Dry Conditions - Part I)*.